Fall 12-6-2011

The Role of Rankl in Prostate Cancer Progression and Bone Metastasis

Chia-Yi Chu
Georgia State University

THE ROLE OF RANKL IN PROSTATE CANCER PROGRESSION AND BONE METASTASIS

by

GINA C. Y. CHU

Under the Direction of Dr. Leland Chung

ABSTRACT

This study focused on the role of RANKL in prostate cancer EMT progression and metastasis. Activation of RANK, a receptor activator of NF-κB, by its ligand RANKL, in a paracrine manner is responsible for osteoclast differentiation and bone remodeling. RANK activation in cancer cells, however, is thought to be promoted by both autocrine and paracrine mechanisms because RANKL has been shown to be derived from either tumor or its microenvironment, such

as osteoblasts, infiltrating inflammatory cells and stromal fibroblasts. In the present study, we demonstrated that autocrine and paracrine RANKL-RANK signaling could be responsible for driving prostate cancer bone metastasis by promoting epithelial to mesenchymal transition (EMT). We further characterized a novel converging RANKL-c-Met signaling network in which the activation of RANKL was found to promote the expression of both RANKL and c-Met in an autocrine manner in prostate cancer cells. The induced RANKL and c-Met in prostate cancer cells is biologically functional and contributes to increased osteoclastogenesis, epithelial to mesenchymal transition (EMT), cell motility, migration and invasion and conferred bone and soft tissue metastases. Remarkably, RANKL expression by 1,000 prostate cancer cells can provoke bone and soft tissue metastases of a "dormant" population of prostate cancer cells which by themselves failed to form tumors and colonize mouse skeleton, suggesting RANKL can serve as a factor in "reawakening" cancer dormancy to initiate the re-growth and metastasis of cancer cells. We also showed that RANKL-induced RANKL feed-forward autocrine regulation is mediated through cMyc transactivation, allowing the establishment of a "vicious cycle" further promoting prostate cancer growth and metastasis. The converging RANKL-c-Met signaling network is therefore a novel target that could be further manipulated for delaying the lethal progression of castration-resistant human prostate cancer bone metastasis.

INDEX WORDS: Rankl, Rank, C-met, C-myc, Castration-resistant, Epithelial to mesenchymal transition, Osteoclast, Prostate cancer, Metastasis, Bone metastasis, Vicious cycle, Cancer dormancy

THE ROLE OF RANKL IN PROSTATE CANCER PROGRESSION AND BONE METASTASIS

by

GINA C. Y. CHU

A Dissertation Submitted in Partial Fulfillment of the Requirements for the Degree of

Doctor of Philosophy

in the College of Arts and Sciences

Georgia State University

2012

THE ROLE OF RANKL IN PROSTATE CANCER PROGRESSION AND BONE METASTASIS

by

Gina C. Y. Chu

Committee Chair: Leland Chung

Committee: Zhi-Ren Liu

Ritu Aneja

Neale Weitzmann

Elctronic Version Approved:

Office of Graduate Studies

College of Arts and Sciences

Georgia State University

August 2012

DEDICATION

This work is dedicated to my family, my mom, Amy Wang, my brother, Aaron Chu, and my husband, Justin Tsai for their never-ending love and support.

ACKNOWLEDGEMENTS

I would like to express my deepest respect and earnest gratitude to my mentor, Dr. Leland W.K. Chung for giving me the opportunity to pursue my doctorate degree under his invaluable and outstanding guidance and supervision as well as his unwavering encouragement and steadfast support. His mentorship and his wisdom have greatly inspired me in every aspect of my professional and personal life. I am also sincerely grateful to Dr. Haiyen E. Zhau and my department chair, Dr. Phang C. Tai for their contribution to my research and constant caring and support over my Ph.D years.

I would also like to thank Dr. Zhi-Ren Liu, Dr. Ritu Aneja, and Dr. Neil Weitzmann for serving as my dissertation committee members and for their support and advice. Special thanks have to go to Dr. Neil Weitzmann for his kindness in offering instrumental advice and assistance toward my research as well as my Qualifying Exam.

Grateful appreciation is also due to my former and present lab members in Dr. Chung's group, Dr. Ruoxiang Wang, Dr. Wen-Chin Huang, Dr. Daqing Wu, Dr. Bekir Cinar, Dr. Sajni Josson, Dr. Murali Gururajan, Dr. Yueming Wang, Dr. Xiaojian Yang, Hui-Wen Lue, Dr. Peizhen Hu, Dr. Chen Shao, Dr. Boyang Wu, Dr. Srinivas Nandana, and Dr. Chun-Peng Liao for their technical advice and support and helpful and inspiring discussion. I deeply cherish every memorable and joyful moment spent in the Chung lab.

Lastly, I would like to express my most heartfelt gratitude to my dearest family, Amy Wang and Aaron Chu and my beloved husband Justin Tsai for their never-ending love, encouragement, and support. Without them, this work would never have been possible.

TABLE OF CONTENTS

LIST OF TABLES

LIST OF FIGURES

CHAPTER 1 INTRODUCTION

Prostate Cancer and its Progression to Castration-Resistant Disease

Prostate cancer is the most commonly diagnosed cancer and the second leading cause of death among men in the United States and other Western countries. In 2004, approximately 230,000 men were diagnosed with prostate cancer and an estimated 30,000 deaths were due to advanced prostate cancer (Jemal et al., 2004). Prostate epithelial cell growth is dependent on androgens, which promote proliferation and inhibit apoptotic death of the prostate epithelium (Isaacs, 1994). Primary prostate tumors derived from the prostate epithelial cells, produce prostate-specific antigen (PSA), which has been used as an initial screening test for prostate cancer detection. The growth of early prostate tumors is androgen dependent, and androgen ablation therapy is the current primary treatment of choice, leading to initial cancer regression with decreased tumor volume and lower PSA levels. However, androgen ablation therapies are not effective for metastatic prostate cancer and a sub-population of prostate cancer cells develops resistance and becomes androgen-independent/insensitive, resulting in metastatic castration-resistant prostate cancers (CRPCs). The underlying mechanism of androgen-independence is not fully understood but androgen receptor (AR) has been identified as the central molecule that mediates androgen independence. Androgen receptor is a ligand-activated transcription factor. Upon androgen stimulation, activated AR translocates to the nucleus and binds to androgen responsive elements (AREs) along with other co-regulators to modulate the genes involved in the differentiation, development, and proliferation of target cells (McEwan, 2000; Trapman & Cleutjens, 1997). In CRPC, AR levels are maintained and not affected by androgen ablation, thus leading to proliferation of prostate cancer cells. The autonomous AR activation in CRPC can arise from AR amplification, gain of function mutations, ligand-independent receptor activation, and increased

interaction and overexpression of AR coactivators (Heinlein & Chang, 2004). Studies have shown that 20% to 30% of CRPC patients are associated with AR gene amplification (Elo & Visakorpi, 2001), and AR protein levels are also increased in tumors without gene amplification (Koivisto & Helin, 1999; Linja et al., 2001). Elevated AR gene and protein expression levels may allow cancer cells to grow and survive in androgen-deprived conditions (Feldman & Feldman, 2001). Moreover, genetic mutations of AR have been detected in CRPC. Approximately 80 mutations have been identified (Gottlieb, Beitel, Wu, & Trifiro, 2004). Most of the AR mutations are gain of functions which have been found to be associated with primary as well as advanced and metastatic tumors (Marcelli et al., 2000). AR mutants have been predominantly characterized with loss of androgen specificity and increased agonistic stimulation through non-androgen hormones or anti-androgens, leading to increased AR sensitivity and/or constitutively active AR (Ceraline et al., 2004; Suzuki et al., 1993; Veldscholte et al., 1992). The most studied AR mutation is AR T877A, which was detected in the human prostatic LNCaP cell line as well as in human prostate tumors (Gaddipati et al., 1994). T877A mutations resulted in increased AR sensitivity to low levels of androgens and allowed mutant AR to become responsive to anti-androgens, such as estrogen, progesterone, and glucorticoid, which act as androgen agonists (Gaddipati et al., 1994; Veldscholte et al., 1992; Veldscholte, Ris-Stalpers et al., 1990; Veldscholte, Voorhorst-Ogink et al., 1990). Coactivators have also been shown to directly interact with AR and enhance AR-dependent gene transcriptional activity (Heinlein & Chang, 2004), and increased levels of a subset of AR coactivators may contribute to the sensitization of AR to low levels of androgen after androgen deprivation therapy (Gregory, Johnson, Mohler, French, & Wilson, 2001). Coactivators, such as SRC-1, TIF-2, and SRC-3 have been found to be overexpressed in hormone refractory prostate cancer and high Gleason

scored prostate cancer (Gnanapragasam, Leung, Pulimood, Neal, & Robson, 2001; Gregory, He et al., 2001; Heinlein & Chang, 2002; McKenna, Lanz, & O'Malley, 1999). In addition, the AR coactivator ARA70 has also been found to be elevated in prostate cancer specimens (Yeh & Chang, 1996) as well as in CWR22 xenograft tumors, which have become hormone refractory after castration (Gregory et al., 1998). Moreover, several tumor suppressor genes have been shown to interact with AR to regulate AR transcriptional activity. Phosphorylated Rb (Yeh et al., 1998) and BRCA1 and 2 can function as AR coactivators and increase AR transcriptional activation (Shin & Verma, 2003; Yeh et al., 2000). Whereas, the umor suppressor PTEN, a negative regulatory of PI3K/Akt survival pathway, inhibits AR transcriptional activity and degradation of AR; loss of PTEN promotes prostate cancer progression through activation of both AR and PI3K/Akt signaling (Heinlein & Chang, 2004).

AR transcriptional activity can also be activated by many growth factors, such as IGF-1, KGF, and EGF, in the absence of androgen (Culig et al., 1994). Cytokines, such as IL-6, also stimulates AR transcriptional activity in LNCaP and DU145 cells (Drachenberg, Elgamal, Rowbotham, Peterson, & Murphy, 1999; Hobisch et al., 1998). Elevated expression of Her2/Neu/ErbB2 receptor tyrosine kinase has been shown to mediate androgen-independent activation of AR in CRPC (Signoretti et al., 2000) through MAPK and PI3K dependent pathways (Campbell, Khosravi-Far, Rossman, Clark, & Der, 1998; Yart et al., 2001). Moreover, overexpression of anti-apoptotic protein Bcl-2 allows survival and cell growth of LNCaP cells and xenograft prostate tumors during androgen ablation by preventing androgen depletion-induced apoptosis of prostate cancer cells. However, Bcl-2 expression was reduced when androgen was re-supplemented, implicating that Bcl-2 might be regulated by AR signaling (Raffo et al., 1995). Therefore, multiple molecular mechanisms potentially promote the

development of CRPC all through modulations of AR function. Androgen ablation leads to amplification and mutation of the AR gene as well as the activation of AR co-activators and many growth factors, which all lead to abnormally up-regulated transcriptional activity of AR allowing the survival and proliferation of prostate cancer cells and progression of CRPC.

Prostate Cancer Lethal Bone Metastasis

Advanced prostate cancers, such as CRPC have a propensity to metastasize to bone, and approximately 90% of CRPC patients will develop bone metastases (Bubendorf et al., 2000; Horwich, 2004; Loberg, Logothetis, Keller, & Pienta, 2005). Prostate cancer-induced bone metastasis is considered incurable (Cheville et al., 2002), and the median survival time for patients with bone metastasis is approximately 20 months (Rajpar et al., 2010). Bone metastases result in significant complications for patients, such as bone pain, pathological fractures, impaired mobility, spinal cord compression, and symptomatic hypercalcemia (Coleman, 1997, 2001; Ye, Kynaston, & Jiang, 2007). Bone metastases can be either osteoblastic (bone forming) or osteoclastic (bone resorbing). Even though prostate cancer bone metastases are predominantly osteoblastic, emerging histological evidence indicates considerable osteolysis is also involved, leading to a heterogeneous mixture of osteolytic and osteoblastic lesions of prostate cancer (Keller & Brown, 2004; Roudier et al., 2008; Zhang et al., 2001). In normal conditions, bone undergoes a balanced and coupled remodeling process initiated by osteoclast-mediated bone resorption and subsequently followed by osteoblast-mediated bone formation (Guise et al., 2010). In prostate cancer bone lesions, the increased bone production is via an overall increased bone remodeling with osteoblast-mediated bone formation outweighing the increased osteoclastic resorption (Keller & Brown, 2004; Vela et al., 2007). Interestingly, the serum levels of the bone-resorption markers, such as N-telepeptide of type-I collagen (NTx), seem to be better correlated

with prostate cancer progression and to be a stronger predictor of overall survival in CRPC patients with bone metastases than the bone-formation marker, bone alkaline phosphatase (BALP) (Sturge, Caley, & Waxman, 2011).

Metastasis of prostate cancer to bone involves a complex and sequential cascade of events dependent on interactions between the cancer cells and their surrounding microenvironment. The metastatic process is generally initiated by detachment of cancer cells from the primary or local site through disruption of the intercellular adhesion and invasion to the surrounding tissues in close proximity by breaking the extracellular matrix. The invasive cancer cells then intravasate to the capillaries generated from tumor vasculature and then to the main circulation as well as the lymphatic system (Guise et al., 2010). Once they survive immune surveillance and mechanical stresses in the circulation, the cancer cells can extravasate from circulation and gain entry to distant hospitable sites to establish and expand through proliferation and induction of angiogenesis. The precise mechanism by which prostate cancer preferentially homes to bone is still unclear, but several hypotheses have been proposed. The essential roles of bone microenvironment and prostate cancer osteomimicry have also been increasing acknowledged and implicated in the process of prostate cancer metastasis to bone.

Batson first proposed the concept of the vertebral vein system, known as the Batson's venous plexus in 1940, which is a network of valveless veins richly surrounding the prostate and connected to the venous plexuses of the internal spine allowing the dissemination of cancer cells to the skeletal system (Batson, 1940). However, such a theory based on anatomical structure could not explain the preferential homing to bone and other common metastatic sites. The "seed and soil" hypothesis proposed by Stephen Paget in 1989 first suggested that the interplay between the metastatic properties of the cancer cells (seed) and the particular organ

microenvironment (soil) determines the favorable and selective homing and growth of the cancer cells (Paget, 1989). Therefore, tumor metastasis involves bi-directional interactions between cancer cells and the bone microenvironment. The "soil", such as the bone microenvironment must provide favorable conditions for the prostate cancer cells to colonize, survive, expand, and establish. Bone is enriched with abundant sources of immobilized growth factors, such as TGF-β, IGF, FGF, PDGF, and BMPs, cytokines, chemokines, and cell adhesion molecules, which can be released and activated during bone resorption, thus serving as a fertile environment for the cancer cells to grow and proliferate (Roodman, 2004). On the other hand, the prostate cancer cells can also alter bone homeostasis by secreting pro-osteoclastic and pro-osteoblastic factors that directly or indirectly impact bone resorption and formation in the bone microenvironment (Vela et al., 2007). Osteolysis is required before osteoblast bone mineralization in metastatic deposits, and prostate cancer cells can secret a number of pro-osteoclastic factors, such as PTHrP, RANKL, and IL-6, which can activate osteoclast precursors and lead to osteoclastic bone resorption (Fili, Karalaki, & Schaller, 2009). Osteolysis then releases all the growth factors stored in the bone matrix, which allows prostate tumor cells to survive and proliferate, leading to more production of the osteolytic factors by the cancer cells. Moreover, prostate cancer cells also have osteomimetic properties and produce many osteotropic factors, such as PDGF, IGFs, FGFs, TGF-β, VEGF, Wnt1, PTHrP, uPA, PSA, ET-1, and BMPs (Ye et al., 2007) and synthesize and deposit bone matrix proteins, such as osteopontin, osteocalcin, osteonectin, and bone sialoprotein in the bone matrix (Cher, 2001; Koeneman, Yeung, & Chung, 1999), thus promoting predominantly osteoblastic metastases. This bidirectional interaction between the prostate cancer cells and the bone microenvironment results in the establishment of a "vicious cycle" that is the key for the development of cancer metastasis to bone.

Pathophysiological Role of RANKL in Bone Remodeling

Bone remodeling is a continuous process during adulthood through the resorption of old bone by bone-degrading osteoclasts and the subsequent formation of new bone by bone-forming osteoblasts (Manolagas & Jilka, 1995). Under normal conditions, bone remodeling continues in cycles where osteoclasts adhere to bone and remove it by acidification and proteolytic degradation, and once osteoclasts leave the resorption sites, osteoblasts subsequently invade the area and begin the process of forming new bone by secreting osteoid (a matrix of collagen and other proteins), which is eventually mineralized. After the bone formation finishes, the surface of the bone is covered by lining cells, characterized as a distinct type of terminally differentiated osteoblasts (Parfitt, 1994). Bone remodeling is a dynamic process that requires coordinated cellular activities among osteoblasts, osteocytes, and osteoclasts to maintain bone homeostasis (Stains & Civitelli, 2005). Osteoclastic bone resorption is always followed by osteoblastic bone formation, which led to the concept that the two processes are mechanistically "coupled" in order to maintain a constant, homeostatically controlled amount of bone (Rodan, 1998).

RANKL, a receptor activator of NF-κB, is a member of the tumor necrosis factor (TNF) super family. RANKL exits both as a membrane-bound and a secreted form, for which the latter is a result of the proteolytic cleavage by MMPs or alternative splicing (Ikeda, Kasai, Utsuyama, & Hirokawa, 2001; Lynch et al., 2005). RANKL is primarily expressed on the surface of osteoblasts and bone marrow stromal cells and the soluble form can be released by activated T cells (Roodman, 2004; Vela et al., 2007). Moreover, RANKL is also found to be expressed in many different tissue types, such as peripheral lymph nodes, bone marrow, thymus, spleen, brain, heart, skeletal muscle, kidney, liver, lung, and mammary gland (Kartsogiannis et al., 1999; Lacey et al., 1998). RANKL expression can be up-regulated by many hormones and growth factors,

such as PTH, PTHrP, prostaglandin E2, vitamin D, and glucocorticoids, as well as by several cytokines, such as IL-1, IL-6, IL-7, IL-17, and TNF-α, (Anandarajah, 2009; Theoleyre et al., 2004). RANKL plays essential roles in multiple aspects of the osteoclastogenesis including osteoclast formation, differentiation, maturation, and survival during bone remodeling (Lacey et al., 1998; Vela et al., 2007). The predominant role of RANKL in osteoclastogenesis was discovered in RANKL knockout mice that developed osteopetrosis with an excess of bone formation due to the complete absence of osteoclasts (Kong et al., 1999), and no factor or combination of factors has been shown to be capable of restoring bone resorption when RANKL is absent (Anandarajah, 2009; Kearns, Khosla, & Kostenuik, 2008). Both membrane-bound and soluble forms of RANKL are implicated as important physiological and pathological mediator of bone resorption (Kearns et al., 2008). The activity of RANKL in bone remodeling is mediated by binding to its cognate receptor RANK on osteoclast precursors in a paracrine manner to promote osteoclastogenesis and hence osteoclast-induced bone resorption (Kong et al., 1999; Yasuda et al., 1998). RANKL-induced osteoclastogenesis can be blocked by OPG, which acts as a decoy receptor of RANKL, leading to suppressed bone resorption and favoring bone formation (Schneeweis, Willard, & Milla, 2005). OPG is also expressed by osteoblasts and bone marrow stromal cells, and the ratio of RANKL and OPG determines the degree of osteoclastogenesis. An imbalance in the ratio of RANKL to OPG is known to be implicated in the pathogenesis of bone remodeling with an increase in RANKL level associated with increased bone resorption. Such imbalance is associated with accelerated bone remodeling rate and manifests as the basis of several bone diseases characterized by bone loss, such as post menopausal osteoporosis, inflammatory arthritis, multiple myeloma, and cancer bone metastases. Moreover, studies from animal models of rheumatoid arthritis and bone metastasis demonstrate that RANKL inhibition

by OPG or RANKL antibody can lead to significantly reduced bone resorption accompanied with increased bone volume, density and strength as well as decreased skeletal tumor burden and development (Kearns et al., 2008).

Autocrine and Paracrine RANK-RANKL Signaling in Prostate Cancer Growth, Survival, and Bone Metastasis

RANKL and RANK are essential mediators in regulating both normal and pathological bone remodeling, but they also play a pivotal role in mammary epithelial cell proliferation and survival during pregnancy as demonstrated by genetic mouse models (Gonzalez-Suarez et al., 2007; Kim et al., 2006). Recently, RANKL-RANK signaling has been demonstrated to be involved in cancer cell proliferation, survival, and metastasis of various cancers, including breast and prostate cancers (Brown et al., 2001; Chen et al., 2006; Fili et al., 2009; Jones et al., 2006). Expression of RANKL and RANK is not restricted to the surface of osteoblasts and stromal cells and on osteoclast precursor cells in the bone environment; emerging evidences from human clinical and in vitro studies have shown that both RANKL and RANK are also expressed by some malignant cancer cells and cell lines, including breast, prostate, lung, and thyroid cancers that have high metastatic potential to bone (Chen et al., 2006; Hanada et al. 2011; Huang, Cheng, Chow, Zheng, & Kumta, 2002; Jones et al., 2006). Moreover, prostate cancer-induced bone metastases exhibit significantly higher RANKL levels expressed by the tumor cells than non-osseous metastases or the primary tumors (Brown et al., 2001; Chen et al., 2006). Similarly, the primary breast tumors that retained RANKL expression correlated with an estrogen receptor-negative and high histological tumor grade (Cross et al., 2006). This suggests that RANKL-RANK signaling may be implicated in cancer malignant progression and bone metastasis.

Cancer growth and survival require reciprocal communications through signals or factors secreted by the cancer cells and the host cells in the immediate tumor microenvironment. For bone metastatic tumors, the cross talk between the tumor cells and the bone microenvironment results in disequilibrium of the bone remodeling and promotes the pathologic "vicious cycle". Cancer cells secrete many cytokines and growth factors, such as IL-6, IL-11, and PTHrP, that stimulate osteoblasts and stromal cells to produce RANKL, and the cancer cells can also express RANKL directly. RANKL produced by both osteoblasts and cancer cells then acts on osteoclast precursors to induce osteoclastogenesis and bone resorption. Increased bone turnover releases more cytokines and growth factors richly stored in the bone matrix, fueling more cancer cell growth and RANKL secretion (Grimaud et al., 2003). Moreover, the increased RANKL may autonomously activate RANK-expressing cancer cells in an autocrine manner, or in a paracrine manner if RANKL is produced by the accessory cells in the bone microenvironment. Autocrine RANKL signaling has been suggested to enhance the malignant progression of breast cancer (Cross et al., 2006). Taken together, the autocrine and paracrine RANKL-RANK signaling can induce cancer cell growth and survival, leading to cancer progression and metastasis (Boyce & Xing, 2007; Schramek, Sigl, & Penninger, 2011). Another possible way RANKL and RANK may be involved in the cancer development and metastasis to the bone is based on the rationale that RANK- expressing cancer cells might sense RANKL produced in the bone microenvironment as a chemoattractant and therefore migrate in a coordinated manner to the bone matrix (Schramek et al., 2010). It has been demonstrated that RANKL can trigger directed migration of human and mouse mammary epithelial cells, breast and prostate cancer cells, and melanoma cells that express RANK (Jones et al., 2006). Reciprocally, RANKL-expressing cancer cells can also be attracted towards RANK-expressing osteoblasts and stromal cells in the

bone microenvironment. Such bidirectional interaction and chemoattraction between cancer cells and the bone microenvironment allows the metastasizing tumor cells, particularly breast and prostate tumors, preferentially colonize, proliferate, and survive in the bone. Moreover, blocking RANKL-RANK signaling has been shown to reduce tumor burden in long bones by 50%, but not metastases in the other tissues in an in vivo model of melanoma bone metastasis (Jones et al., 2006). In the MDA-MB-231 breast cancer bone metastasis model, inhibition of RANKL with OPG-Fc, which consists of the ligand-binding domain of human OPG fused to the Fc domain of human IgG (Morony et al., 1999), demonstrated a reduction in both tumor number and size in the bone marrow, leading to a total decrease of tumor burden by 80% (Morony et al., 2001). Mice treated with OPG-Fc also exhibited decreased skeletal tumor volume and tumor growth while increasing tumor cell apoptosis (Canon et al., 2008). In several prostate cancer models, RANKL inhibition with either OPG-Fc or RANK-Fc prevented tumor growth in the bone and/or reduced skeletal tumor burden accompanied with decreased serum PSA level in the bone. However, both OPG-Fc and RANK-Fc treatments had no effects on the growth of subcutaneous prostate tumors (Kiefer et al., 2004; Yonou et al., 2003; Zhang et al., 2001; Zhang et al., 2003). Furthermore, in the colon cancer model, OPG-Fc also showed inhibition of tumor growth in bone (Morony et al., 2001). Together, these studies further confirmed that RANKL inhibition can reduce bone metastases and tumor growth in bone, leading to improved survival in multiple myeloma, breast, prostate, and colon cancer models; however, RANKL inhibition cannot directly decrease tumor cell proliferation in other tissue metastases. These data strongly support the notion that RANKL/RANK interaction may not directly stimulate tumor cell proliferation; however, autocrine and paracrine RANKL-RANK signaling can promote tumor cell growth and survival through reciprocal feedback and interdependence between tumor cells and the bone

microenvironment by creating vicious cycle with tumor cells promoting bone resorption and the resorbing bone matrix supporting the growth and survival of tumor cells in return, eventually leading to cancer progression and bone metastasis. Targeting the RANKL system with small molecule inhibitors not only can inhibit bone resorption but also prevent tumor growth and block bone metastasis.

Epithelial to Mesenchymal Transition in Prostate Cancer Progression and Metastasis

Epithelial to mesenchymal transition (EMT) is considered a critical and evolutionarily conserved process during embryonic development (Thiery, 2003). During EMT, epithelial cells undergo profound morphogenetic changes by losing their characteristic cell-cell adhesion structures, modulating their polarity, and reorganizing their cytoskeleton switching from cytokeratin- to vimentin-based filaments, thus resulting in the formation of isolated and migratory mesenchymal cells that have invasive properties and resistance to apoptosis (Klymkowsky & Savagner, 2009; Savagner, 2010; Singh & Settleman, 2010). EMT was first recognized in the context of cellular remodeling during embryogenesis, including heart morphogenesis, mesoderm and neural crest formation in the early 1980s (Savagner, 2001; Thiery, Acloque, Huang, & Nieto, 2009). In adults, EMT can occur during wound healing, tissue regeneration, and organ fibrosis to generate repair-associated mesenchymal cells or fibroblasts. Today, EMT is strongly implicated in tumor progression and metastasis (Kalluri, 2009; Kang & Massague, 2004; Thiery, 2002). Even though some pathologists remain skeptical whether EMT is apparent in human tumor specimens because it cannot be followed in time and space in human tumors, a growing body of evidence strongly suggests that EMT, if transient, is an essential step for the progression of many carcinomas to give rise to the great diversity of phenotypes and malignant potential, and it may be a permanent phenomenon in tumors with mixed carcinoma (epithelial origin) and sarcomas (mesenchymal

origin) (Kang & Massague, 2004; Sethi, Macoska, Chen, & Sarkar, 2010; Tarin, Thompson, & Newgreen, 2005; Thiery, 2002; Thompson, Newgreen, & Tarin, 2005). Moreover, recently, EMT has also been mechanistically linked with stemness of the cancer cells, leading to increased resistance to apoptosis, diminished senescence and escape from immune surveillance (Kong et al., 2010; Lynch et al., 2010; Mani et al., 2008; Morel et al., 2008), eventually leading to drug resistance (Singh & Settleman, 2010; van der Pluijm, 2010).

The hallmark of EMT is the disruption of intercellular contacts through the loss of E-cadherin components, which are essential molecules providing the cell-cell adhesion junctions for the formation of epithelia and maintenance of the epithelial homeostasis. Cells with lost E-cadherin expression can dissociate from the neighboring cells and gain mesenchymal phenotype with enhanced cell motility and invasiveness, allowing them to migrate away from the original tissue into the adjacent ones. Such morphological and behavioral transition can promote the progression of many cancer cells, including breast, prostate, and pancreas, from an indolent to a malignant state, thus favoring their migration, invasion, dissemination, and metastasis (Guarino, Rubino, & Ballabio, 2007; Kang & Massague, 2004; Klymkowsky & Savagner, 2009). During EMT, the loss of the epithelial-specific marker, E-cadherin is accompanied by up-regulation of mesenchymal-associated genes, such as N-cadherin, vimentin, or fibronectin. Such changes in gene expression with decreased E-cadherin and increased N-cadherin or vimentin expression during EMT are consistently observed in various cancers with enhanced tumor growth and invasiveness, leading to tumor progression and metastasis (Huber, Kraut, & Beug, 2005; Thiery, 2002). In the context of tumor progression, EMT has been studied extensively in detail in vitro using epithelial cell models and in vivo using transgenic mouse tumor models. Therefore, the molecular mechanisms underlying the EMT process have been unraveled and several

interconnected transduction pathways and a number of signaling molecules governing the initiation of EMT have been elucidated. These include receptor tyrosine kinase (RTK), Ras/MAPK, Src, PI3K/Akt, Wnt/β-catenin, Rho-GTPases, TGF-β, NF-κB, and integrins pathways (Guarino et al., 2007; Klymkowsky & Savagner, 2009; Thiery, 2003). Most of these pathways converge on the repression of E-cadherin expression as an event that is critical for the onset of EMT, followed by activation of mesenchymal gene expression through the modulation of many transcription factors, contributing to the molecular mechanisms of EMT. The loss of E-cadherin function during tumor progression can be genetically or epigenetically regulated. E-cadherin expression is frequently inhibited by various epigenetic mechanisms (Thiery, 2002), and the loss of E-cadherin expression through promoter hypermethylation is observed in some primary tumors as well as some metastases (Chang, Chow, Lam, Wei, & Yuen, 2002; Machado et al., 2001). However, in most cases, E-cadherin expression is inhibited through transcription repression by zinc-finger transcription factors Snail or Slug (Bolos et al., 2003; Nieto, 2002) and basic helix-loop-helix transcription factors Twist or E47 (Yang et al., 2004), which are all strong repressors of E-cadherin transcription and potent inducers of EMT. Other E-cadherin repressors, such ZEB1 and SIP1 are also implicated in EMT (Peinado, Portillo, & Cano, 2004). E-cadherin repressors negatively regulate E-cadherin transcription by recognizing and binding to the common proximal E-boxes in E-cadherin promoter (Nieto, 2002; Yang et al., 2004), and presumably display overlapping functional redundancy. Overexpression of Snail, Twist, Slug, or SIP1 not only suppresses E-cadherin expression but also up-regulates N-cadherin expression in human pancreatic, prostate, and gastric cancer (Alexander et al., 2006; Hotz et al., 2007; Odero-Marah et al., 2008; Rosivatz et al., 2002). A model of E-cadherin suppressors participated during EMT and invasion has been suggested by which Snail and SIP1 may induce the initial

invasiveness of EMT, whereas Slug, E47, and perhaps ZEB1 would be involved in the maintenance of the migratory and invasive phenotype of EMT (Peinado et al., 2004); Twist is likely to play a role in the development of distant metastasis by promoting cancer cells to enter the bloodstream (Yang et al., 2004). Moreover, Snail and Twist expression has been reported to correlate with prostate and breast cancer progression and metastasis (Karreth & Tuveson, 2004; Kwok et al., 2005).

The process of EMT can be initiated by many growth factors, such as EGF, FGF, HGF, IGF, and PDGF binding to their cognate receptors and stimulating the receptor tyrosine kinases that mediate the phosphorylation and activation of downstream substrates and signaling, including Ras/MAPK, PI3K/Akt, Rho/Rac, NF-κB, Src, and β-catenin. Activation of RTK by growth factors is known to be required for cell scattering, therefore contributing to the migratory and invasive phenotype implicated in EMT (Boyer, Valles, & Edme, 2000). Ras is a small GTP-binding protein that activates a cascade of effectors with kinase activity, and each of which defines a pathway with specific functions. The best characterized Ras effector is the serine/threonine kinase Raf, which can initiate a series of phosphorylations leading to the activation of MAPK (ERK), which translocates into the nucleus and phosphorylates various transcription factors, such as Ets factors, Jun and Fos, and Slug (Boyer, Roche, Denoyelle, & Thiery, 1997). These Ras/MAPK-activated downstream transcription factors are essential mediators of EMT. Slug is known as a direct repressor of E-cadherin transcription and an inducer of EMT (Thiery, 2003), and AP-1 formed from complex of Jun and Fos, and Ets factors are also regarded as inducers of EMT (Davies et al., 2005; Hsu, Trojanowska, & Watson, 2004). Other than directly triggering MAPK, Ras can also synergistically activate PI3K and Rho/Rac signaling which are also important players in EMT (Guarino et al., 2007).

PI3K is fundamentally involved in the regulation of cell growth and apoptosis, and the PI3K/Akt pathway plays a central role in tumorigenesis by promoting cell survival and cell proliferation and inhibiting apoptosis. Activated Akt can directly up-regulate Snail expression, or it can phosphorylate and inhibit GSK-3β in the Wnt/β-catenin pathway and prevent the degradation of both β-catenin and Snail, thus leading to an increase in both signaling β-catenin and Snail levels, ultimately promoting EMT (Bakin, Tomlinson, Bhowmick, Moses, & Arteaga, 2000; Zhou et al., 2004).

Rho and Rac are small GTPases involved in the regulation of the actin cytoskeleton, polarization, cell-cell and cell-matrix adhesion, membrane trafficking, and cell proliferation (Burridge & Wennerberg, 2004; Jiang, Sha, & Schacht, 2006). Therefore, they are recognized as key mediators governing cell dissociation, cell shape changes and migratory ability during EMT and invasion process. Growth factor-activated receptor tyrosin kinases and their downstream mediators Ras and PI3K, as well as signals from extracellular matrix can all modulate the activity of Rho and Rac, and their activation are required for induction of cell motility during EMT possibly through the breakdown of the intercellular junctions (Guarino et al., 2007).

Src is a non-receptor SH2 domain-containing cytoplasmic tyrosin kinase involved in the regulation of cell growth, adhesion, and migration. Src can modulate the cell adhesiveness state by altering the balance between the cadherin-mediated cell-cell adhesion and integrin-mediated cell-matrix adhesion and inducing a more motile phenotype. Src is considered as a potent EMT inducer because activated Src can promote an 'adhesion switch' through disruption of E-cadherin-based intercellular contacts and up-regulation of dynamic integrin-mediated cell-matrix adhesion, leading to a conversion from a cohesive to a dispersed, migratory phenotype. The underlying mechanism of Src-induced migration is based on the activation and accumulation of

phosphomyosin through FAK- and MAPK-dependent activation, which results in the breakdown of cell-cell contacts and gain of acto-myosin contractility, leading to a mesenchymal phenotype suitable for migration and invasion (Avizienyte, Brunton, Fincham, & Frame, 2005).

TGF-β is a cytokine expressed in most human cancer and plays a dual role in tumor development. In the early phases of tumor formation, TGF-β acts as a strong anti-proliferative, pro-apoptotic, and tumor growth inhibiting factor; however, in the later stages it converts to promote tumor progression by stimulating EMT, migration, and invasion. Activation of TGF-β signaling results in the formation of a Smad complex, which is able to translocate into the nucleus and activate transcription factor LEF-1/TCF, which is a crucial mediator of EMT. However, TGF-β can also induce EMT in a Smad-independent manner through the activation of Ras/MAPK, PI3K, p38, Rho and Rac signaling (Bakin et al., 2000; Bhowmick et al., 2001; Xie et al., 2004). In tumor cells, it seems that the cooperation between TGF-β and either RTK or downstream Ras and PI3K can overcome the suppressive effects of TGF-β on cell proliferation, thereby allowing EMT to take place. Moreover, TGF-β can induce epithelial cells to undergo EMT and become mesenchymal-like cells that are capable to produce more TGF-β, thus creating an autocrine feed-forward loop, allowing the maintenance of the mesenchymal-like phenotype and reinforcing the EMT process (Guarino et al., 2007).

β-catenin has been shown to play central roles in both the cell adhesion complex as well as in Wnt signaling; therefore, β-catenin represents a converging point where cadherins intersect and modulate the Wnt signaling system in EMT (Nelson & Nusse, 2004). The canonical Wnt signaling pathway is initiated by Wnt ligands binding to LRP5 and LRP 6 receptors, which then complex with the transmembrane Frizzled receptors and activate Dishevelled protein, leading to inhibition of glycogen synthase kinase 3β (GSK-3β)-mediated β-catenin phosphorylation and

accumulation of unphosphorylated β-catenin in the cytoplasm. β-catenin can be present in the membrane associated to E-cadherin, in cytosol, or in the nucleus. Upon Wnt activation, the cytosolic β-catenin can translocate into the nucleus, replace the co-repressors and bind with LEF/TCF transcription factors to activate the transcription of downstream genes required for EMT, such as Ets, Jun, Slug, fibronectin, and vimentin (Brabletz et al., 2005; Mason & Patterson, 2003; Nelson & Nusse, 2004). In the absence of a Wnt-mediated signal, most of the cytosolic β-catenin is sequestered by E-cadherin at the cell junctions, and the remaining β-catenin is rapidly degraded through GSK-3β-mediated phosphorylation. Down-regulation of E-cadherin during EMT not only increases cell motility through loss of cell-cell adhesion but also results in an increase of free cytosolic β-catenin for nuclear signaling, leading to enhanced EMT induction and maintenance. In addition to Wnts and loss of E-cadherin, activation of PI3K/Akt, integrin-linked kinase (ILK), or Ras/MAPK can also stimulate β-catenin nuclear signaling through phosphorylation and inhibition of GSK-3β (Ding et al., 2005). Moreover, GSK-3β is found to be highly expressed in the epithelial cells and it can block Snail transcription and promote its degradation; conversely, inhibition of GSK-3β through Wnt or other signaling leads to up-regulation of Snail and promotes EMT (Brabletz et al., 2005; Zhou et al., 2004).

Recently, NF-κB has been identified as a central mediator of EMT in a model of breast cancer progression, and Ras and TGF-β-mediated EMT and activation of their downstream genes are at least in part via NF-κB signaling (Huber et al., 2004). Importantly, the NF-κB family of transcription factors can promote EMT progression through activation of E-cadherin repressors, such as Snail (Brabletz et al., 2005; Kim et al., 2007), Slug (Belguise et al., 2007), ZEB1/2 (Chua et al., 2007), and Twist (Pham et al., 2007; Sosic & Olson, 2003; Sosic, Richardson, Yu, Ornitz, & Olson, 2003), leading to the up-regulation of mesenchymal markers vimentin, MMP2,

and MMP9 (Brabletz et al., 2005; Huber et al., 2004; Kong et al., 2010; Min, Eddy, Sherr, & Sonenshein, 2008). Therefore, NF-κB signaling is widely recognized for its pivotal roles in cell survival, EMT induction, maintenance of invasiveness, and progression to metastasis in many human cancers.

Molecular Mechanism of RANKL-Activated RANK Signaling

Binding of RANKL to RANK triggers intricate and distinct signaling cascades that induce the differentiation of osteoclast precursor cells and stimulate the resorption function and survival of mature osteoclasts. RANK-stimulation induces signaling pathways of NF-κB, MAPKs, MAPK-P38, Src/PI3K/AKT, and NFATc1 through the initial activation of TNF receptor-associated factor (TRAF) adaptor proteins, especially TRAF6 (Galibert, Tometsko, Anderson, Cosman, & Dougall, 1998; Wada, Nakashima, Hiroshi, & Penninger, 2006). RANKL-RANK interaction induces strong NF-κB activation in osteoclasts through activation of TRAF6. RANK stimulation induces phosphorylation and degradation of IκBα and the nuclear translocation and DNA binding of the NF-κB proteins of p50, p52, and p65 (Jimi et al., 1999). Genetic ablation of NF-κB p50 and p52 proteins in mice leads to decreased osteoclastogenesis and osteopetrosis (Iotsova et al., 1997). Moreover, NF-κB activation can also mediate cellular proliferation, invasion, angiogenesis, and metastasis (Aggarwal, 2004; Bhat-Nakshatri, Sweeney, & Nakshatri, 2002; Biswas, Cruz, Gansberger, & Pardee, 2000; Bond, Fabunmi, Baker, & Newby, 1998; Chilov et al., 1997; Helbig et al., 2003). MAPK family members of p38-MAPKs, JNK, and ERK are also activated by RANK stimulation (Jimi et al., 1999). Activated p38 downstream of RANK leads to direct phosphorylation of STAT1, controlling various target genes (Kwok et al., 2005) and might be involved in regulation of mRNA stability (Chang & Karin, 2001). Activation of JNK from RANK-signaling also up-regulates AP-1 transcription factor family members, including cJun,

JunB, c-Fos, and Fra, which are essential for osteoclast differentiation (David, Sabapathy, Hoffmann, Idarraga, & Wagner, 2002; Wagner, 2002). ERK is also activated upon RANKL activation during osteoclastogenesis (Wada et al., 2006). ERK, p38-MAPK, and JNK MAPK pathways are also known to be associated with cancer development, proliferation, differentiation, survival and migration (Dhillon, Hagan, Rath, & Kolch, 2007; Wagner & Nebreda, 2009).

Another downstream target of RANK signaling is nuclear factor of activated T cells, calcineurin-dependent 1 (NFATc1) (Takayanagi et al., 2002). RANKL-RANK signaling induces increased NFATc1 expression to promote osteoclast differentiation through activation of osteoclastic genes, such as TRAP and calcitonin receptors in cooperation with c-Fos. NFATc1 can also be activated via calcineurin with elevated intracellular Ca^{+2} levels upon RANK activation (Takayanagi, 2005; Takayanagi et al., 2002). Recently, NFATc1 has been shown to promote tumor migration, invasion, and metastasis through activation of numerous target genes, including COX2, autotoxin, and prostaglandin E_2, particularly in breast cancer cells (Mancini & Toker, 2009; Muller et al., 2010).

PI3K-AKT signaling is also involved in RANKL-induced osteoclastogenesis mediated through Src activation (Nakashima et al., 2000). Among the many molecules downstream of Src, PYK2 (Protein Tyrosine Kinase-2) and c-Cbl are implicated in osteoclast adhesion signaling and bone resorption function (Miyazaki et al., 2004; Walsh & Choi, 2003). Src and PI3K function mediates RANK and adhesion signals convergence, transmitting the signals for proper actin cytoskeletal organization and facilitating the resorption activity of osteoclasts (Chellaiah, Fitzgerald, Alvarez, & Hruska, 1998). Additionally, Src is a proto-oncogene that has been strongly implicated in the development, growth, progression, and metastasis of many human cancers (Irby & Yeatman, 2000).

Activation of RANKL-RANK-signaling pathways also plays an important role in cancer progression and metastasis. RANK-mediated signaling might act as a link between osteoclastogenesis during bone resorption and cancer progression and metastasis.

Overarching Hypotheses and Aims of This Study

The goal of this thesis is to identify and evaluate the role of prostate cancer cell-derived RANKL in EMT progression and bone and soft tissue metastases.

The overarching hypothesis of this study is that autocrine and paracrine cell signaling networks, mediated by RANKL-RANK interaction, promotes EMT progression and metastasis of prostate cancer cells. RANKL-RANK interaction provides a "reawakening" signal for the "dormant" non-tumorigenic prostate cancer cells to re-engage in tumorigenesis and metastasis cascade through a mechanism mediated by RANKL-induced autocrine feed-forward activation in which RANKL induced RANKL and c-MET expression. Responsiveness of RANK and c-MET in prostate cancer cells to external converging signals, from RANKL, HGF and or VEGF, are responsible for driving EMT and prostate cancer bone and soft tissue metastases.

The first aim is to examine whether RANKL induces prostate cancer cell EMT *in vitro* at both the biochemical and morphological levels.

The second aim is to examine whether RANKL promotes *in vivo* tumorigenesis and metastasis of prostate cancer cells.

The third aim is to investigate whether the presence of RANKL-expressing prostate cancer cells confers the ability of RANKL-null and non-tumorigenic prostate cancer cells to grow and metastasize.

The fourth aim is to determine the underlying molecular mechanism that regulates RANKL-induced RANKL expression in an autocrine manner.

CHAPTER 2 MATERIALS AND METHODS

Cell Culture

The LNCaP, C4-2, and C4-2B human prostate cancer progression models were established by our laboratory as previously described (Thalmann et al., 1994). PC-3, PC-3M and DU145 human prostate cancer cells and MG63 human osteosarcoma cells were obtained from ATCC (Manassas, VA). LNCaP, C4-2, C4-2B, PC3, PC3-M, DU145, and MG63 were all maintained in RPMI 1640 supplemented with 5% FBS. $ARCaP_E$ and $ARCaP_M$ cells, established by our lab (Xu et al., 2006; Zhau et al., 1996), were maintained in T-medium (Invitrogen, Carlsbad, CA) supplemented with 5% FBS. SaOS-2 and RAW264.7 cells (kindly provided by Dr. Neale Weitzmann, Emory University, Atlanta, GA) were maintained in DMEM supplemented by 10% FBS.

Cloning of RANKL Expression Vectors

Human RANKL cDNA ORF (NM_003701) was purchased from OriGene (Rockville, MD). Human RANKL cDNA was amplified by PCR and subcloned into p3×FLAG- myc-CMV-25 (Sigma-Aldrich, St. Louis, MO) at the NotI and XbaI restriction enzyme sites. The amplified human RANKL cDNA was also subcloned into Plvx-AcGFP-N1 plasmids (Clontech, Mountain View, CA) at the XhoI and XmaI restriction enzyme sites. The sequences of both p3×FLAG-RANKL and Plvx-AcGFP-RANKL were confirmed by DNA sequencing.

Cell Transfection and Transduction

$ARCaP_E$ or $ARCaP_M$ cells were seeded into 6-well plates and transiently transfected with flag-tagged RANKL or neo plasmid DNA under the regulation of CMV-promoter or 20 pmole RANKL siRNA (Santa Cruz Biotechnology, Inc., Santa Cruz, CA) with a universal siRNA

serving as the control (Invitrogen, Carlsbad, CA). After 48 h of transfection, cells were harvested for western blotting and RT-PCR analyses. For stable transfection, LNCaP cells were first transfected with either p3xFlag-tagged RANKL- or neo-control-plasmid (p3×FLAG- myc-CMV-25) cDNA (Sigma–Aldrich, St. Louis, MO) in a 6-well plate for 48h, and the cells were trypsinized and seeded into a 15 cm dish. The cells containing the transfected vectors were selected in 400 μg/ml of G418 until individual colonies containing the transfected construct were formed. LNCaP cell colonies expressing flag-tagged RANKL or neo plasmid were picked and the cells were amplified from a 48-well plate to a 10 cm dish in the presence of G418. Stable clones were maintained in 200 μg/ml of G418 and routinely checked for flag-RANKL expression by western blot analysis.

ARCaP$_E$-RANKL and ARCaP$_E$-Neo stably transfected cell lines were established by a lentiviral infection protocol. In brief, lentiviral particles containing RANKL-GFP or GFP alone (Neo control) were produced by 293FT cells after transfection with Plvx-RANKL-AcGFP or Plvx-AcGFP-N1 plasmids (Clontech, Mountain View, CA) for 24 to 48 h. The supernatant containing the lentiviral particles was centrifuged at 4000 rpm for 10 min, and the lentiviral particles were aliquotted for storage at -80°C until use. ARCaP$_E$ cells were infected with lentiviruses containing DMEM media in a 1 to 1 ratio in the presence of 8 μg/ml of polybrene (Sigma-Aldrich, Inc., St. Louis, MO) for 48h, and the cells were selected, characterized and maintained in T Medium containing 4 μg/ml of puromycin.

In Vitro Osteoclastogenesis Assay

Osteoclast precursor cells (RAW 264.7 cells) and prostate cancer cells were co-cultured in 48-well plates containing 500 μl of α-MEM media supplemented with 10% FBS, and were set up in

quadruplicates. Osteoclast precursor cells were seeded with prostate cancer cells in an 8:1 ratio (15,000 RAW 264.7 cells and 1,875 prostate cancer cells) per well. Recombinant mouse RANKL (100 ng/ml, provided by Dr. Xu Feng, (McHugh et al., 2000; Zhang, Feng, & McDonald, 2003)) was added to the assay as the positive control. Additionally, recombinant OPG (1 μg/ml) was added to designated wells to block RANKL-mediated increased osteoclastogenesis. The cells were checked under the microscope daily from day 4 to day 7. Cells were fixed and subjected to tartrate-resistant acid phosphatase (TRAP) staining (Sigma-Aldrich, Inc., St. Louis, MO). $TRAP^+$ multinucleated cells (≥3 nuclei) in the entire well were counted as mature osteoclasts and images were taken under light microscopy.

In Vitro Osteogenic Assay

Osteoblast precursor cells (MC3T3-E14 cells) and prostate cancer cells were co-cultured in 24-well plates in 500 μl of osteogenic media containing α-MEM media supplemented with 10% FBS, 10 mM β-glycerophosphate, 50 μg/ml of L-ascorbate, and 10^{-8} M dexamethasome, and were set up in triplicates. Osteoblast precursor cells were seeded with prostate cancer cells in a 10:1 ratio (20,000 MC3T3 cells and 2000 prostate cancer cells) per well. The cells were co-cultured for 14 days with a daily check under the microscope, and the osteogenic media were changed every two days. Cells were washed with PBS, fixed with ice cold 75% ethanol at 4°C for 30 min, and subjected to Alizarin Red-S (40 mM) staining for 10 min at RT. Cells were then washed with water and air dried before being photographed by a scanner. For quantification, Alizarin Red-S dye was eluted with 200 μl of 10% cetylpyridinium chloride (CPC) at RT for 30-45 min with continuous rocking, and the eluted dye was transferred to a 96-well plate and measured at an absorbance of 570 nm using a microplate reader.

In Vitro Migration and Invasion Assays

Migration and invasion by cancer cells were examined in 24-well plates using collagen I and growth factor reduced Matrigel (BD Biosciences, Bedford, MA) coated transwells (8 μm pore size), respectively, as previously described (Nomura et al., 2006; Odero-Marah et al., 2008). Cells were serum-starved in RPMI 1640 or T-medium (Invitrogen, Carlsbad, CA) overnight and dissociated in 10 mM EDTA/HEPES. The lifted cells were washed and counted, and $5x10^4$ cells were seeded in 100 μl of serum-free RPMI 1640 or T-medium in the upper chamber of the transwells in the presence or absence of 1 μg/ml OPG, and 400 μl of RPMI 1640 or T-medium supplemented with 5% FBS was placed in the lower chamber of the transwells. After 24h (migration) and 48h (invasion) of culturing at 37 °C, the migrated and invaded cells were fixed with 10% formaldehyde, stained with 0.5% crystal violet, and the cells at the upper side of the membrane of the chamber were removed and quantified (Gleave, Cancer Res 1991).

In Vitro Proliferation Assay

RANKL- or Neo vector-expressing $ARCaP_E$ and LNCaP cells were seeded into 96-well plate at 5,000 cells per well. For R1881 treatment, LNCaP-RANKL or LNCaP-Neo cells were serum starved in serum-free RPMI1640 overnight and treated in the presence or absence of 10 nM of R1881. Cell proliferation was examined daily by adding 20 μl of CellTiter 96 AQ_{ueous} One Solution Reagent (Promega, Madison, WI) into each well and incubating for 2h. The plate was read at absorbance of 490 nm using a 96-well plate reader. The CellTiter 96 AQ_{ueous} One Solution Cell proliferation Assay is a colorimetric method capable of determining cell proliferation by assessing the total number of viable cells in each well (Berridge & Tan, 1993).

Reverse Transcription (RT)-Polymerase Chain Reaction (PCR)

Total RNA from cells was isolated using RNeasy Mini Kit (Qiagen, Valencia, CA) according to the manufacturer's instructions. Complementary DNA (cDNA) was generated from 3 μg of total RNA using SuperScript® III First-Strand Synthesis System (Invitrogen, Carlsbad CA), and 1 μl of cDNA was subjected to PCR analyses using the following primers : RANKL F, 5'-TGG ATC ACA GCA CAT CAG AGC AG-3'; RANKL R, 5'-TGG GGC TCA ATC TAT ATC TCG AAC-3'; RANK F, 5'-GGG AAA GCA CTC ACA GCT AAT TTG-3'; RANK R, 5'-GCA CTG GCT TAA ACT GTC ATT CTC C-3'; OPG F, 5'-GCT AAC CTC ACC TTC GAG-3'; OPG R, 5'-TGA TTG GAC CTG GTT ACC-3'; E-cadherin F, 5'-GCC AAG CAG CAG TAC ATT CTA CAC G-3'; E-cadherin R, 5'-GCT GTT CTT CAC GTG CTC AAA ATC C-3'; N-cadherin F, 5'-GAT GTT GAG GTA CAG AAT CGT; N-cadherin R, 5'-GGT CGG TCT GGA TGG CGA-3'; Snail F, 5'-CAG ACC CAC TCA GAT GTC AA-3'; Snail R, 5'-CAT AGT TAG TCA CAC CTC GT-3'; Vimentin F, 5'-GGA CTC GGT GGA CTT CTC; Vimentin R, 5'-CGC ATC TCC TCC TCG TAG-3'; c-Met F, TGGGAATCTGCCTGCGAA; c-Met R, CCAGAGGACGACGCCAAA. The PCR reaction cycles involved an initial denaturation at 94°C for 10 min, followed by 36 cycles of 94°C,1 min; 55 °C,30 sec for RANKL and RANK and 48°C, 1 min for OPG; 72°C, 1 min and a final extension at 72°C for 10 min. For E-cadherin and N-cadherin gene amplification, the PCR reactions ran for a total of 32 cycles with annealing temperatures of 55°C and 47°C, respectively for 30 sec. For Snail, Vimentin, and GAPDH amplification, the PCR reactions ran for a total of 28 cycles with annealing temperatures at 48°C for 30 sec. The amplified PCR products were detected and analyzed on 1% agarose gel.

Western Blot Analysis

$ARCaP_E$ and LNCaP cells were cultured in 6-well plates. At 70% confluency, the cells were serum-starved overnight and then treated with 200 ng/ml of trimerized RANKL in serum-free and phenol-red free RPMI-1640 medium for three days before cell harvesting. $ARCaP_E$-RANKL and LNCaP-RANKL cells were cultured in 6-well plates and treated with 20 μM of LY294002, a PI3K inhibitor, 20 μM of SB203580, an inhibitor of MAP kinase reactivating kinase, or 2 μM of PS341 (bortezomib), a proteasome inhibitor, at 90% confluency for four hours. Cells were lysed in RIPA buffer containing 1x protease inhibitor cocktail (Thermo Fisher Scientific, Waltham, MA) and centrifuged, and the supernatants were collected and quantified using the Bradford Protein Assay (Thermo Fisher Scientific, Waltham, MA). Cell lysates (20-30 μg) were resolved on a 4-12% Bis-Tris gradient SDS-PAGE (Invitrogen, Carlsbad, CA) under reducing conditions, followed by transblotting onto nitrocellulose membrane (BioRad, Hercules, CA). The membranes were blocked in 5% non-fat milk in PBST for one hour at room temperature (RT) and incubated with diluted primary antibodies in blocking buffer at 4°C overnight. The primary antibodies used were RANKL, E-cadherin, vimentin, OPG, c-Met (Santa Cruz Biotechnology, Inc., Santa Cruz, CA), p-Met (Tyr-1230/34/35) (Invitrogen, Carlsbad, CA), RANK (Amgen, Thousand Oaks, CA), N-cadherin (BD Transduction Laboratories, San Jose, CA), phospho-Akt (Ser 473), Akt, phospho-p38 (Thr180/Tyr182), p38, phospho-ERK1/2 (Thr202/Tyr204), ERK, phospho-SAPK/JNK (Thr183/Tyr185), JNK, phospho-NF-κB p65 (Ser536), and NF-κB p65 (Cell Signaling Technology, Danvers, MA). Production and usage of androgen receptor antibody (PG21) were previously reported (Prins, Birch, & Greene, 1991). The membranes were washed with PBST three times before incubating with peroxidase-

conjugated anti-mouse or anti-rabbit secondary antibodies at RT for one hour. After three washes, the membranes were visualized using ECL Plus reagent (GE Healthcare, Piscataway, NJ).

The nuclear extracts of LNCaP, RANKL-treated LNCaP, LNCaP-Neo, and LNCaP-RANKL cells were prepared using the NE-PER Nuclear and Cytoplasmic Extraction Kit (Thermo Fisher Scientific, Waltham, MA) and resolved on a 4-12% Bis-Tris gradient SDS-PAGE (Invitrogen, Carlsbad, CA) under reducing conditions, followed by transblotting onto nitrocellulose membrane (BioRad, Hercules, CA). Membranes were probed with cMyc (D84C12XP), phospho-Lamin A/C (Ser 22) (Cell Signaling Technology, Danvers, MA), and Max (sc-197X) antibodies (Santa Cruz Biotechnology, Inc., Santa Cruz, CA).

Soft Agar Colony Formation

Six well plates were first coated with 1 ml of 0.5% Agarose mixed in RPMI1640 supplemented with 10% FBS and placed at room temperature until they solidified. One thousand prostate cancer cells were then mixed in 1 ml of 0.3% agarose in RPMI1640 supplemented with 10% FBS and laid over the pre-coated 0.5% agarose layer, and 1 ml feeding media (RPMI1640 containing 10% FBS) were added into the well after the top agarose layer solidified. Media were changed every three days. Once the colonies were formed, the plates were stained with 0.5% crystal violet for 30 min at room temperature and washed with distilled water until the crystal violet in the agarose became clear and only the colonies were stained blue. The colonies (>100 um) were then counted and images of each well were taken by camera.

In Vivo Experiments

All animal procedures were performed according to an approved protocol from the Institutional Animal Care and Use Committee. LNCaP-RANKL and LNCaP-Neo cells or $ARCaP_E$-RANKL and $ARCaP_E$-Neo cells ($1x10^6$ cells/50µl PBS) were inoculated intracardially into 5- to 7-week-old male athymic nude mice (Charles River, Wilmington, MA), using a 28G1/2 needle (LNCaP-RANKL n=20; LNCaP-Neo n=15) as described previously (Odero-Marah et al., 2008). For the co-inoculation experiment, LNCaP-RANKL and LNCaP-RFP cells were pre-mixed at 1 to 9 or 9 to 1 ratios in a total of a million cells and intracardially inoculated into 5- to 7-week-old male athymic nude mice. A million LNCaP-Neo and LNCaP-RFP cells premixed at a 1 to 1 ratio were also intracardially co-inoculated into the nude mice. A million LNCaP-RANKL cells were also inoculated intratibially in nude mice a week before the intracardial inoculation of a million LNCaP-RFP cells. All mice were constantly monitored for tibial or metastatic tumor formation on a weekly basis. Mice bearing metastatic bone tumors were first observed at 2 months, and mice were sacrificed 3 to 4 months after injection. Before euthanasia, all mice were scanned with X-ray or µCT analysis to examine the skeleton and determine the types of bone lesions. All metastatic tumors to bone or soft tissues were harvested and processed for histomorphological and histochemical analyses. For the co-inoculation experiments, the harvested bone or soft tissue tumors were subjected to fluorescent imaging using the Xenogen imaging system for detecting the red fluorescent signal (excitation: 570; emission: 620).

Immunohistochemical Analysis

All reagents from the DAKO system were used for immunoperoxidase staining of section slides. Paraffin-embedded sections of bone and soft tissue tumors were rehydrated and antigenic epitopes were retrieved in citrate buffer using a pressure cooker. After antigen retrieval, slides were blocked with dual endogenous enzyme block (DEEB) at RT for 10 min and incubated with primary antibodies against Flag (Cell Signaling Technology, Danvers, MA), RANKL IMG-185A (Imgenex, San Diego, CA), RANKL NB100-56512 (Novus, Littleton, CO), RANKL FL-317 (Santa Cruz Biotechnology, Inc., Santa Cruz, CA), RFP (Antibodies-online, Atlanta,GA), E-cadherin, N-cadherin, vimentin, c-Met, neuropilin 1, Mcl-1, p-NF-κB p65 (Ser 536), VEGF (Santa Cruz Biotechnology, Inc., Santa Cruz, CA), and p-c-Met (pYpYpY1230/1234/1235) (Invitrogen, Carlsbad,CA) at 4°C overnight. The slides were placed at RT for 1 h and rinsed in Tris-buffered saline with 0.05% Tween (TBST) and incubated with Envision + Labeled Polymer-HRP at RT for 30 min. The slides were incubated with peroxidase substrate buffer with a chromogen, diaminobenzidine (DAB) to detect the staining signal, followed by hematoxylin counterstaining of nuclei. After dehydration and cover-slipping, the slides were examined by light microscopy. The intensity of IHC staining was scored based on a combined intensity and percentage positive scoring method as previously reported (De Marzo, Knudsen, Chan-Tack, & Epstein, 1999). Strong intensity was scored as 3, intermediate as 2, weak as 1, and negative as 0. Each intensity score was then summed with the score of percentage of cells that were stained, with >50% of the cells as 2, <50% of the cells as 1, and none as 0. One-way ANOVA was used to analyze the population scores between the two stages of cancer progression (Bone vs. benign, well-differentiated, or poorly-differentiated, or well-differentiated vs. benign).

Tartrate-Resistant Acid Phosphatase Staining

The osteoclasts in tissue samples were detected by Tartrate-Resistant Acid Phosphatase (TRAP) staining. The bone tumors were harvested and decalcified in 10% ethylenediamine tetraacetic acid (EDTA)/ PBS for 14 days. The decalcifying solution was changed every other day. The decalcified bone tissues were processed, paraffin embedded, and cut into sections. The bone tissue sections were deparaffinized and stained with a TRAP staining kit purchased from Sigma (St. Louis, MO) according to the manufacturer's instructions, followed by Orange G staining.

Goldner's Trichrome Osteoid Staining

Paraffin-embedded tissue sections were de-paraffinized and rehydrated in a series of alcohol and rinsed in water. The tissue sections were first stained for nuclei in Weigert's iron hematoxylin for 20 min and rinsed in water for 1 min. The slides were then differentiated in acid alcohol (1% hydrochloric acid in 70% alcohol) for less than 5 sec followed by rinsing in water for 10 min. The slides were stained in a sequence of solution A (0.075g Ponceau 2R, 0.025g acid fuchsin, 0.01g azophloxin, and 0.2ml acetic acid in 100 ml distilled water) for 5 min, rinsed with 1% acetic acid, solution B (2g orange G and 4g phosphomolybdic acid in 100 ml water) for 3 min, rinsed with 1% acetic acid, solution C (0.2g light green and 0.2 ml acetic acid in 100 ml water) for 5 min, and rinsed with 1% acetic acid for 5 min. The slides were blot dried, cleared in 100% alcohol and xylene, and mounted (Murphy, Simmons, Kaigler, & Mooney, 2004).

Chromatin Immunoprecipitation (ChIP) Assay

ChIP was performed by a ChIP-IT kit (Active Motif, Inc., Carlsbad, CA). LNCaP and LNCaP-RANKL cells were serum-starved overnight and treated with 200 µg/ml of RANKL, 200 µg/ml of RANKL plus 200 µg/ml of OPG, or 1 µg/ml of OPG for LNCaP-RANKL cells for an

additional 48h. The cells were formaldehyde-fixed and sheared into 200-1500 bp of DNA fragments by enzymatic shearing mixture for 10 min at 37 °C. A portion of the cross-linked protein-DNA complexes was reserved as input DNA, and the rest of the protein-DNA complexes were subjected to immunoprecipitation with anti-cMyc antibody (Cell Signaling Technology, Danvers, MA) and anti-rabbit IgG as a negative control. The precipitated DNA was extracted and purified for both semi-quantitative and quantitative real-time PCR analyses. The PCR primers 5'-CCTGGTCACTCTTCCTCAAC-3' (forward) and 5'-CTCTAGGCAAGATTTGTGAC-3' (reverse) were used to amplify cMyc DNA from the input and anti-cMyc- and anti-rabbit IgG-precipitated DNA. The amplified PCR products were detected and analyzed on a 3% agarose gel. Quantitative real-time PCR was also conducted to further quantify the PCR products from the ChIP analysis. The purified DNA was mixed with SYBR Green PCR Master Mix (Applied Biosystems, Foster City, CA) and the cMyc primer pair and amplified using the ABI 7500 Fast detection system (Applied Biosystems, Foster City, CA). The relative expression of each sample was then normalized with that of input to get the fold change.

Electrophoretic Mobility Shift Assay (EMSA)

Nuclear extracts of LNCaP, RANKL-treated LNCaP, and LNCaP-RANKL cells were prepared using the NE-PER Nuclear and Cytoplasmic Extraction Kit (Thermo Fisher Scientific, Waltham, MA). EMSA was performed using the non-invasive LightShift Chemiluminescent EMSA kit according to the manufacturer's instructions. The double-stranded oligonucleotide of cMyc/Max binding motif (underlined) within the RANKL promoter is 5'-CAATTTAGAACACATGCTTTAATAAC-3', which was used as biotin-labeled and unlabeled probes (and later was used as competitors at 400x) in the binding reactions. For the supershift

assay, 2 µg of cMyc (sc-764X) and Max (sc-197X) antibodies (Santa Cruz Biotechnology, Inc., Santa Cruz, CA) were pre-mixed with the nuclear extracts for 30 min on ice before adding the binding reaction mixture, which further incubated at RT for 20 min. The samples were subjected to electrophoresis on a 5% TBE gel in 0.5x TBE buffer for 1h and transferred onto a nylon membrane in 0.5x TBE buffer for 1h. The nylon membrane was UV cross-liked at 120 mJ/cm^2 for 1 min, blocked, and incubated with streptavidin-HRP solution at RT for 15 min. The membrane was washed for four times for 5 min each before adding the substrate. The membrane was then exposed to X-ray film to detect the biotin-labeled DNA by chemiluminescence.

PCR Array

The PCR arrays, Osteogenesis (PAHS-026) and TNF-α ligands and receptors (PAHS-063) were purchased from SABiosciences (Qiagen, Frederick, MD). The RNA was extracted from LNCaP and LNCaP-RANKL cells and converted to cDNA by reverse transcription PCR using a RT^2 First Strand Kit (C-03) from SABiosciences (Qiagen, Frederick, MD). The mixture of cDNA and SYBR Green Master Mix was added to each well of the array plate containing the primer pairs for different genes. Quantitative real-time PCR was performed using the ABI 7500 Fast detection system (Applied Biosystems, Foster City, CA) at 95°C for 10 min and 40 cycles of 95°C, 15 sec and 60 °C, 1 min, and followed by a dissociate curve. The relative expression was analyzed using the SABiosciences online analyzing tool based on the ΔΔCt method.

Cytokine antibody array

The data for the cytokine antibody arrays (RayBiotech Inc. Norcross, GA) were kindly provided by Dr. Sue-Hwa Lin.

Construction of RANKL Promoter-Luciferase Reporter Plasmid and Deletion Mutants

The 2.5kb human RANKL promoter was constructed by amplifying from the human BAC clone RP11-86N24 using primers 5'-GTGCACAGAATTCTTCAGGGGGCAAGTC-3' (forward) and 5'-GCGAAGCTTCATGGCGCTCGGCCCTCTCG-3' (reverse). The amplified fragment was subsequently subcloned into a firefly luciferase expression vector pGL3-basic (Promega, Madison, WI). The authenticity of the 2.5kb RANKL promoter region was confirmed by DNA sequencing. A series of deletion mutants of the RANKL promoter were generated from the 2.5kb RANKL promoter using QuikChange II XL Site-Directed Mutagenesis Kit following the manufacturer's instructions (Stratagene, Santa Clara, CA).

Transient Transfection and Luciferase Reporter Assay

The RANKL promoter and deletion mutants plus the β-galactosidase plasmid (for transfection efficiency control) were transiently transfected into prostate cancer cells using Lipofectamine 2000 (Invitrogen, Carlsbad, CA) for 48h. In the treatment experiments, after the 48h transfection the cells were serum-starved for 24h before treatment with RANKL, OPG, or RANKL plus OPG for another 48h. For cMyc inhibition, the cells were pre-treated with 20 μM cMyc inhibitor, 10058-F4 for 4h before treatment with RANKL for LNCaP cells. The cells were then harvested and extracted for protein lysate using 1X passive lysis buffer (Promega, Madison, WI). The lysate was centrifuged at 13,200 rpm at 4°C for 10 min, and the supernatant was collected for luciferase assay by mixing 20 μl of protein lysate with 100 μl of substrate (luciferin). The luciferase activity of each sample was measured by a BD Monolight 3010 luminometer (BD-Pharmingen, San Diego, CA). The rest of the protein lysate was used for measuring β-gal activity,

and the relative luciferase activity of each sample was calculated by normalizing to the β-gal activity.

Prostate Cancer Tissue Specimens

Formalin-fixed and paraffin-embedded (FFPE) human prostate cancer specimens were obtained from Department of Pathology of the Cedars-Sinai Medical Center (IRB# Pro 00021228). Additional clinical prostate cancer tissue specimens were obtained from Dr. Fouad Habib at the University of Edinburgh, Scotland, and Dr. Hua Yang at the Jilin University, China. Usage of clinical specimens was approved by the human tissue institutional review committees at the respective institutions.

CRPC Xenografts

To establish working protocols for single and sequential multiple QD labeling, we chose to use a LTL-313 CRPC xenograft model since it mimics castration-resistant prostate cancer and provides consistent and readily available multiple tissue specimens critical for the development and establishment of a new MQDL protocol. FFPE tissues from a castration resistant prostate cancer (CRPC) LTL-313 (Living Tumor Laboratory, www.livingtumorcentre.com) xenograft model were obtained from Vancouver Cancer Center, BC Cancer Agency, Vancouver, Canada. The LTL-313 tumor line was developed from prostate needle biopsy specimen from an 80-year old patient diagnosed with Gleason Score 8 prostate cancer with a serum PSA level of 17 ng/ml at the time of diagnosis (Andersen et al., 2010). The tumor line development protocol was approved by the Clinical Research Ethics Board of the University of British Columbia, in accordance with the Laboratory Animal Guidelines of the Institute of Experimental Animal Sciences (Human specimen use was with approvals from University of British Columbia,

Canada (IRB# UBC BCCA REB #H04-60131). Briefly, to establish castration-resistant prostate cancer, fresh LTL-313 tumor tissues from the 5th generation of grafting were cut into 3 × 3 × 1 mm pieces and re-grafted into the subrenal capsules of male NOD-SCID mice. The animals were maintained for tumor formation for two months before castration to remove androgens. Three weeks after castration, when the tumor volume was significantly reduced, the remaining tumor tissues were harvested and prepared as FFPE tissue blocks. Xenongraft tissues used in this study were derived from 9 tumors from castrated mice and 5 tumors from 5 intact mouse hosts supplemented with testosterone that had undergone sham operation.

Single QD Labeling (SQDL)

The IHC staining protocol was modified for single QD labeling. Streptavidin-conjugated QDs (565-, 585-, 605-, 625-, 655- and 705 nm) were prepared as 10 nM in PBS with 6% IgG-free, protease-free BSA (Jackson Immunoresearch; West Grove, PA). Antigen retrieved tissues or fixed cell samples were incubated in PBS containing 2.5% horse serum (Vector Laboratories) and 20% Streptavidin Block Reagent (Invitrogen) for 20 minutes, followed by treatment with primary Abs as described above in the above immunoreagents section in PBS plus 1% horse serum and 20% Biotin Block Reagent (Invitrogen) at 4^{o}C overnight. After a 3 × 5 min PBST (PBS+ 0.4% Triton X-100) rinse specimens were incubated with the secondary Ab cocktail at room temperature for 30 min and then incubated with the respective streptavidin-QD at 37^{o}C for 60 min. At the end of each incubation, the specimens were subjected to routine 3 x 5 min PBST (PBS+ 0.4% Triton X-100) rinse. After the final rinse, the slides were mounted in aqueous mounting media containing 4'6-diamidino-2-phenylindole (DAPI) (Vector Laboratories) for imaging. The Ab dilutions were described in the IHC section above.

Multiplexed QD Labeling (MQDL)

The single QD labeling protocol was modified for MQDL, in which a single tissue section was subjected to staining for multiple markers in a sequential manner. For each biomarker test, labeling started with a streptavidin blocking, followed by primary Ab reaction and biotinylated secondary Ab incubation, and reaction with streptavidin-conjugated QD at a specified wavelength. Sections were incubated sequentially (with a 3 x 5 min PBST rinse after each incubation). Primary Abs and dilutions in MQDL were identical to those used for SQDL. The immunoreaction sequences were: 1) Anti-Neuropilin-1 Ab, 2 hours, room temperature; biotinylated horse anti-goat IgG, at room temperature, 30 min; streptavidin-QD705, at 37°C, 1 hour. 2) Anti- p-c-Met Ab, at 4°C, overnight; biotinylated horse anti-rabbit IgG, at room temperature, 30 min; streptavidin-QD655 at 37°C, 1 hour. 3) Anti-VEGF Ab, at room temperature, 2 hours; biotinylated horse anti-rabbit IgG, at roomtemperature, 30 min; streptavidin-QD625 at 37°C, 1 hour. 4) Anti- p-p65-NFκB Ab at 4°C, overnight; biotinylated horse anti-rabbit IgG at room temperature, 30 min; streptavidin-QD565 at 37°C, 1 hour. 5) Anti-RANKL Ab at room temperature, 2 hours; biotinylated horse anti-mouse IgG at room temperature, 30 min; streptavidin-QD585 at 37°C, 1 hour. 6) Mounting in aqueous mounting media containing DAPI. Ab concentrations were described in the IHC section. Sections of FFPE LNCaP-RANKL human prostate cancer cells were used as a positive control. For negative control, primary Abs were replaced with isotype- and species-matched control Abs and applied to an immediately adjacent tissue section, and MQDL was performed in parallel with the tissue slide labeled with the testing primary Abs.

Spectral imaging

Image acquisition

A CRi spectral imaging system (Caliper Life Sciences, Hopkinton, MA) with built-in Nuance v3.1 software was used to document multispectral images following the manufacturer's recommended protocol. For each field of cancer tissue, serial images were acquired at a 10 nm wavelength interval from 450 to 800 nm, a range chosen corresponding to the active fluorescent QDs. It generates an unprocessed image "cube" as a stack of 36 separate images with each image containing the complete spectral information for every pixel at that given wavelength. All images were acquired at 400 × magnification, with a 50 milliseconds exposure. To avoid variations in labeling due to cell heterogeneity, five images from different cancerous tissue sites were taken for each tissue specimen for subsequent quantification.

Image deconvolution

Image deconvolution or unmixing protocol was used to extract specific labeling by a specified QD. A spectral library for 565, 585, 605, 625, 655, and 705 nm was built for deconvolution by performimg multiple SQDLs using androgen receptor (AR) antibody without final DAPI counterstaining on serially adjacent tissue sections. The positive labeling of AR was confirmed by parallel IHC staining on adjacent tissues. The spectrum of DAPI was obtained by mounting the adjacent tissue in the aqueous mounting medium containing DAPI. Spectra of tissue autofluorescence were acquired for each tissue from a negative control slide (see MQDL section) prepared by IHC without fluorescent markers. Autofluorescence reduction was performed using Real Component Analysis plug-in software. The spectral library was then used to unmix the cube. The separate spectral contributions to the data 'cube' are outputted as designated colored

intensity maps. These images represent the distribution of each of the QDs and autofluorescence in the tissue. After the deconvolution of the images, the background labeling was filtered and only the true positive signals were shown on the images of the Figures presented.

Signal quantification

The spectral library was used to deconvolute the imaging cube to extract labeling of individual QD using inForm v1.3 software (Caliper) following the recommended strategy. First, a training set comprising two classes of tissue was created: 'cancer' and 'non-cancer'. The software was trained on these areas using the spectra of both the DAPI counterstain and the multiplexed QD immunolabeling and tested on 50 randomly selected cells from each image to determine the accuracy of differentiating the two classes. This process was repeated until further iterations no longer improved the accuracy. Histological H/E images were then used to localize cancer cells based on nuclear DAPI labeling. A built-in algorithm was then used to define the cytoplasmic vs. nuclear subcellular regions. Based on an analysis of images at 400 × magnification, the optimal threshold settings approximated: fixed scale 200, minimum blob size 20, maximum blob size 10,000, circularity threshold 0, edge sharpness 0, fill hole enabled (nuclear parameters); inner distance to nucleus 1, outer distance to nucleus 7, minimum cytoplasm sample size 1, minimum signal range 0, maximum signal range 65535 (cytoplasmic parameters). To eliminate non-specific signals at the specified spectrum, an acellular area within the field being analyzed was used as background labeling. QD fluorescence intensity in each cell was exported to an Excel spreadsheet (Microsoft, Seattle, WA) and subjected to statistical analysis (Ghazani et al., 2006; Liu et al., 2010).

Statistical Analysis

Student's t-test was used for statistical analysis between most of the experimental groups and control groups. Significance (*P* value) between the experimental and the control smaple smaller than 0.05 is annotated as * ,and if *P* value smaller than 0.005 is annotated as **.

One-way ANOVA was used to analyze the population scores between the two stages of cancer progression (Bone vs. benign, well-differentiated, or poorly-differentiated, or well-differentiated vs. benign) for RANKL IHC scoring (*** = $P<0.001$; ** = $P<0.05$ over the benign tumors).

CHAPTER 3 AUTOCRINE AND PARACRINE CELL SIGNALING MEDIATED BY RANKL-RANK INTERACTION PROMOTES EPITHELIAL TO MESENCHYMAL TRANSITION AND PROGRESSION OF HUMAN PROSTATE CANCER CELLS

Introduction

Epithelial to mesenchymal transition (EMT), an essential process during embryonic development, is an event where epithelial cells lose their polarity and cell-cell contacts and undergo extensive cytoskeleton remodeling at the migration and invasion front (Kang & Massague, 2004). EMT is also known to play an important role in tumor progression and metastasis (Boyer et al., 2000; Hotz et al., 2007). Cells undergoing EMT are characterized by loss of intercellular contacts and gain of mesenchymal phenotype with enhanced motility and invasiveness, and such morphological and behavioral switches allow the transition of cancer cells from an indolent state to a malignant state, leading to tumor invasion, dissemination, and metastasis. This morphological transition is accompanied by the loss of the epithelial-specific marker E-cadherin, which is the first and most critical event during EMT, followed by up-regulation of mesenchymal-associated genes such as N-cadherin, vimentin, or fibronectin. Such changes in gene expression with decreased E-cadherin and increased N-cadherin or vimentin expression during EMT are consistently observed in various cancers with enhanced tumor growth and invasiveness leading to tumor progression and metastasis (Huber et al., 2005; Thiery, 2002).

The process of EMT can be triggered by many growth factors, such as TGF-β, EGF, IGF, and FGF, leading to the activation of multiple interrelated signaling pathways and various signaling molecules, including tyrosine kinsases (RTK), Ras/MAPK, Src, PI3K/AKT, Wnt/β-catenin, and NF-κB-, Notch-, and Hedgehog-dependent signaling (Boyer et al., 2000; Guarino et al., 2007;

Huber et al., 2005; Thiery & Sleeman, 2006). Most of these pathways converge on the repression of E-cadherin expression and the activation of mesenchymal gene expression through the modulation of many transcription factors, contributing to the molecular mechanisms of EMT. The loss of E-cadherin function during tumor progression can be genetically or epigenetically regulated. In most cases, E-cadherin expression is down-regulated at the transcriptional level by zinc-finger transcription factors Snail or Slug (Bolos et al., 2003; Nieto, 2002) and a basic helix-loop-helix transcription factor Twist (Yang et al., 2004), which are both strong repressors of E-cadherin transcription and potent inducers of EMT. Snail and Twist negatively regulate E-cadherin transcription by binding to E-box motifs in E-cadherin promoter (Nieto, 2002; Yang et al., 2004), and they are capable of increasing N-cadherin expression in human prostate and gastric cancer (Alexander et al., 2006; Hotz et al., 2007; Rosivatz et al., 2002). Moreover, their expression has been reported to be correlated with prostate and breast cancer progression and metastasis (Karreth & Tuveson, 2004; Kwok et al., 2005).

Prostate cancer is the most commonly diagnosed cancer and the leading cause of death among men in the United States. Advanced and metastatic prostate cancer frequently causes bone metastases (Y. Li et al., 2006), and about 80% of prostate cancer patients (Landis, Murray, Bolden, & Wingo, 1999) will have bone metastasis, which is usually incurable. The bone microenvironment particularly serves as a growth-factor and extracellular-matrix-rich site for prostate cancer cells to colonize. Two major cell types in bone, the bone-resorbing osteoclasts and the bone-forming osteoblasts, are known to interact with prostate cancer cells contributing to the subsequent mixed osteosclerotic and osteolytic lesions found in clinical human prostate cancer bone metastatic specimens (Boyce & Xing, 2007; Roato et al., 2008; Roodman, 2004; Rosivatz et al., 2002).

RANKL, a receptor activator of NF-κB ligand, is a member of the tumor necrosis factor (TNF) superfamily and a master regulator of bone remodeling. RANKL exits in both a membrane-bound and a secreted form. The latter is a result of proteolytic cleavage by MMPs or alternative splicing (Ikeda et al., 2001; Lynch et al., 2005). RANKL is primarily expressed on the surface of osteoblasts and marrow stromal cells and is released by activated T cells (Roodman, 2004). RANKL exerts its action by binding to its receptor RANK on osteoclasts in a paracrine manner to promote osteoclast maturation and hence osteoclast-induced bone resorption (Kong et al., 1999; Yasuda et al., 1998). Osteoblasts also express and secrete OPG, which is a decoy receptor of RANKL, to regulate or fine-tune the RANKL activity. RANKL has recently been shown by our laboratory (Odero-Marah et al., 2008; Zhau et al., 2008) and others (Boyce & Xing, 2007; Chen et al., 2006; Huang et al., 2002; Jones et al., 2006) to be expressed in malignant prostate cancer cells, which also express its receptor, RANK. Our previous data also showed that RANKL was up-regulated along with other mesenchymal markers in Snail- or EGF plus TGF-β-induced EMT of prostate cancer cells, therefore indicating RANKL as a novel EMT marker during prostate cancer progression (Odero-Marah et al., 2008; Zhau et al., 2008).

In this study, we further examined whether RANKL could be a mediator of EMT in human prostate cancer cells. Using the $ARCaP_E$/$ARCaP_M$ prostate cancer progression model and non-metastatic LNCaP cells, we demonstrated that RANKL was capable of inducing EMT progression, migration, and invasion of prostate cancer cells. Moreover, RANKL stimulated its own expression in an autocrine fashion in prostate cancer cells, and the increased RANKL expression by prostate cancer cells could further activate osteoclast precursors in a paracrine fashion to induce osteoclastogenesis and subsequently increase bone resorption, leading to osteolytic lesions. Together, RANKL promoted survival, EMT progression, and bone metastasis

in human prostate cancer cells. Therefore, it is essential to understand the cellular mechanisms and the downstream targets by which RANKL promotes prostate cancer survival, EMT progression, and bone metastasis, which can be exploited for the future development of potential therapeutic treatments for the prevention of prostate cancer-induced bone metastasis.

Results

RANKL Expression Is Correlated with Human Prostate Cancer Progression

We previously identified RANKL as a novel marker for prostate cancer EMT progression (Odero-Marah et al., 2008). To further confirm the significance of RANKL in human prostate tumor progression, we examined RANKL expression in clinical prostate cancer tissue specimens of differing Gleason grade and tumor stage using an established IHC protocol. We took special steps including the use of multiple anti-RANKL antibodies from commercial sources, immunoadsorption of these antibodies by recombinant RANKL protein, and validation of RANKL expression in experimental human prostate cancer cells and xenograft tissues by RT-PCR and western blots. Using the well-characterized anti-RANKL monoclonal antibody, we assessed RANKL expression on one commercial TMA of benign and prostate cancer specimens and two custom-made TMAs containing well- and poorly-differentiated and bone metastatic prostate cancer specimens. We observed low levels of staining for RANKL in benign prostate tumor (N=20) but positive staining in both the nucleus and cytoplasm in well- and poorly-differentiated human prostate cancer specimens (Fig.1A, well differentiated N=18; poorly differentiated N=39). Significantly stronger immunostaining for RANKL was observed in the bone metastases (Fig.1A N=43). Statistical analysis (one-way ANOVA) further confirmed the significantly higher expression of RANKL in the bone metastatic specimens over benign, well-differentiated ($P<0.001$), and poorly-differentiated prostate cancers ($P=0.035$) (Fig. 1B). RANKL expression in primary tumor was also higher compared to benign tumor ($P=0.023$). These immunohistochemical results support a positive correlation between the level of RANKL expression and the progression of clinical prostate cancer specimens with increased RANKL expression from benign to locally invasive status, and to skeletal metastases.

We next examined RANKL, RANK, and OPG expression at both the mRNA and protein levels in several pairs of isogenic human prostate cancer cell lines with differential propensity for bone and soft tissue metastases. Two osteosarcoma cell lines, MG-63 and SaOS-2, served as positive controls. Differential expression at mRNA and protein levels of RANKL, RANK, and OPG was observed in each pair of these isogenic cell lines (Fig. 1B and 1C). Positive correlations of RANKL expression and the aggressiveness of human prostate cancer cell lines were observed with higher expression in $ARCaP_M$, C4-2/C4-2B, and PC-3M cells than the corresponding parental, $ARCaP_E$, LNCaP, and PC-3 cells. Higher levels of RANKL expression were found in more aggressive osteosarcoma MG-63 than in indolent SaOS-2 cells. The RANKL receptor, RANK, was expressed by all of the prostate cancer cell lines, and strong expression was observed in $ARCaP_M$ and PC3M cells. RANK mRNA expression is not always correlated with RANK protein expression in LNCaP cells. While an inverse relationship of protein expression was observed between RANKL and OPG, there was no correlation between RANKL and OPG mRNAs. In the ARCaP EMT prostate cancer progression cell model (Xu et al., 2006), we demonstrated consistently that the more invasive and metastatic $ARCaP_M$ cells had stronger expression of the RANKL/RANK/OPG triad than the less invasive $ARCaP_E$ cells. Among these isogenic prostate cancer cell line pairs, $ARCaP_E$ and LNCaP cells showed the lowest expression level of RANKL, RANK, and OPG. Collectively, these results indicated that RANKL, RANK, and OPG were expressed by most of the human prostate cancer cell lines we examined, and their levels of expression generally correlated with the virulence of these cells.

A.

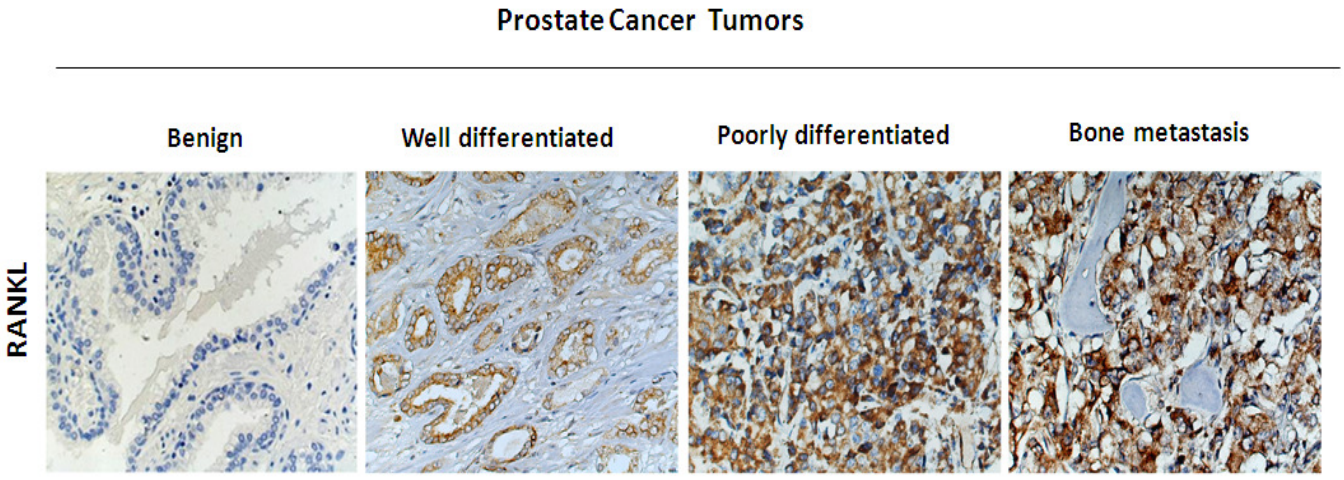
Prostate Cancer Tumors
Benign
Well differentiated
Poorly differentiated
Bone metastasis
RANKL

B.

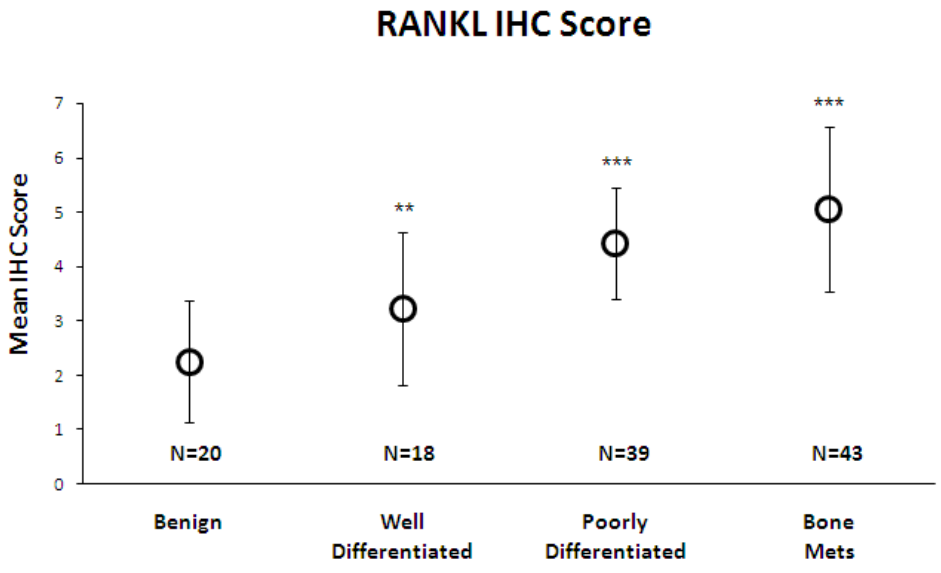
RANKL IHC Score
Mean IHC Score
0
1
2
3
4
5
6
7
**
***
***
N=20
N=18
N=39
N=43
Benign
Well Differentiated
Poorly Differentiated
Bone Mets

C.

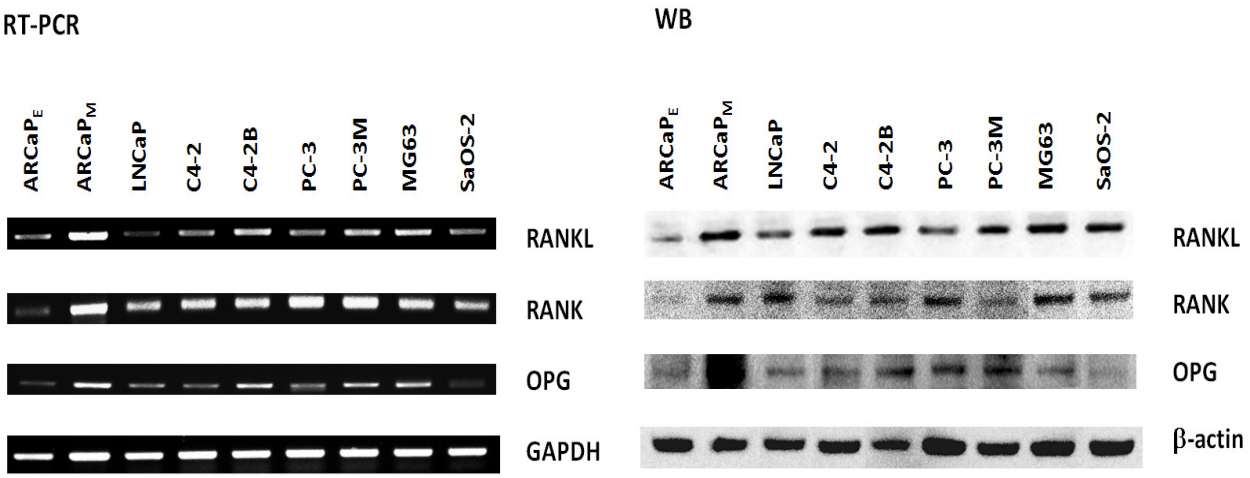

Figure 1. RANKL expression is expressed in clinical prostate cancer and cancer bone metastasis. RANKL, RANK, and OPG are differentially expressed in human prostate cancer cell lines. **A,** RANKL expression was examined in clinical human prostate cancer specimens by immunohistochemical (IHC) staining. RANKL expression is negative or low in benign tumors but positively stained in well- and poorly- differentiated primary human prostate tumors and in prostate tumors metastasized to the skeleton. RANKL expression may be correlated with human prostate cancer progression and bone metastasis. **B,** Relative score of RANKL IHC staining in benign (N=20), well-differentiated (N=18), poorly-differentiated (N=39), and bone metastatic prostate tumors (N=43). (*** = P<0.001; ** = P<0.05 over the benign tumors). **C,** RANKL/RANK/OPG expression was examined in different human prostate cancer (ARCaP$_E$, ARCaP$_M$, LNCaP, C4-2, C4-2B, PC-3, PC-3M) and human osteoblastic tumor cell lines (MG-63 and SaoS-2). The expression was shown by both RT-PCR (left panel) and western blot (WB, right panel).

RANKL Induces EMT Progression of Prostate Cancer

Given our early observation that RANKL expression increased corresponding to EMT induced in $ARCaP_E$ cells upon addition of soluble growth factors (Odero-Marah et al., 2008; Zhau et al., 2008), we examined if exogenously added recombinant RANKL, or forced RANKL expression genetically in prostate cancer cells, may contribute directly to their mesenchymal transition. We used two cell models for this study, the ARCaP EMT cell model (Xu et al., 2006) and the LNCaP cell model (Thalmann et al., 2000). Our previous investigations revealed that ARCaP cells when provoked to assume EMT by soluble growth factors underwent morphologic, biochemical and behavioral changes, whereas the LNCaP cell model when provoked to undergo EMT by soluble growth factors only exhibited biochemical and behavioral but not morphologic transition (Josson et al., 2011). $ARCaP_E$ cells exposed to 200 ng/ml recombinant RANKL protein gradually changed their morphology from cobble-stoned clusters to more dispersed and fibroblastic-like appearance over the 8-day period (Fig. 2A). RANKL treatment down-regulated E-cadherin but up-regulated N-cadherin expression, reflecting a 'cadherin switch' with a replacement of E-cadherin by N-cadherin during EMT (Fig. 2B-1) (Maeda, Johnson, & Wheelock, 2005; Voulgari & Pintzas, 2009). RANKL also induced up-regulation of Snail, vimentin, and RANKL expression, consistent with the previous observation that these markers are associated with EMT (Zhau et al., 2008). The ability of recombinant RANKL to induce its own expression is restricted to such cancers as prostate (ARCaP and LNCaP) and osteosarcoma (MG-63 and Saos-2) cells but not normal prostate (PrEC and RWPE-1) or bone (RAW264.7) cells (data not shown). OPG, a decoy receptor of RANKL, was found to antagonize RANKL-RANK interaction and block RANKL-induced EMT and cadherin switch in $ARCaP_E$ cells (Fig. 2B-2). Further, Figure 2B-3 shows that by exposing $ARCaP_M$ to OPG, EMT was reversed, both

morphologically (reversal to epithelial morphology) and biochemically (expression of mesenchymal cell associated genes and reversal of cadherin switch). These results were confirmed by a genetic approach where depleting endogenous RANKL by RANKL siRNA induced mesenchymal to epithelial transition (MET) (Fig. 2B-4). The functional role of exogenously added RANKL in the induction of EMT was also confirmed in the LNCaP cell model (Fig. 2B-5).

The functional role of RANKL in provoking EMT in the ARCaP cell model is also supported by the *in vitro* migration and invasion behaviors of ARCaP and LNCaP cells. Recombinant RANKL treatment increased the migration and invasion of $ARCaP_E$ and LNCaP cells, and these changes were abrogated by the presence of OPG (Fig. 2C). Likewise, $ARCaP_M$ and LNCaP-RANKL cells expressed higher intrinsic levels of RANKL and also gained increased migratory and invasive phenotypes, which were antagonized by OPG treatment. These results are consistent with the presence of an autocrine loop involving RANKL-RANK that is capable of driving the morphologic, biochemical and/or behavioral transition of ARCaP and LNCaP cells from their lesser invasive epithelial phenotype to a more aggressive mesenchymal phenotype.

A.

RANKL Treatment of $ARCaP_E$

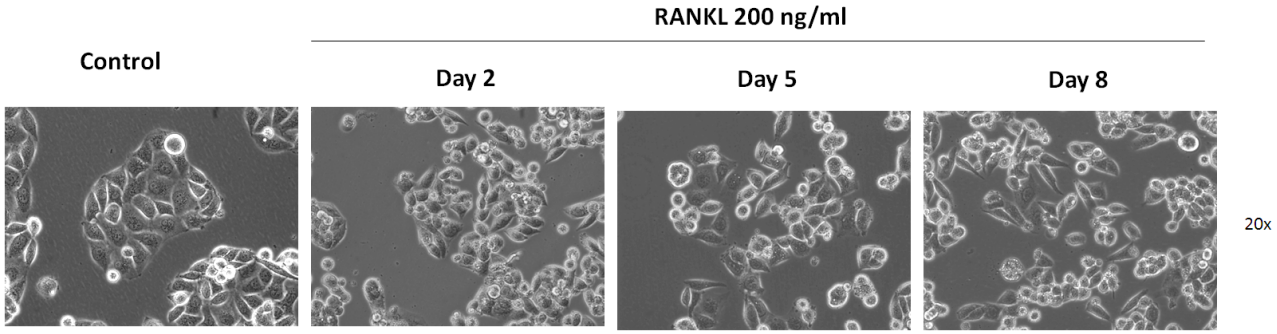

B.

$ARCaP_E$ and $ARCaP_M$

(1) RANKL Treatment of $ARCaP_E$

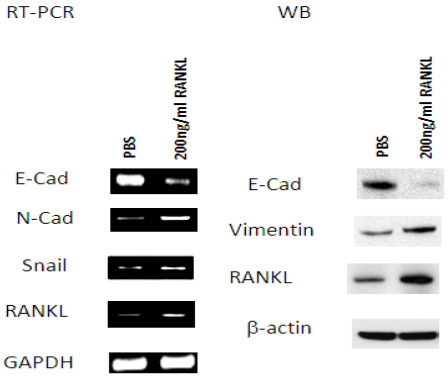

(2) RANKL Plus OPG Treatment of $ARCaP_E$

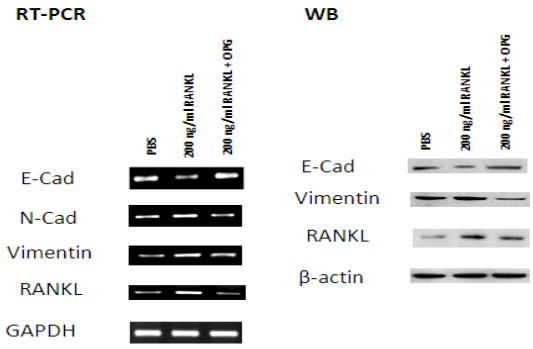

(3) OPG Treatment of $ARCaP_M$

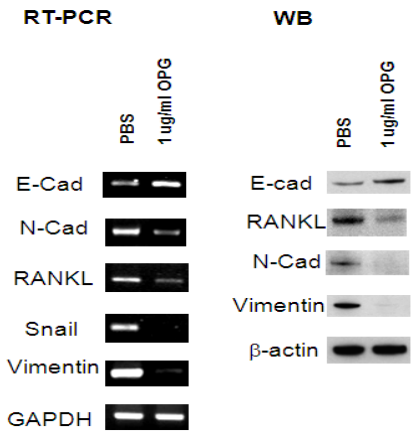

(4) Transient RANKL Knockdown in $ARCaP_M$

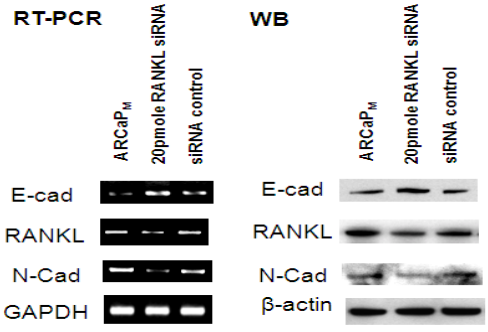

LNCaP

(5) RANKL Treatment of LNCaP Cells

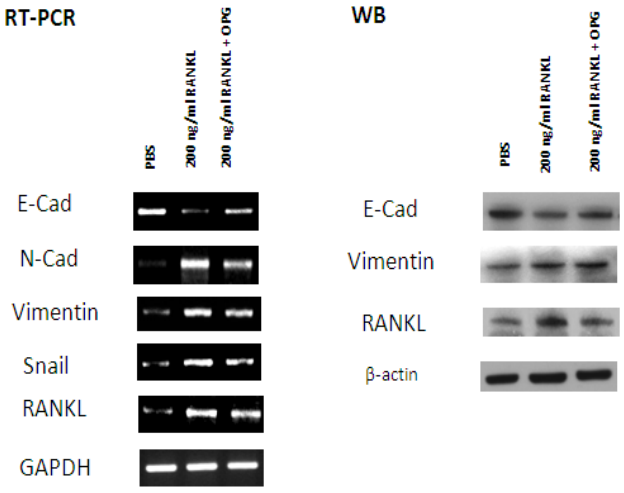

C.

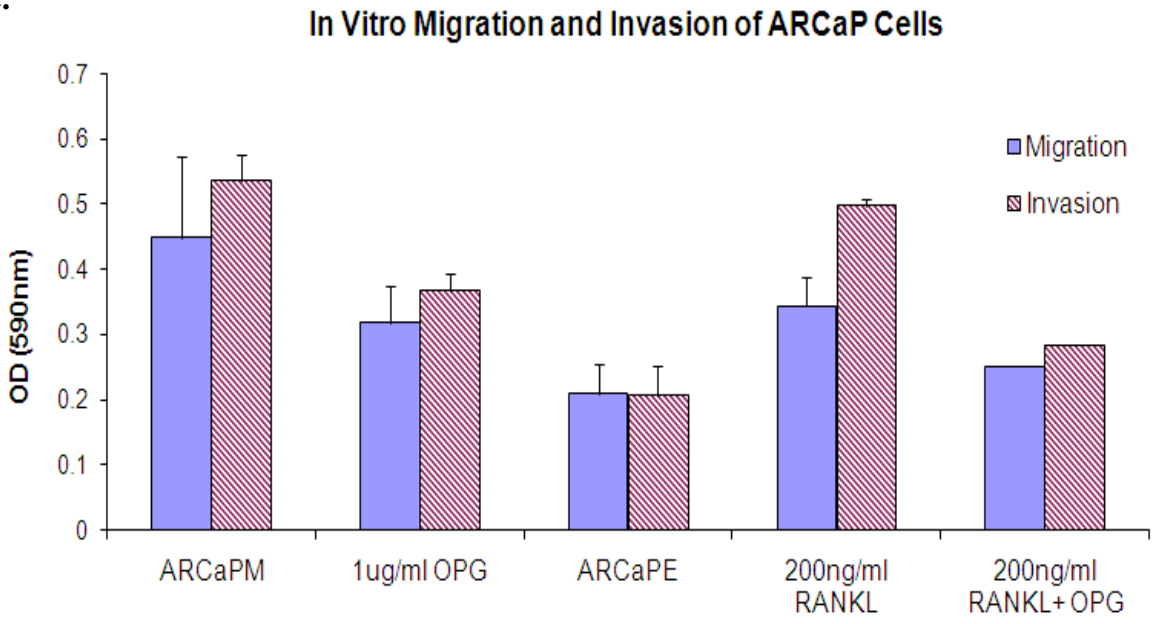

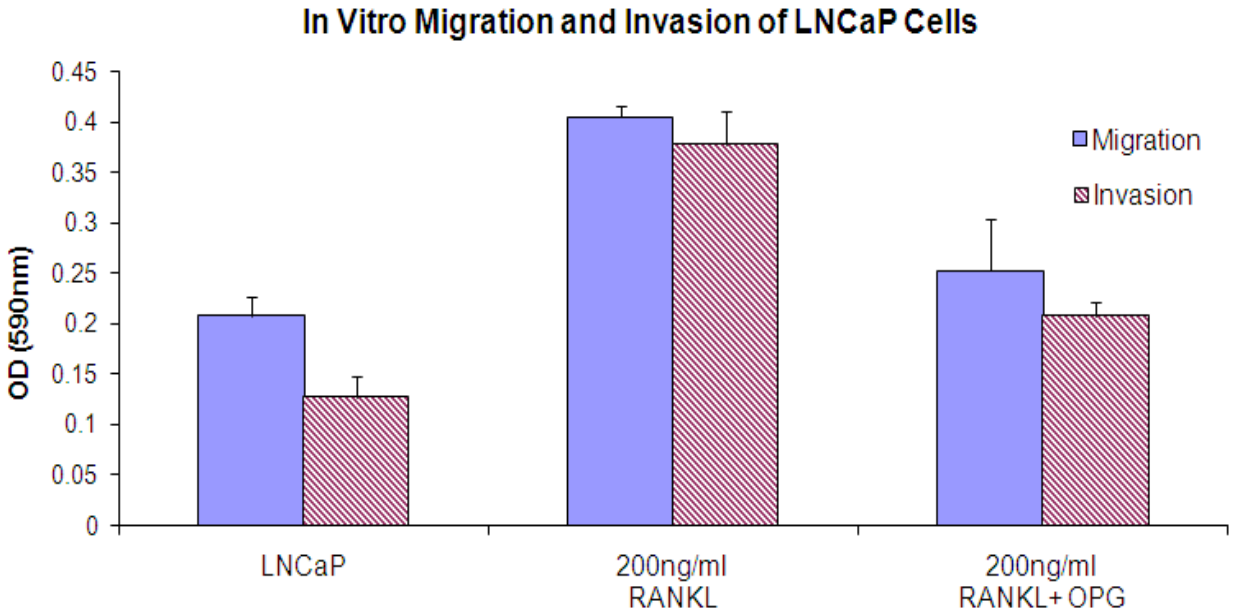

Figure 2. RANKL treatment induces morphological and biochemical changes wherein prostate cancer cells undergo EMT progression, leading to increased *in vitro* migration and invasion in ARCaPM cells. Addition of OPG can prevent the RANKL-induced EMT transformation of prostate cancer cells. **A,** $ARCaP_E$ cells were serum-starved overnight and treated with 200 ng/ml of trimerized recombinant RANKL protein (rRANKL) for 8 days. Cell morphological changes were observed at day 2, 5, and 8. Images were taken with light microscopy (20x magnification). **B1, B2, and B5,** Prostate cancer progression model; ARCaP and LNCaP cells were treated with 200 ng/ml of rRANKL proteins alone or in the presence of OPG, a decoy RANK receptor, and biochemical changes of EMT-specific markers were examined by RT-PCR and Western blot analyses. RANKL decreased the epithelial marker E-cadherin and increased the mesenchymal markers vimentin, N-cadherin, and Snail. RANKL also increased its own expression. Addition of OPG abolished RANKL-induced biochemical EMT changes. **B3** and **B4,** mesenchymal $ARCaP_M$ cells when treated with 1 µg/ml of OPG or transiently knocked down RANKL showed increased expression of epithelial marker but decreased expression of mesenchymal markers, indicating a reversal of EMT phenotype. **C,** RANKL protein treatment enhanced the migration and invasion of $ARCaP_E$ and LNCaP cells, which could be diminished in the presence of OPG. Consistently with these findings, $ARCaP_M$ cells when treated with 1 µg/ml of OPG, showed decreased migration and invasion potential.

Ectopic RANKL Expression Promotes EMT in Human Prostate Cancer Cells

To establish a genetic basis defining the autocrine roles of RANKL in the promotion of EMT and prostate cancer progression, ectopically RANKL, tagged with either GFP or Flag, was enforced respectively in $ARCaP_E$ and LNCaP human prostate cancer cell lines. Clones stably expressing RANKL were isolated, characterized and *in vivo* tumorigenic and metastatic potential determined. Western blot analysis demonstrated the expression of RANKL with slightly shifted molecular weight corresponding to the sizes of GFP or Flag tag (Fig. 3A). $ARCaP_E$-RANKL showed morphologic transition to a mesenchymal phenotype, from a cobblestone to a more dispersed spindle-shaped appearance, when compared to the neo transfected controls (Fig. 3B). A lesser morphologic change was seen in LNCaP-RANKL cells, from their original spindle- and neuron-like morphology to a more round and oval shape morphology, when compared to neo-transfected LNCaP cells. These morphologic features induced by increased RANKL expression were also reflected in their biochemical properties, i.e. a switch of E-cadherin to N-cadherin, vimentin, Snail, and RANKL expression. Moreover, RANKL overexpression in both $ARCaP_E$ and LNCaP cells also stimulated endogenous RANKL expression at both transcript and protein levels (Fig. 3A), supporting earlier results where adding exogenous recombinant RANKL to these human prostate cancer cells induced RANKL expression (see Fig. 2B). The functional roles of RANKL in $ARCaP_E$ and LNCaP cells were determined *in vitro*. Enforced RANKL exerted no growth effects on either $ARCaP_E$ or LNCaP cells (Fig. 3D). $ARCaP_E$-RANKL and LNCaP-RANKL transfectants, however, displayed enhanced migration and invasion compared to the Neo control cells (Fig. 3E). The increase in cell migration and invasion were suppressed by OPG, suggesting increased autocrine RANKL-RANK interaction upon enforced RANKL expression. Moreover, $ARCaP_E$-RANKL and LNCaP-RANKL also promoted *in vitro* soft agar

colony formations, implying an enhanced tumorigenic potential of these cells conferred by RANKL expression. The enhanced tumorigenicity of $ARCaP_E$-RANKL and LNCaP-RANKL cells can be attenuated upon the addition of OPG, lowering the number of colony formations in soft agar (Fig. 3F).

A.

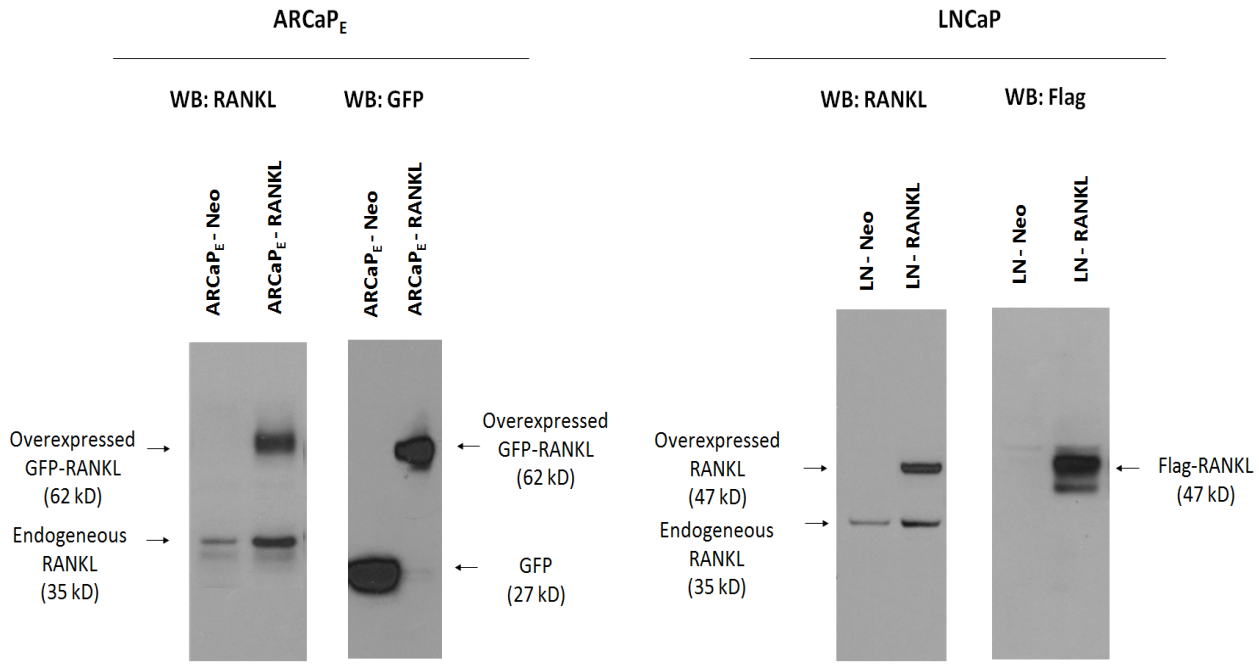

B.

RANKL Stable Transfection

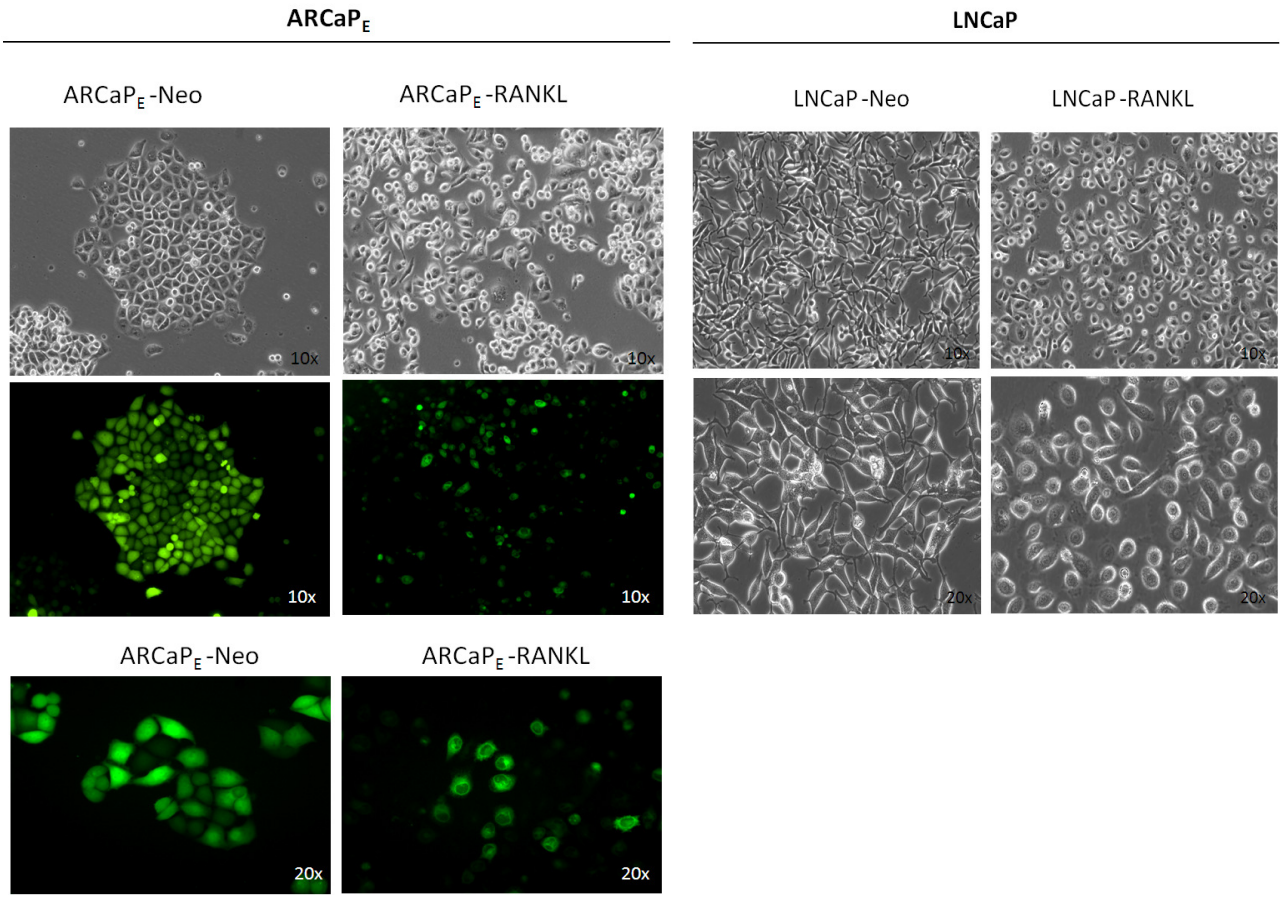

C.

RANKL Overexpression in ARCaP$_E$ Cells

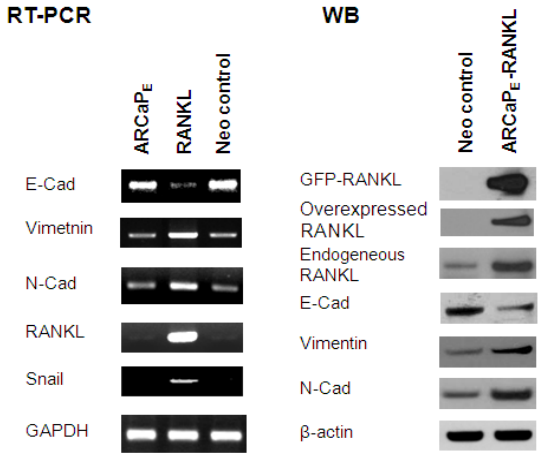

RANKL Overexpressing LNCaP Cells

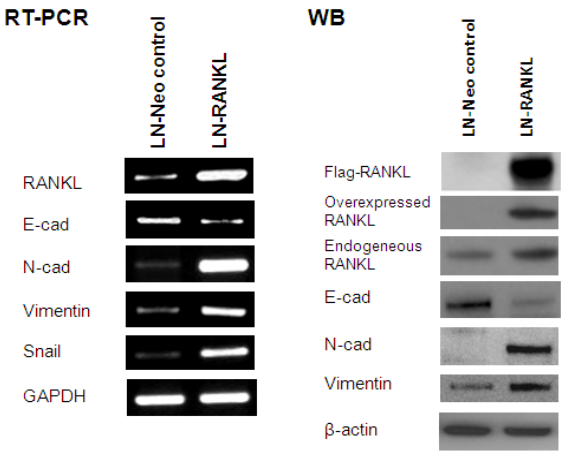

D.

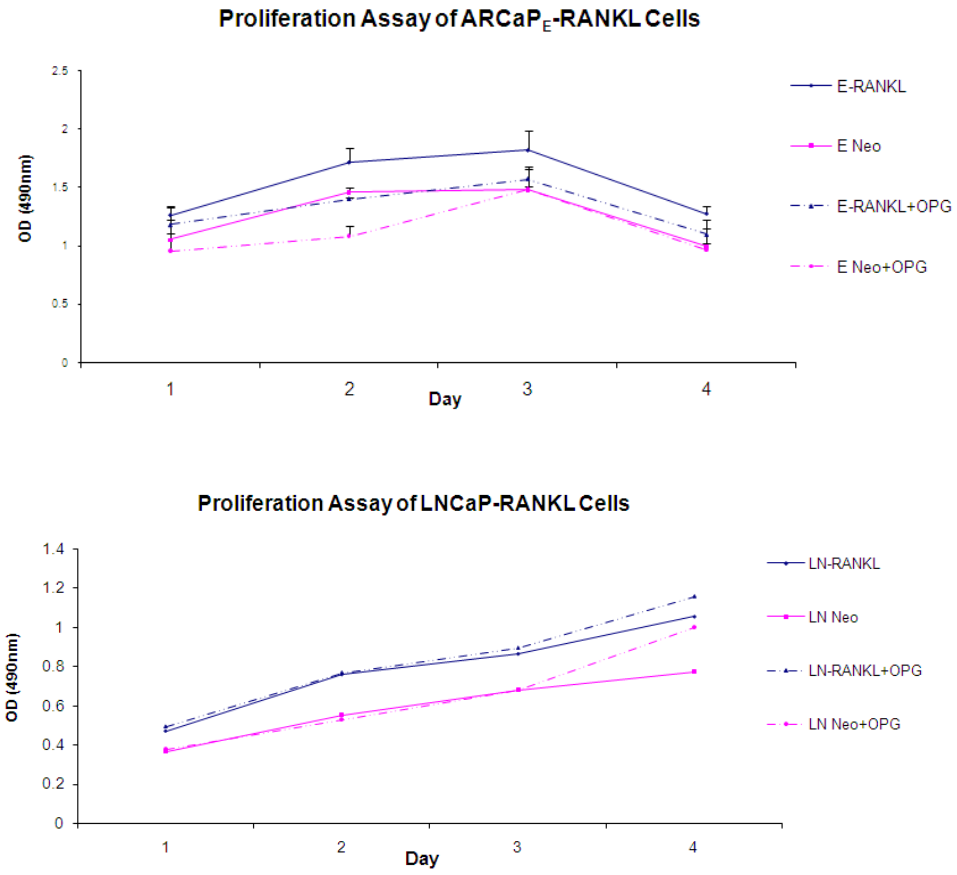
Proliferation Assay of ARCaP$_E$-RANKL Cells
OD (490nm)
Day
E-RANKL
E Neo
E-RANKL+OPG
E Neo+OPG
Proliferation Assay of LNCaP-RANKL Cells
OD (490nm)
Day
LN-RANKL
LN Neo
LN-RANKL+OPG
LN Neo+OPG

E.

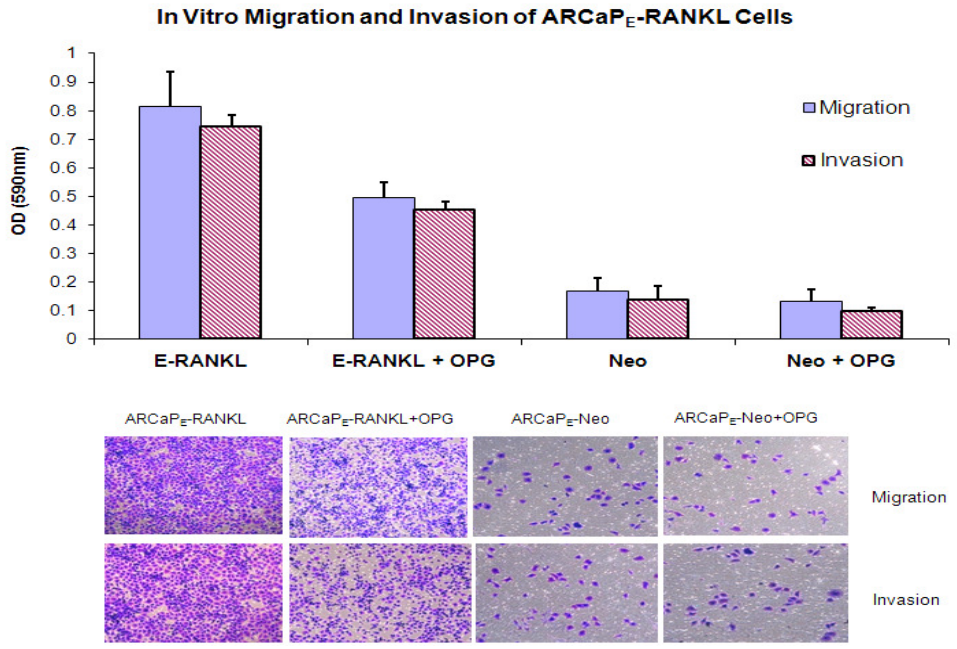
In Vitro Migration and Invasion of ARCaP$_E$-RANKL Cells
OD (590nm)
Migration
Invasion
E-RANKL
E-RANKL + OPG
Neo
Neo + OPG
ARCaP$_E$-RANKL
ARCaP$_E$-RANKL+OPG
ARCaP$_E$-Neo
ARCaP$_E$-Neo+OPG
Migration
Invasion

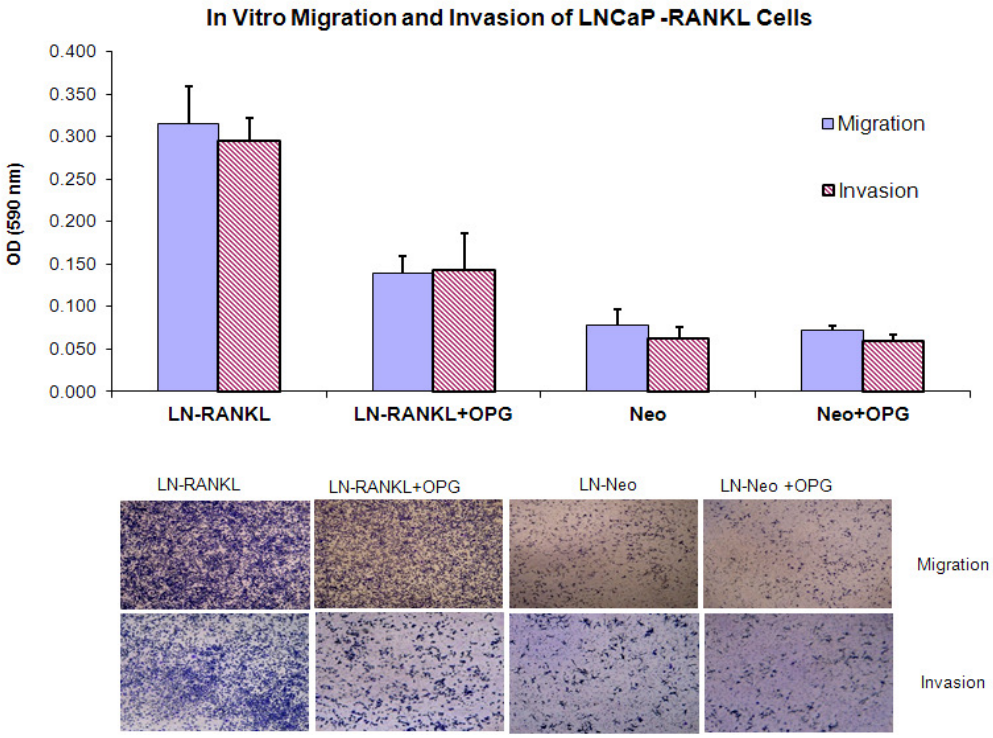
In Vitro Migration and Invasion of LNCaP -RANKL Cells
OD (590 nm)
0.400
0.350
0.300
0.250
0.200
0.150
0.100
0.050
0.000
Migration
Invasion
LN-RANKL
LN-RANKL+OPG
Neo
Neo+OPG
LN-RANKL
LN-RANKL+OPG
LN-Neo
LN-Neo +OPG
Migration
Invasion

F.

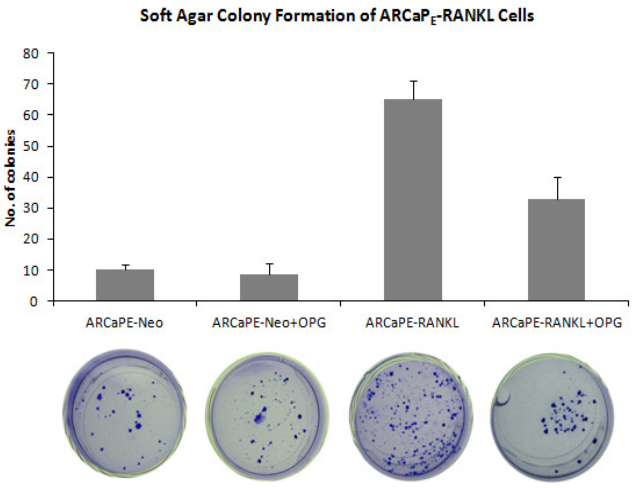
Soft Agar Colony Formation of ARCaP$_E$-RANKL Cells
No. of colonies
80
70
60
50
40
30
20
10
0
ARCaPE-Neo
ARCaPE-Neo+OPG
ARCaPE-RANKL
ARCaPE-RANKL+OPG

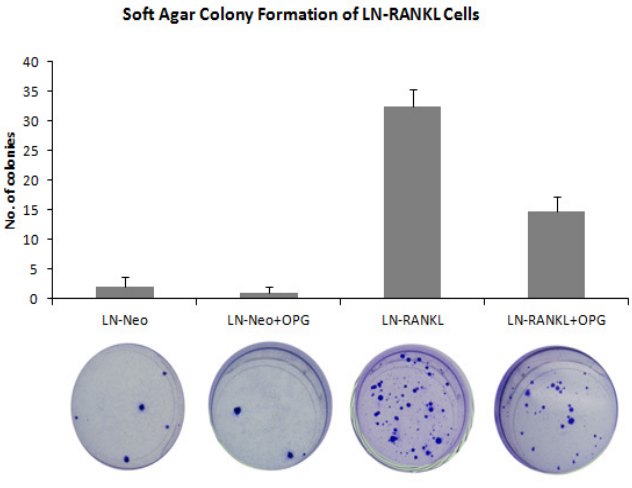
Soft Agar Colony Formation of LN-RANKL Cells
No. of colonies
40
35
30
25
20
15
10
5
0
LN-Neo
LN-Neo+OPG
LN-RANKL
LN-RANKL+OPG

Figure 3. RANKL overexpression also promoted EMT progression of prostate cancer cells and increased their migration and invasion potential. **A,** Characterization of RANKL overexpression in $ARCaP_E$ and LNCaP cells by Western blot analysis. RANKL expression constructs were tagged with GFP or Flag proteins, and RANKL overexpression was detected by RANKL, GFP, or Flag antibodies. **B,** RANKL overexpression changed the morphology of $ARCaP_E$ and LNCaP cells detected under light microscopy (10x and 20x magnification). Since the RANKL expression construct introduced into the $ARCaP_E$ cells had a GFP tag, RANKL overexpression was also detected using fluorescent microscopy. RANKL was shown to be expressed on the membrane, cytosol and nuclei of the genetically tagged cells (10x and 20x magnification). Progressive morphological changes in LNCaP cells were induced by RANKL expression, but LNCaP-Neo cells demonstrated no morphological change. **C,** RANKL overexpression also induced EMT changes at the molecular level. **D,** Stable clones overexpressing RANKL or Neo constructs were established in both $ARCaP_E$ and LNCaP cells, and their proliferation rates were examined by MTS assay. RANKL was found not to affect the basal cell proliferation rate of $ARCaP_E$ and LNCaP cells. **E,** RANKL overexpression, however, increased cell migration and invasion of $ARCaP_E$ and LNCaP cells, which were antagonized upon addition of OPG. **F.** RANKL increased the tumorigenic potential of both LNCaP and ARCaP cells by inducing increased anchorage-independent colony formation compared to LNCaP-Neo and $ARCaP_E$-Neo cells, and such induction could be attenuated upon addition of OPG.

RANKL Expression in ARCaP$_E$ and LNCaP Cells Induces I*n Vitro* Osteoclastogenesis

To determine if the enforced RANKL is biologically functional, we compared the ability of both the Neo controls and RANKL-expressed ARCaP$_E$ and LNCaP cells to induce osteoclast maturation in an *in vitro* osteoclastogenesis assay to quantify the numbers of matured osteoclasts (Lacey et al., 1998; Yasuda et al., 1998). Mouse macrophage RAW264.7 cells, known to be osteoclast precursors, were co-cultured with ARCaP$_E$-RANKL or LNCaP-RANKL cells; stably Neo-expressed ARCaP$_E$ and LNCaP cells served as controls. Ectopically expressed RANKL in ARCaP$_E$ and LNCaP cells induced significantly increased numbers of large and matured osteoclasts (no. of nuclei >3), which were equivalent to that induced by 100 ng/ml of trimerized RANKL protein; ectopically Neo-expressed ARCaP$_E$ and LNCaP cells induced only a few mature osteoclasts (Fig. 4). Addition of OPG decreased by approximately two-fold the formation of mature osteoclasts induced by ARCaP$_E$-RANKL and LNCaP-RANKL cells, but had very minimal blocking effects against osteoclastogenesis induced by Neo-transfected control cells. These results further confirmed that RANKL produced by ARCaP$_E$-RANKL or LNCaP-RANKL cells is biologically functional and capable of mounting an enhanced osteoclastogenesis reaction *in vitro*.

A.

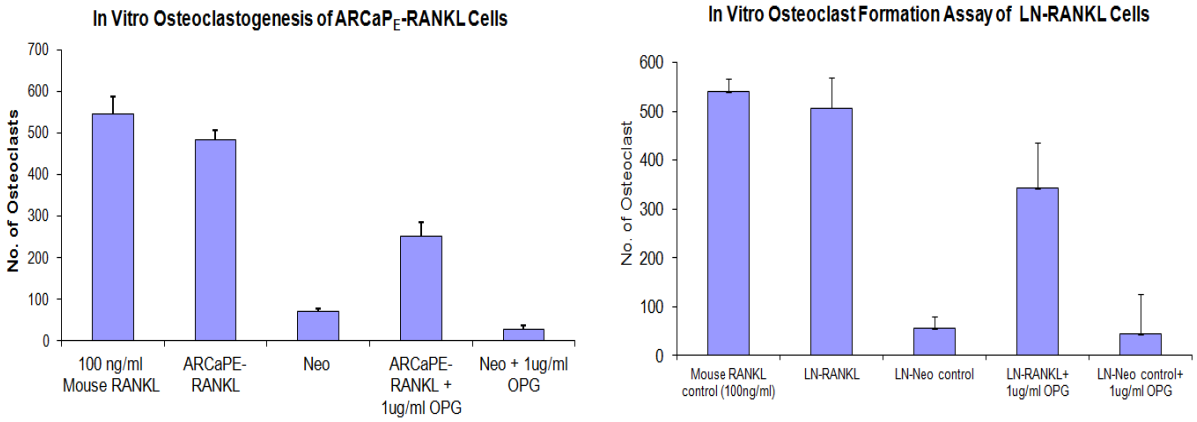

B.

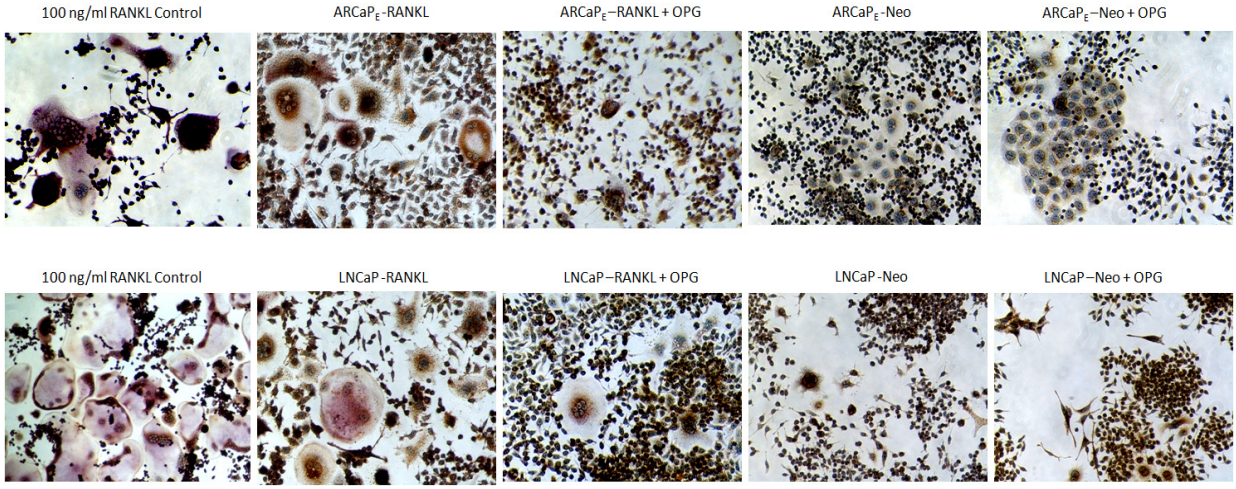

Figure 4. RANKL expressed in ARCaP$_E$ and LNCaP cells was found to be biologically active driving the maturation of cancer cell-adjacent osteoclast precursor cells in a paracrine fashion. **A,** RANKL-expressing ARCaP$_E$ and LNCaP cells were co-cultured with osteoclast precursor RAW-264.7 cells in the presence or absence of OPG for five days, and TRAP+ multinucleated mature osteoclasts were stained and counted under light microscopy. Addition of 100 ng/ml of RANKL protein to RAW264.7 cells served as positive control. RANKL overexpressed by ARCaP$_E$ and LNCaP cells induced five-fold more TRAP+ mature osteoclasts than Neo control cells, indicating that RANKL expressed by ARCaP$_E$ and LNCaP cells was functional. **B,** Representative images of TRAP+ multinucleated mature osteoclasts induced by RANKL protein in ARCaP$_E$-RANKL and LNCaP-RANKL as well as Neo control cells in the presence or absence of OPG (20x magnification).

RANKL Promotes EMT by Activation of NF-κB through an Akt and P38 Dependent Mechanism in Prostate Cancer Cells

The autocrine action of tumor cell-derived RANKL on the cell surface receptor RANK in prostate cancer cells was studied. RANKL expressed in both $ARCaP_E$ and LNCaP cells significantly activated the PI3K-Akt, P38 MAPK, and NF-κB signaling pathways by increasing the phosphorylated levels of Akt on serine 473, P38 on tyrosine 180, and P65 on serine 536. Nevertheless, RANKL did not activate other MAPKs, such as Erk1/2 and JNK/SAPK (Fig. 5A). RANKL-RANK interaction is therefore capable of inducing multiple downstream signaling pathways in prostate cancer cells similar to RANK activation in osteoclasts (Boyle, Simonet, & Lacey, 2003; Wada et al., 2006). Subsequently, we examined the effect of kinase inhibitors specific for Akt, P38, and NF-κB on RANKL-induced EMT. We treated both $ARCaP_E$-RANKL and LNCaP-RANKL cells with 20 μM of a PI3K inhibitor, LY294002, 20 μM of a P38 inhibitor, SB203580, and 2 μM of NF-κB or proteasome inhibitor, PS341 respectively for 4h followed by western blot analysis. As can be seen in Fig. 5B, PI3K and NF-κB inhibitors both increased E-cadherin and decreased vimentin and RANKL expression in $ARCaP_E$-RANKL cells, leading to a reversal of EMT, and similar results were observed in LNCaP-RANKL cells treated with either a P38 or a NF-κB inhibitor. This result shows that direct inhibition of NF-κB signaling prevented RANKL-induced EMT in both $ARCaP_E$-RANKL and LNCaP-RANKL cells. Moreover, we observed that PI3K inhibitor also reduced the phosphorylated level of P38, and subsequently P38 inhibitor resulted in a reduction in phosphorylated level of P65 in both cell types, thus suggesting transactivation of cell signaling axes in the sequence of Akt, P38, and P65 stimulation by RANKL in prostate cancer cells. These findings are consistent with previous studies showing that PI3K-Akt transactivates P38, which further activates NF-κB transcriptional activity through

phosphorylation of P65 upon TNF-α stimulation (Madrid, Mayo, Reuther, & Baldwin, 2001; Viatour, Merville, Bours, & Chariot, 2005). Therefore, we conclude that RANKL promoted EMT by activation of the NF-κB pathway through an Akt and P38 dependent mechanism in prostate cancer cells.

A.

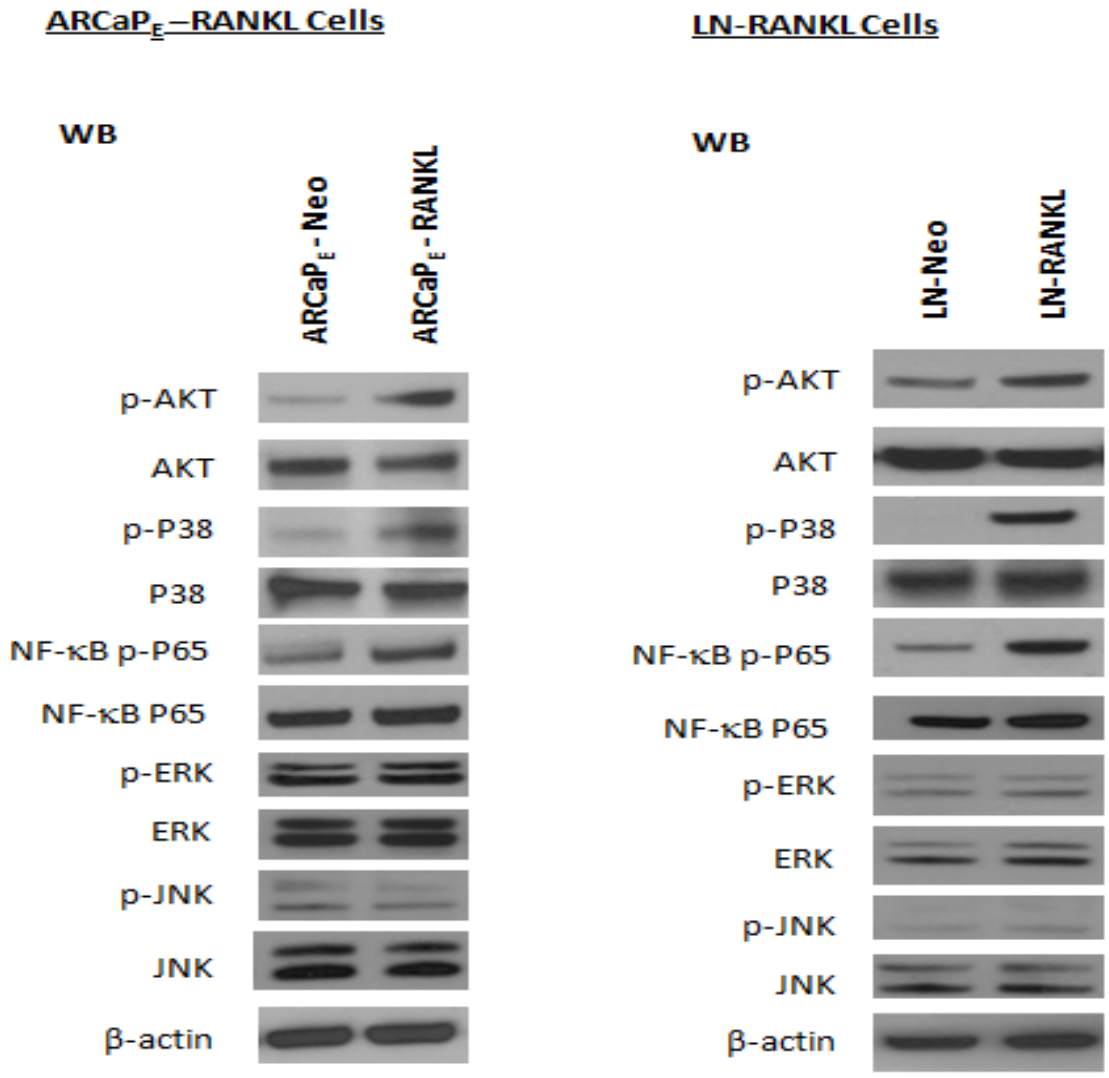

B.

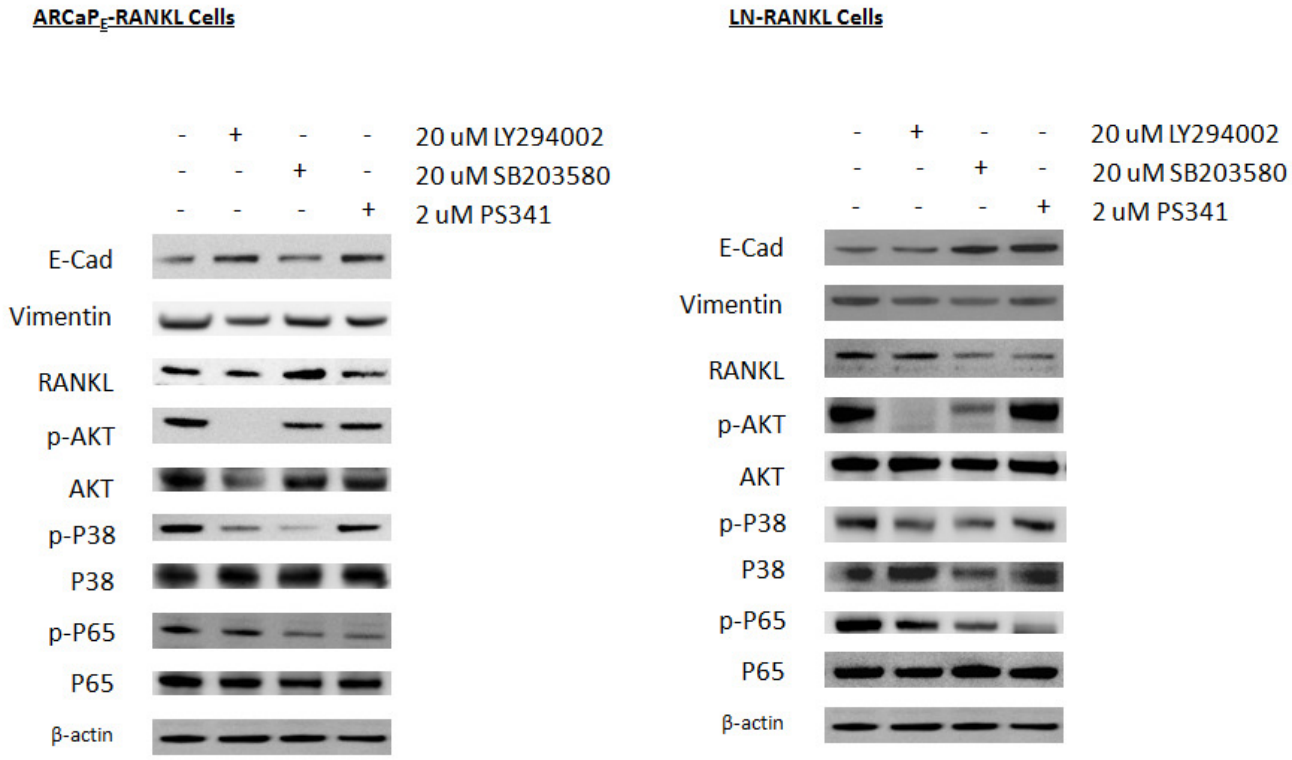

Figure 5. RANKL induced EMT in prostate cancer cells by activating NF-κB signaling through AKT and p38 dependent pathways. **A,** RANKL activated PI3K-AKT, p38, and NF-κB by increasing their phosphorylation levels in ARCaP$_E$ and LNCaP cells as detected by Western blot analysis. **B,** ARCaP$_E$-RANKL and LNCaP-RANKL cells were treated with PI3K (20 μM LY294002), p38 (20 μM, SB203580), and NF-κB (2 μM, PS341) inhibitors for 4 hours, and the cells were harvested for cell lysis followed by Western blot analysis.

Discussion

Apart from the major role of RANKL in regulating bone remodeling in osteoclasts, there is a growing body of evidence to support the idea that RANKL-RANK signaling also exerts important functions in other tissue types, such as mammary gland development during pregnancy (Fata et al., 2000; Kong et al., 1999), lymph node organogenesis (Kong et al., 1999), and monocyte function and inflammatory responses (Seshasayee et al., 2004). However, how RANKL-RANK interaction might be involved in cancer development and progression has not yet been clearly elucidated. We previously showed that RANKL was expressed by malignant prostate cancer cells and its expression was up-regulated during prostate cancer EMT progression, serving as a novel EMT marker. In this study, we further show that RANKL is directly involved in driving the EMT progression and bone metastasis of prostate cancer cells. Moreover, blocking RANKL with OPG can reduce prostate cancer-induced osteolytic lesions.

Our data first demonstrated that RANKL expression was closely associated with clinical human prostate tumor progression where RANKL expression is significantly elevated in bone metastases and poorly-differentiated prostate cancer compared to a low level of expression in benign and a moderate level in well-differentiated prostate cancer specimens. RANKL/RANK/OPG triad was found to be expressed by various prostate cancer cell lines at different levels (Fig 1). Importantly, we further demonstrated that RANKL treatment or overexpression induced indolent human prostate cancer cells, such as $ARCaP_E$ and LNCaP cells, to undergo EMT, leading to increased migration and invasion *in vitro* (Fig. 2 and 3). In agreement with other studies, activation of RANK can enhance cell migration and invasion of prostate cancer cells as well as other epithelial cancer cells (Armstrong et al., 2008; Jones et al., 2006; Sabbota et al.). Blocking RANKL with its decoy receptor OPG not only prevented

RANKL-induced EMT of $ARCaP_E$ and LNCaP cells, but also converted the mesenchymal phenotype and behavior of $ARCaP_M$ cells to become more epithelial-like with decreased levels of mesenchymal markers and reduced migration and invasion, a phenomenon known as EMT reversal (Fig. 2). RANKL expression is stimulated by many osteotropic and growth factors, such as TGF-β, PTHrP, and prostaglandin E2 (Roodman, 2004; Virk & Lieberman, 2007). To our knowledge, we are the first to demonstrate that RANKL treatment or overexpression triggered auto-induction of RANKL expression in prostate cancer cells (Fig. 2B and 3A). Increased levels of RANKL can therefore activate RANK on prostate cancer cells in an autocrine manner to further substantiate their EMT progression and malignancy. Since our data showed that RANKL produced by prostate cancer cells is functional in inducing *in vitro* osteoclastogenesis (Fig. 4), one can further speculate that increased RANKL expression by prostate cancer cells can simultaneously bind to RANK on the surrounding osteoclast precursors in a paracrine manner to activate osteoclast maturation and bone resorption in the bone microenvironment.

Since prostate cancer cells are well-known for their osteomimetic properties, which allow them to imitate the gene expression and behavior of the bone cells, we speculated that RANK activation in prostate cancer cells during EMT transformation might share similar signaling transductions with the differentiating osteoclast precursors. During osteoclastogenesis, RANKL-RANK interaction activates multiple downstream signaling cascades, such as the NF-κB, P38, ERK, JNK, and Src-Akt pathways (Boyle et al., 2003; Jones et al., 2006). We therefore examined these signaling molecules in RANKL-overexpressing LNCaP and $ARCaP_E$ cells. We observed that only the NF-κB, P38, and PI3K-Akt pathways were activated in $ARCaP_E$- and LNCaP-RANKL cells as well as RANKL-treated $ARCaP_E$ cells, but not the ERK or JNK pathways (Fig. 5A). We further asked which one of the three pathways is predominantly

activated and responsible for the RANKL-induced EMT progression and RANKL auto-induction in prostate cancer cells. We inhibited each of the three pathways with their specific inhibitors and examined the EMT markers as well as RANKL expression. Our data indicated that RANKL-induced EMT was abrogated by inhibiting NF-κB signaling in both $ARCaP_E$- and LNCaP-RANKL cells; however, P38 or PI3K inhibitors also partially reverted the EMT markers and decreased RANKL expression in $ARCaP_E$- or LNCaP-RANKL cells. Moreover, we observed that both p38 and PI3K inhibitors diminished the level of p65 phosphorylation, and p38 inhibitor had a stronger inhibitory effect on NF-κB activation than PI3K inhibitor, and in addition, PI3K inhibitor significantly reduced the phosphorylated level of p38 in both cells (Fig. 5B). Our results are therefore in agreement with several studies which have shown that activation of p38 MAPK is required for p65 phosphorylation and transcription function (Bergmann, Hart, Lindsay, Barnes, & Newton, 1998; Kuphal, Poser, Jobin, Hellerbrand, & Bosserhoff, 2004; Wesselborg, Bauer, Vogt, Schmitz, & Schulze-Osthoff, 1997), and AKT can transactivate the p65 subunit of NF-κB through the activation of p38 MAPK (Madrid et al., 2001; Viatour et al., 2005). Furthermore, studies using malignant melanoma also showed that the ERK pathway is not involved in NF-κB activation (Kuphal et al., 2004; Wang & Richmond, 2001). These results suggested that RANKL induces a sequential activation of signaling cascades from PI3K-AKT, p38, and then to NF-κB in $ARCaP_E$- and LNCaP-RANKL cells. Therefore, RANKL mediates EMT transformation of prostate cancer cells by transactivating NF-κB signaling through AKT and P38 dependent pathways which are known to be involved in cancer cell survival, progression, and metastasis.

In summary, RANKL expressed by prostate cancer cells or other cell types in the microenvironment binds to RANK on prostate cancer cells to drive EMT progression through the transactivation of NF-κB signaling in a p38 and/or PI3K-AKT dependent mechanism, and

RANKL-RANK interaction can further stimulate RANKL expression in prostate cancer cells, forming an auto-induction signaling loop. Furthermore, increased RANKL expression by prostate cancer cells can also activate osteoclast precursors in the bone microenvironment in a paracrine fashion to induce osteoclastogenesis and increase bone resorption, which subsequently releases growth factors richly stored in the bone. Together, the autocrine and paracrine signaling mediated by RANKL-RANK interaction creates a vicious cycle that steadily promotes the survival, EMT progression, and bone metastasis of human prostate cancer cells. Targeting of RANKL and its downstream molecules may be a potential new therapeutic strategy for preventing prostate cancer progression and bone metastasis.

CHAPTER 4 RANKL EXPRESSING PROSTATE CANCER CELLS PROMOTE BONE METASTASIS AND TRANSFORM NON-TUMORIGENIC AND NON-METASTATIC PROSTATE CANCER CELLS TO CO-COLONIZE AT METASTATIC SITES

Introduction

Advanced prostate cancer, such as CRPC, has a propensity to metastasize to bone, and more than 80% of CRPC patients will develop bone metastases with a high level of morbidity (Bubendorf et al., 2000; Horwich, 2004; Loberg et al., 2005) for which there is presently no cure. Bone metastasis is also associated with hypercalcemia, anemia, bone pain, recurrent infection, spinal cord compression, fractures and paralysis (Coleman, 1997, 2001; Ye et al., 2007). Although tumor genetic constituents and behavioral anomalies are now shown to be regulated by interactions between cancer cells and their microenvironment (Josson et al., 2011 ; Mundy, 1997), the molecular mechanism of PCa bone colonization still remains elusive. Moreover, it is now well established that prostate cancer cells can home to bone but not necessarily colonize bone successfully; prostate cancer cells must interact reciprocally with bone cells by promoting bone resorption and new bone formation (Coleman, 1997; Mundy, 1997; Roodman, 2004).

Even though emerging evidence has recently suggested the importance of RANKL-RANK interaction in breast and prostate cancer progression and metastasis (Jones et al., 2006; Josson et al., 2011 ; Odero-Marah et al., 2008; Zhang et al., 2001; Zhau et al., 2008), there is no animal model available depicting the role and behavior of RANKL-overexpressing prostate cancer cells *in vivo*. We have demonstrated that RANKL exogenous treatment or endogenous overexpression can induce EMT progression of prostate cancer cells such as LNCaP and $ARCaP_E$ at both the biochemical and morphological levels and enhance their *in vitro* migration, invasion, and

tumorigenic potential. In this study we investigated the *in vivo* role of RANKL in prostate cancer growth and metastases using RANKL-overexpressing LNCaP and $ARCaP_E$ cell models and examined their *in vivo* tumorigenic and metastatic potential through interaction with the microenvironments.

Results

RANKL Facilitates Tumor Formation and Bone Metastasis of Human Prostate Cancer Cells *In Vivo*

Though we showed the *in vitro* EMT progression of prostate cancer cells induced by RANKL, it is crucial to determine the *in vivo* effect of RANKL in terms of tumor formation and metastases. Therefore, we inoculated LNCaP-RANKL or LNCaP-Neo and $ARCaP_E$-RANKL or $ARCaP_E$-Neo cells intracardially into male athymic nude mice to determine their tumorigenic and metastatic potentials. We found that RANKL expression significantly enhanced the metastatic potential of LNCaP and $ARCaP_E$ cells. LNCaP-RANKL and $ARCaP_E$-RANKL cells induced 100% and 70% incidence of gross bone metastases to various anatomical sites, including the legs, skull, ribs and spine, and an average of 72% and 65% incidence of gross soft tissue metastases to lymph nodes, adrenal glands, and lungs over a three-month observation period (Table 1; Fig. 6A). LNCaP-Neo cells, in contrast, failed to produce any tumor or metastasis, consistent with the known indolent nature of LNCaP cells (Wu et al., 1998). $ARCaP_E$-Neo cells also failed to induce any bone metastasis but showed 20% metastatic incidence to adrenal glands. Mice bearing LNCaP-RANKL and $ARCaP_E$-RANKL cells also developed serious cachexia with extensive tumor burden mostly in the skeleton. We inspected mice with bone lesions using μCT analysis to determine the type of bone lesions induced by LNCaP-RANKL and $ARCaP_E$-RANKL cells. Previous studies by our laboratory (Thalmann et al., 1994; Wu et al., 1998) and others (Corey et al., 2002) showed that intratibial or orthotopic injection of LNCaP lineage-derived C4-2, and C4-2B cells in immune-compromised mice produced mixed osteolytic and osteoblastic bone lesions. LNCaP or LNCaP-Neo cells, when injected intrafemorally or orthotopically in immune-compromised mice, however, failed to form tumors (Wu et al., 1994;

Wu et al., 1998), Table 1). Figure 6B shows 3D μCT scans of skeletons of mice bearing the LNCaP-Neo, LNCaP-RANKL, $ARCaP_E$-Neo, and $ARCaP_E$-RANKL cells. Extensive bone destruction at femoral, pericranial, jaw, and spinal sites was observed in most of the mice bearing the LNCaP-RANKL and $ARCaP_E$-RANKL cells with gross skeletal metastases but not in mice bearing the Neo control cells. These results indicated that LNCaP-RANKL and $ARCaP_E$-RANKL cells induced severe osteolytic bone lesions where the bones were heavily resorbed compared to the bone structure of the Neo control mice.

We next sought histochemical evidence of RANKL expression and EMT phenotype in metastatic tumors from mice bearing the LNCaP-RANKL cells using IHC staining against flag-tagged RANKL and EMT markers. We observed that RANKL expression when detected with either Flag or RANKL antibody showed a stronger signal in the bone tumor at the bone/tumor interface compared to lymph node tumor. Both bone and lymph node metastatic tumors expressed high levels of N-cadherin and vimentin but low levels of E-cadherin expression, demonstrating the EMT progression of the tumor cells. Interestingly, we demonstrated that E-cadherin expression in both bone and lymph node metastatic tumors appeared to be in clusters or subsets of the tumor cells, showing a heterogeneous tumor cell population/clone. This phenomenon can be explained as the re-expression of E-cadherin during mesenchymal-to-epithelial transition (MET) to allow the establishment of metastatic tumor cells in the microenvironment at distant sites, following the metastases of disseminated tumor cells resulting from EMT. Such re-expression of E-cadherin during MET of metastatic tumor cells has been well demonstrated in many breast and prostate cancer metastases to bone and liver, indicating the epithelial plasticity of tumor cells (Chao, Shepard, & Wells, ; Kowalski, Rubin, & Kleer, 2003; van der Pluijm, 2010; Wells, Yates, & Shepard, 2008; Yates, Shepard, Stolz, & Wells, 2007). Since RANKL expressed by LNCaP cells

was biologically functional in inducing in vitro osteoclastogenesis, we further examined the osteoclastic activity in the bone tumors induced by LNCaP-RANKL cells intracardially inoculated in nude mice using TRAP staining. We observed an increased number of TRAP-positive mature osteoclasts at the bone/tumor interface compared to normal bone from mice bearing the LNCaP-Neo cells (Fig 6D), which further confirms the biological functionality of RANKL produced by LNCaP cells in activating osteoclastogenesis in vivo.

Table 1. Metastatic incidence of LNCaP-RANKL and $ARCaP_E$-RANKL vs LNCaP-Neo and $ARCaP_E$-Neo cells in nude mice. RANKL- and Neo-expressing LNCaP and $ARCaP_E$ cells were intracardially inoculated into male athymic nude mice. Mice were sacrificed three months after injection, and the tumors metastasized to the soft tissues and bone were harvested and evaluated for the metastatic incidence. Mice inoculated with LNCaP-Neo cells failed to form any visible metastatic tumor.

Metastatic Incidence of LNCaP-RANKL and $ARCaP_E$-RANKL Cells in Nude Mice

Cells \ Metastatic Sites	Lymph Node	Bone Metastases (Limbs, Rib, Jaw, Skull)	Adrenal Gland	Lung
LNCaP Neo Control	0/15	0/15	0/15	0/15
LNCaP-RANKL	18/20 (90%)	20/20 (100%)	17/20 (85%)	8/20 (40%)
$ARCaP_E$-Neo Control	0/5 (0%)	0/5 (0%)	1/5 (20%)	0/5 (0%)
$ARCaP_E$-RANKL	6/10 (60%)	7/10 (70%)	7/10 (70%)	0/10 (0%)

A.

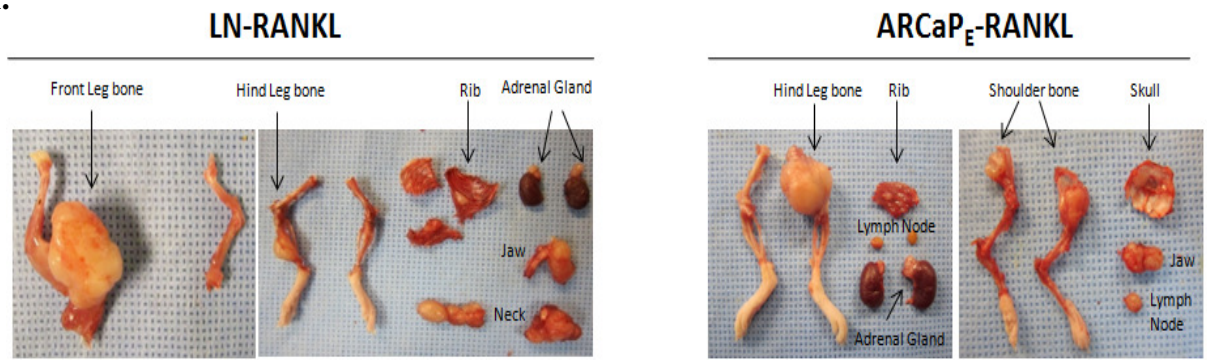

B.

μCT demonstration of osteolytic bone lesions induced by the inoculation of LN-RANKL cells in nude mice

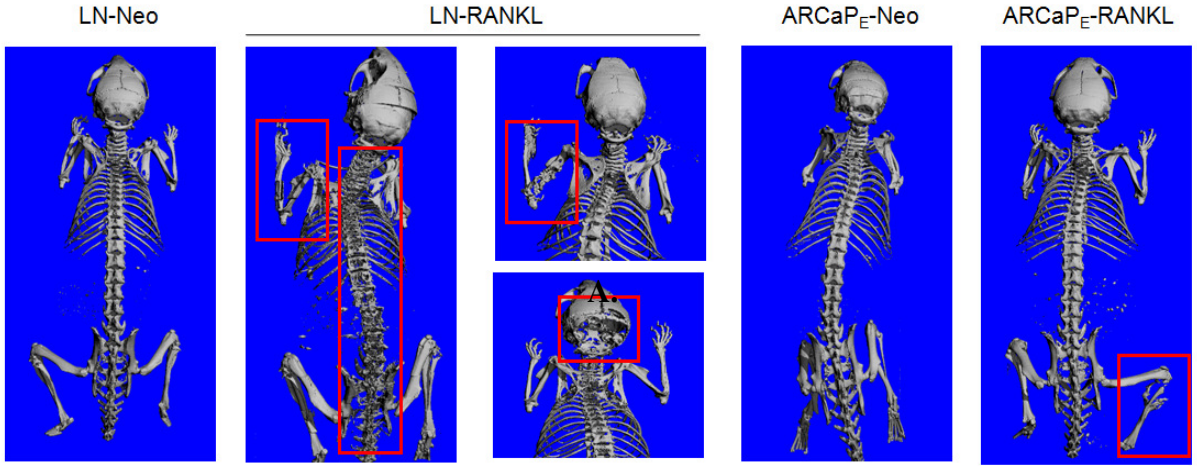

C.

IHC Staining of RANKL and EMT Markers in Metastatic Tumors Induced by LN-RANKL Cells

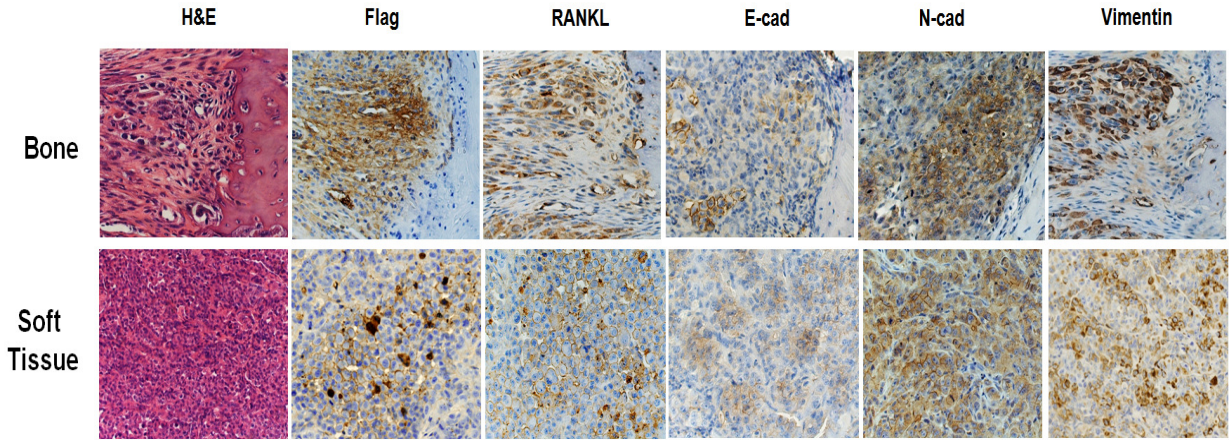

D.

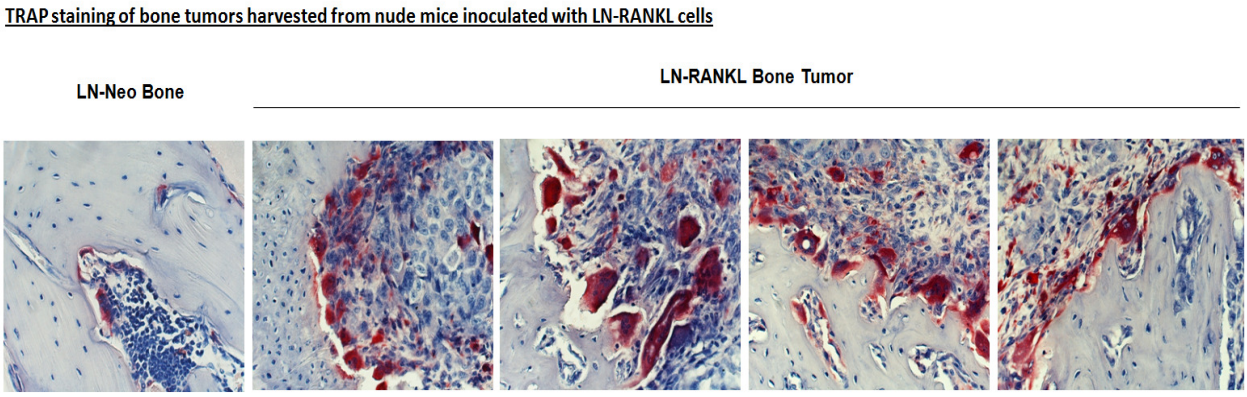

Figure 6. RANKL increased the metastatic potential of both LNCaP and ARCaP$_E$ cells and induced osteolytic lesions in bone. RANKL-induced tumors expressed mesenchymal phenotype and exhibited increased osteoclastic activity in bone. **A,** Representative images of metastatic tumors in bone and soft tissues induced by LNCaP-RANKL and ARCaP$_E$-RANKL cells inoculated in nude mice (Metastatic sites are labeled and indicated by arrows). **B,** Representative 3D μCT scans demonstrate osteolytic lesions in mouse femur, spine, skull, and tibia (outlined in red) induced by the LNCaP-RANKL and ARCaP$_E$-RANKL cells inoculation in nude mice. **C,** Immunohistochemical (IHC) staining of RANKL and EMT marker expression in bone and soft tissue (lymph nodes) tumors induced by LNCaP-RANKL cells inoculated in nude mice. Using LNCaP-RANKL cells as a model, we showed that a small number of LNCaP-RANKL cells are sufficient to induce bone metastases in the presence of bystander RANKL non- or low-expressing cells. Importantly, histomorphology showed that both RANKL-expressing and low-expressing cells reside in the bone metastasis tumors, suggesting the important function of RANKL in contributing to the overall bone metastases irrespective of the basal steady-state level of RANKL expression. **D,** TRAP staining of mature osteoclast lining (red) in bone tumor induced by the inoculation of LNCaP-RANKL cells in nude mice compared to the normal bone

RANKL Expressing Prostate Cancer Cells Promote Tumorigenesis of RANKL Non-Expressing Prostate Cancer Cells in the Bone

We further examined if there is cross-talk between RANKL-expressing and RANKL-non-expressing prostate cancer cells to mimic the heterogeneous population of cancer cells in the bone microenvironment. We co-inoculated a thousand, ten thousand, and a hundred thousand LNCaP-RANKL cells and a million RANKL-low-or-non expressing LNCaP cells labeled with red fluorescent protein (LNCaP-RFP) intratibially and examined whether RANKL-expressing prostate cancer cells are capable of inducing neighboring RANKL-non-expressing prostate cancer cells to form tumors in the bone. We demonstrated that as few as a thousand LNCaP-RANKL cells can promote the non-tumorigenic, RANKL-non-expressing LNCaP-RFP cells to grow tumors in mice tibia (Fig 7). We detected the presence of LNCaP-RFP cells using fluorescent imaging of the harvested tumors. We also found that as the number of LNCaP-RANKL cells increased, the tibial tumors were bigger and the red fluorescent signal detected was stronger, implicating RANKL-expressing LNCaP cells augmentation of the tumorigenic potential of RANKL-non expressing LNCaP-RFP cells in the tumor microenvironment.

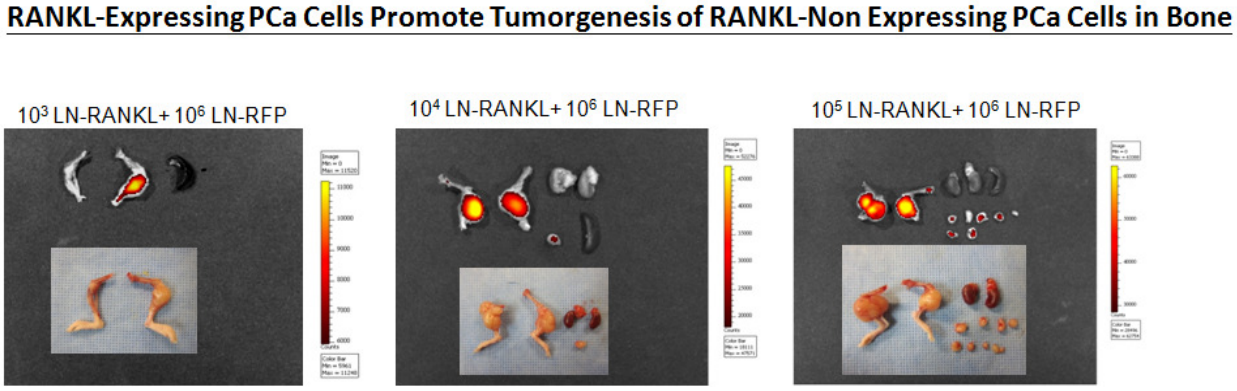

Figure 7. Small numbers of RANKL-expressing PCa cells conferred tumorgenicity of RANKL-non-expressing PCa cells in bone. One thousand, ten thousand, and a hundred thousand RANKL-expressing LNCaP (LNCaP-RANKL) cells were co-inoculated with a million RANKL non-expressing LNCaP cells tagged with red fluorescent protein (LNCaP-RFP) in both tibia of nude mice. Tibial and soft tissue tumors were harvested and subjected to fluorescent imaging for detection of the red fluorescent signal using the Xenogen imaging system at an excitation of 535 nm and emission of 620 nm. Spleens were also harvested and used as controls.

RANKL-expressing PCa Cells Promote Co-colonization of Non-metastatic and RANKL-non-expressing PCa Cells to the Metastatic Sites

We next used the bone metastatic LNCaP-RANKL cell model plus indolent LNCaP-RFP cells to examine if RANKL-expressing prostate cancer cells are capable of promoting RANKL-low-or-non-expressing and non-metastatic prostate cancer cells to proliferate and metastasize in vivo. We co-inoculated LNCaP-RANKL and LNCaP-RFP cells intracardially at a ratio of 1 to 9 and 9 to 1, respectively. We also intratibially inoculated the LNCaP-RANKL cells first, followed by intracardial inoculation of the LNCaP-RFP cells. Mice bearing the LNCaP-RANKL plus LNCaP-RFP at a 9 to 1 ratio demonstrated 100% metastases to bone and an average of 65% metastases to soft tissues such as adrenal glands and lymph nodes. However, when co-inoculation of LNCaP-RANKL and LNCaP-RFP cells at a 1 to 9 ratio, metastases to bone and soft tissues occurred only at a 60% and 30% incidence, respectively. When inoculating LNCaP-RANKL cells intratibially followed by intracardial inoculation of LNCaP-RFP cells, all of the mice (n=5) demonstrated 100% tumor growth in the tibial bone as well as metastases to either adrenal glands or lymph nodes. When inoculating non-tumorigenic LNCaP-RFP cells intratibially followed by intracardial inoculation of LNCaP-RANKL cells, 50% of the mice (n=4) developed tibial tumors but we observed no soft tissue metastasis (Table 2).

Table 2. Metastatic incidence of LNCaP-Neo or LNCaP-RANKL plus LNCaP-RFP cells in nude mice. LNCaP-RANKL and LNCaP-RFP cells were intracardially co-inoculated into male athymic nude mice at a ratio of either 1 to 9 or 9 to 1 in a total of a million cells. Half a million of LNCaP-Neo plus half a million of LNCaP-RFP cells were also intracardially co-inoculated into nude mice but failed to form any tumor or metastasis. A million LNCaP-RANKL or LNCaP-RFP cells were also inoculated intratibially followed by intracardiac implantation of a million LNCaP-RFP or LNCaP-RANKL cells. Tumors metastasized to the soft tissues and bone were harvested and evaluated for the metastatic incidence.

	Metastatic Sites		
Groups	**Bone**	**Adrenal Gland**	**Lymph Node**
Intracardial Injection of $5x10^5$ LN-Neo + $5x10^5$ LN-RFP	0/10	0/10	0/10
Intracardial Injection of $9x10^5$ LN-RANKL + 10^5 LN-RFP	10/10	8/10	5/10
Intracardial Injection of 10^5 LN-RANKL + $9x10^5$ LN-RFP	6/10	0/10	3/10
Intratibial Injection of 10^6 LN-RANKL + Intracardial Injection of 10^6 LN-RFP	5/5	3/5	2/5
Intratibial Injection of 10^6 LN-RFP + Intracardial Injection of 10^6 LN-RANKL	2/4	0/4	0/4

We further examined the red fluorescent signals of the metastatic tumors harvested from the mice of all three groups using fluorescent imaging *ex vivo* to detect any presence of the LNCaP-RFP cells in the tumors. Interestingly, we found that the metastatic bone and soft tissue tumors from all three groups exhibited the red fluorescent signals, especially the bone tumors compared to the normal organs such as spleen, bone, and kidney acting as negative controls. In addition, red fluorescent signal was also detected in the tibia of mice bearing intratibial LNCaP-RFP cells plus intracardial LNCaP-RANKL cells, but not if the LNCaP-Neo cells were injected intracardially instead (Fig. 8A). Moreover, we also detected red fluorescent signals from frozen as well as paraffin-embedded tissue sections of the metastatic tumors under the fluorescent microscope (Fig. 8B and 8C). Alternatively, we stained the RFP on the paraffin-embedded tumor sections with antibody and further confirmed the presence of LNCaP-RFP cells in the bone tumors (Fig. 8C). We also performed multiplexed quantum dot (QD) labeling of RANKL and RFP on paraffin-embedded tumor sections to confirm the co-presence of LNCaP-RANKL and LNCaP-RFP cells in the bone tumor as well as to examine the level of RANKL expression by the bone-colonizing LNCaP-RFP cells (Fig. 8D). We found that the number of colonizing LNCaP-RFP cells corresponds with the number of co-inoculated LNCaP-RFP cells in mice. We also observed that RANKL expression in the LNCaP-RANKL induced bone tumors is heterogeneous, suggesting the possibility that RANKL expression can be switched on/off by the prostate cancer cells depending on the surrounding microenvironment. Moreover, we discovered that the colonized LNCaP-RFP cells in the bone tumors also express high or moderate level of RANKL indicated by the co-localization (yellow) of RANKL (green) and RFP (red) labeling (Fig. 8D). This result further indicated that RANKL-expressing LNCaP-RFP cells lead to transformation from an indolent state to become metastatic. RANKL expression in LNCaP-RFP

cells may be induced by a mechanism of RANKL autocrine induction through a paracrine interaction with LNCaP-RANKL cells. Together, these results suggested that LNCaP-RFP cells co-colonized with the LNCaP-RANKL cells in the metastatic sites. LNCaP cells are known to be non-tumorigenic and non-metastatic; however, the co-existence of LNCaP-RANKL cells might transform and convey metastatic potential to the indolent LNCaP-RFP cells, allowing their co-colonization to the bone and soft tissues with LNCaP-RANKL cells. Moreover, tumors induced by LNCaP-RANKL cells in the tibial bone also promoted homing of the LNCaP-RFP cells to the tumor sites. This observation might be well explained by the 'seed and soil' theory where the disseminated LNCaP-RANKL cells initially created a favorable environment by inducing osteolytic lesions in the bone, leading to the release of growth factors and cytokines that subsequently allowed the circulating LNCaP-RFP cells to colonize and grow in the bone lesions.

A.

9 LN-RANKL+ 1 LN-RFP

Intratibial LN-RANKL+ Intracardiac LN-RFP

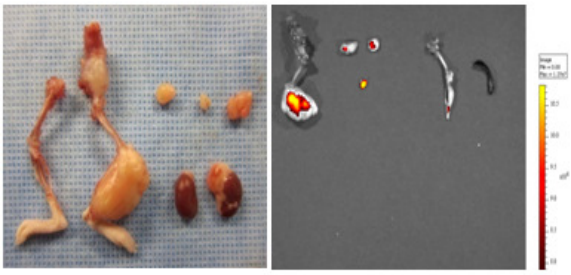

1 LN-RANKL+ 9 LN-RFP

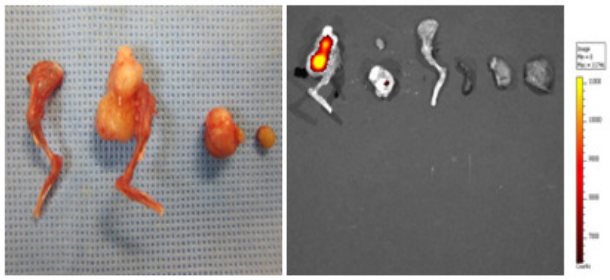

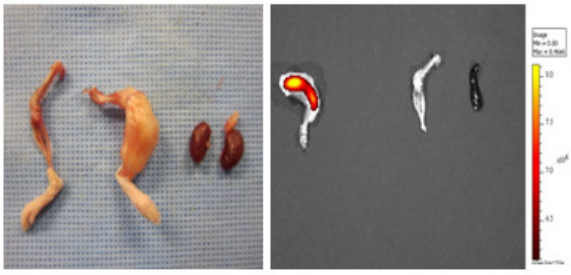

Intratibial Injection LN-RFP
+
Intracardial Injection LN-Neo

Intratibial Injection LN-RFP
+
Intracardial Injection LN-RANKL

B.

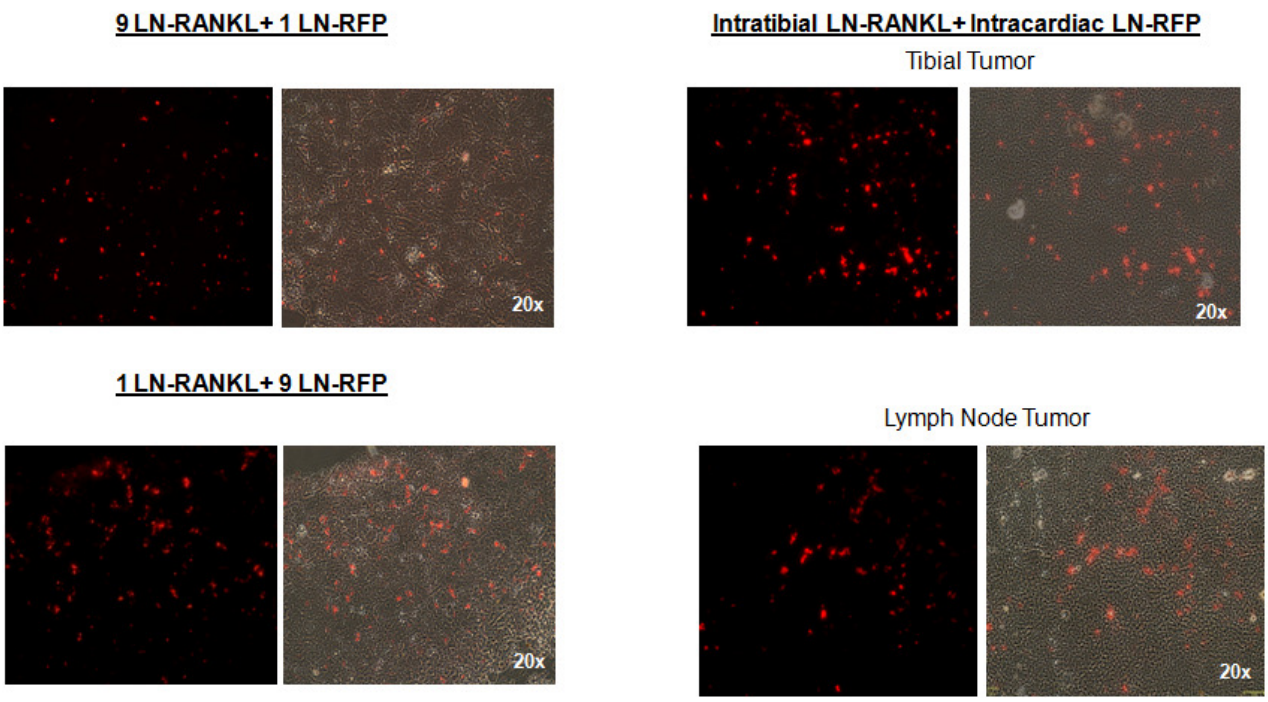
9 LN-RANKL+ 1 LN-RFP
20x
Intratibial LN-RANKL+ Intracardiac LN-RFP
Tibial Tumor
20x
1 LN-RANKL+ 9 LN-RFP
20x
Lymph Node Tumor
20x

C.

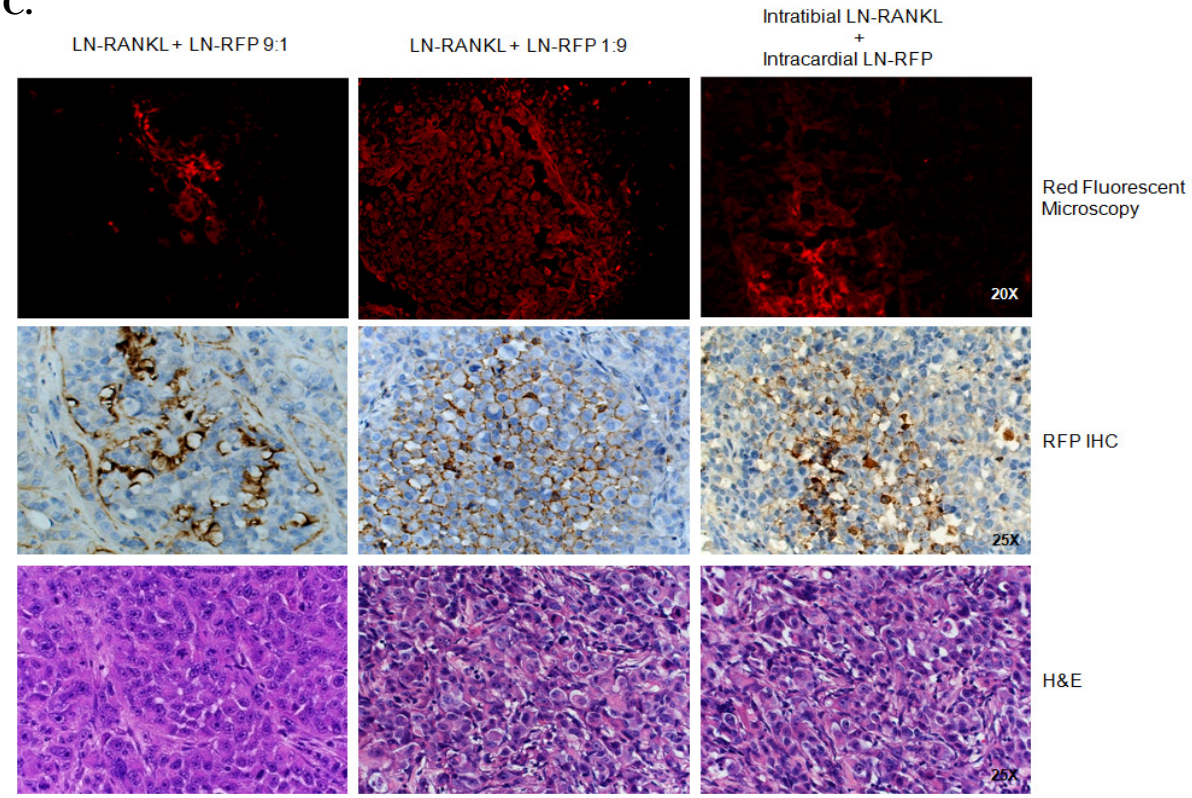
LN-RANKL + LN-RFP 9:1
LN-RANKL + LN-RFP 1:9
Intratibial LN-RANKL
+
Intracardial LN-RFP
20X
Red Fluorescent Microscopy
25X
RFP IHC
25X
H&E

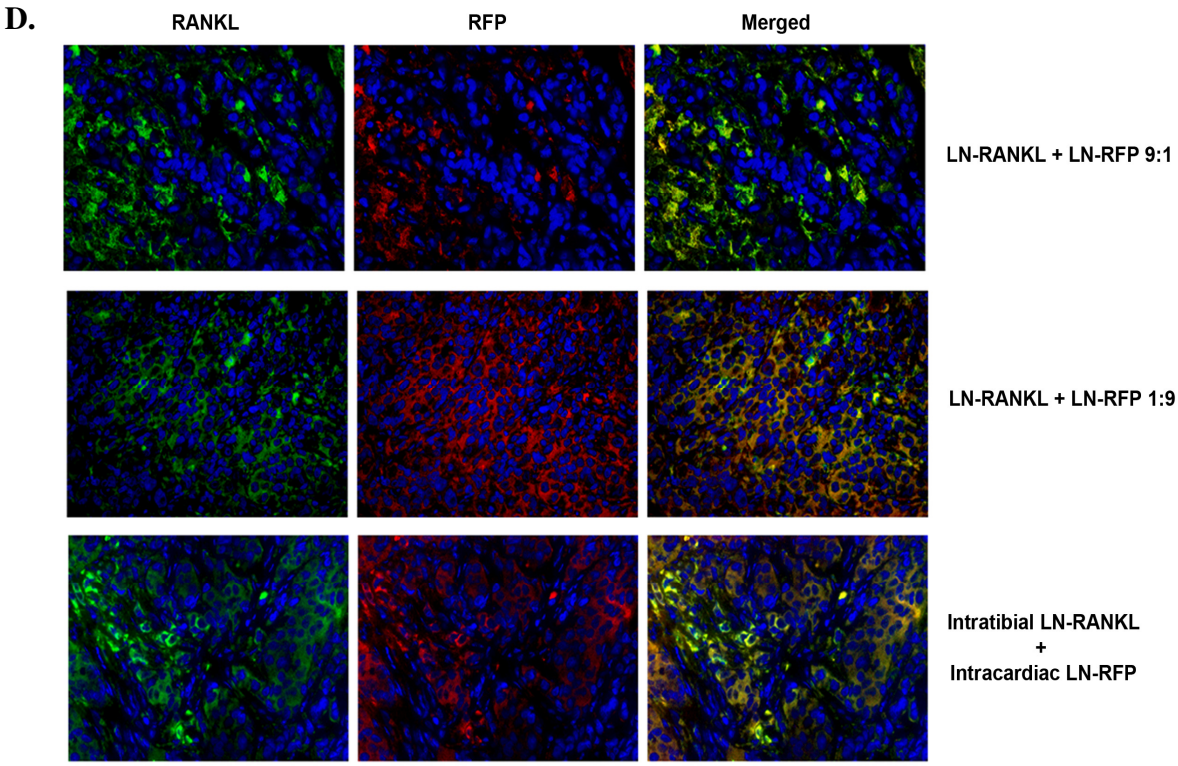

Figure 8. RANKL-expressing PCa cells promote co-colonization of non-metastatic and RANKL-non-expressing PCa cells at metastatic sites. **A.** Representative images and corresponding red fluorescent signal intensity of bone and soft tissue tumors harvested from nude mice bearing tumors with LNCaP-RANKL plus LNCaP-RFP cells at 1 to 9 and 9 to 1 ratios and intratibial inoculation of LNCaP-RANKL cells followed by intracardiac inoculation of LNCaP-RFP cells. Representative *in vivo* X-ray and fluorescent images (Ex: 740; Em: 840) of intratibial inoculation of LNCaP-RFP cells followed by intracardiac inoculation of LNCaP-RANKL cells. **B.** Representative red fluorescent microscopy detected from frozen sections of bone and soft tissue tumors harvested from each group (20x magnification). Parts of the tumors were fixed in OCT and sectioned using Cryostat at -25 ºC and the red fluorescent signals of the frozen sections were detected using fluorescent microscopy. **C.** Representative images of red fluorescent microscopy and corresponding immunohistochemical staining of RFP and hematoxylin and eosin (H&E) staining from paraffin-embedded tumors of each group detected by light and fluorescent microscopy (25x magnification). **D.** Representative images of multiplexed quantum dot (QD) labeling of RANKL (green) and RFP (red) as well as merged QD labeling of paraffin-embedded tumor sections counterstained with DAPI nuclear staining (blue). Individual QD labeled protein expression is presented alone in pseudocolor, followed by a composite of the superimposed QD signals overlaid with nuclear DAPI staining. Images were acquired using the Cri spectral imaging system at 40x magnification.

Co-culture of RANKL-expressing and RANKL-non-expressing PCa Cells Induces Increased Osteoblastic Activity *In Vitro* and Mixed Osteolytic and Osteoblastic Lesions *In Vivo*

We next sought to determine *in vitro* osteoblastic and osteoclastic activity in a co-culture of LNCaP-Neo or LNCaP-RANKL cells with LNCaP-RFP cells. We performed *in vitro* osteoclastogenesis and osteogenic assays by incubating the osteoclast (RAW 264.7 cells) and osteoblast (MC3T3 cells) precursors with LNCaP-RANKL, LNCaP-Neo, and LNCaP-RFP cells as well as with the co-culture of LNCaP-RANKL or LNCaP-Neo with LNCaP-RANKL cells at a 1 to 9 ratio. We demonstrated that LNCaP-RANKL cells induced high levels of osteoclast differentiation but low levels of osteoblast mineralization compared to LNCaP-Neo or LNCaP-RFP cells (Fig. 9A and 9B). Nevertheless, upon co-culture with LNCaP-RFP cells, the number of mature osteoclasts formed decreased and the osteoblast mineralization increased significantly compared to the LNCaP-RANKL cells alone. The levels of osteoclast maturation and osteoblast mineralization were comparable between the LNCaP-Neo, LNCaP-RFP cells and co-culture of both cell types (Fig. 9A and 9B). These results suggested that the presence of LNCaP cells can switch predominantly osteoclastic LNCaP-RANKL cells to become more osteoblastic-like.

Furthermore, μCT scans demonstrated that mice bearing either a 1 to 9 or 9 to 1 ratio of LNCaP-RANKL and LNCaP-RFP cells or intratibial LNCaP-RANKL plus intracardial LNCaP-RFP cells all displayed mixed osteolytic and osteoblastic lesions in the bone (Fig. 9C). Intratibial co-inoculation of a thousand, ten thousand, and a hundred thousand LNCaP-RANKL cells plus LNCaP-RFP cells also led to mixed osteolytic and osteoblastic lesions (Fig. 9C). Next, we sought to examine the histological evidence of the mixed osteoyltic and osteoblastic phenotype in paraffin-embedded tumor sections. We combined TRAP (red staining of multinucleated

osteoclasts) as well as orange G (yellow orange staining of new bone formation) staining and demonstrated that the bone tumors from all three groups exhibited osteolytic as well as osteoblastic activities at the bone and tumor interface. Higher osteoblastic but lower osteolytic activity was observed in the bone tumors induced by a 1 to 9 ratio of LNCaP-RANKL and LNCaP-RFP cells as well as by the intratibial LNCaP-RANKL plus intracardial LNCaP-RFP cells (Fig. 9D). We alternatively demonstrated the increased level of osteoblastic activity in the tumors induced by the co-inoculation of LNCaP-RANKL and LNCaP-RFP cells by detecting the osteoid formation/thickness using Trichrome staining (Fig. 9E). The osteoid stained in red, and the mineralized bone stained in turquoise. The level of osteoid formation and thickness can reflect the level of bone formation (Ott, 2008). Together, these results indicated that the level of osteoblastic and osteoclastic phenotype displayed in the bone lesions seemed to be correlated with the number of LNCaP-RFP and LNCaP-RANKL cells, respectively, during the co-inoculation.

A.

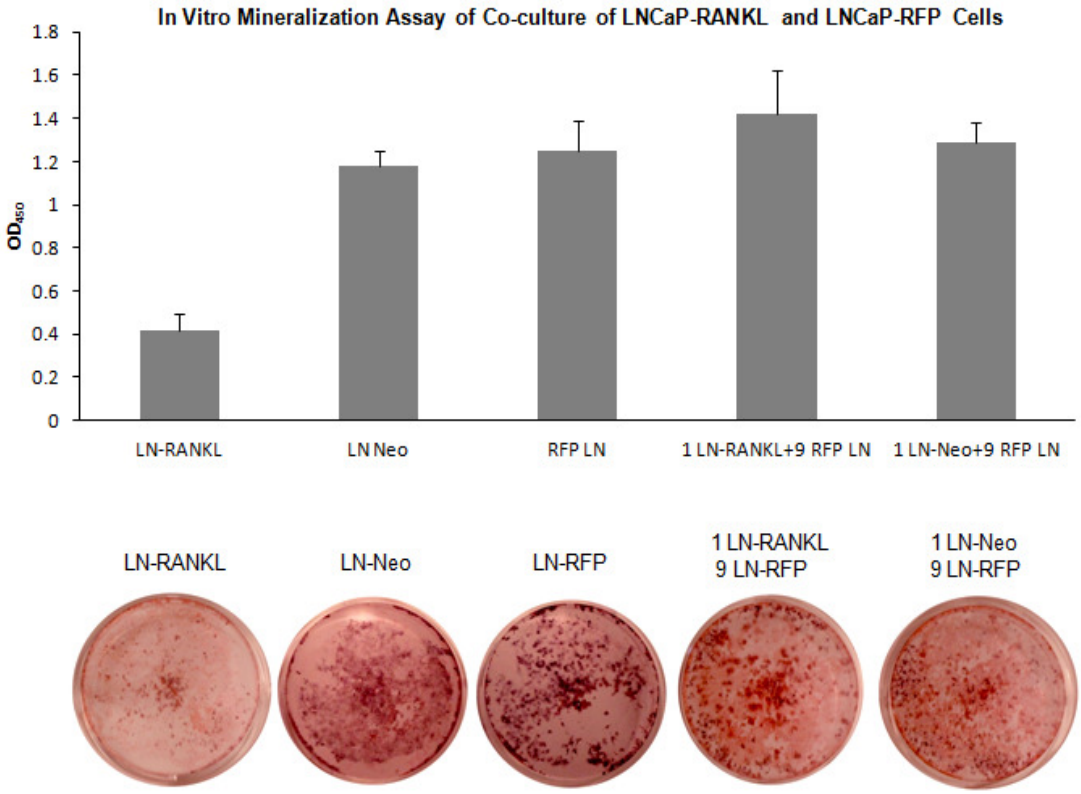
In Vitro Mineralization Assay of Co-culture of LNCaP-RANKL and LNCaP-RFP Cells
OD450
1.8
1.6
1.4
1.2
1
0.8
0.6
0.4
0.2
0
LN-RANKL
LN Neo
RFP LN
1 LN-RANKL+9 RFP LN
1 LN-Neo+9 RFP LN
LN-RANKL
LN-Neo
LN-RFP
1 LN-RANKL 9 LN-RFP
1 LN-Neo 9 LN-RFP

B.

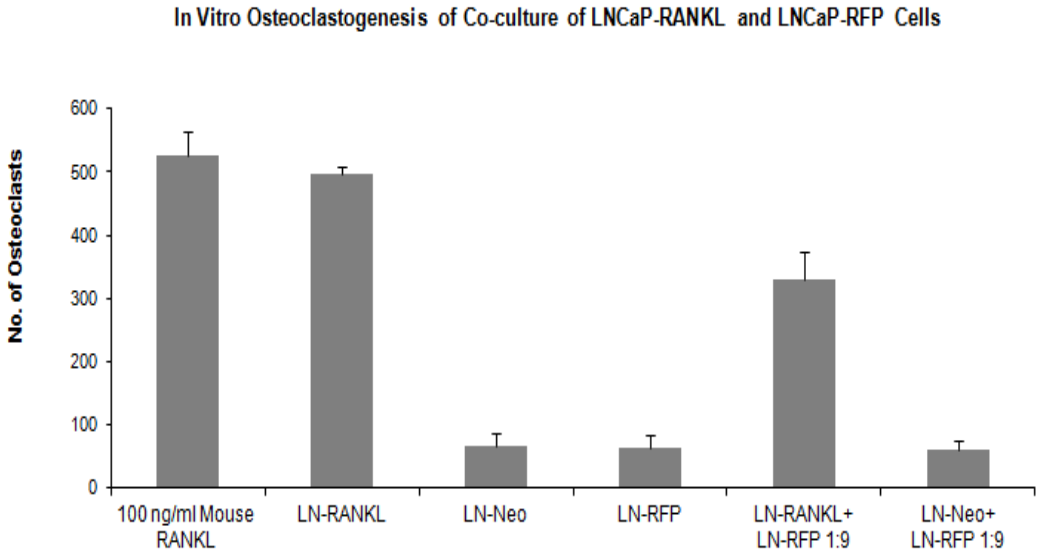
In Vitro Osteoclastogenesis of Co-culture of LNCaP-RANKL and LNCaP-RFP Cells
No. of Osteoclasts
600
500
400
300
200
100
0
100 ng/ml Mouse RANKL
LN-RANKL
LN-Neo
LN-RFP
LN-RANKL+ LN-RFP 1:9
LN-Neo+ LN-RFP 1:9

C.

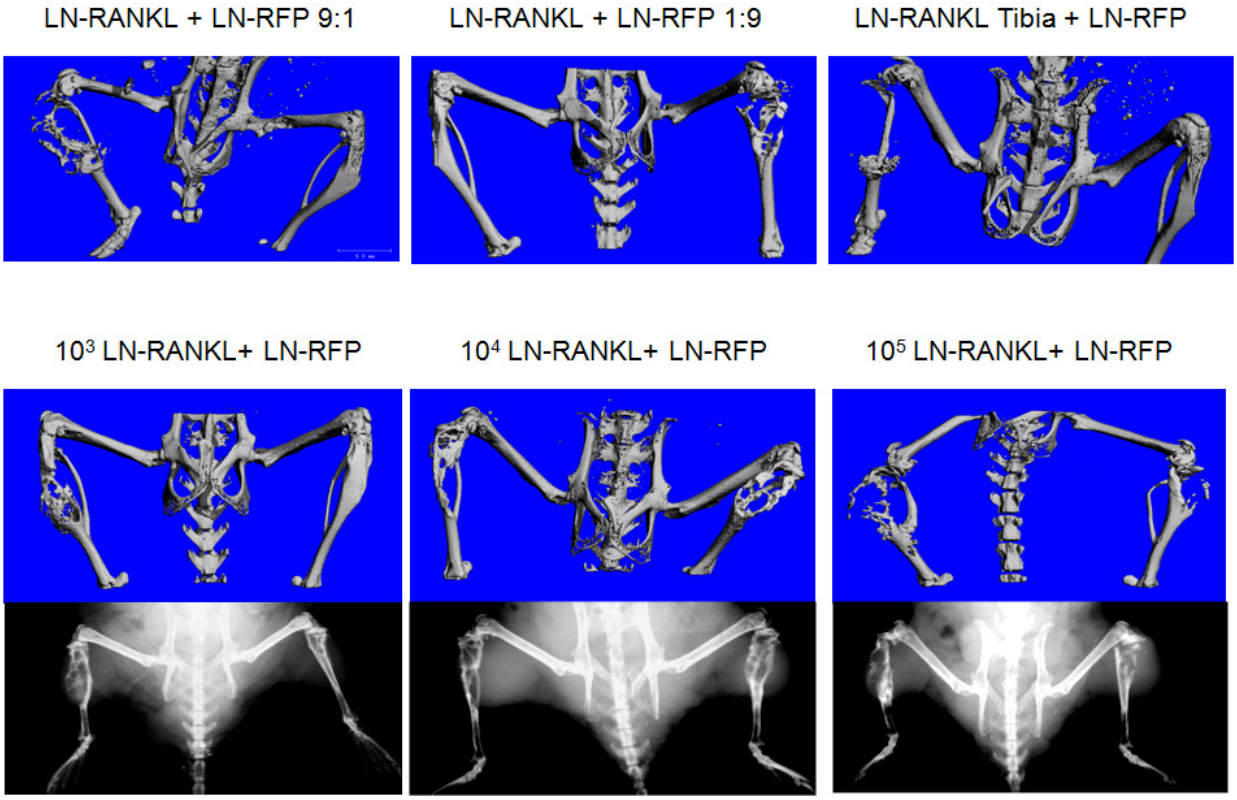

D.

TRAP Staining

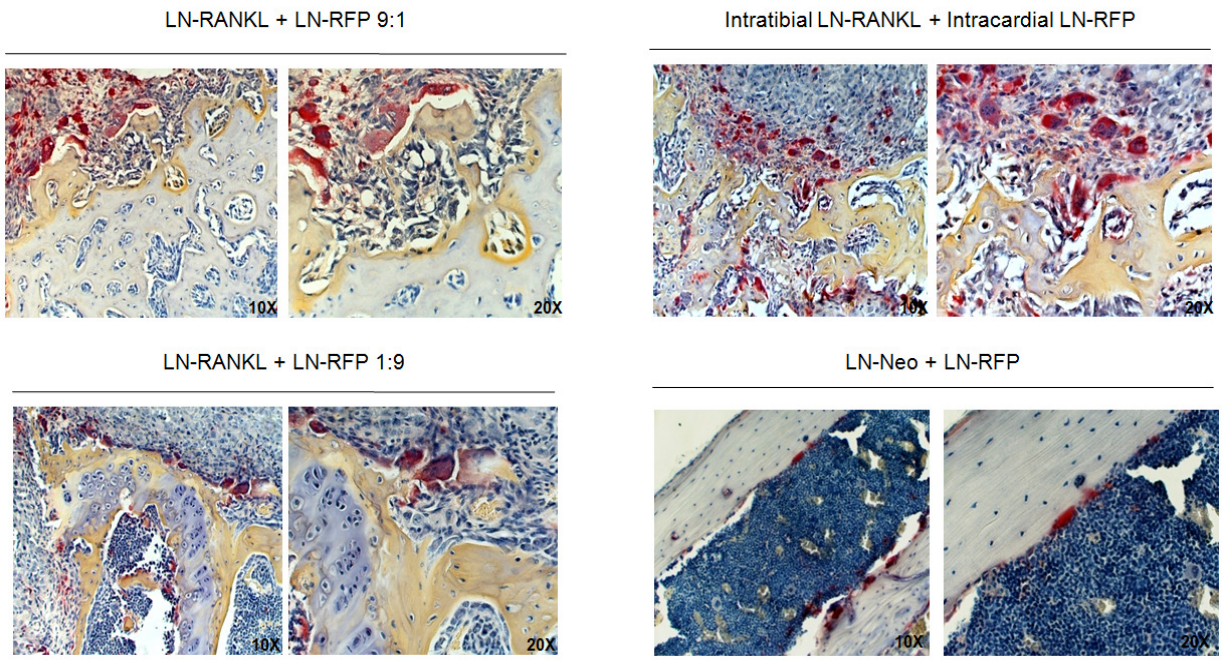

E.

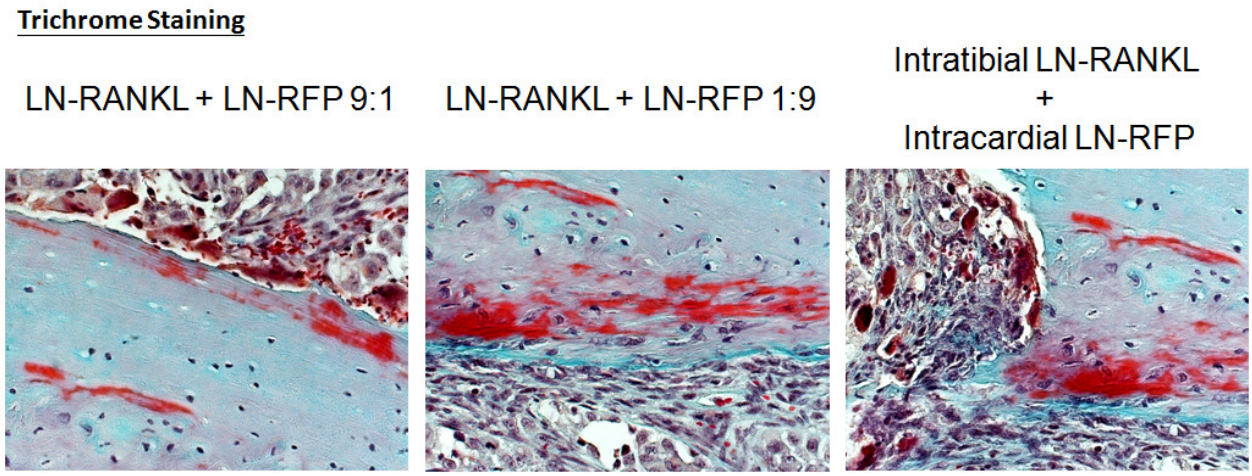

Figure 9. Co-culture of RANKL-expressing and non-expressing PCa cells induces increased osteoblastic activity *in vitro* and mixed osteolytic and osteoblastic lesions *in vivo*. **A.** LNCaP-RANKL and LNCaP-Neo cells were cultured alone or co-cultured with LNCaP-RFP at a 1 to 9 ratio in the presence of pre-osteoblast MC3T3-E1-14 cells for 14 days, and the cells were stained with Alizarin Red, which was then extracted and quantitated by measuring at an absorbance of 450 nm. **B.** LNCaP-RANKL and LNCaP-Neo cells were cultured alone or co-cultured with LNCaP-RFP at a 1 to 9 ratio in the presence of osteoclast precursor RAW264.7 cells for 7 days, and TRAP+ multinucleated mature osteoclasts were stained and counted under light microscopy. Addition of 100 ng/ml of RANKL protein to RAW264.7 cells served as positive control. **C.** Representative 3D μCT scans demonstrate a mix of osteolytic and osteoblastic lesions in mouse tibia induced by the LNCaP-RANKL and LNCaP-RFP tumor cell inoculation in nude mice. **D.** TRAP staining of mature osteoclast lining (red) and orange G staining of new bone formation (yellow orange) in bone tumor induced by the co-inoculation of LNCaP-RANKL and LNCaP-RFP cells in nude mice. Images were taken by light microscopy at 12.5x and 25x magnification. **E.** Trichrome staining of osteoids and active bone formation (red), mineralized bone (green), and cartilage (purple) in bone tumor induced by the co-inoculation of LNCaP-RANKL and LNCaP-RFP cells in nude mice (Magnification 25x).

RANKL Induced Expressional Changes of Soluble Factors Associated with Prostate Cancer Progression and Mixed Bone Metastasis

We further examined the changes of gene expression associated with osteoblastic regulation and prostate cancer progression upon RANKL expression of LNCaP cells as well as the co-culture of LNCaP-RANKL and LNCaP-RFP cells *in vitro*. We first analyzed the transcriptional expression of osteoblastic markers such as OPG (Gori et al., 2000; G. H. Thomas, 2001), Runx2 (Komori et al., 1997; Otto et al., 1997), activating transcription factor 4 (ATF4) (Yang et al., 2004), and alkaline phosphatase (ALP) (Szulc, Garnero, Marchand, Duboeuf, & Delmas, 2005) in LNCaP-RANKL, LNCaP-Neo, and LNCaP-RFP cells alone or a co-culture of both cells at a 1 to 9 ratio. Figure 10A shows that co-culture of LNCaP-RANKL and LNCaP-RFP cells significantly induced OPG, Runx2, and ALP expression but only a moderate level of ATF4 expression compared to LNCaP-Neo/LNCaP-RFP and LNCaP-RANKL cells or LNCaP-Neo plus LNCaP-RFP cells. We also observed that LNCaP-RANKL cells have a higher expression of OPG and Runx2 but not ATF4 or ALP compared to LNCaP-Neo/LNCaP-RFP cells. We previously identified that OPG and RANK expression was up-regulated along with RANKL overexpression in LNCaP and $ARCaP_E$ cells (data not shown). It is also interesting to find that the Runx2 expression level is higher in LNCaP-RANKL than in LNCaP-Neo even though Runx-2 is an important transcriptional factor involved in osteoblastic differentiation (Komori, 2006; K. Nakashima & de Crombrugghe, 2003). These results explain the increased level of osteoblastic activity observed in bone lesions induced by the co-inoculation of LNCaP-RANKL and LNCaP-RFP cells *in vivo*, likely through the up-regulation of these osteoblastic regulatory genes.

We next examined various cytokine, chemokine, and growth factor expressions using cytokine antibody arrays probed with conditioned media (CM) from parental LNCaP, LNCaP-RANKL,

and co-cultured LNCaP and LNCaP-RANKL cells (Fig. 10B) as well as qRT-PCR array for LNCaP and LNCaP-RANKL cells to indicate the differential production of the soluble factors. Interestingly, the cytokine array revealed an induction of MCP-2 protein, a chemotaxis factor, specifically in the mixed cell co-culture but not in the LNCaP or LNCaP-RANKL CM (Fig. 10C). Its induction may be a result of the inter-reactive cross-talk between LNCaP and LNCaP-RANKL cells. Furthermore, the results from both cytokine antibody and qRT-PCR arrays indicated five categories of soluble factors involved in mediating chemotaxis, bone resorption, bone formation, proteolytic cleavage, and angiogenesis that were up-regulated in LNCaP-RANKL cells (Table 3).

Taken together, these results demonstrate that an increased RANKL level in prostate cancer cells can alter both the production and secretion of chemokines, cytokines and growth factors. These alterations could affect the balance of osteolytic/osteoblastic activities when prostate cancer cells colonize bone. The secreted factors will be further refined, validated and developed as predictive biomarkers for prostate cancer progression. We will also further investigate the role of MCP-2 in osteoblast/osteoclast differentiation.

A.

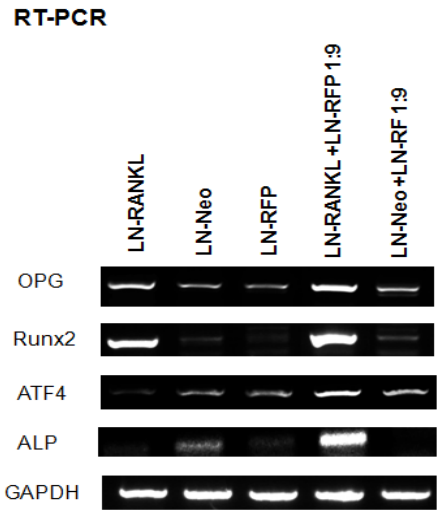

B.

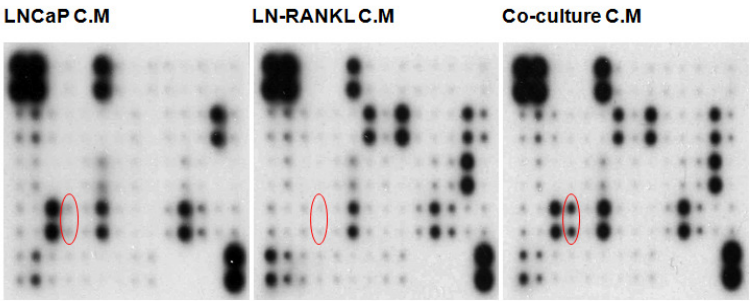

C.

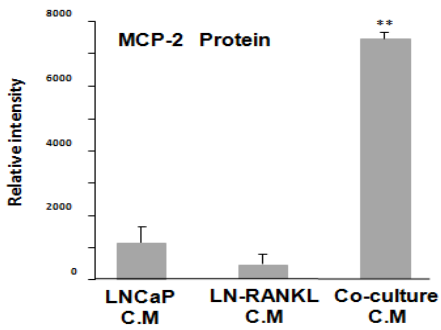

Figure 10. RANKL induced expressional changes of soluble factors associated with prostate cancer progression and mixed bone metastasis. **A.** Co-culture of LNCaP-RANKL and LNCaP-Neo cells with LNCaP-RFP cells at a ratio of 1 to 9 in vitro. The total RNA was extracted for RT-PCR analysis of osteoblastic markers OPG, Runx2, ATF4, and ALP. **B.** Representative RayBio antibody arrays probed with parental LNCaP, LNCaP-RANKL, and LNCaP and LNCaP-RANKL co-cultured conditioned media indicated altered soluble factor production in LNCaP-RANKL as well as co-cultured conditioned media. Red circles indicate a unique MCP-2 induction upon co-culture with the parental LNCaP cells. **C.** Quantification of the increased MCP-2 induction in co-culture. Asterisks indicate statistical significance ($P<0.01$).

Table 3. A selected list of soluble factor production up-regulated in LNCaP-RANKL cells compared to LNCaP-Neo cells. The altered expression was confirmed at the protein level, which is shown in black, and differential expression at the mRNA level is shown in red.

Chemotaxis	Bone Resorption		Bone Formation		Proteolytic Activation		Angiogenesis	
MCP-2	HGF	BMP-3	OPG	FGF-1	TIMP-1	MMP9	VEGF	RANKL
GRO	IL-6	TGFβ1	TIMP-1	FGF-2	uPAR	MMP10	CD40	TNFα
GCP-1	IL-8	RANKL	PDGF-BB	BMP-4	MMP1	Cathepsin K	CD40 ligand	FGF-1/2
GM-CSF		MMP1	Runx2	BMP-5	MMP8		MMP1	TGFβ1
			CTGF				MMP9	CTGF

RANKL Induces Functional cMet Expression and Leads to HGF-Induced cMet Phosphorylation in Prostate Cancer Cells

Interestingly, we further discovered that EMT-inducing RANKL and scatter factor HGF (Chang, Kao, Way, Ho, & Fu, ; Hung et al.) are capable of inducing cMet expression as well as activating downstream cMet signaling through increased levels of phosphorylated cMet in prostate cancer cells. As shown in Figure 11A, exogeneous RANKL and HGF treatments significantly increased cMet expression as well as the phosporylated level of cMet in both LNCaP and $ARCaP_E$ cells, and such induction can be abrogated upon the addition of OPG or anti-HGF antibody. Similarly, RANKL overexpression in LNCaP cells also up-regulated cMet and phosphorylated cMet expression at both the RNA and protein levels (Fig. 11B). As demonstrated by single quantum dot labeling (SQDL), LNCaP-RANKL cells expressed high levels of membrane-bound and cytoplasmic cMet and phosphorylated cMet compared to RANKL-low and cMet-null expressing LNCaP-Neo cells (Fig. 11C). As shown in Fig. 11D, multiplexed QD labeling (MQDL) further illustrated strong co-expression and co-localization of RANKL, c-Met, and p-c-Met on the membrane as well as in the cytoplasm of LNCaP-RANKL cells but was not observed in LNCaP-Neo cells. Moreover, the induced c-Met is biologically functional since the p-c-Met expression increased upon the addition of HGF, and this activation of p-c-Met can be antagonized by anti-HGF monoclonal antibody (Fig. 11E). Promoter reporter assay further confirmed that RANKL treatment or overexpression induced up-regulation of cMet transcriptional activity (Fig. 11F). Up-regulation of cMet and p-c-Met expression level was also observed in histological sections of bone and soft tissue tumors induced by LNCaP-RANKL cells *in vivo* (Fig. 11G).

A.

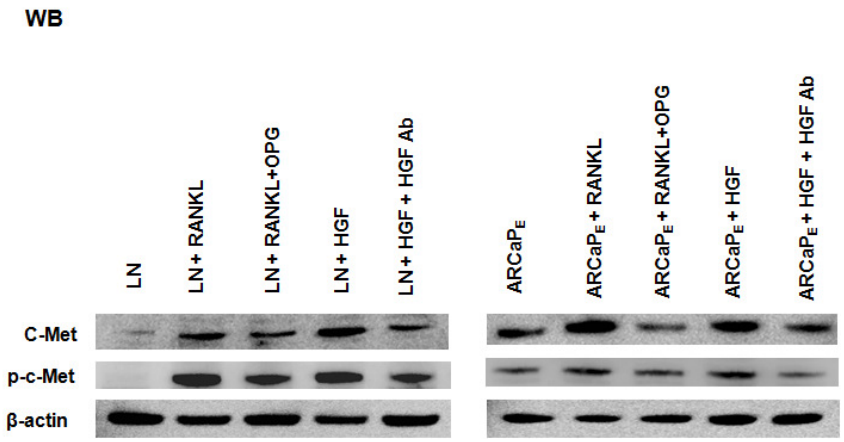
WB
LN
LN+ RANKL
LN+ RANKL+OPG
LN+ HGF
LN+ HGF + HGF Ab
ARCaP$_E$
ARCaP$_E$ + RANKL
ARCaP$_E$ + RANKL+OPG
ARCaP$_E$ + HGF
ARCaP$_E$ + HGF + HGF Ab
C-Met
p-c-Met
β-actin

B.

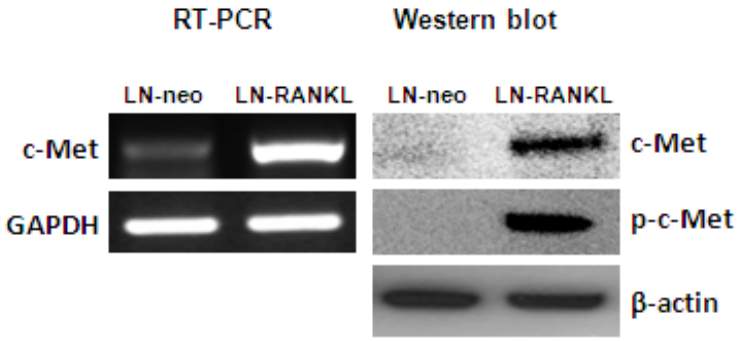
RT-PCR
Western blot
LN-neo
LN-RANKL
LN-neo
LN-RANKL
c-Met
GAPDH
c-Met
p-c-Met
β-actin

C.

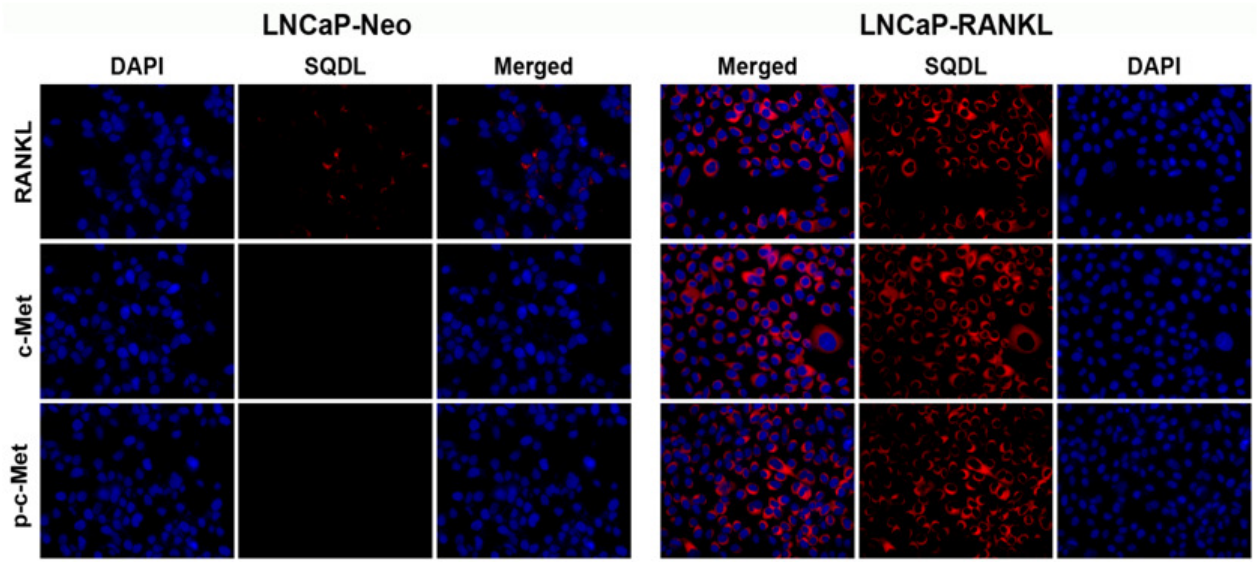
LNCaP-Neo
LNCaP-RANKL
DAPI
SQDL
Merged
Merged
SQDL
DAPI
RANKL
c-Met
p-c-Met

D.

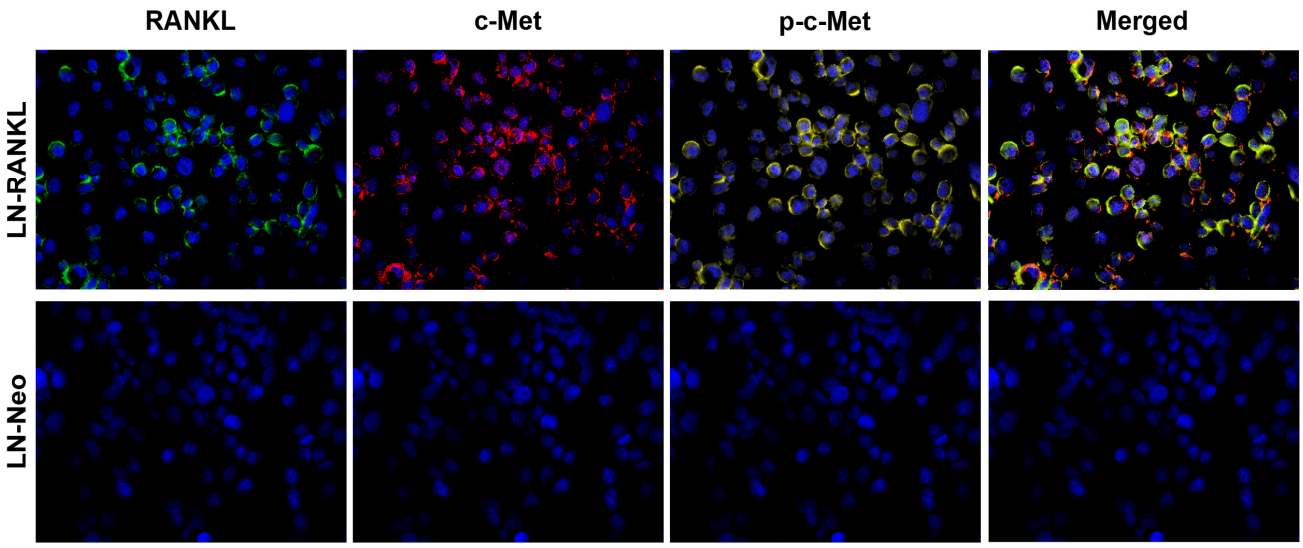
RANKL
c-Met
p-c-Met
Merged
LN-RANKL
LN-Neo

E.

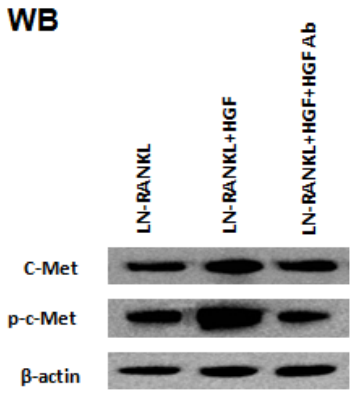
WB
LN-RANKL
LN-RANKL+HGF
LN-RANKL+HGF+HGF Ab
C-Met
p-c-Met
β-actin

F.

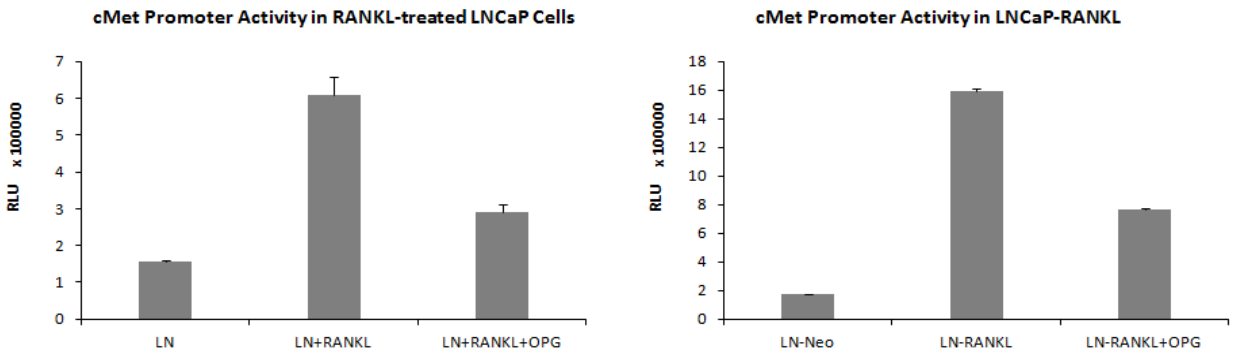
cMet Promoter Activity in RANKL-treated LNCaP Cells
RLU x 100000
0
1
2
3
4
5
6
7
LN
LN+RANKL
LN+RANKL+OPG
cMet Promoter Activity in LNCaP-RANKL
RLU x 100000
0
2
4
6
8
10
12
14
16
18
LN-Neo
LN-RANKL
LN-RANKL+OPG

G.

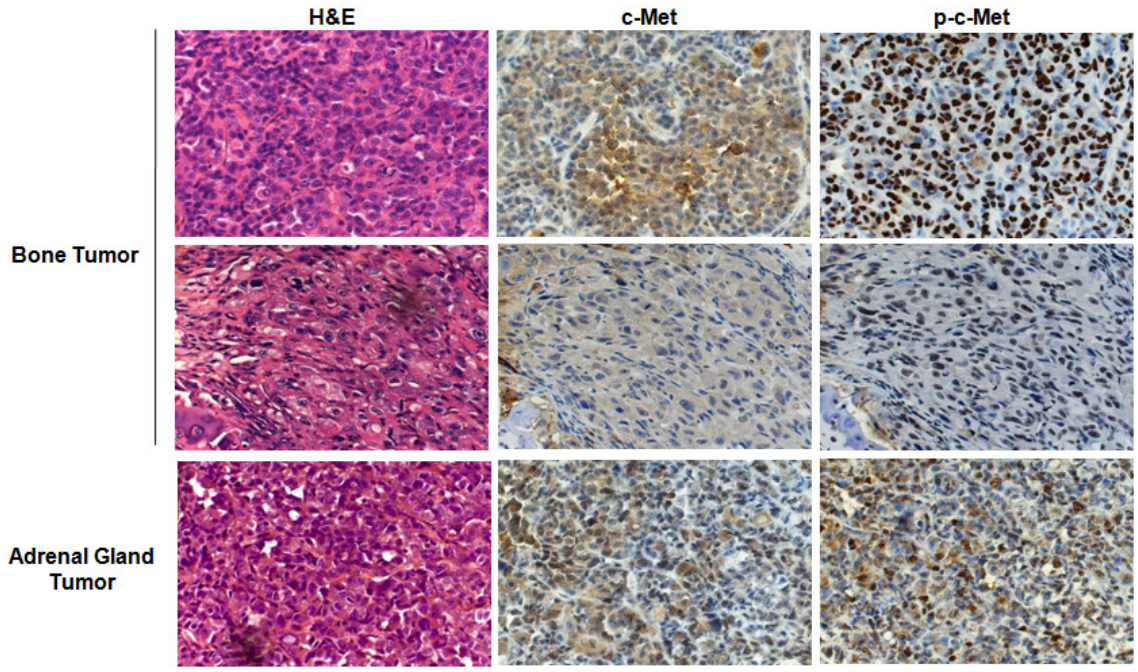

Figure 11. RANKL and HGF induce c-MET expression and phosphorylated levels of c-Met. **A.** RANKL and HGF treatments induced c-Met and p-c-Met expression in LNCaP and $ARCaP_E$ cells detected by western blot analysis. Such induction can be attenuated upon the addition of OPG and HGF neutralizing antibody. **B.** LNCaP-RANKL cells expressed high levels of cMet and phosphorylated cMet at both the RNA and protein levels as detected by RT-PCR and western blot analyses. **C.** Representative images of DAPI and single quantum dot labeling (SQDL) of RANKL, c-Met, and p-c-Met in LNCaP-Neo and LNCaP-RANKL cells as well as overlaid images (40x magnification). **D.** Representative images of multiplexed quantum dot (QD) labeling of RANKL (green), c-Met (red), and p-c-Met (yellow) of LNCaP-RANKL and LNCaP-Neo cells counterstained with DAPI nuclear staining (blue). Individual QD labeled protein expression is first presented alone in pseudocolor followed by a composite image of the superimposed QD signals overlaid with nuclear DAPI staining. Images were acquired using the Cri spectral imaging system at 40x magnification. **E.** RANKL-induced cMet is functional in responding to HGF treatment with increased cMet as well as phosphorylated cMet at protein levels as detected by western blot analysis. **F.** RANKL treatment or overexpression up-regulated cMet transcriptional activity, which can be attenuated by OPG treatment. *, $P<0.05$; **,$P<0.005$ **G.** Representative images of c-Met and p-c-Met IHC staining of LNCaP-RANKL-induced bone and adrenal gland tumors.

Discussion

We examined the metastatic and osteolytic potential of LNCaP-RANKL and ARCaP$_E$-RANKL cells *in vivo* following intracardial inoculation to male athymic nude mice. We observed that both LNCaP-RANKL and ARCaP$_E$-RANKL cells induced a high incidence of both bone and soft tissue metastases, which could be observed at two months after the injections, while LNCaP-Neo cells failed to produce any tumor or metastasis and ARCaP$_E$-Neo cells failed to form any bone metastasis (Table 1 and Fig. 6A). Mice bearing either LNCaP-RANKL or ARCaP$_E$-RANKL cells demonstrated extensive osteolytic lesions in the skeleton but not mice bearing LNCaP-Neo and ARCaP$_E$-Neo cells (Fig. 6B). Both bone and soft tissue metastases dissected from mice bearing the LNCaP-RANKL cells expressed the EMT phenotype with high expression of the mesenchymal markers N-cadherin and vimentin and low expression of the epithelial marker E-cadherin (Fig. 6C). Moreover, RANKL expression exhibited heterogeneity in subsets of the metastatic tumor cells, indicating a mixed population of LNCaP-RANKL cells and RANKL non- or low-expressing cells residing in the metastatic tumors. Importantly, the histomorphology suggested that a small number of RANKL-expressing cells may be sufficient to induce bone metastases in the presence of bystander RANKL non- or low-expressing cells, implicating the important function of RANKL in contributing to overall bone and soft tissue metastases irrespective of the basal steady-state level of RANKL expression. With RANKL overexpression, all of the bone metastases were expected to be highly osteolytic with severe degradation of the bones shown by both μCT demonstrations (Fig. 6B) as well as the high level of TRAP-positive staining of dissected tumors (Fig. 6D). Several studies showed that LNCaP cells are highly indolent and non-metastatic for both intracardial and intraosseous inoculations in the nude mice model, but they are capable of inducing osteoblastic or mixed lesions in the SCID

mouse model after intratibial injection (Corey et al., 2002; Fisher et al., 2002; Wu et al., 1998). Therefore, our animal model is to our knowledge the first to show that intracardial inoculation of LNCaP cells overexpressing RANKL can promote EMT progression and bone metastases. RANKL confers the malignant and metastatic potential of LNCaP cells to home to the bone, leading to predominantly osteolytic lesions. Even though the majority of prostate cancer patients develop osteoblastic bone metastasis, there is also considerable evidence of tumor-induced osteoclastic bone resorption as an initial and a constant event, leading to overall elevated bone remodeling, since these two processes are mechanistically coupled. In our animal models where RANKL is overexpressed by the prostate cancer cells, the balance is completely tilted towards to the osteolytic phenotype of bone metastases.

However, the underlying mechanism of RANKL-induced bone metastasis is not yet clear. One potential mechanism may be explained by the 'seed and soil' theory where RANK expressing osteoclast precursors present in the bone microenvironment attract the circulating RANKL expressing tumor cells in the bloodstream to land in bone, resulting in the activation of osteoclast maturation followed by increased resorption. This results in the release of a plethora of growth factors richly stored in the bone, which can further activate the surrounding prostate cancer cells to express more RANKL in a paracrine fashion. Subsequently, increased RANKL expression can further stimulate RANKL expression by the prostate cancer cells in an autocrine manner, leading to a vicious cycle.

Since LNCaP-RANKL cells provoked osteoclastogenesis in mouse skeleton, we further tested the hypothesis that these characteristics of LNCaP-RANKL cells may facilitate the growth and colonization of otherwise non-tumorigenic, non-metastatic and RANKL-null LNCaP cells. We provided evidence that small numbers of RANKL-expressing prostate cells are capable of

conferring tumorigenicity to RANKL-low or-null expressing prostate cancer cells *in vivo*. As low as one thousand LNCaP-RANKL cells are sufficient to facilitate the growth of LNCaP-RFP tumors in mouse skeleton and soft tissues. Bigger tibial tumors with more intensified RFP signals were detected in chimeric tumors consisting of an increasing number of LNCaP-RANKL cells. This further implies that the RANKL-expressing LNCaP cells augmented the tumorgenic potential of RANKL-non expressing LNCaP-RFP cells in the tumor microenvironment (Fig. 7). We also discovered that RANKL-expressing prostate cancer cells promoted co-colonization of RANKL-non-expressing and non-metastatic prostate cancer cells to metastatic sites. Intracardial co-inoculation of LNCaP-RANKL cells and LNCaP-RFP at a ratio of 9 to 1 or 1 to 9 significantly increased the metastatic incidence compared to intracardial co-inoculation of LNCaP-Neo plus LNCaP-RFP cells, which failed to form any metastasis *in vivo* (Table 2). *Ex vivo* imaging of bone and soft tissue tumors as well as histological examinations of frozen and paraffin-embedded tumor sections all displayed red fluorescent signals, revealing the presence of LNCaP-RFP cells at the metastatic sites. Similar observations were also made in bone and soft tissue tumors when LNCaP-RFP cells were injected intracardially in mice harboring LNCaP-RANKL cells in the skeleton. Interestingly, fluorescent imaging also showed that intracardial inoculation of LNCaP-RANKL cells in mice harboring LNCaP-RFP cells in the tibial bone induced skeletal tumor formation by these non-tumorigenic LNCaP-RFP cells, as a strong intensity of red fluorescent signaling was detected in the tibial tumor (Fig. 8). These experiments together demonstrated unequivocally the ability of non-tumorigenic or "dormant" LNCaP-RFP cells to participate in tumorigenesis and metastases to bone and soft tissues in the presence of LNCaP-RANKL cells. In addition, QD labeling results revealed that the number of LNCaP-RFP cells colonized to the bone corresponds with the proportion of co-inoculated LNCaP-RFP cells in

mice. We also observed that RANKL expression in LNCaP-RANKL induced bone tumors is heterogeneous, indicating the possibility that RANKL expression can be switched on/off by the prostate cancer cells depending on the surrounding microenvironment. Moreover, we discovered that the colonized LNCaP-RFP cells in bone tumors also express high or moderate levels of RANKL as indicated by the co-localization (yellow) of RANKL (green) and RFP (red) labeling (Fig. 10D), suggesting the induction of RANKL expression in RFP-tagged LNCaP cells by RANKL-expressing LNCaP cells, which do not express RFP. Since co-inoculation of LNCaP-Neo plus LNCaP-RFP cells failed to form tumor or metastasis in mouse skeleton, this result further implies that the RANKL-expressing LNCaP cells can "reawaken" dormant LNCaP-RFP cells, leading to their participation in tumorigenesis and metastasis possibly through the induction of RANKL expression. Such an observation might also be well explained by the 'seed and soil' theory where the disseminated LNCaP-RANKL cells initially create a favorable environment by inducing osteolytic lesions in the bone, leading to the release of growth factors and cytokines that subsequently allow the circulating and presumably dormant LNCaP-RFP cells to colonize and grow at the bone sites.

We further observed that co-culture of RANKL-expressing and RANKL-low-expressing prostate cancer cells induced increased osteoblastic activity *in vitro* and mixed osteolytic and osteoblastic lesions *in vivo*. Since LNCaP-RANKL cells induced predominately osteolytic reactions in mouse skeleton, we examined whether mixed osteolytic/osteoblastic reactions can be provoked by the co-presence of RANKL-high-expressing and –low-expressing LNCaP cells. Osteoblastogenesis and osteoclastogenesis assays *in vitro* showed that LNCaP-RANKL cells induced predominately osteoclast differentiation with low levels of osteoblast mineralization while LNCaP-Neo or LNCaP-RFP cells either cultured alone or together with LN-RANKL cells produced

substantially increased osteoblast mineralization (Fig. 9A). These results are in agreement with the 3D μCT scans of representative chimeric tumors composed of intracardial 1 to 9 or 9 to 1 ratios of LNCaP-RANKL and LNCaP-RFP cells, intratibial LN-RANKL plus intracardial LN-RFP cells, or intratibial LNCaP-RANKL plus LNCaP-RFP cells, which all displayed mixed osteolytic and osteoblastic lesions in the bone (Fig. 9C). TRAP staining of mature osteoclast lining (red) and orange G staining of new bone formation (yellow orange) in bone tumor were observed in the chimeric tumors co-inoculated with LN-RANKL and LN-RFP cells in nude mice (Fig. 9D). Alternative evidence of the increased level of osteoblastic activity in the tumors induced by the co-inoculation of LN-RANKL and LN-RFP cells is illustrated by detecting the osteoid formation/thickness using Trichrome staining (Fig. 9E). The osteoid stained in red, and the mineralized bone stained in turquoise. The level of osteoid formation and thickness can reflect the level of bone formation (Ott, 2008). Moreover, co-culture of LNCaP-RANKL and LNCaP-RFP cells *in vitro* further demonstrated elevated expression of important osteoblastic regulatory genes, such as OPG, Runx2, ALP, and ATF4, as well as a chemotactic factor, MCP-2, which is specifically induced in the mixed cell co-culture (Fig. 10A-C). Analyses from Cytokine Antibody array as well as qRT-PCR array generated an expression profile of regulatory factors involved in chemotaxis, bone resorption, bone formation, proteolytic cleavage, and angiogenesis that are elevated in RANKL-expressing LNCaP cells (Table 3). These results demonstrated that increased RANKL levels in prostate cancer cells can alter the production of chemokines, cytokines, and growth factors, and such alterations can directly affect the progression of prostate cancer cells as well as the balance of osteolytic and osteoblastic activities when prostate cancer cells colonize the bone.

We further discovered a previously unrecognized forward feedback loop in which RANKL-c-Met signaling converges. RANKL expression induced both RANKL and c-Met expression by prostate cancer cells (Fig. 11). RANKL or HGF treatment of LNCaP and $ARCaP_E$ cells demonstrated an up-regulated expression of cMet as well as phosphorylated level of p-c-Met. Similar results were also observed in LNCaP-RANKL cells at both the RNA and protein levels. The RANKL and c-Met expressed by prostate cancer cells are both biologically functional as evidenced respectively by increased osteoclastogenesis (Fig. 4) and phosphorylation of c-Met when RANKL-expressing prostate cancer cells are exposed to mononuclear osteoclasts in co-culture or exogenous recombinant HGF (Fig. 11).

We observed that the extent of osteolysis can be switched from osteolytic to osteoblastic depending on the proportion of RANKL-positive and RANKL-negative prostate cancer cells used in the mixed populations. For example, using LNCaP-RANKL cells as a model, we showed that a small number of LNCaP-RANKL expressing cells are sufficient to induce bone metastases in the presence of bystander RANKL non- or low-expressing cells. Importantly, histology showed that both RANKL-expressing and low-expressing cells reside in the bone metastasis tumors, suggesting the important function of RANKL in contributing to overall bone metastases irrespective of the basal steady-state level of RANKL expression. Since RANKL low and non-expressing LNCaP cells failed to form tumors in mice without the co-presence of RANKL-positive LNCaP cells, we believe that RANKL is an important factor activating the "dormancy" of prostate cancer cells to form tumors in mouse bone. This well explains the clinical observation of cancer dormancy in which prostate cancer cells are often found in the bone but fail to colonize the bone (Aguirre-Ghiso, 2007). In the presence of RANKL-positive LNCaP cells, RANKL low or non-expressing prostate cancer cells participated in bone

colonization. RANKL-c-Met signaling converges, whereby RANKL expression induces both RANKL and c-Met expression by prostate cancer cells, further committing them to EMT progression and metastasis. These results have important clinical implications in which further justify the targeting of RANKL as an effective therapeutic approach for human prostate cancer bone metastasis targeting not only existing tumors but also preventing the activation of tumor dormancy.

CHAPTER 5 RANKL STIMULATED AN AUTOCRINE FEED-FORWARD INDUCTION OF RANKL EXPRESSION MEDIATED BY C-MYC/MAX TRANSACTIVATION IN PROSTATE CANCER CELLS

Introduction

RANKL expression can be positively and negatively regulated by many hormones and growth factors, such as PTH, PTHrP, prostaglandin E2, estradiol, glucocorticoids, testosterone, vitamin D3 ($1\alpha,25(OH)_2D_3$), and progesterone/progestin as well as by several cytokines, such as IL-1, IL-6, IL-7, IL-17, and TNF-α, (Anandarajah, 2009; Theoleyre et al., 2004) through various molecular mechanisms. These RANKL-stimulating factors can be secreted by bone cells and certain tumor cells, including breast and prostate cancer cells, which have high propensity to invade bone and cause skeletal complications and metastases (Mundy, 2002). Recently, we have identified that both exogenous and endogenous RANKL can induce RANKL expression in an autocrine feed-forward manner in prostate cancer cells but not in normal cells. Blocking the source of RANKL using RANKL natural decoy receptor, OPG, can attenuate the up-regulated RANKL expression at both the RNA and protein levels. The augmented RANKL has been shown to be biologically functional in increasing *in vitro* osteoclastogenesis. Moreover, since prostate cancer cells express both RANKL and its receptor RANK (Armstrong et al., 2008; Chen et al., 2006; Jones et al., 2006; Odero-Marah et al., 2008; Zhang et al., 2001), the autocrine induction of RANKL in prostate cancer cells allows EMT progression and enhanced metastatic potential, demonstrated by increased *in vitro* migration, invasion, and tumorigenic activities as well as enhanced *in vivo* bone and soft tissue metastases. Therefore, it is crucially important to unravel the molecular mechanism of RANKL-induced autocrine regulation. In this study, we investigated the transcriptional regulation of RANKL expression using a 2.5kb RANKL

promoter reporter to identify the important transcription factor(s) involved in RANKL-induced autocrine feed-forward activation.

Results

Validation of 2.5kb Human RANKL Promoter Activity in Human Osteosarcoma and Prostate Cancer Cells

We previously determined that RANKL is capable of inducing its own expression in prostate cancer cells through an autocrine feed-forward regulation. In order to study the transcriptional regulation of RANKL gene expression, we constructed a 2.5kb human RANKL promoter amplified from a BAC clone containing the 5' upstream promoter region of RANKL using PCR. We first sought to validate the 2.5kb RANKL promoter reporter activity in human osteoblastic osteosarcoma, SaOS-2 cells stimulated with osteotropic factors, such as PTH and vitamin D_3 (Anandarajah, 2009; Theoleyre et al., 2004), which are known to stimulate RANKL expression in osteoblasts. The RANKL promoter activity was increased in SaOS-2 cells by approximately 3 fold upon treatment with 10 nM of PTH or 20 nM of vitamin D_3 (Fig. 12A). We further examined the RANKL transcriptional activity in prostate cancer $ARCaP_M$, $ARCaP_E$, LNCaP, C4-2, and PC3 cells as well as in SaOS-2 cells as a positive control. We found that RANKL promoter activity was much higher in PC3 and $ARCaP_M$ cells, which are known to express high levels of RANKL, compared to RANKL-low expressing $ARCaP_E$, LNCaP, or C4-2 cells (Fig. 12B). This finding therefore correlates with the endogenous level of RANKL expression in these prostate cancer cells detected by either RT-PCR or by western blot analyses in the previous results (Fig. 1B).

A.

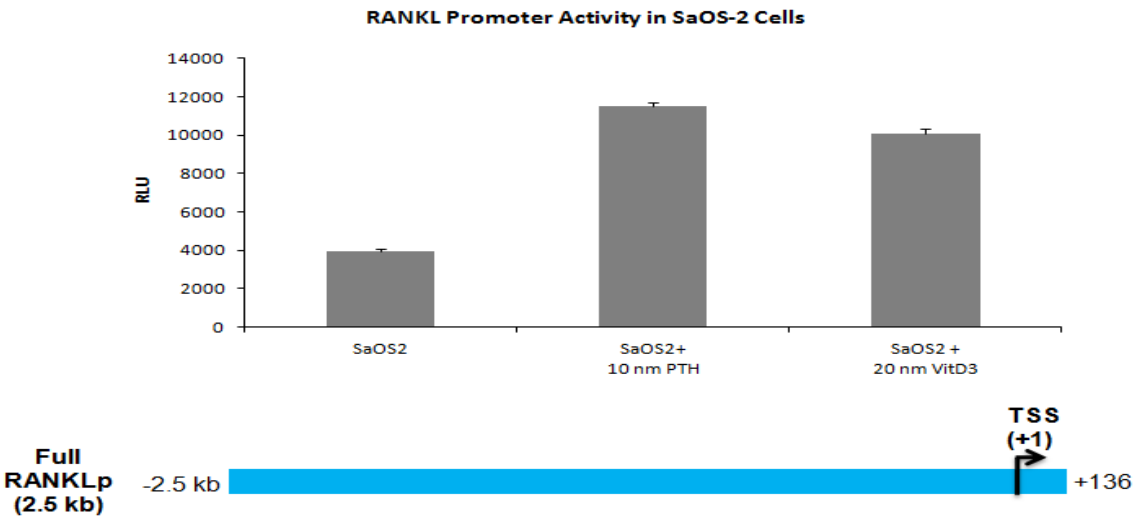

B.

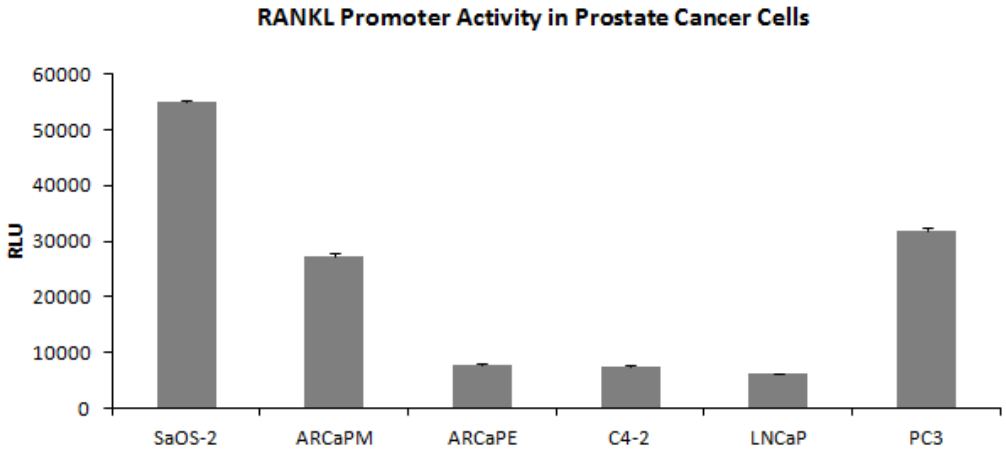

Figure 12. RANKL promoter (2.5Kb) activity in human osteosarcoma and prostate cancer cells. **A.** The 2.5Kb RANKL promoter was introduced into human osteosarcoma SaOS-2 cells to examine RANKL basal promoter activity as well as the stimulated promoter activity by exogenous treatments with PTH and vitamin D_3. **B.** RANKL promoter activity was examined in prostate cancer $ARCaP_E$, $ARCaP_M$, LNCaP, C4-2, and PC3 cells and compared to osteosarcoma SaOS-2 cells as a positive control. * , *$p<0.05$*

RANKL Induced an Autocrine Feed-forward Induction of RANKL Expression in Prostate Cancer Cells

We discovered that exogenous RANKL treatment can induce endogenous RANKL expression in prostate cancer cells, such as $ARCaP_E$ and LNCaP cells, which express low levels of RANKL. Treatment of $ARCaP_M$ cells with OPG can decrease the RANKL production by $ARCaP_M$ cells at both the RNA and protein levels (Fig. 13A). We also introduced the RANKL promoter to the ARCaP cell model to examine RANKL transcriptional activity upon treatment with RANKL, OPG or RANKL plus OPG. We found that RANKL promoter activity is consistent with the biochemical data where RANKL treatment induced a significant induction of RANKL transcriptional activity in both $ARCaP_E$ and $ARCaP_M$ cells. Such increased RANKL promoter activity can be attenuated upon exposure to OPG. Furthermore, treating $ARCaP_M$ cells with OPG resulted in a reduction in RANKL promoter activity, but OPG treatment has minimal effect on RANKL transcription in $ARCaP_E$ cells (Fig. 13B). Similarly, RANKL promoter activity was greatly activated upon RANKL treatment but addition of OPG decreased the RANKL-induced RANKL transcriptional activity in LNCaP cells (Fig. 13C).

We also examined the RANKL promoter activity in RANKL-overexpressing LNCaP and $ARCaP_E$ cells to further confirm the RANKL autocrine activation. As shown by Figure 13D and 13E, endogenous RANKL overexpression greatly up-regulated RANKL promoter activity by approximately 8 fold compared to Neo controls in both LNCaP and $ARCaP_E$ cells, and exposure to OPG decreased the RANKL promoter activity in these cells. RANKL promoter activity was not affected by OPG treatment in LNCaP-Neo and $ARCaP_E$-Neo cells.

A.

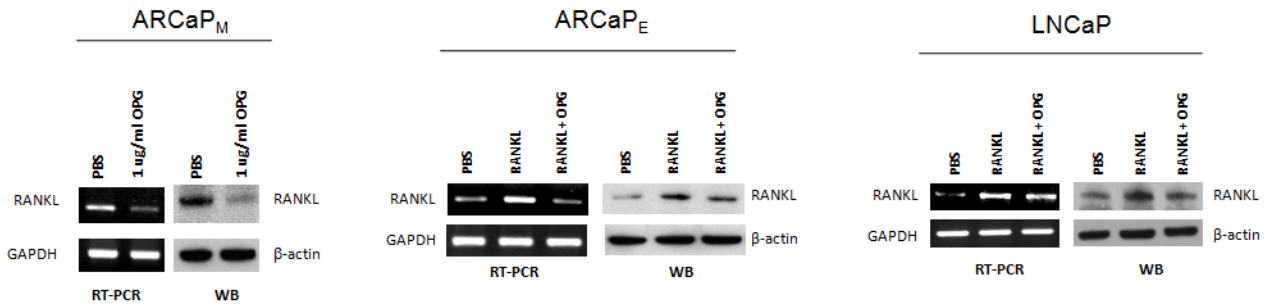
ARCaP$_M$
ARCaP$_E$
LNCaP
PBS
1 ug/ml OPG
RANKL
RANKL+OPG
RANKL
GAPDH
β-actin
RT-PCR
WB

B.

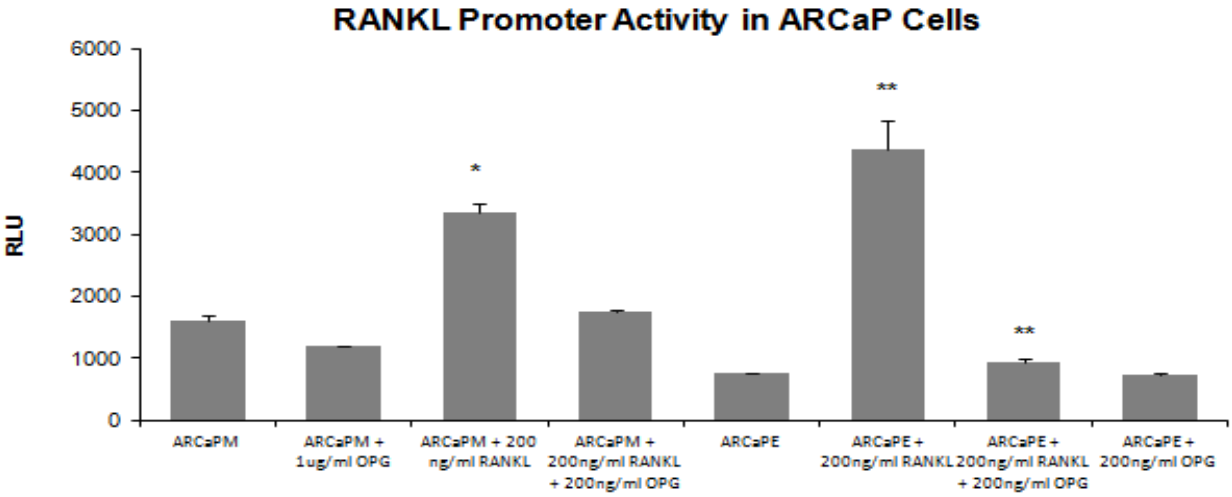
RANKL Promoter Activity in ARCaP Cells
RLU
6000
5000
4000
3000
2000
1000
0
*
**
**
ARCaPM
ARCaPM + 1ug/ml OPG
ARCaPM + 200 ng/ml RANKL
ARCaPM + 200ng/ml RANKL + 200ng/ml OPG
ARCaPE
ARCaPE + 200ng/ml RANKL
ARCaPE + 200ng/ml RANKL + 200ng/ml OPG
ARCaPE + 200ng/ml OPG

C.

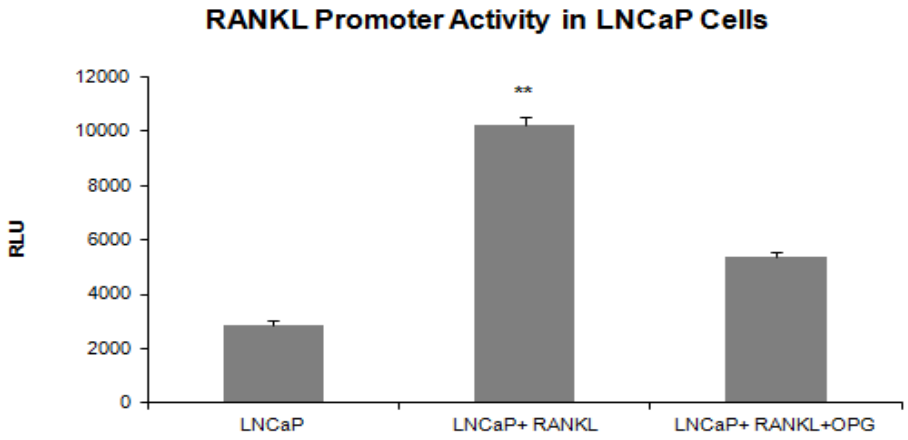
RANKL Promoter Activity in LNCaP Cells
RLU
12000
10000
8000
6000
4000
2000
0
**
LNCaP
LNCaP+ RANKL
LNCaP+ RANKL+OPG

D.

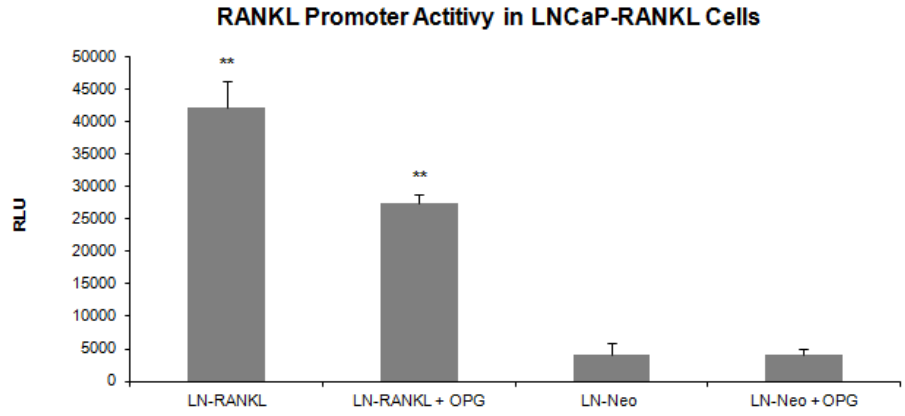

E.

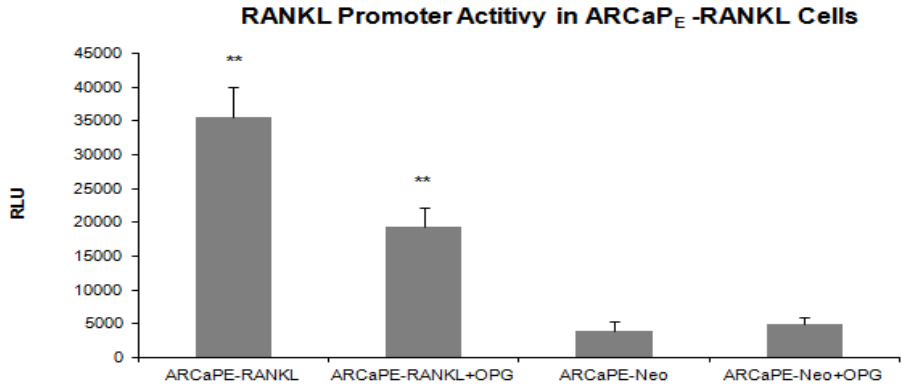

Figure 13. RANKL induced an autocrine feed-forward induction of RANKL expression in prostate cancer cells. **A.** RANKL treatment up-regulated RANKL expression at both mRNA and protein levels in $ARCaP_E$ and LNCaP cells, which can be attenuated upon addition of OPG. RANKL expression in $ARCaP_M$ cells can be down-regulated by the addition of 1 ug/ml of OPG. **B.** Corresponding results were also observed using a RANKL promoter reporter assay in which RANKL promoter activity was induced by RANKL treatments in $ARCaP_E$ and $ARCaP_M$ cells. OPG treatment could dampen the RANKL promoter activity in $ARCaP_M$ cells and abolish the RANKL autocrine induction. **C.** RANKL autocrine induction was also observed in LNCaP cells as demonstrated by RANKL promoter reporter assay. RANKL promoter activity was significantly up-regulated in **D.** LNCaP-RANKL and **E.** $ARCaP_E$-RANKL cells compared to Neo controls of both cell types, and OPG treatment attenuated the increased RANKL promoter activity in both LNCaP-RANKL and $ARCaP_E$-RANKL cells * , $p<0.05$*; ***, $p<0.005$.

Identification of the cMyc Binding Motif within the -1884 and -1384 Region of RANKL Promoter that Mediates the RANKL Autocrine Feed-forward Induction by RANKL

We discovered that RANKL is capable of inducing its own expression in prostate cancer cells. We next further identified the *cis*-acting element(s) in the RANKL promoter region that are responsible for RANKL autocrine transcriptional regulation using a promoter deletion study. We first generated five deletion mutants of the 2.5 kb RANKL promoter: D1 (deletion from -2383 to -1884), D2 (deletion from -1884 to -1384), D3 (deletion from -1384 to -884), D4 (deletion from -884 to -384), and D5 (deletion from -384 to -101) (Fig. 14A). We transfected these five deletion constructs as well as the full-length promoter into RANKL-expressing LNCaP-RANKL cells and RANKL-low or –non-expressing LNCaP-Neo cells. As shown in Figure 14B, full-length RANKL promoter activity was significantly induced in LNCaP-RANKL cells but not in the LNCaP-Neo cells, and among the five deletion constructs only the D2 deletion construct (-1884 to -1384) abolished RANKL promoter activity in LNCaP-RANKL cells. However, the basal promoter activity was very minimal and remained unchanged for these RANKL deletion mutants in the LNCaP-Neo cells. These results suggested that the potential *cis*-acting element mediating the RANKL-induced autocrine regulation might reside at region D2 between -1884 and -1384 of the RANKL promoter.

We next tried to characterize the precise *cis*-acting element(s) within the 500-bp D2 region (-1884 and -1384) of the RANKL promoter. Database searching revealed two putative *cis*-acting elements in the D2 region: the CRE binding site (-1177~-1184) and the cMyc/Max binding site (-1372~-1384) (Fig. 14C). We subsequently generated the respective CRE and cMyc deletion mutants, and we transfected the D2, CRE, and cMyc deletion mutants as well as the full-length promoter to examine their luciferase reporter activities in LNCaP-RANKL and LNCaP-Neo cells.

Consistently, RANKL overexpression greatly induced RANKL promoter activity in LNCaP cells but such induction was abolished upon deletion of the 500-bp D2 region of the promoter (Fig. 14D). The cMyc/Max deletion construct completely abolished RANKL basal promoter activity in LNCaP-RANKL cells but not by the CRE deletion mutant. Similar results were also observed for the promoter activities of the CRE and cMyc/Max deletion mutants in LNCaP cells treated with RANKL (Fig. 14E). The RANKL promoter activity was not significantly changed by the deletion mutants in LNCaP-Neo and LNCaP cells. Taken together, these data demonstrated that the cMyc/Max binding site within the RANKL promoter region is important for RANKL promoter activity regulated by RANKL autocrine induction.

A.

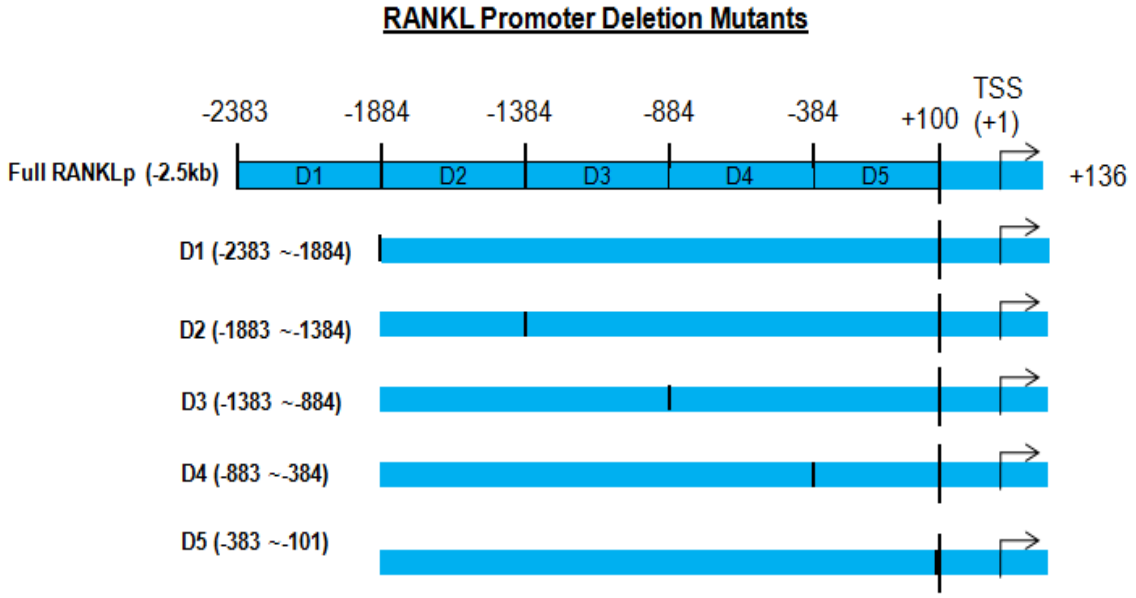
RANKL Promoter Deletion Mutants
-2383
-1884
-1384
-884
-384
+100
TSS
(+1)
Full RANKLp (-2.5kb)
D1
D2
D3
D4
D5
+136
D1 (-2383 ~-1884)
D2 (-1883 ~-1384)
D3 (-1383 ~-884)
D4 (-883 ~-384)
D5 (-383 ~-101)

B.

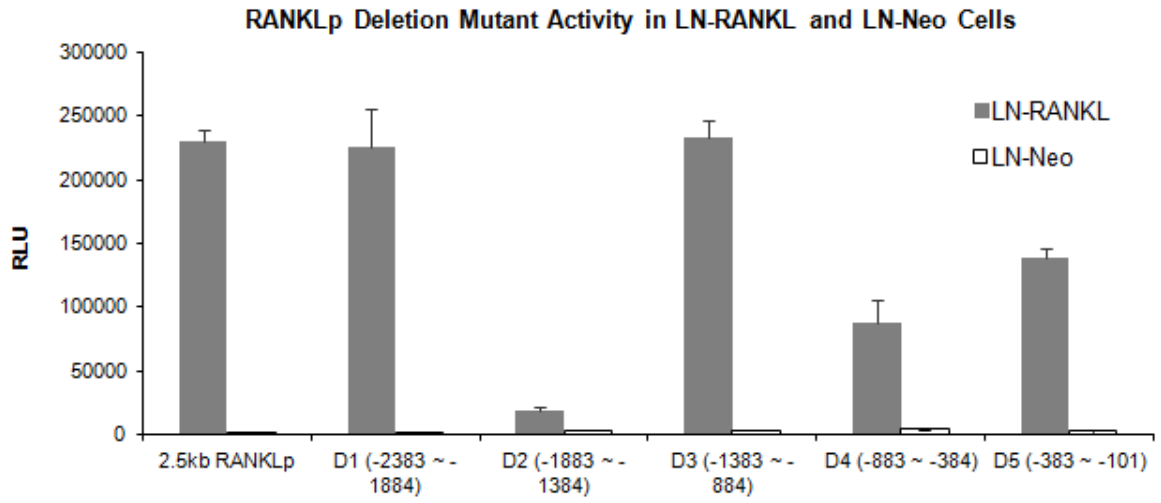
RANKLp Deletion Mutant Activity in LN-RANKL and LN-Neo Cells
RLU
300000
250000
200000
150000
100000
50000
0
LN-RANKL
LN-Neo
2.5kb RANKLp
D1 (-2383 ~ -1884)
D2 (-1883 ~ -1384)
D3 (-1383 ~ -884)
D4 (-883 ~ -384)
D5 (-383 ~ -101)

C.

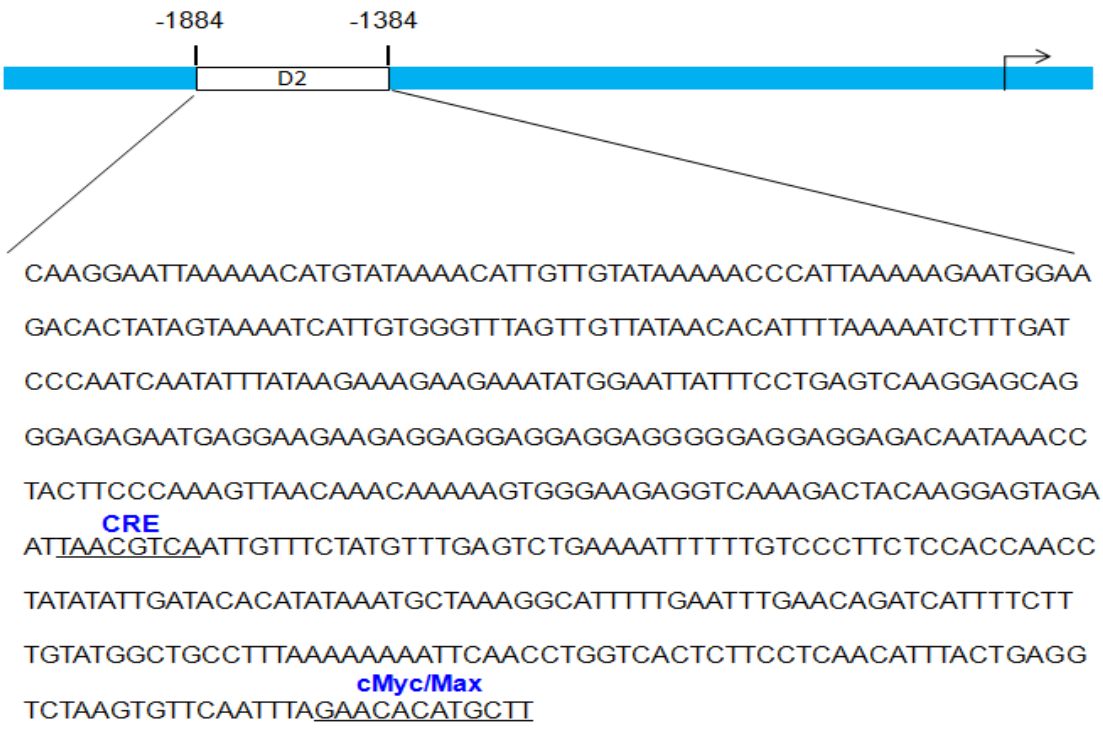
-1884
-1384
D2
CAAGGAATTAAAAACATGTATAAAACATTGTTGTATAAAAACCCATTAAAAAGAATGGAA
GACACTATAGTAAAATCATTGTGGGTTTAGTTGTTATAACACATTTTAAAAATCTTTGAT
CCCAATCAATATTTATAAGAAAGAAGAAATATGGAATTATTTCCTGAGTCAAGGAGCAG
GGAGAGAATGAGGAAGAAGAGGAGGAGGAGGAGGGGGAGGAGGAGACAATAAACC
TACTTCCCAAAGTTAACAAACAAAAAGTGGGAAGAGGTCAAAGACTACAAGGAGTAGA
CRE
ATTAACGTCAATTGTTTCTATGTTTGAGTCTGAAAATTTTTTGTCCCTTCTCCACCAACC
TATATATTGATACACATATAAATGCTAAAGGCATTTTTGAATTTGAACAGATCATTTTCTT
TGTATGGCTGCCTTTAAAAAAAATTCAACCTGGTCACTCTTCCTCAACATTTACTGAGG
cMyc/Max
TCTAAGTGTTCAATTTAGAACACATGCTT

D.

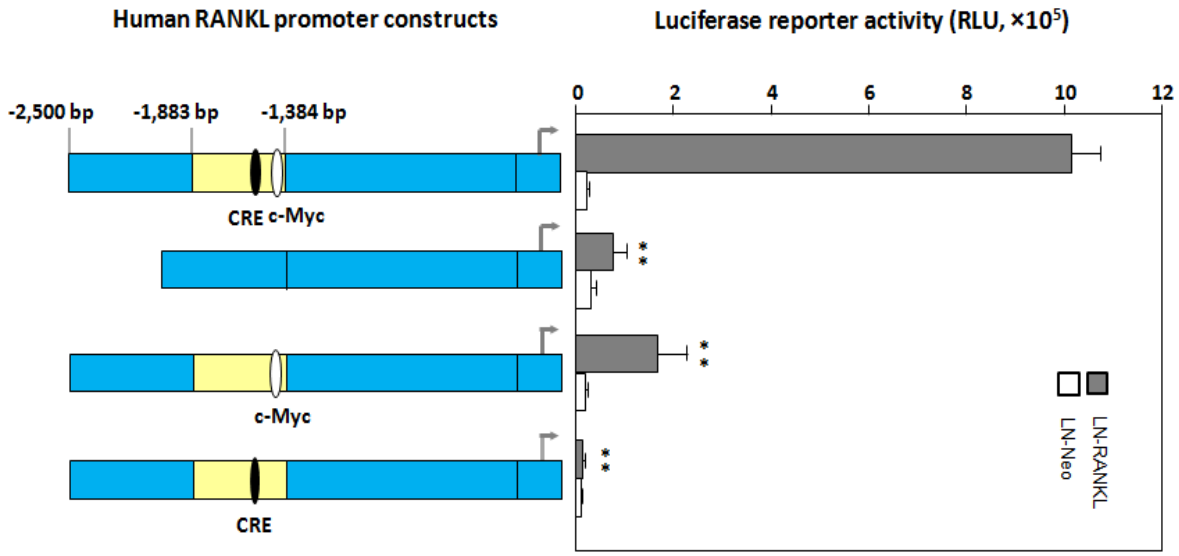
Human RANKL promoter constructs
Luciferase reporter activity (RLU, ×10^5)
-2,500 bp
-1,883 bp
-1,384 bp
CRE c-Myc
c-Myc
CRE
0
2
4
6
8
10
12
LN-Neo
LN-RANKL

E.

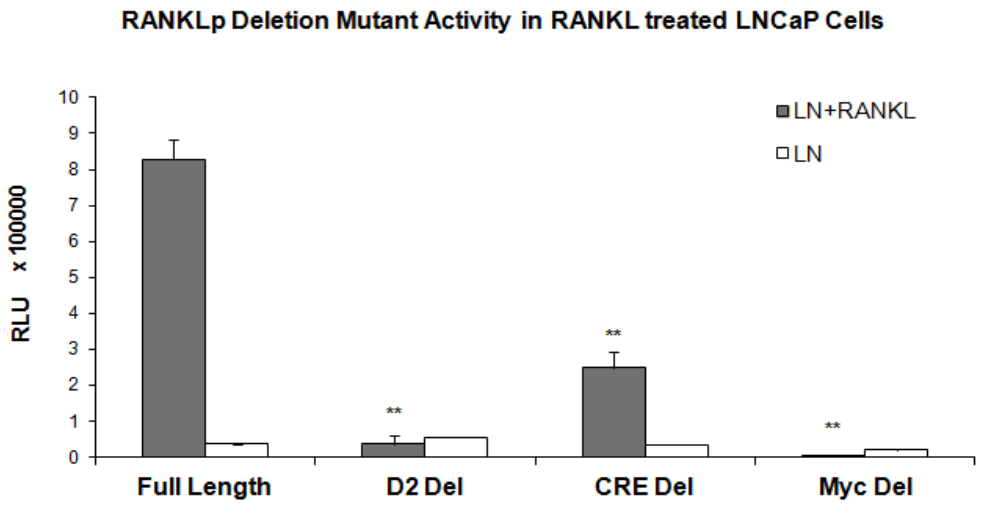

Figure 14. Identification of the cMyc binding motif within the -1884 and -1384 region of RANKL promoter that mediates the RANKL autocrine feed-forward induction by RANKL. **A.** Diagram of RANKL full promoter construct and deletion mutants, D1 deleted from -2383 to -1884, D2 deleted from -1884 to -1384, D3 deleted from -1384 to -884, D4 deleted from -884 to -384, and D5 deleted from -384 to -101. **B.** The transcriptional activities of these RANKL promoter deletion mutants were examined in LNCaP-RANKL and LNCaP-Neo cells. D2 mutant showed a significant reduction of RANKL transcriptional activity to a minimal level in LNCaP-RANKL cells, and all deletion mutants showed minimal responsiveness in LNCaP-Neo cells. **C.** The DNA sequence of D2 region (500bp) within the RANKL promoter (-1884~-1384). CRE (-1177~-1184) and cMyc/Max (-1372~-1384) binding sites were identified within the D2 region (underlined). **D.** The full length RANKL promoter and D2, CRE, and cMyc/Max deletion mutants were examined for their RANKL transcriptional activity in LNCaP-RANKL and LNCaP-Neo cells or **E.** in LNCaP cells treated with or without RANKL. The RANKL transcriptional activity was significantly inhibited with the cMyc/Max deletion mutant in LNCaP-RANKL and RANKL-treated LNCaP cells. **, $p<0.005$.

RANKL Autocrine Activation Is Mediated through Direct Interaction of cMyc to Its *cis*-acting Binding Element within the RANKL Promoter Region in Prostate Cancer Cells

We next wanted to further validate whether cMyc transcription factor is the key protein mediating RANKL-induced autocrine gene regulation in prostate cancer cells. We therefore conducted ChIP analysis to investigate the *in vivo* interaction between nuclear cMyc and its binding *cis*-acting elements in RANKL-treated and RANKL-overexpressing LNCaP cells in the presence or absence of OPG. The binding of cMyc to the chromatin was detected by PCR amplification of the cMyc binding region within the RANKL promoter using the original protein-DNA complexes (input) and anti-cMyc- or anti-rabbit IgG immunoprecipitated DNA-protein complexes as templates. As shown in Fig. 15A, no cMyc amplified PCR product was detected in either LNCaP or LNCaP-Neo cells whereas the levels of cMyc PCR product were greatly increased in LNCaP cells treated with RANKL or in LNCaP-RANKL cells, and the level of cMyc amplification was decreased upon OPG treatment of these cells. In addition, using quantitative real-time PCR as readouts, we observed that RANKL significantly increased the binding of cMyc transcription factor to its binding site within the RANKL promoter region by 20-fold and 8-fold in LNCaP-RANKL and RANKL-treated LNCaP cells, respectively. OPG treatment attenuated the interaction of cMyc with its binding site by 13-fold in LNCaP-RANKL cells and by 4-fold in LNCaP cells treated with RANKL (Fig. 15B). Furthermore, activation of the cMyc target gene requires direct binding of cMyc/Max heterodimers to the consensus binding sites containing the E-box box sequence (CACGTG) within the promoter sequence (Walhout, Gubbels, Bernards, van der Vliet, & Timmers, 1997).

To further determine whether there is a direct binding of cMyc/Max heterodimer to its binding motif within the RANKL promoter, we performed an electrophoretic mobility shift assay

(EMSA) using non-invasive biotin-labeled cMyc/Max oligonucleotides as probes and detecting the formation of DNA-protein complexes. One band indicating the DNA-protein complex was detected on gel after the nuclear extracts from LNCaP-RANKL or RANKL-treated LNCaP cells were incubated with the probes. The band was absent in the presence of a 400-fold excess of unlabeled probes as competitors, suggesting that the binding of cMyc/Max oligonucleotides to the nuclear proteins in LNCaP-RANKL or RANKL-treated LNCaP cells is specific (Fig. 15C). Furthermore, the band of the DNA-protein complex was supershifted when anti-cMyc or anti-Max antibodies were incubated with the DNA-protein binding reaction due to retardation of the DNA-protein-antibody complex, but the shift was not observed with incubation with anti-rabbit IgG. Moreover, no DNA-protein binding complex was observed for LNCaP cells. Together, these results suggest that RANKL promotes the direct binding of cMyc/Max heterodimers to the corresponding binding sequence within the RANKL promoter and activates RANKL expression, leading to cMyc-mediated RANKL autocrine feed-forward induction.

Moreover, we examined the level of nuclear cMyc and Max in RANKL-treated LNCaP and LNCaP-RANKL cells, and we found significant up-regulation of nuclear cMyc and Max levels compared to LNCaP cells (Fig. 15D). This suggests that RANKL treatment or overexpression also induced cMyc and Max expression levels, leading to the subsequent activation of RANKL transcription through increased cMyc/Max heterodimer binding to the RANKL promoter. We further examined RANKL promoter activity in LNCaP-RANKL and RANKL-treated LNCaP cells in the presence of a cMyc inhibitor, 10058-F4, which disrupts cMyc and Max interaction and prevents transactivation of c-Myc target gene expression. We observed that the cMyc inhibitor induced a significant decrease in RANKL transcriptional activity in both RANKL-treated LNCaP and LNCaP-RANKL cells but had no effect on RANKL promoter activity in

LNCaP or LNCaP-Neo cells (Fig. 15E). Moreover, cMyc inhibitor also greatly decreased RANKL expression in LNCaP-RANKL or RANKL-treated LNCaP cells at protein levels, further suggesting that disruption of the cMyc/Max heterodimer inhibits the transactivation of RANKL expression (Fig. 15F).

A.

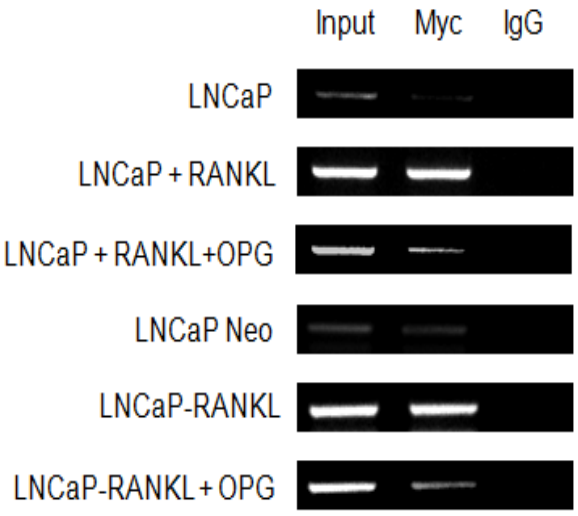
Input
Myc
IgG
LNCaP
LNCaP + RANKL
LNCaP + RANKL+OPG
LNCaP Neo
LNCaP-RANKL
LNCaP-RANKL + OPG

B.

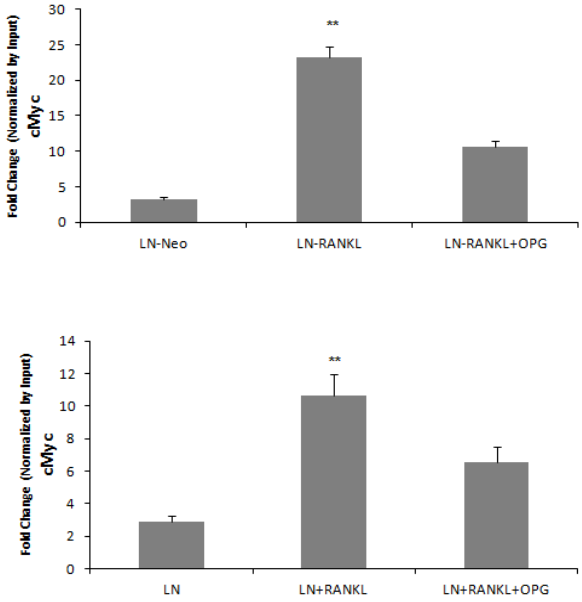
Fold Change (Normalized by Input) cMyc
30
25
20
15
10
5
0
**
LN-Neo
LN-RANKL
LN-RANKL+OPG
Fold Change (Normalized by Input) cMyc
14
12
10
8
6
4
2
0
**
LN
LN+RANKL
LN+RANKL+OPG

C.

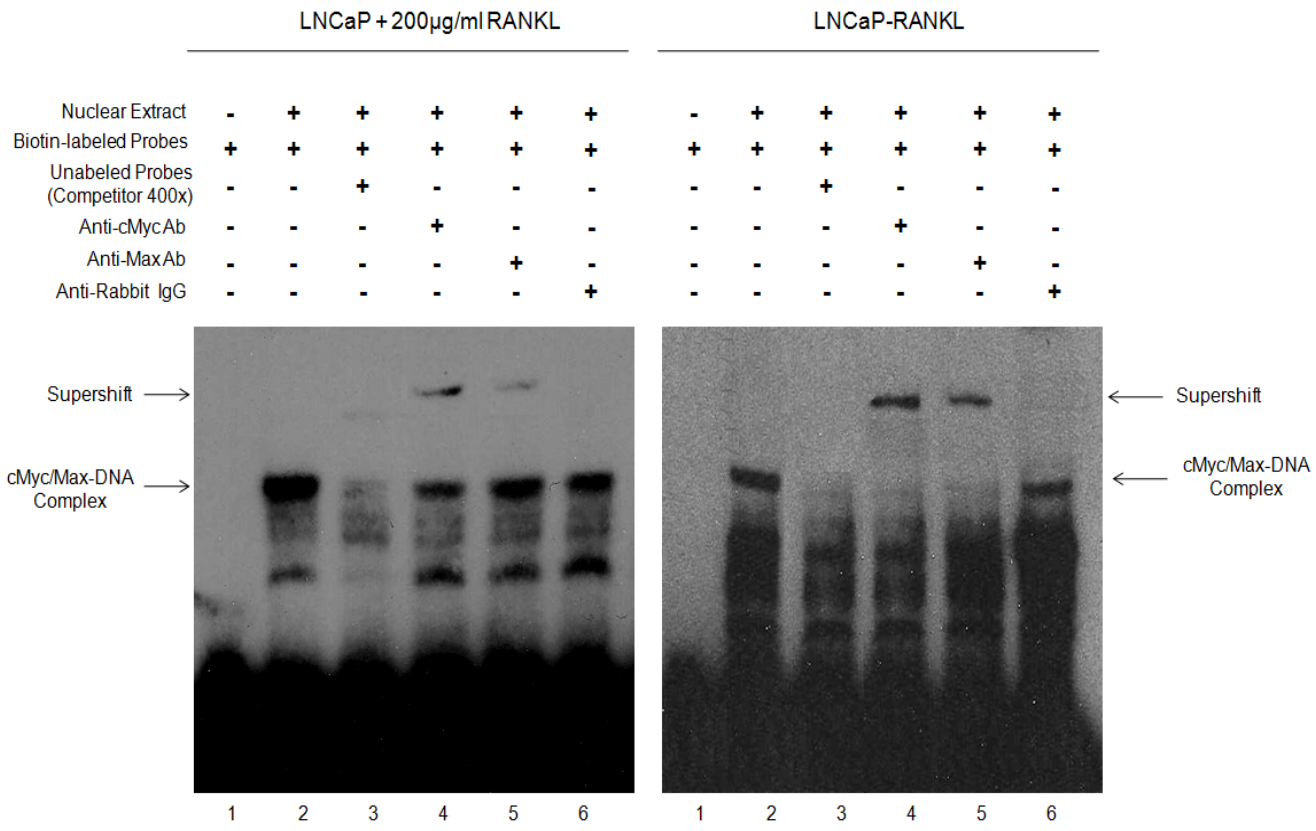
LNCaP + 200µg/ml RANKL
LNCaP-RANKL
Nuclear Extract
Biotin-labeled Probes
Unabeled Probes (Competitor 400x)
Anti-cMyc Ab
Anti-Max Ab
Anti-Rabbit IgG
Supershift
cMyc/Max-DNA Complex
1 2 3 4 5 6
1 2 3 4 5 6

D.

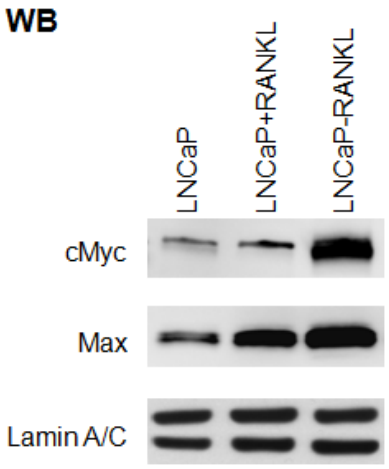
WB
LNCaP
LNCaP+RANKL
LNCaP-RANKL
cMyc
Max
Lamin A/C

E.

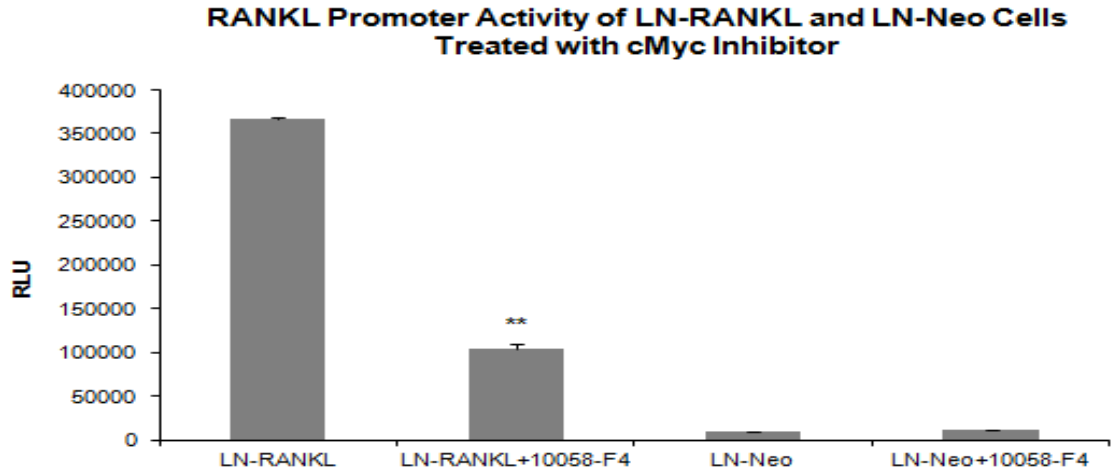
RANKL Promoter Activity of LN-RANKL and LN-Neo Cells Treated with cMyc Inhibitor
RLU
400000
350000
300000
250000
200000
150000
100000
50000
0
**
LN-RANKL
LN-RANKL+10058-F4
LN-Neo
LN-Neo+10058-F4

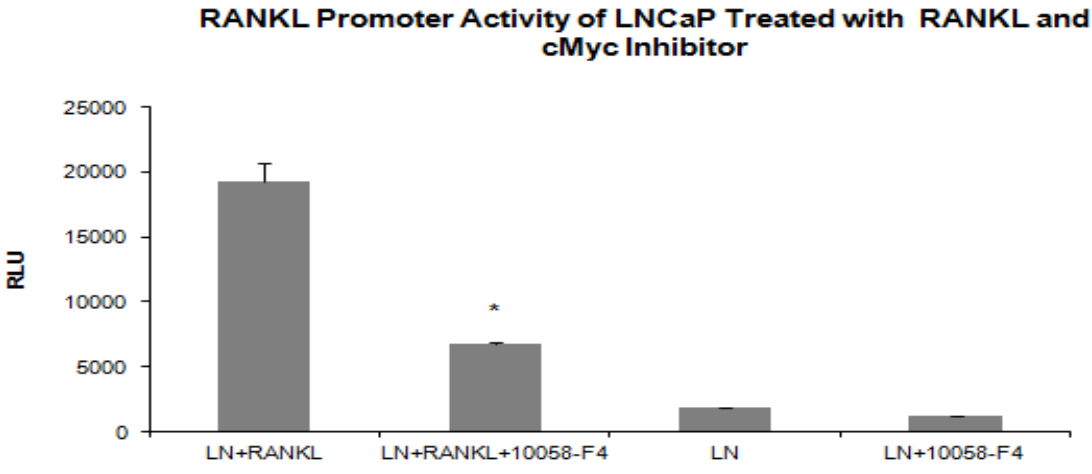
RANKL Promoter Activity of LNCaP Treated with RANKL and cMyc Inhibitor
RLU
25000
20000
15000
10000
5000
0
*
LN+RANKL
LN+RANKL+10058-F4
LN
LN+10058-F4

F.

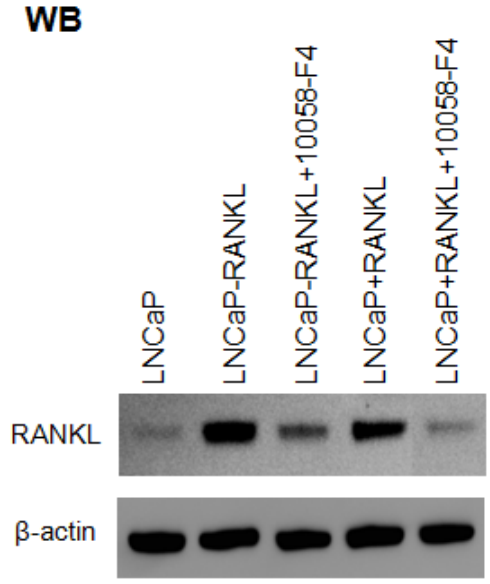

Figure 15. RANKL autocrine activation is mediated through direct interaction of cMyc to its *cis*-acting binding element within the RANKL promoter region in prostate cancer cells. **A.** ChIP analysis of LNCaP cells treated with 200 µg/ml of RANKL or RANKL plus OPG as well as LNCaP-RANKL cells and LNCaP-RANKL cells treated with OPG. The chromatin and nuclear proteins were cross-linked with formaldehyde, sheared by enzymatic shearing mixture and subjected to immunoprecipitation (IP) using anti-cMyc antibody or anti-rabbit IgG as a negative control. The input and cMyc antibody- and IgG-pull-downed cMyc-DNA complex was subjected to semi-quantitative RT-PCR for cMyc DNA amplification. **B.** Quantitative real-time PCR was also performed for cMyc amplification in the ChIP analysis. **C.** EMSA analysis demonstrating nuclear cMyc/Max heterodimer binding to cMyc oligonucleotides in RANKL-treated LNCaP and LNCaP-RANKL cells *in vitro.* Nuclear extract from both cells was incubated with biotin-labeled cMyc/Max probe (lanes 2-6). An excess of unlabeled probe (400x) as competitor (lane 3), anti-cMyc antibody (lane 4), anti-Max antibody (lane 5), and anti-rabbit IgG as negative control (lane 6) were added to the binding reaction. Arrows indicate free probe, cMyc/Max-DNA complex, and supershifted cMyc/Max-DNA complex conjugated with anti-cMyc or anti-Max antibodies. **D.** The nuclear protein levels of cMyc and Max in LNCaP cells treated with RANKL and LNCaP-RANKL cells were examined by Western blot analysis, and lamin A/C was used as the internal control. **E and F,** RANKL treated LNCaP cells and LNCaP-RANKL cells were treated with 20 µM of cMyc inhibitor, 10058-F4 and examined for the RANKL promoter reporter activity as well as protein expression level. cMyc inhibitor significantly decreased RANKL transcriptional activity (**E**) and protein expression (**F**) in LNCaP-RANKL cells or in LNCaP cells treated with RANKL. * , $p<0.05$; **, $p<0.005$.

Discussion

We demonstrated for the first time that RANKL can induce autocrine feed-forward induction of RANKL expression at both the transcriptional and translational levels. To study the transcriptional regulation of RANKL autocrine induction, we constructed a 2.5kb RANKL promoter reporter using a BAC clone containing RANKL 5' upstream promoter regions. The promoter was functional in RANKL-producing osteosarcoma SaOS-2 cells, and upon stimulation with RANKL-stimulating or osteotropic factors, such as PTH and vitamin D_3, RANKL promoter activity was significantly induced (Fig. 12A). RANKL promoter activity was also examined in prostate cancer cells, and the level of RANKL transcriptional activity was correlated with the endogenous level of RANKL expression and paralleled the aggressiveness and malignancy of the cells (i.e. RANKL promoter activity was high in aggressive $ARCaP_M$ and PC3 cells but low in indolent cells, such as $ARCaP_E$ and LNCaP (Fig. 12B). RANKL treatment and overexpression both induced up-regulation of RANKL expression in prostate cancer cells at both the RNA and protein levels (Fig. 13A). RANKL-induced autocrine activation was further demonstrated by RANKL promoter reporter assay. RANKL promoter activity was augmented in $ARCaP_E$, $ARCaP_M$, and LNCaP cells when treated with RANKL, and the induced activity was abrogated upon exposure to OPG (Fig. 13B and 13C). Furthermore, overexpression of RANKL in LNCaP and $ARCaP_E$ cells also significantly activated the RANKL promoter activity compared to the Neo-transfected cells (Fig. 13D and 13E).

Our RANKL promoter deletion study identified the region from -1884 to -1384 within the RANKL promoter as responsible for the RANKL-mediated autocrine induction since deletion of that region abolished the RANKL basal promoter activity (Fig. 14A and 14B). Within that region of RANKL promoter, we predicted two potential *cis*-acting elements, including CREB and

cMyc/Max motifs that might be potentially involved in RANKL autocrine transcriptional regulation (Fig 14C). Further characterization of these two binding sites by a deletion study revealed that cMyc/Max binding to RANKL promoter is required for RANKL-induced RANKL transcription in LNCaP-RANKL as well as RANKL-treated LNCaP cells (Fig. 14D and 14E). ChIP and EMSA analyses further confirmed that RANKL treatment or overexpression induced direct and specific binding of nuclear cMyc/Max heterodimer to its binding site within the RANKL promoter to activate RANKL transcription, and such binding can be attenuated upon OPG treatment (Fig. 15A, 15B, and 15C). RANKL also greatly increased both cMyc and Max nuclear protein levels in LNCaP cells (Fig.14D). Disruption of cMyc and Max interaction by cMyc inhibitor (10058-F4) prevented transactivation of RANKL promoter, leading to a significant reduction in RANKL transcription as well as protein expression in both RANKL-treated or overexpressing LNCaP cells (Fig.15E and 15F).

Together, these results demonstrate a novel regulatory mechanism of RANKL-induced RANKL autocrine gene expression via cMyc/Max heterodimer transactivation. Such auto-induction of RANKL expression promotes EMT progression and metastasis by prostate cancer cells and also leads to the establishment of the "vicious cycle" between prostate cancer cells and their surrounding microenvironment, especially in the bone.

CHAPTER 6 THE USE OF ENGINEERED HUMAN PROSTATE CANCER CELL LINE AND XEONGRAFT MODEL FOR THE STUDY OF CELL SIGNALING NETWORK IN CASTRATION-RESISTANT PROSTATE CANCER: A MULTIPLEX QUANTUM DOT LABELING APPROACH (PLOS ONE 2011 IN PRESS)

Introduction

Semi-conductor quantum dots (QDs) fluorescent nanoparticles have been recognized as one of the great recent advances for our ability to detect relevant biomarkers expressed by cells, tissues and sera (Hu et al., 2010; Leung, 2004; Shi et al., 2008; Sweeney et al., 2008; Wagner, Li, Li, Li, & Le, 2010). The unique optical and electronic properties of QDs include their narrow and symmetrical emission bands, size- and material-tunable light emission, high surface to volume ratio, photostability, signal brightness and sensitivity, and simultaneous excitation of multiple fluorescence colors making it possible to detect multiple targets simultaneously at the single cell level (Shi et al., 2008; Xing et al., 2007). Quantum dot labeling, QDL, is superior to conventional organic dyes for cell and tissue staining, especially since the latter yield broad bandwidth with overlapping signal emissions and are highly susceptible to photobleaching. Multiplexing biomarkers with different colors provides significant advantages over traditional organic or fluorescent dyes for the detection and analysis of dynamic changes in proteins and nucleic acids in cells or tissues under pathophysiologic conditions. QDL has been applied successfully to detect the levels of expression of genes *in situ* associated with important biologic processes such as epithelial to mesenchymal transition (Xing et al., 2007) in cancer metastasis (R. Li et al., 2009), protein biomarkers in the blood, the presence of nucleic acids, microRNA and DNA methylation in sera or tissue extracts with samples barcoded for rapid processing by automated protocols (Bailey, Puleo, Ho, Yeh, & Wang, 2009; Kong et al., 2010; Liang et al.,

2005). In the present study, we employed multiplexed quantum dot labeling (MQDL) to detect the activated c-Met-mediated cell signaling pathway leading to EMT, cancer growth and bone and soft tissue metastasis in a novel prostate cancer metastasis model (Thalmann et al., 1994; Thalmann et al., 2000; van Leenders et al., 2003). We confirmed the levels of gene expression assessed by MQDL with gene expression as determined by RT-PCR and western blots. We then applied the MQDL protocol to determine if the c-Met cell signaling pathway and EMT are activated in a castration-resistant prostate cancer (CRPC) animal model and in clinical prostate cancer specimens obtained from patients with high Gleason scores and bone metastasis. We observed that activation of c-Met is closely linked to EMT in cancer cells and their subsequent increased migration, invasion and metastasis (Chung et al., 1992; Pisters et al., 1995; Zhang et al., 2010). c-Met signal activation in human prostate cancer has important clinical implications: 1) c-Met downstream signaling drives EMT and cancer cell migration, invasion, metastasis and survival in several human solid tumor models including prostate cancer (Lengyel et al., 2005; Torres et al., 2011; Zhang et al., 2010; Zhou et al., 2011). 2) Since targeting c-Met and VEGFR2 downstream signaling with a synthetic multiple tyrosine kinase inhibitor, cabozantinib (XL-184), resulted in remarkable resolution of bone and soft tissue metastases in a large number of patients with solid tumors including CRPC patients (Smith et al., 2010; Zhang, Guessous, Kofman, Schiff, & Abounader, 2010), it would be important to show if these cell signaling pathways might be activated in clinical specimens and in relevant tumor xenograft models. We used a human prostate cancer cell line to demonstrate that c-Met activation confers EMT and prostate cancer bone and soft tissue metastases and investigated in depth the c-Met signaling activation by molecular analyses with results confirmed by MQDL. We then employed MQDL to evaluate c-Met signaling activation in clinical prostate cancer tissue specimens and correlated the results

with a castration-resistant human prostate cancer xenograft model. We showed that MQDL, coupled with Vectra Image Analysis, enhances the quantitative profiling capability of individual biomarkers at the single cell level. A series of biomarkers associated with EMT, such as decreased expression of EpCAM, and increased expression of N-cadherin, vimentin and RANKL, and c-Met signal activation, including VEGF, neuropilin 1, p-c-Met and phospho(p)-NF-κB p65 (Tobar, Villar, & Santibanez, 2010; Zhang et al., 2010), were analyzed. The results of these studies showed a remarkable parallelism of EMT and c-Met activation between the prostate cancer cell model, the CRPC xenograft model and clinical prostate cancer specimens. The methodologies established in the present study could be of significant value in the near future to characterize other activated signaling pathways in clinical specimens, interrogate molecular mechanisms underlying cancer progression, identify druggable targets, and follow up the clinical response of patients to therapeutic intervention.

Results

Development of a quantitative QD labeling protocol for the assessment of gene expression associated with the activation of c-Met signaling and EMT in cultured human LNCaP cells stably tansfected with RANKL

LNCaP bone and soft tissue metastases model

A novel LNCaP bone metastasis model was developed by stable transfection of this cell line with RANKL (LNCaP-RANKL), which drives EMT in the transfected cells. When RANKL overexpressing LNCaP cells were injected intracardially in mice they exhibited an increased incidence of bone and soft tissue metastases (Table 4).

Table 4. RANKL overexpressing LNCaP cells induced high incidences of bone and soft tissue metastases. LNCaP-RANKL and LNCaP-neo cells (1x106 cells/50µl PBS) were inoculated intracardially into 5- to 7-week-old male athymic nude mice (LNCaP-RANKL n=20; LNCaP-neo n=15). Metastatic lesions were observed between 2 - 3 months after injection. * Micro-CT tomography detected bone lesions in limbs, ribs, jaw, and skull determined by X-ray radiography and confirmed by histopathologic staining (H&E).

	Lymph nodes	Bones*	Adrenal glands	Lung
LNCaP-neo	0/15	0/15	0/15	0/15
LNCaP-RANKL	18/20 (90%)	20/20 (100%)	17/20 (85%)	8/20 (40%)

Validation of Activated c-Met Signaling Components That Lead to EMT by RT-PCR, Western Blot and Single Quantum Dot Labeling, SQDL

Comparison of gene expression between stable LNCaP-neo control and LNCaP-RANKL cells using RT-PCR and Western blot showed evidence of activated c-Met signaling through increased expression of c-Met, p-c-Met, and p-NFκB p65 (Fig. 16). The cells underwent morphologic (Panel A) and biochemical (Panels B and C) epithelial to mesenchymal transition, with decreased intercellular adhesion mediated by E-cadherin and EpCAM, and increased N-cadherin, vimentin and RANKL. These assessments of c-Met signaling activation and EMT were subjected to SQDL analyses with a specific effort to confirm if c-Met activation and EMT occurred in this cell model of prostate cancer progression. SQDL confirmed that in comparison to control LNCaP-neo cells (Fig. 17A), LNCaP-RANKL cells (Fig. 17B) had activated c-Met signaling as revealed by an elevated expression of RANKL, c-Met, p-c-Met and p-NFκB p65 and evidence of EMT, a cadherin switch of elevated expression of N-cadherin, vimentin and RANKL but decreased expression of E-cadherin and AR. Quantitative analyses (Fig. 18) of 1,000 randomly selected cancer cells by inForm software (Caliper) supported the imaging data in which both AR and E-cadherin expression was drastically decreased and activated c-Met signaling components led to EMT, such as elevated expression of c-Met, p-c-Met, p-NFκB p65, N-cadherin, vimentin, and RANKL were observed in LNCaP-RANKL, when compared to LNCaP-neo cells. This quantitative SQDL protocol was adopted for gene expression analyses of an established CRPC LTL-313 xenograft model.

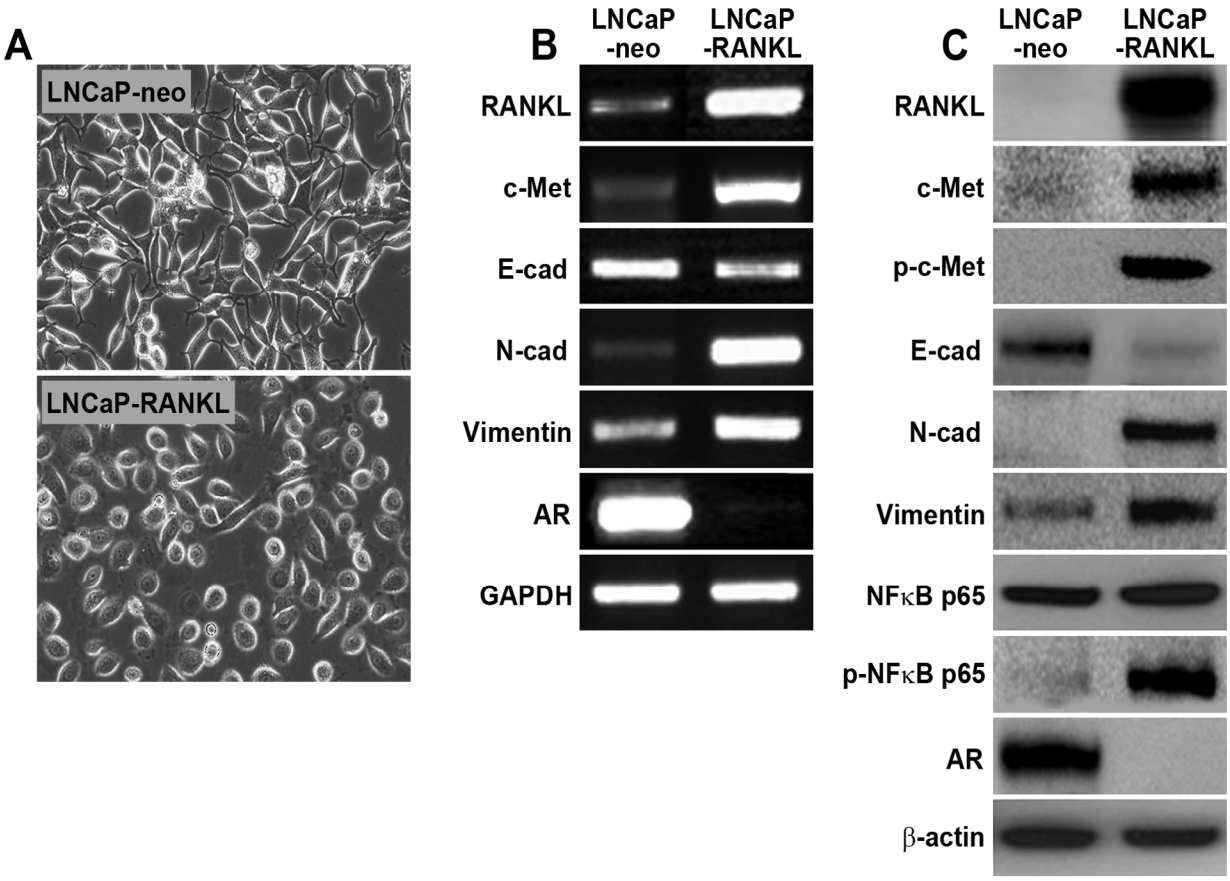

Figure 16. RANKL-transfected LNCaP cells induced epithelial to mesencymal transition in histomorphology (A) and gene expression in mRNA (B) and protein (C). Data represent one of 3 RANKL-stably transfected and 2 neo-stably transfected LNCaP cell clones.

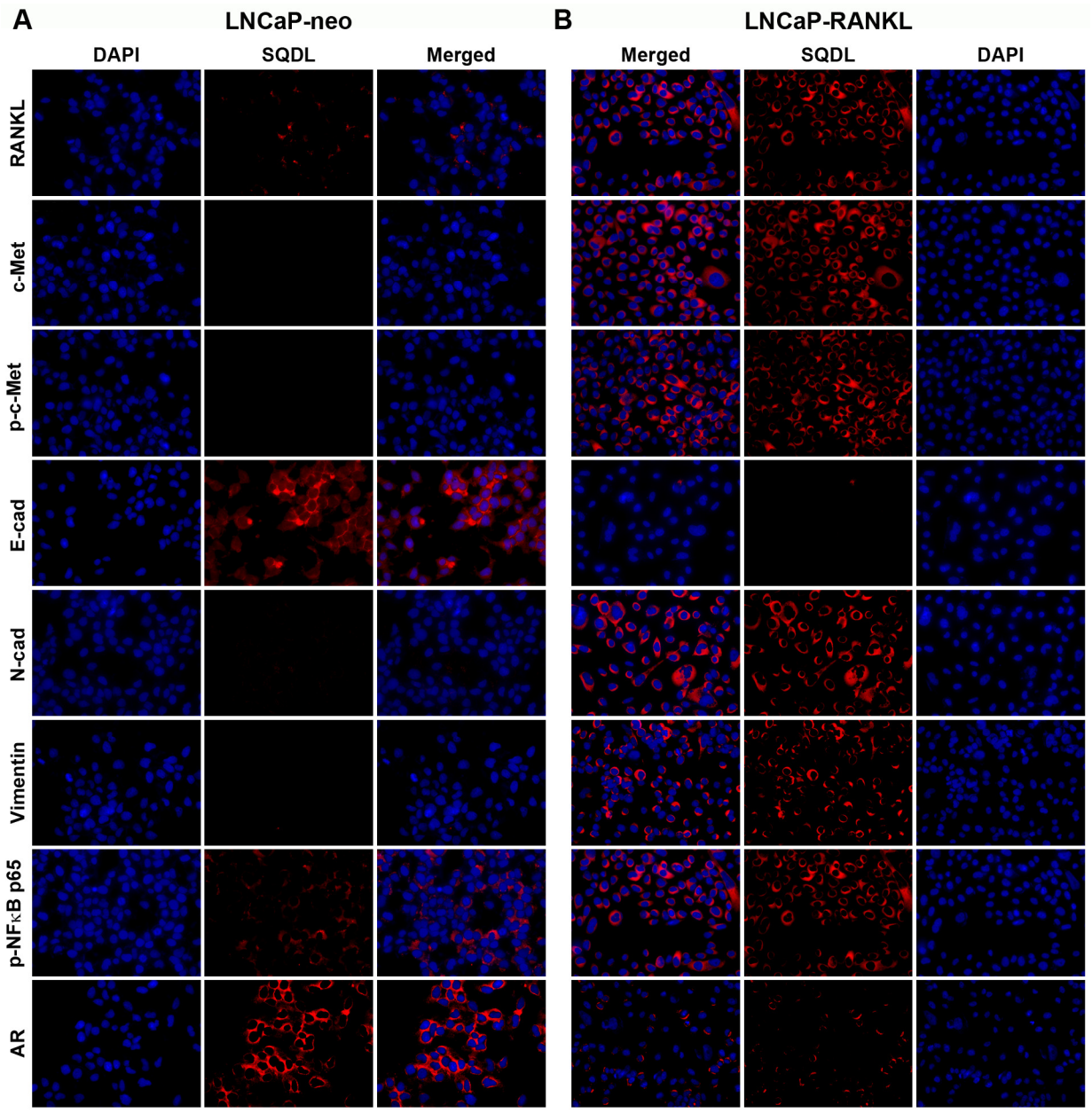

Figure 17. RANKL overexpression activated c-Met signaling components detected by single quantum dot labeling, SQDL. Differential QD labeling of proteins was performed in LNCaP-neo (**A**) and LNCaP-RANKL (**B**) cells using DAPI nuclear staining as reference. For each analysis, QD labeled protein expression is presented in pseudocolor, with the overlaid image of DAPI and QD signals (Merged). ×400.

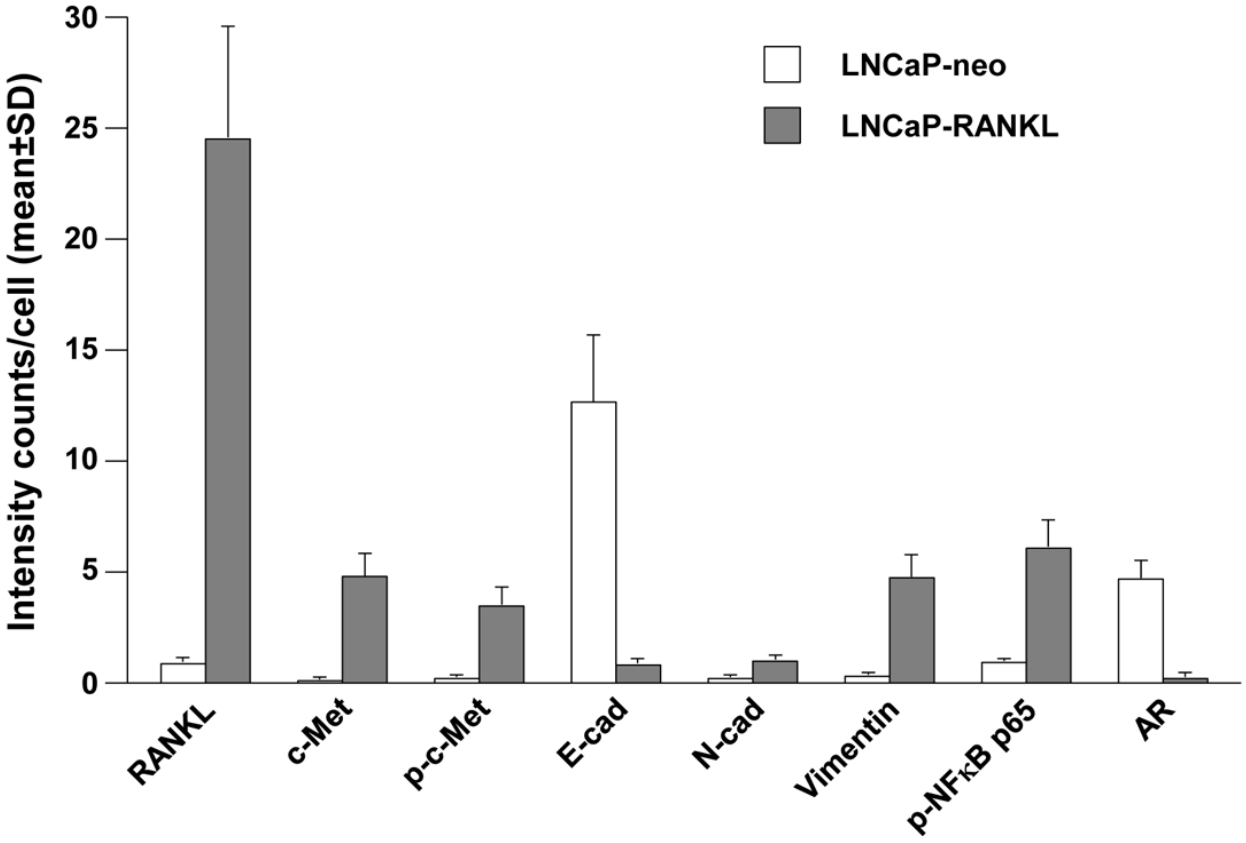

Figure 18. Quantification of differential gene expression subsequent to RANKL overexpression in LNCaP cells. Cell-based average intensity counts from 1,000 each of neo- and RANKL-transfected LNCaP clones were quantified using inForm software. Statistically significant changes in protein expression were observed ($P < 0.05$).

Validation of c-Met signaling activation and EMT in the CRPC LTL-313 model with results confirmed by IHC and SQDL

To understand the clinical significance of c-Met signaling activation and EMT in the LNCaP-RANKL model and the associated increases in prostate cancer metastases, we defined the c-Met signaling pathway and EMT in a CRPC LTL-313 xenograft model obtained from the Living Tumor Laboratory (livingtumorcentre.com). We included additional c-Met signaling associated genes such as neuropilin-1, VEGF, p-Akt, VEGFR2, Mcl-1 and AR, which were characterized as mediators of c-Met downstream survival signaling (Coloff et al., 2011; Huynh et al., 2009; D.C Smith et al., 2010; Zhang et al., 2010). Figure 19 shows that increased c-Met signaling-associated genes and decreased AR expression in CRPC LTL-313 xenografts maintained in castrated male hosts, as assessed by IHC (Panel A) and SQDL (Panel B) compared to the xenografts maintained in intact mice with androgen supplementation.

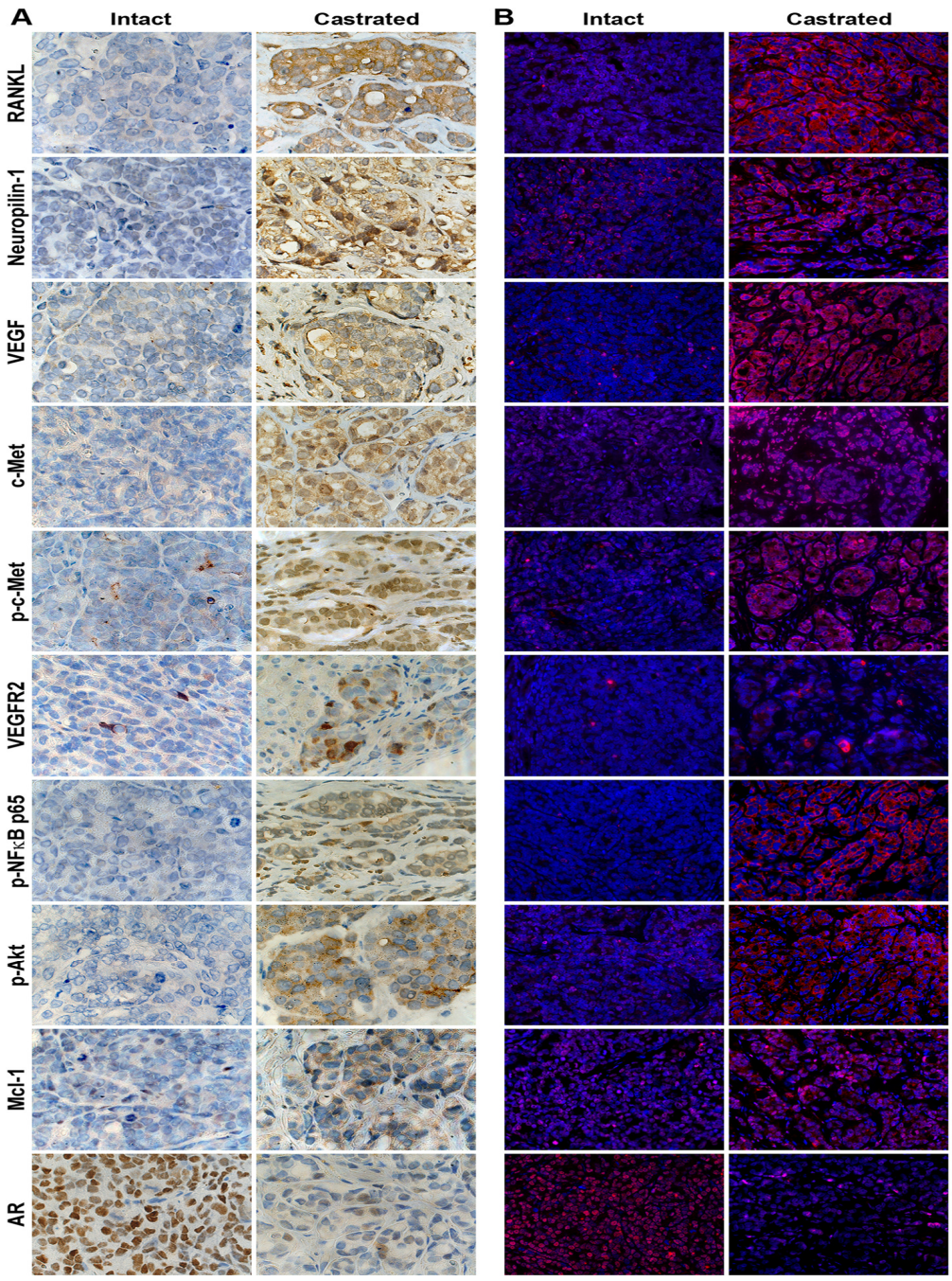

Figure 19. Detection of c-Met activated and EMT associated proteins in the CRPC LTL-313 xenograft model by conventional IHC (A) and SQDL (B). Castration increased a panel of genes in LTL-313 xenograft prostate cancer and decreased AR expression compared to xenografts obtained from intact hosts by both IHC and SQDL. ×400.

MQDL Analysis Demonstrated Activated c-Met and EMT in a CRPC LTL-313 Xenograft Model and Primary and Metastatic Human Prostate Cancer Tissue Specimens

A series of human prostate cancer xenografts obtained from the Living Tumor Laboratory was used to test the quantitative MQDL protocol. We selected the LTL-313 model for this task because this model exhibits CRPC characteristics with a propensity for primarily lymph node, lung and liver metastases with infrequent bone metastasis, when the tumors are implanted and grown under the renal capsules. We tested the hypothesis that tumors grown in castrated mice would develop castration resistance and have activated c-Met signaling leading to EMT, when compared to tumors grown in mice supplemented with exogenous androgen (Fig. 20A). Three approaches were taken: 1) to establish a robust MQDL protocol to detect and quantify a panel of gene expressions on the CRPC LTL-313 model tissue specimen with results compared with SQDL; 2) to use this established quantitative MQDL protocol to confirm if activation of c-Met and EMT occur in the CRPC LTL-313 tissues maintained in the castrated hosts; and 3) to demonstrate by the standardized MQDL protocol the activation of c-Met and EMT induction in both primary and skeletal metastatic human prostate cancer tissues. Figure 20B shows the quantitative MQDL analyses of neuropili-1, p-c-Met, VEGF, p-NFκB p65, and RANKL, previously reported to be associated with c-Met signal activation (Tobar et al., 2010; Zhang et al., 2010) and EMT (Odero-Marah et al., 2008; H. E. Zhau et al., 2008) in human prostate cancer cells and in the CRPC LTL-313 model. We showed activated c-Met signaling and EMT, as exhibited by increased expression of neuropilin-1, VEGF, and RANKL protein and activation of p-c-Met and p-NFκB p65 in the CRPC LTL-313 tumor model with higher expression and activation of these genes in LTL-313 tumor xenografts maintained in castrated compared to intact mice. As an internal control for minimizing the possible fluorescence interference of

multiple QD probes, we performed MQDL side by side with the SQDL protocol (see above). The elevated expression of the 5 studied genes was found to be statistically significant by inFom quantitative analyses (Fig. 20B). We determined this panel of 5 genes in primary prostate cancer specimens with different Gleason scores and found that expression of neuropilin-1, VEGF, p-c-Met, RANKL, and p-NFκB p65 were more elevated in poorly differentiated (Gleason score 10) than moderately differentiated (Gleason score 7, 3+4) prostate cancer (Fig. 21). These results, taken together, confirmed that QD labeling is highly sensitive and versatile and can be used for multiplexing gene expression profiles in experimental models at the single cell level.

Furthermore, we showed that some clusters of LTL-313 tumor cells grown as xenografts in castrated male hosts underwent EMT (marked as M in Fig. 22A, Composite panel) and others only partially transitioned to express both E and M markers (marked as E/M in Fig. 22A, Composite panel). Decreased expression of EpCAM, an epithelial biomarker, with concomitant increased expression of mesenchymal markers, such as N-cadherin and RANKL, was observed (Fig. 22A, Deconvoluted panels). These data support the conclusion that castration promotes EMT in prostate cancer cells *in situ.* Similar EMT was detected by MQDL in clinical primary prostate cancers (Fig. 22B). A cluster of prostate cancer cells underwent EMT (M) while the other clusters of cells underwent partial EMT (E/M) (Fig. 22B, Composite panel). Furthermore, Figure 23 demonstrates the co-expression of epithelial EpCAM and mesenchymal RANKL, and vimentin biomarkers in a metastatic bone tissue specimen.

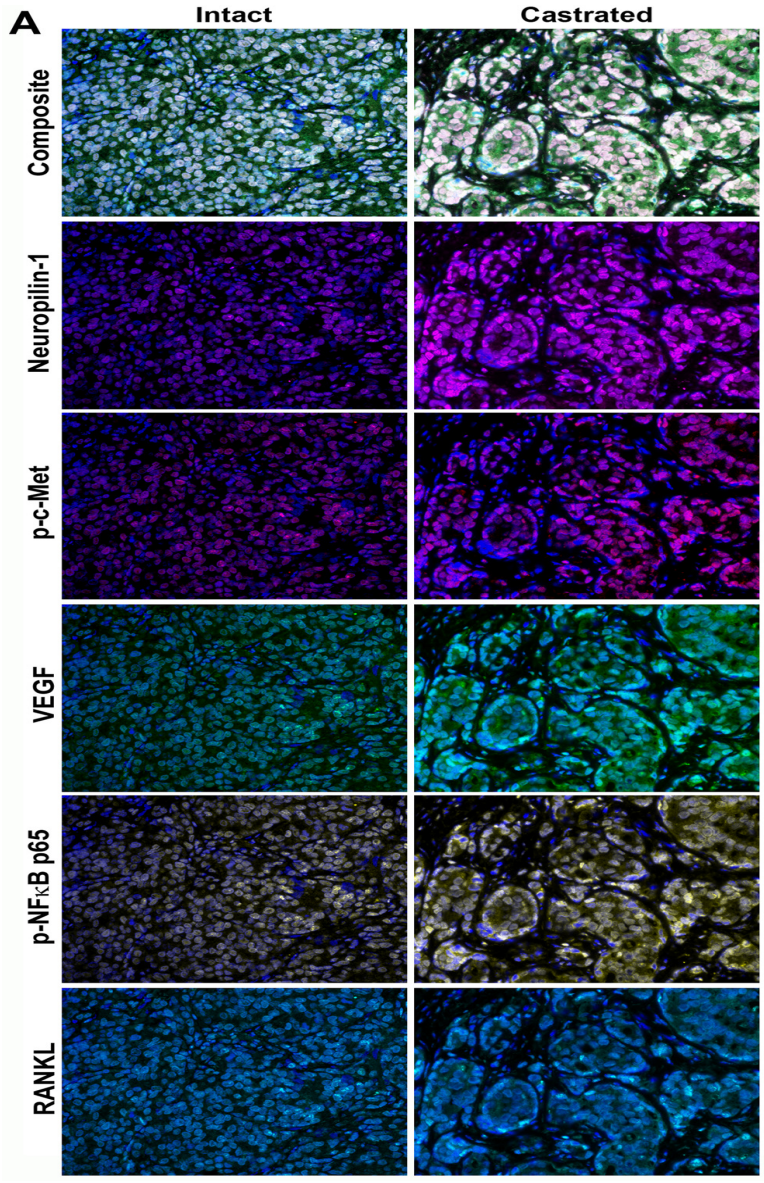
A
Intact
Castrated
Composite
Neuropilin-1
p-c-Met
VEGF
p-NFκB p65
RANKL

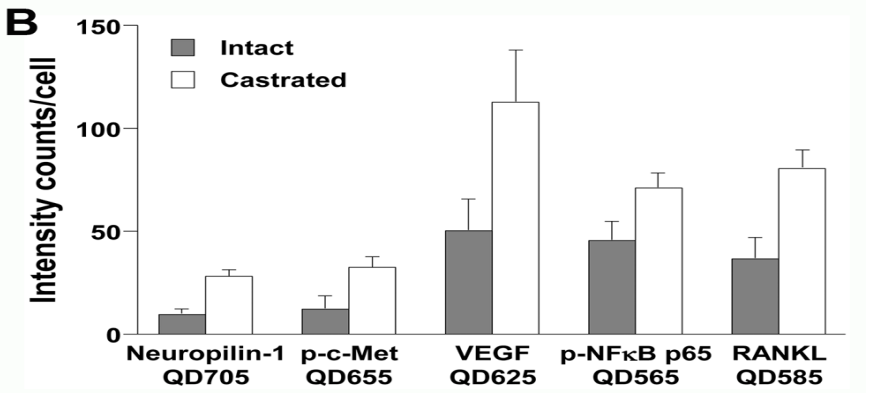
B
Intensity counts/cell
150
100
50
0
Intact
Castrated
Neuropilin-1 QD705
p-c-Met QD655
VEGF QD625
p-NFκB p65 QD565
RANKL QD585

Figure 20. Multiplexed quantum dot labeling (MQDL) simultaneously detected c-Met activated and EMT genes in a CRPC LTL-313 xenograft model. Single tumor tissue sections from intact and castrated hosts were subjected to sequential MQDL. Enhanced expression of c-Met activated genes was detected in tumor tissues from castrated hosts. **A,** A stack of multiple images (Cube), nuclear staining (DAPI), and individual gene expression (in pseudocolors) are shown. Gene expression signals were superimposed with DAPI nuclear signals to yield a composite image for analysis. ×400. **B**, Significant differences in gene expression were found by quantification analysis of 1,000 cells in each tumor specimen using inForm software ($P < 0.05$).

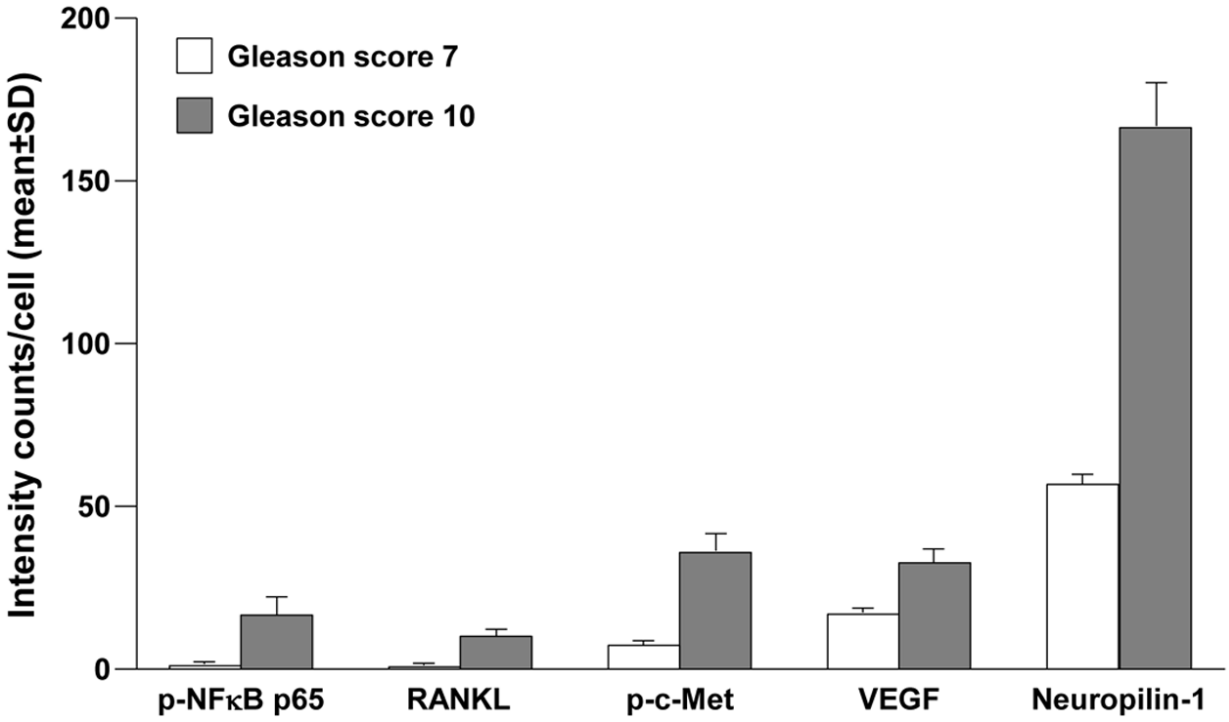

Figure 21. MQDL assesses differential gene expression in clinical primary prostate cancer specimens. C-Met-activated and EMT protein expressions in 5,000 cells of each representative prostate cancer tissues of Gleason scores 7 (3+4) and 10 (5+5) were compared. Expression intensities were quantified with the inForm software and statistically compared ($P < 0.05$).

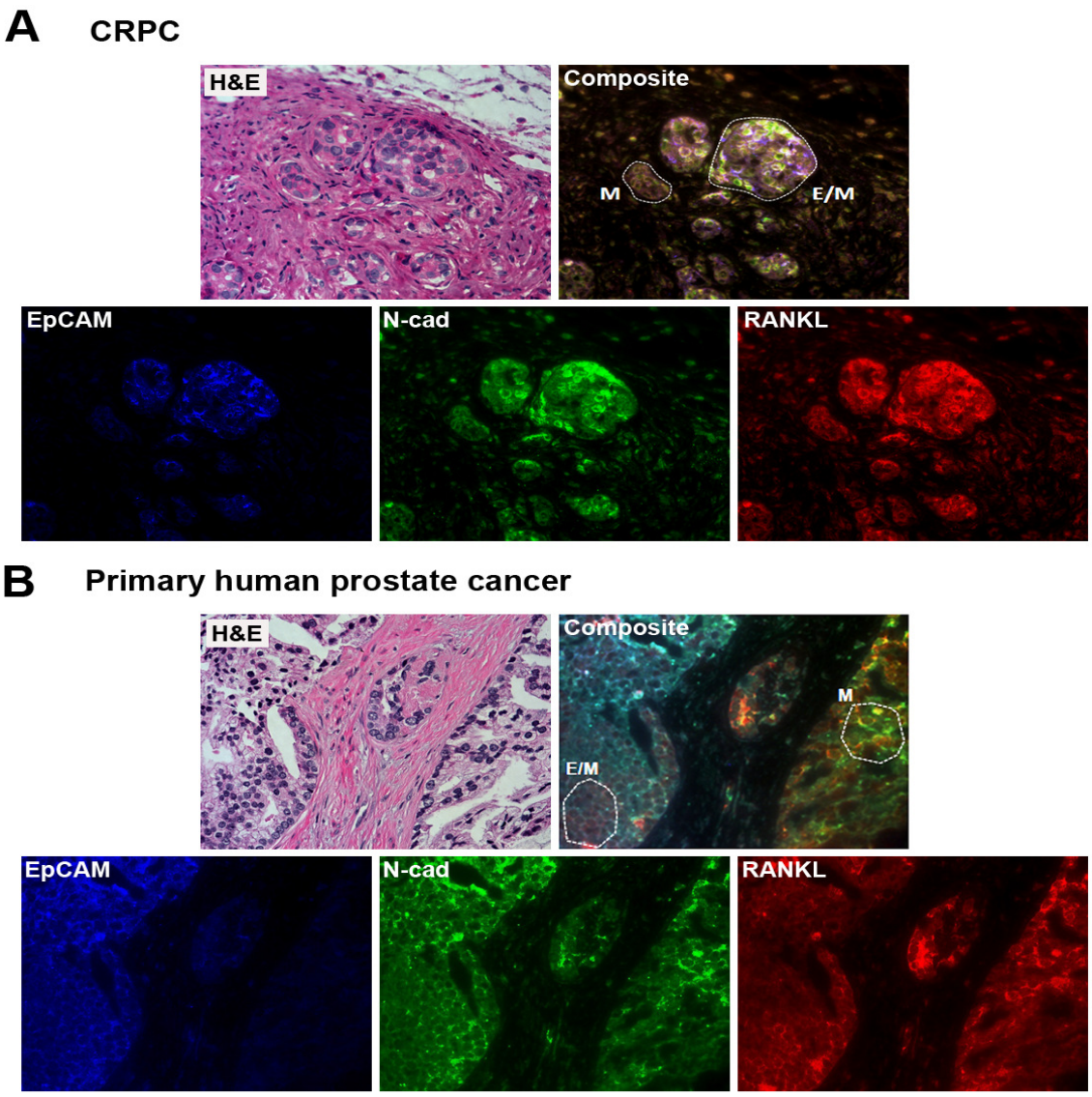

Figure 22. MQDL detects EMT biomarkers in CRPC LTL-313 prostate tumors harvested from castrated hosts and from clinical prostate cancer. **A**, The CRPC LTL-313 model showed androgen deprivation induced more abundant expression of EMT markers in a cluster of cells within the tumor region, as revealed by QD labeling of EpCAM, N-Cad, and RANKL. **B**, Similar EMT biomarkers were detected in a clinical primary prostate cancer specimen (Gleason score 6; 3+3) with documented bone metastasis. M denotes cells that completed EMT and E/M indicates cells undergoing partial EMT. ×400.

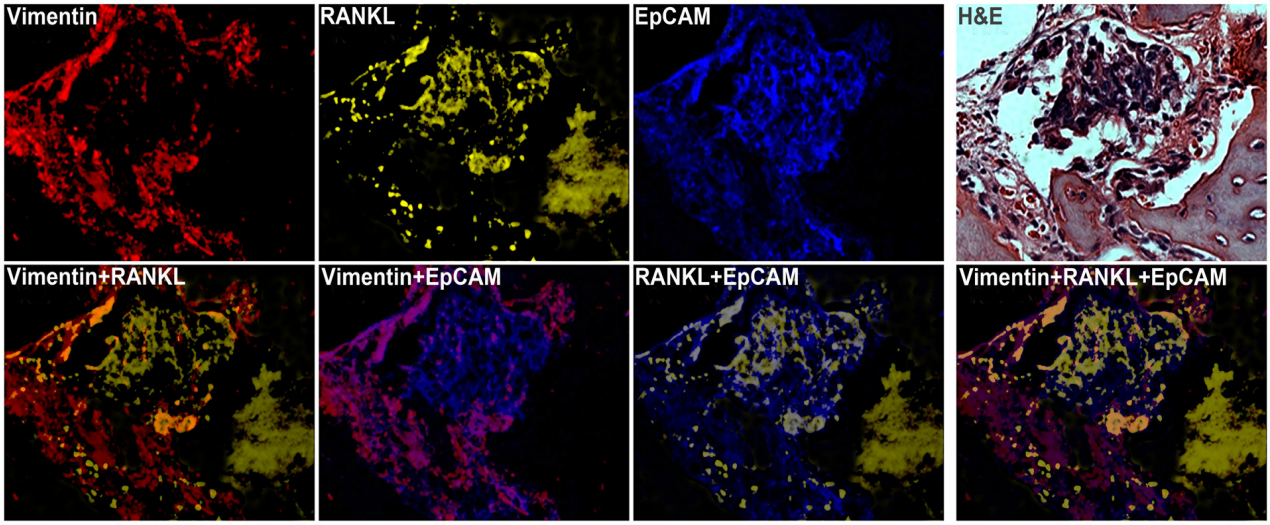

Figure 23. MQDL detects EMT biomarkers in clinical bone tissue specimens. A representative specimen of human prostate cancer bone metastasis co-expressed high levels of epithelial EpCAM, and mesenchymal RANKL and vimentin proteins. ×400.

Discussion

Understanding the underlying molecular signaling pathway in CRPC and prostate cancer bone and soft tissue metastases could benefit patient care through improved disease surveillance and selection of patients for more effective targeting. Considering the limited amount of tissues and cells available from biopsies and needle aspirates, and the challenges of tumor cell heterogeneity, MQDL offers a valuable multiplexing capability to analyze changes in cell signaling network components, at the single cell level during prostate cancer progression in both preclinical models and clinical specimens. The advantages of quantitative MQDL over conventional IHC are: 1) Data obtained by quantitative MQDL could contain spatial and temporal information on the tissue specimens at the single cell level that can be easily integrated into the already-known histomorphometric and immnohistochemical information obtained from the tumor tissues or cells. 2) The cell signaling network defined in tissue specimens could have predictive value for assessing the progression and therapeutic responsiveness of the prostate cancer. 3) Quantitative MQDL is highly efficient for tissue and cell utilization and can be further developed to monitor simultaneously multiple cell signaling networks in human cancer cells *in situ*. The results of our studies using quantitative MQDL suggest that activation of c-Met signaling is responsible for driving prostate cancer cells to undergo EMT, with prostate cancer cells acquiring increased capability for cell migration, invasion and metastasis. The quantitative aspect of the MQDL protocol is supported by a preclinical animal model in which LNCaP-RANKL cells, shown to overexpress RANKL, had activated c-Met signaling (Table 1, Figures 1 - 3), and underwent EMT by acquiring increased ability to metastasize to mouse skeleton and soft tissues, compared to parental LNCaP-neo cells. In parallel, we presented evidence of activated c-Met and EMT in a preclinical CRPC LTL-313 tumor xenograft model (Figures 4, 5, and 7A). Using the

established and validated MQDL protocol, we consistently observed activated c-Met with evidence of EMT in poorly differentiated (high Gleason score) and bone metastatic clinical prostate cancer specimens (Figures 6 and 8) (Zhang et al., 2011; Zhang et al., 2010; Zhau et al., 2008). Taken together, we suggest that activation of c-Met signaling and subsequent induction of EMT is probably a common feature of prostate cancer cells, xenograft models and clinical prostate cancer specimens exhibiting an increased propensity for lethal progression. These results suggest the possible link between c-Met-mediated signaling activation, EMT and prostate cancer aggressiveness developed in a castration-resistant state. This increased c-Met signaling network in prostate cancer cells could be considered as one of the reasons why targeting c-Met and VEGFR2 kinases with a small molecule, cabozantinib (XL-184), resolved bone and soft tissue metastases in a broad spectrum of solid tumors in patients (Smith et al., 2010; Zhang et al., 2010). Because of the small sample size used for the determination of c-Met signal activation in clinical prostate cancer specimens, a large scale of evaluation using clinical prostate cancer specimens with known status of c-Met activation (e.g. sensitive vs. resistant to cabozantinib) is warranted.

Several technical issues with MQDL deserve special attention. 1) Conjugation non-covalently of streptavidin-coated QD to biotinylated secondary whole Ab is preferred to the direct conjugation of QD to secondary Ab fragments via reduced sulfhydryl-amine coupling. The former non-covalent method of QD detection through the biotin-avidin complex in our practice provides high labeling specificity and intensity. 2) Florescence interference and florescence resonance energy transfer can present a challenge for designing a suitable protocol to assess gene expression in cells. Sweeney (Sweeney et al., 2008) provided earlier evidence that order of the addition of antibodies and QDs could affect cell labeling read-outs. We suggest conducting a

series of combinational tests to determine the optimal reaction sequence and using matched primary Abs and QDs, a parallel set of negative control Ab IgGs, and when possible confirming the MQDL results with SQDL, IHC and Western blots. 3) The quality of the tissues and cells and non-specific labeling should be carefully determined in the immediately adjacent tissue sections to the actual sections used for data acquisition and analyses. 4) For internal controls, β-actin and EF1-α, two routinely used internal protein loading controls for western blotting, were assessed in our current protocol. We found that β-actin and EF1-α expression levels fluctuated depending on the QD-conjugates used and the levels were different between prostate tissues obtained from intact and castrated hosts in preclinical models. These results are in agreement with the report of Yurube T *et al.* (Yurube et al., 2011) using β-actin as a control gene for immunofluorescence detection of gene expression in a rat tail disc degeneration model and found that β-actin was significantly down-regulated rather than staying unchanged. Before establishing a well-accepted internal control for MQDL, we used stringent negative subtype matched antibodies as controls.

In summary, MQDL is demonstrated to be a highly dynamic technique for assessing multiple gene expression at the single cell level in formalin-fixed cell and tissue specimens. This protocol could be of great value for assessing cell signaling network in tissues and cells obtained from the clinic or from the laboratory. Because of the unique photo-physical properties of QDs, MQDL could provide a sensitive method to determine levels of gene expression relevant to cell signaling networks or special biomarker expression even when clinical materials are limited.

CHAPTER 7 GENERAL DISCUSSION AND FUTURE DIRECTIONS

Understanding the biology and targeting of prostate cancer bone metastasis holds promise for improving the survival of patients with castration-resistant and lethal progressive disease (Beltran et al., 2011; Lee, Saylor, & Smith, 2010; Sturge et al., 2011). Among the many biologic processes studied, we and others found that the induction of EMT by soluble growth factors can provoke increased cancer cell growth, invasion, migration and ultimately metastasis to distant organs (Josson et al., 2011; Odero-Marah et al., 2008; Xu et al., 2006; Zhau et al., 2008). Previous elegant studies have demonstrated the paracrine roles of tumor-derived PTHrP which promotes RANKL expression by osteoblasts, increasing bone turnover through a "vicious cycle", and linked cellular interactions among cancer (which expresses PTHrP), osteoblasts (which express RANKL) and osteoclasts (which express RANK) (Guise et al., 2010 ; Roodman, 2004; Vela et al., 2007; Ye et al., 2007; Yin, Pollock, & Kelly, 2005). Potential paracrine roles of RANKL in mediating hormone-induced stromal-epithelial interaction in mammary gland development (Fata et al., 2000; Fernandez-Valdivia et al., 2009; Gonzalez-Suarez et al., 2007; Gonzalez-Suarez et al., 2010; Schramek et al., 2010; Schramek et al., 2011), and expansion of the "stem cell niche" providing an escape route for cancer cells to gain altered behaviors such as increased EMT and resistance to hormone-, chemo- and/or radiation-therapy (Al-Ejeh et al., 2011; Gangemi et al., 2009; Ghotra, Puigvert, & Danen, 2009; Nicolini et al., 2011; Schwarz-Cruz-y-Celis & Melendez-Zajgla, 2011) have also been proposed. The present study added to our understanding of the roles of tumor cell-derived RANKL in EMT, and further defined the converging RANKL-c-Met forward feedback loop to explain the roles of prostate cancer cell-derived RANKL in bone and soft tissue metastases. The significance of these observations includes: 1) RANKL derived from tumor cells or the microenvironment could amplify RANKL

downstream growth and survival signaling by promoting RANKL and c-Met expression. Both RANKL (Chu, 2010; Odero-Marah et al., 2008; Zhau et al., 2008) and HGF (Chang et al., 2011; Hung et al., 2011) have been shown to induce EMT in prostate cancer cells and activation of a downstream signaling network involving c-Met which is activated primarily by VEGF in the ARCaP cell model through its co-receptor, neuropilin-1, to promote survival by activating an anti-apoptotic gene, Mcl-1 (Zhang et al., 2010). 2) The expressed RANKL and c-Met in cancer cells are biologically functional and participate in enhanced osteoclastogenesis and increased c-Met phosphorylation and downstream survival signaling (Eder, Vande Woude, Boerner, & LoRusso, 2009; Sutherland, Rogers, Tosh, & Rogers, 2009; Zhang et al., 2010). 3) A small number of RANKL-expressing prostate cancer cells are sufficient to facilitate the growth and colonization of RANKL-null cells in mouse skeleton suggesting that RANKL can serve as a factor in "reawakening" cancer dormancy in mouse bone. Based on the trafficking of LNCaP-RFP cells, we observed that prostate cancer bone metastasis contributed directly to its secondary soft tissue metastases. 4) The feed-forward RANKL autocrine induction is mediated by activation of an oncogenic transcription factor, cMyc, that regulates RANKL expression as well as a wide spectrum of downstream genes involved in cancer cell growth, progression, and metastasis (Grandori, Cowley, James, & Eisenman, 2000; Gustafson & Weiss, 2010; Wolfer et al., 2010; Xu, Chen, & Olopade, 2010). Our findings support the significant clinical insights gained from targeting RANKL and c-Met/VEGF based signaling by an anti-RANKL monoclonal antibody, denosumab (Adler & Gill, 2011; Bishr et al., 2011; Fizazi et al.,2011 ; George & Moul, 2011; Scott & Muir, 2011), and the small molecule cabozantinib (XL-184, (Smith, 2011)) which were shown to delay or prevent the progression of castration-resistant prostate cancer (CRPC) in patients with bone metastasis.

The functional roles of RANKL derived from prostate cancer and its contribution to bone and soft tissue metastases have not been investigated previously in part due to the lack of evidence of a predominant expression of RANKL by prostate cancer cells found to colonize to bone. Our results showing RANKL amplifying RANKL and c-Met expression and the facilitating roles of a small number of RANKL-expressing prostate cancer cells to promote RANKL-null cells to co-colonize bone reaffirmed the potential dynamic role of RANKL in prostate cancer bone and secondary soft tissue metastases. Our evidence is further supported by the facts that: 1) RANKL, RANK and OPG are expressed by clinical human prostate cancer tissues and also by a wide-spectrum of isogenic human prostate cancer cell lines (Fig. 1A and 1B). The steady-state level of RANKL expression in these cell lines seems to correlate with the increased invasiveness and bone metastatic potential of prostate cancer tissues and cells (Fig. 1B). 2) Interrupting RANKL-RANK interaction with denosumab in men with clinical progressive prostate or breast cancers reduced their skeletal related events and improved patients' survival (Lee et al., 2010; Lipton, 2011; Stopeck et al., 2010; Sturge et al., 2011). 3) Using human prostate, breast, lung and renal cancer cell lines as experimental models for the study of the underlying mechanisms driving cancer bone metastasis, we found a consistent elevation of RANKL that was provoked by soluble factors (Zhau et al., 2008) which drove EMT and cancer bone and soft tissue metastases and induced lethality in experimental mice (Odero-Marah et al., 2008). 4) Previous studies have focused on the sources of RANKL from normal cells, such as osteoblasts B- or T-cells (Kartsogiannis et al., 1999; Manolagas & Jilka, 1995; Roodman, 2004; Vela et al., 2007), which often activate their receptor RANK in the neighboring normal cells in a paracrine manner (Boyce & Xing, 2007; Hanada et al., 2011; Tripodo et al., 2011). Results of this study support a model in which prostate cancer cell-derived RANKL plays a pivotal role in conferring the ability of tumor

cells to metastasize to bone by induction of EMT driven by PI3K-Akt, P38-MAPK and NF-κB signaling (Fig 9A). This model, however, does not exclude the important functional roles of paracrine RANKL-RANK interaction. The positive feedback loop of RANKL regulation of its own expression in prostate and bone cancer but not normal cells (Fig. 2B, 3A, 3C) mediated by cMyc transactivation (Fig. 15) makes possible a "vicious cycle" in cancer but not normal cells in which autocrine RANKL-RANK signaling is amplified in prostate cancer bone metastasis. RANKL-RANK signaling, however, also occurs with paracrine interaction between osteoblasts and osteoclasts during bone remodeling (Kearns et al., 2008; Lemaire, Tobin, Greller, Cho, & Suva, 2004; Sims & Gooi, 2008) as well as with neighboring cancer cells, conferring the ability to grow and metastasize. RANKL autocrine and paracrine signaling can initiate the reactivation or reawakening of tumor cells from dormancy (Fig. 8). RANKL also serves as a paracrine mediator in steroid hormone action in mammary gland development and stem cell renewal during pregnancy (Fata et al., 2000; Kong et al., 1999), and is also involved in lymph node organogenesis (Kong et al., 1999), monocyte function and inflammatory responses (Seshasayee et al., 2004).

Autocrine RANKL-RANK interaction within prostate cancer cells was shown to modulate a "cadherin switch" which controls EMT and its reversal MET. EMT is considered as an important early invasive step in prostate cancer bone metastasis but once tumor cells reach distant organs a reversal of EMT, called MET, occurs (Chao et al., 2010; Kowalski et al., 2003; van der Pluijm, 2010; Wells et al., 2008; Yates et al., 2007). Data obtained from the ARCaP EMT model support this suggestion since by antagonizing RANKL-RANK interaction genetically by RANKL siRNA (Fig. 2B-4) or blocking downstream signaling by pathway-specific inhibitors (Fig. 9B), we have observed a reversal of EMT, or MET. The reversal could

offer an explanation of why the bulk of prostate cancer cells in circulating blood and in bone appear epithelial in morphology and express E-cadherin and EpCAM (Armstrong et al., 2011; Klymkowsky & Savagner, 2009; Saha et al., 2008; van der Pluijm, 2010; Wells et al., 2008; Yates et al., 2007). The exact mechanisms for how this occurs remain speculative at this time but understanding the RANKL-RANK switch in EMT and its reversal to MET could offer such an explanation. Clinical prostate cancer bone metastasis is predominately osteoblastic, yet our animal models revealed primarily osteolytic bone reactions (Fig. 8B). We suggest that factors yet to be identified within the tumor microenvironment could play a pivotal role in attenuating autocrine RANKL-RANK signaling in prostate cancer cells. For example, elevated OPG or decreased osteoclast activating factors such as IL-11, MIP-1α, and secreted factors that control the shedding of activated RANKL by cathepsins and MMPs could dampen RANKL-RANK signaling. Attenuating RANKL expression by downregulating osteotropic growth factors, such as TGF-β, PTHrP, and prostaglandin E2 (Roodman, 2004; Virk & Lieberman, 2007) could play a role. These factors secreted in the tumor microenvironment could be responsible for fine-tuning the RANKL-RANK signaling which ultimately determines the cadherin and EMT/MET switches, cancer cell growth, survival and therapeutic responsiveness (Zhau et al., 2008). Since stem cell properties have been observed in cancer cells undergoing EMT and RANKL-RANK signaling could be responsible for the expansion of the stem cell niche, an appropriate balance of RANKL-RANK signaling could have profound implications in determining the status of malignancy of cancer cells. Additionally, RANKL-RANK interaction and downstream signaling could also convey the ability of cancer bone colonization and the coupling between osteolytic versus osteoblastic responses observed in clinical prostate cancer bone metastasis (Keller & Brown, 2004). Consistent with other studies, activation of RANK can enhance cell migration and

invasion of prostate and non-prostate cancer epithelial cells (Armstrong et al., 2008; Jones et al., 2006; Sabbota et al.2010).

Prostate cancer cells have been shown to exhibit osteomimetic properties, allowing them to imitate the gene expression and functions of bone cells (Keller, 2002; Koeneman et al., 1999; Lecrone, Li, Devoll, Logothetis, & Farach-Carson, 2000; Thomas, True, Bassuk, Lange, & Vessella, 2000; Zhang et al., 2001). We found that one of the factors controlling prostate cancer cell synthesis and deposition of osteocalcin and bone sialoprotein is β2-microglobulin (Huang et al., 2006). Interestingly, β2-microglobulin expression in human prostate, breast, lung and renal cancers increased RANKL expression (Josson et al., 2011) and promoted EMT and cancer skeletal and soft tissue metastases resulting in increased lethality in mice (Josson et al., 2011). We speculated that RANKL expression by these cancer cells might be responsible, in an autocrine manner, for the morphologic, biochemical and behavioral transition of prostate cancer cells to express their migratory, invasive and metastatic behaviors through EMT. Since RANKL expressed by prostate cancer cells is functional in the induction of osteoclastogenesis in vitro, this suggests RANKL-RANK interaction in prostate cancer cells must be involved also with the host microenvironment. We examined the role of three RANKL-RANK downstream signaling networks, PI3K-Akt, P38-MAPK, and NF-κB, in EMT by the use of appropriate pathway-specific metabolic inhibitors. Results indicate that RANKL-induced EMT was abrogated by inhibiting NF-κB signaling in both the ARCaP$_E$-RANKL and LNCaP-RANKL cell models. However, inhibition of P38-MAPK or PI3K-Akt also partially reverted the EMT marker and decreased RANKL expression in both ARCaP$_E$-RANKL and LNCaP-RANKL cells (Fig. 9B). We observed significant pathway "cross-talk" since both P38 and PI3K inhibitors diminished the level of P65 phosphorylation, and P38 inhibitor had a stronger inhibitory effect on NF-κB

activation than PI3K inhibitor (Fig. 9B). Additionally, PI3K inhibitor significantly reduced the phosphorylated level of P38 in both cells (Fig. 9B). Our results are therefore in agreement with several studies showing that activation of P38 MAPK is required for P65 phosphorylation and transcription function (Bergmann et al., 1998; Kuphal et al., 2004; Wesselborg et al., 1997), and that Akt can transactivate the P65 subunit of NF-κB through the activation of P38-MAPK (Madrid et al., 2001; Viatour et al., 2005). Furthermore, studies using malignant melanoma also showed that the ERK pathway is not involved in NF-κB activation (Kuphal et al., 2004; Wang & Richmond, 2001). These results suggested that RANKL induced a sequential activation of signaling cascades from PI3K-Akt, P38, and then to NF-κB in ARCaP$_E$-RANKL and LNCaP-RANKL cells. Therefore, RANKL mediates the EMT transformation of prostate cancer cells by transactivating NF-κB signaling through Akt and P38 dependent pathways, which are known to be involved in cancer cell proliferation, survival, and distant metastasis.

In summary, our study identified an important role for prostate cancer cell derived RANKL in prostate cancer bone and soft tissue metastases through the induction of EMT. We observed an intriguing RANKL autocrine signal amplification system in which RANKL induced its own expression in cancer but not normal cells through activation of the oncogenic cMyc transcription factor. We showed that RANKL-RANK interaction activated downstream PI3K-Akt, P38-MAPK, and NF-κB. We suggest that fine-tuning the RANKL-RANK switch in prostate cancer cells could elicit insights in the biology of EMT and the osteoblastic versus osteolytic lesions induced by metastatic prostate cancer, and improve the therapeutic targeting of the RANKL-RANK axis. Understanding the roles of tumor cell-derived RANKL in EMT and tumor dormancy could strengthen our rationale for targeting RANKL-c-Met-mediated downstream signaling and improve the effectiveness of targeting lethal bone metastasis in CRPC.

Future Directions

Ectopic expression of RANKL induced EMT progression and metastasis in indolent prostate cancer cells, such as LNCaP and $ARCaP_E$ cells. Also, we could ablate the expression of RANKL or RANK in aggressive $ARCaP_M$ and PC3 cells, which express high levels of RANKL, using a shRNA approach. We will examine both the *in vitro* and *in vivo* behavior of these RANKL or RANK knock-down $ARCaP_M$ and PC3 cells.

Since RANKL-c-Met signaling converges, by which RANKL expression induced both RANKL and c-Met expression by prostate cancer cells, we will treat mice bearing intracardially-injected or intratibially-injected LNCaP-RANKL cells with the anti-RANKL monoclonal antibody denosumab (Adler & Gill, 2011; Bishr et al., 2011; Fizazi et al., 2011; George & Moul, 2011; Scott & Muir, 2011) and the small molecule cabozantinib (XL-184, (Smith, 2011), which targets c-Met to determine if these drugs alone or in combination can prevent LNCaP-RANKL-induced bone and soft tissue metastasis or prevent local tumor growth in the tibial bone.

We also aim to further study the reawakening of tumor dormancy by RANKL. We will generate tetracycline inducible (Tet-on) RANKL expressing prostate cancer cell lines using LNCaP and $ARCaP_E$ cells. We will repeat the *in vivo* co-inoculation experiment using RFP-tagged LNCaP cells and tetracycline inducible RANKL expressing LNCaP cells, for which we can control the time point for switching on the RANKL expression, and study LNCaP-RFP behavior *in vivo*. Alternatively, we will inoculate LNCaP-RFP cells either intracardially or intratibially in nude mice for a month followed by administration of recombinant human/mouse RANKL proteins via i.p. injection to examine if LNCaP-RFP cells can metastasize or grow in the tibia.

Furthermore, we will also be interested in ectopically overexpressing cMet in LNCaP cells to examine if cMet expression can drive EMT progression and metastasis in LNCaP cells similar to RANKL-expressing LNCaP cells. In conjunction, we are also generating cMet knock-down LNCaP-RANKL, $ARCaP_{M,}$ and PC3 cells. We found that their morphology changed from mesenchymal to more epithelial-like, suggesting a reversal of EMT or MET phenotype, which coincides with decreased *in vitro* migration and invasion potential. We will therefore further examine their tumorigenic and metastatic potential *in vivo.*

BIBLIOGRAPHY

Adler, R. A., & Gill, R. S. (2011). Clinical utility of denosumab for treatment of bone loss in men and women. *Clin Interv Aging, 6*, 119-124.

Aggarwal, B. B. (2004). Nuclear factor-kappaB: the enemy within. *Cancer Cell, 6*(3), 203-208.

Aguirre-Ghiso, J. A. (2007). Models, mechanisms and clinical evidence for cancer dormancy. *Nat Rev Cancer, 7*(11), 834-846.

Al-Ejeh, F., Smart, C. E., Morrison, B. J., Chenevix-Trench, G., Lopez, J. A., Lakhani, S. R., et al. (2011). Breast cancer stem cells: treatment resistance and therapeutic opportunities. *Carcinogenesis, 32*(5), 650-658.

Alexander, N. R., Tran, N. L., Rekapally, H., Summers, C. E., Glackin, C., & Heimark, R. L. (2006). N-cadherin gene expression in prostate carcinoma is modulated by integrin-dependent nuclear translocation of Twist1. *Cancer Res, 66*(7), 3365-3369.

Anandarajah, A. P. (2009). Role of RANKL in bone diseases. *Trends Endocrinol Metab, 20*(2), 88-94.

Andersen, R. J., Mawji, N. R., Wang, J., Wang, G., Haile, S., Myung, J. K., et al. (2010). Regression of castrate-recurrent prostate cancer by a small-molecule inhibitor of the amino-terminus domain of the androgen receptor. *Cancer Cell, 17*(6), 535-546.

Armstrong, A. J., Marengo, M. S., Oltean, S., Kemeny, G., Bitting, R. L., Turnbull, J. D., et al. Circulating tumor cells from patients with advanced prostate and breast cancer display both epithelial and mesenchymal markers. *Mol Cancer Res, 9*(8), 997-1007.

Armstrong, A. P., Miller, R. E., Jones, J. C., Zhang, J., Keller, E. T., & Dougall, W. C. (2008). RANKL acts directly on RANK-expressing prostate tumor cells and mediates migration and expression of tumor metastasis genes. *Prostate, 68*(1), 92-104.

Avizienyte, E., Brunton, V. G., Fincham, V. J., & Frame, M. C. (2005). The SRC-induced mesenchymal state in late-stage colon cancer cells. *Cells Tissues Organs, 179*(1-2), 73-80.

Bailey, V. J., Puleo, C. M., Ho, Y. P., Yeh, H. C., & Wang, T. H. (2009). Quantum dots in molecular detection of disease. *Conf Proc IEEE Eng Med Biol Soc, 2009*, 4089-4092.

Bakin, A. V., Tomlinson, A. K., Bhowmick, N. A., Moses, H. L., & Arteaga, C. L. (2000). Phosphatidylinositol 3-kinase function is required for transforming growth factor beta-mediated epithelial to mesenchymal transition and cell migration. *J Biol Chem, 275*(47), 36803-36810.

Batson, O. V. (1940). The Function of the Vertebral Veins and Their Role in the Spread of Metastases. *Ann Surg, 112*(1), 138-149.

Belguise, K., Guo, S., Yang, S., Rogers, A. E., Seldin, D. C., Sherr, D. H., et al. (2007). Green tea polyphenols reverse cooperation between c-Rel and CK2 that induces the aryl hydrocarbon receptor, slug, and an invasive phenotype. *Cancer Res, 67*(24), 11742-11750.

Beltran, H., Beer, T. M., Carducci, M. A., de Bono, J., Gleave, M., Hussain, M., et al. (2011). New Therapies for Castration-Resistant Prostate Cancer: Efficacy and Safety. *European Urology, In Press, Corrected Proof.*

Bergmann, M., Hart, L., Lindsay, M., Barnes, P. J., & Newton, R. (1998). IkappaBalpha degradation and nuclear factor-kappaB DNA binding are insufficient for interleukin-1beta and tumor necrosis factor-alpha-induced kappaB-dependent transcription. Requirement for an additional activation pathway. *J Biol Chem, 273*(12), 6607-6610.

Berridge, M. V., & Tan, A. S. (1993). Characterization of the cellular reduction of 3-(4,5-dimethylthiazol-2-yl)-2,5-diphenyltetrazolium bromide (MTT): subcellular localization, substrate dependence, and involvement of mitochondrial electron transport in MTT reduction. *Arch Biochem Biophys, 303*(2), 474-482.

Bhat-Nakshatri, P., Sweeney, C. J., & Nakshatri, H. (2002). Identification of signal transduction pathways involved in constitutive NF-kappaB activation in breast cancer cells. *Oncogene, 21*(13), 2066-2078.

Bhowmick, N. A., Ghiassi, M., Bakin, A., Aakre, M., Lundquist, C. A., Engel, M. E., et al. (2001). Transforming growth factor-beta1 mediates epithelial to mesenchymal transdifferentiation through a RhoA-dependent mechanism. *Mol Biol Cell, 12*(1), 27-36.

Bishr, M., Lattouf, J. B., Gannon, P. O., & Saad, F. (2011). Updates on therapeutic targets and agents in castration-resistant prostate cancer. *Minerva Urol Nefrol, 63*(2), 131-143.

Biswas, D. K., Cruz, A. P., Gansberger, E., & Pardee, A. B. (2000). Epidermal growth factor-induced nuclear factor kappa B activation: A major pathway of cell-cycle progression in estrogen-receptor negative breast cancer cells. *Proc Natl Acad Sci U S A, 97*(15), 8542-8547.

Bolos, V., Peinado, H., Perez-Moreno, M. A., Fraga, M. F., Esteller, M., & Cano, A. (2003). The transcription factor Slug represses E-cadherin expression and induces epithelial to mesenchymal transitions: a comparison with Snail and E47 repressors. *J Cell Sci, 116*(Pt 3), 499-511.

Bond, M., Fabunmi, R. P., Baker, A. H., & Newby, A. C. (1998). Synergistic upregulation of metalloproteinase-9 by growth factors and inflammatory cytokines: an absolute requirement for transcription factor NF-kappa B. *FEBS Lett, 435*(1), 29-34.

Boyce, B. F., & Xing, L. (2007). Biology of RANK, RANKL, and osteoprotegerin. *Arthritis Res Ther, 9 Suppl 1*, S1.

Boyer, B., Roche, S., Denoyelle, M., & Thiery, J. P. (1997). Src and Ras are involved in separate pathways in epithelial cell scattering. *Embo J, 16*(19), 5904-5913.

Boyer, B., Valles, A. M., & Edme, N. (2000). Induction and regulation of epithelial-mesenchymal transitions. *Biochem Pharmacol, 60*(8), 1091-1099.

Boyle, W. J., Simonet, W. S., & Lacey, D. L. (2003). Osteoclast differentiation and activation. *Nature, 423*(6937), 337-342.

Brabletz, T., Hlubek, F., Spaderna, S., Schmalhofer, O., Hiendlmeyer, E., Jung, A., et al. (2005). Invasion and metastasis in colorectal cancer: epithelial-mesenchymal transition, mesenchymal-epithelial transition, stem cells and beta-catenin. *Cells Tissues Organs, 179*(1-2), 56-65.

Brown, J. M., Corey, E., Lee, Z. D., True, L. D., Yun, T. J., Tondravi, M., et al. (2001). Osteoprotegerin and rank ligand expression in prostate cancer. *Urology, 57*(4), 611-616.

Bubendorf, L., Schopfer, A., Wagner, U., Sauter, G., Moch, H., Willi, N., et al. (2000). Metastatic patterns of prostate cancer: an autopsy study of 1,589 patients. *Hum Pathol, 31*(5), 578-583.

Burridge, K., & Wennerberg, K. (2004). Rho and Rac take center stage. *Cell, 116*(2), 167-179.

Campbell, S. L., Khosravi-Far, R., Rossman, K. L., Clark, G. J., & Der, C. J. (1998). Increasing complexity of Ras signaling. *Oncogene, 17*(11 Reviews), 1395-1413.

Canon, J. R., Roudier, M., Bryant, R., Morony, S., Stolina, M., Kostenuik, P. J., et al. (2008). Inhibition of RANKL blocks skeletal tumor progression and improves survival in a mouse model of breast cancer bone metastasis. *Clin Exp Metastasis, 25*(2), 119-129.

Ceraline, J., Cruchant, M. D., Erdmann, E., Erbs, P., Kurtz, J. E., Duclos, B., et al. (2004). Constitutive activation of the androgen receptor by a point mutation in the hinge region: a new mechanism for androgen-independent growth in prostate cancer. *Int J Cancer, 108*(1), 152-157.

Chang, H. W., Chow, V., Lam, K. Y., Wei, W. I., & Yuen, A. (2002). Loss of E-cadherin expression resulting from promoter hypermethylation in oral tongue carcinoma and its prognostic significance. *Cancer, 94*(2), 386-392.

Chang, H. Y., Kao, M. C., Way, T. D., Ho, C. T., & Fu, E. (2011). Diosgenin suppresses hepatocyte growth factor (HGF)-induced epithelial-mesenchymal transition by down-regulation of Mdm2 and vimentin. *J Agric Food Chem, 59*(10), 5357-5363.

Chang, L., & Karin, M. (2001). Mammalian MAP kinase signalling cascades. *Nature, 410*(6824), 37-40.

Chao, Y. L., Shepard, C. R., & Wells, A. (2010). Breast carcinoma cells re-express E-cadherin during mesenchymal to epithelial reverting transition. *Mol Cancer, 9*, 179.

Chellaiah, M., Fitzgerald, C., Alvarez, U., & Hruska, K. (1998). c-Src is required for stimulation of gelsolin-associated phosphatidylinositol 3-kinase. *J Biol Chem, 273*(19), 11908-11916.

Chen, G., Sircar, K., Aprikian, A., Potti, A., Goltzman, D., & Rabbani, S. A. (2006). Expression of RANKL/RANK/OPG in primary and metastatic human prostate cancer as markers of disease stage and functional regulation. *Cancer, 107*(2), 289-298.

Cher, M. L. (2001). Mechanisms governing bone metastasis in prostate cancer. *Curr Opin Urol, 11*(5), 483-488.

Cheville, J. C., Tindall, D., Boelter, C., Jenkins, R., Lohse, C. M., Pankratz, V. S., et al. (2002). Metastatic prostate carcinoma to bone: clinical and pathologic features associated with cancer-specific survival. *Cancer, 95*(5), 1028-1036.

Chilov, D., Kukk, E., Taira, S., Jeltsch, M., Kaukonen, J., Palotie, A., et al. (1997). Genomic organization of human and mouse genes for vascular endothelial growth factor C. *J Biol Chem, 272*(40), 25176-25183.

Chua, H. L., Bhat-Nakshatri, P., Clare, S. E., Morimiya, A., Badve, S., & Nakshatri, H. (2007). NF-kappaB represses E-cadherin expression and enhances epithelial to mesenchymal transition of mammary epithelial cells: potential involvement of ZEB-1 and ZEB-2. *Oncogene, 26*(5), 711-724.

Chung, L. W., Li, W., Gleave, M. E., Hsieh, J. T., Wu, H. C., Sikes, R. A., et al. (1992). Human prostate cancer model: roles of growth factors and extracellular matrices. *J Cell Biochem Suppl, 16H*, 99-105.

Coleman, R. E. (1997). Skeletal complications of malignancy. *Cancer, 80*(8 Suppl), 1588-1594.

Coleman, R. E. (2001). Metastatic bone disease: clinical features, pathophysiology and treatment strategies. *Cancer Treat Rev, 27*(3), 165-176.

Coloff, J. L., Macintyre, A. N., Nichols, A. G., Liu, T., Gallo, C. A., Plas, D. R., et al. (2011). Akt-dependent glucose metabolism promotes Mcl-1 synthesis to maintain cell survival and resistance to Bcl-2 inhibition. *Cancer Res, 71*(15), 5204-5213.

Corey, E., Quinn, J. E., Bladou, F., Brown, L. G., Roudier, M. P., Brown, J. M., et al. (2002). Establishment and characterization of osseous prostate cancer models: intra-tibial injection of human prostate cancer cells. *Prostate, 52*(1), 20-33.

Cross, S. S., Harrison, R. F., Balasubramanian, S. P., Lippitt, J. M., Evans, C. A., Reed, M. W., et al. (2006). Expression of receptor activator of nuclear factor kappabeta ligand (RANKL) and tumour necrosis factor related, apoptosis inducing ligand (TRAIL) in breast cancer, and their relations with osteoprotegerin, oestrogen receptor, and clinicopathological variables. *J Clin Pathol, 59*(7), 716-720.

Culig, Z., Hobisch, A., Cronauer, M. V., Radmayr, C., Trapman, J., Hittmair, A., et al. (1994). Androgen receptor activation in prostatic tumor cell lines by insulin-like growth factor-I, keratinocyte growth factor, and epidermal growth factor. *Cancer Res, 54*(20), 5474-5478.

David, J. P., Sabapathy, K., Hoffmann, O., Idarraga, M. H., & Wagner, E. F. (2002). JNK1 modulates osteoclastogenesis through both c-Jun phosphorylation-dependent and -independent mechanisms. *J Cell Sci, 115*(Pt 22), 4317-4325.

Davies, M., Robinson, M., Smith, E., Huntley, S., Prime, S., & Paterson, I. (2005). Induction of an epithelial to mesenchymal transition in human immortal and malignant keratinocytes by TGF-beta1 involves MAPK, Smad and AP-1 signalling pathways. *J Cell Biochem, 95*(5), 918-931.

De Marzo, A. M., Knudsen, B., Chan-Tack, K., & Epstein, J. I. (1999). E-cadherin expression as a marker of tumor aggressiveness in routinely processed radical prostatectomy specimens. *Urology, 53*(4), 707-713.

Dhillon, A. S., Hagan, S., Rath, O., & Kolch, W. (2007). MAP kinase signalling pathways in cancer. *Oncogene, 26*(22), 3279-3290.

Ding, Q., Xia, W., Liu, J. C., Yang, J. Y., Lee, D. F., Xia, J., et al. (2005). Erk associates with and primes GSK-3beta for its inactivation resulting in upregulation of beta-catenin. *Mol Cell, 19*(2), 159-170.

Drachenberg, D. E., Elgamal, A. A., Rowbotham, R., Peterson, M., & Murphy, G. P. (1999). Circulating levels of interleukin-6 in patients with hormone refractory prostate cancer. *Prostate, 41*(2), 127-133.

Eder, J. P., Vande Woude, G. F., Boerner, S. A., & LoRusso, P. M. (2009). Novel therapeutic inhibitors of the c-Met signaling pathway in cancer. *Clin Cancer Res, 15*(7), 2207-2214.

Elo, J. P., & Visakorpi, T. (2001). Molecular genetics of prostate cancer. *Ann Med, 33*(2), 130-141.

Fata, J. E., Kong, Y. Y., Li, J., Sasaki, T., Irie-Sasaki, J., Moorehead, R. A., et al. (2000). The osteoclast differentiation factor osteoprotegerin-ligand is essential for mammary gland development. *Cell, 103*(1), 41-50.

Feldman, B. J., & Feldman, D. (2001). The development of androgen-independent prostate cancer. *Nat Rev Cancer, 1*(1), 34-45.

Fernandez-Valdivia, R., Mukherjee, A., Ying, Y., Li, J., Paquet, M., DeMayo, F. J., et al. (2009). The RANKL signaling axis is sufficient to elicit ductal side-branching and alveologenesis in the mammary gland of the virgin mouse. *Dev Biol, 328*(1), 127-139.

Fili, S., Karalaki, M., & Schaller, B. (2009). Mechanism of bone metastasis: the role of osteoprotegerin and of the host-tissue microenvironment-related survival factors. *Cancer Lett, 283*(1), 10-19.

Fisher, J. L., Schmitt, J. F., Howard, M. L., Mackie, P. S., Choong, P. F., & Risbridger, G. P. (2002). An in vivo model of prostate carcinoma growth and invasion in bone. *Cell Tissue Res, 307*(3), 337-345.

Fizazi, K., Carducci, M., Smith, M., Damiao, R., Brown, J., Karsh, L., et al. (2011). Denosumab versus zoledronic acid for treatment of bone metastases in men with castration-resistant prostate cancer: a randomised, double-blind study. *Lancet, 377*(9768), 813-822.

Gaddipati, J. P., McLeod, D. G., Heidenberg, H. B., Sesterhenn, I. A., Finger, M. J., Moul, J. W., et al. (1994). Frequent detection of codon 877 mutation in the androgen receptor gene in advanced prostate cancers. *Cancer Res, 54*(11), 2861-2864.

Galibert, L., Tometsko, M. E., Anderson, D. M., Cosman, D., & Dougall, W. C. (1998). The involvement of multiple tumor necrosis factor receptor (TNFR)-associated factors in the signaling mechanisms of receptor activator of NF-kappaB, a member of the TNFR superfamily. *J Biol Chem, 273*(51), 34120-34127.

Gangemi, R., Paleari, L., Orengo, A. M., Cesario, A., Chessa, L., Ferrini, S., et al. (2009). Cancer stem cells: a new paradigm for understanding tumor growth and progression and drug resistance. *Curr Med Chem, 16*(14), 1688-1703.

George, D., & Moul, J. W. (2011). Emerging treatment options for patients with castration-resistant prostate cancer. *Prostate*.

Ghazani, A. A., Lee, J. A., Klostranec, J., Xiang, Q., Dacosta, R. S., Wilson, B. C., et al. (2006). High throughput quantification of protein expression of cancer antigens in tissue microarray using quantum dot nanocrystals. *Nano Lett, 6*(12), 2881-2886.

Ghotra, V. P., Puigvert, J. C., & Danen, E. H. (2009). The cancer stem cell microenvironment and anti-cancer therapy. *Int J Radiat Biol, 85*(11), 955-962.

Gina C.Y. Chu, R. W., Haiyen Zhau, Xu Feng and Leland W.K. Chung. (2010). Autocrine and Paracrine Cell Signaling Mediated by RANKL-RANK Interaction Promotes Epithelial to Mesenchymal Transition of Human Prostate Cancer Cells. *Society For Basic Urologic Research*.

Gnanapragasam, V. J., Leung, H. Y., Pulimood, A. S., Neal, D. E., & Robson, C. N. (2001). Expression of RAC 3, a steroid hormone receptor co-activator in prostate cancer. *Br J Cancer, 85*(12), 1928-1936.

Gonzalez-Suarez, E., Branstetter, D., Armstrong, A., Dinh, H., Blumberg, H., & Dougall, W. C. (2007). RANK overexpression in transgenic mice with mouse mammary tumor virus promoter-controlled RANK increases proliferation and impairs alveolar differentiation in the mammary epithelia and disrupts lumen formation in cultured epithelial acini. *Mol Cell Biol, 27*(4), 1442-1454.

Gonzalez-Suarez, E., Jacob, A. P., Jones, J., Miller, R., Roudier-Meyer, M. P., Erwert, R., et al. (2010). RANK ligand mediates progestin-induced mammary epithelial proliferation and carcinogenesis. *Nature, 468*(7320), 103-107.

Gori, F., Hofbauer, L. C., Dunstan, C. R., Spelsberg, T. C., Khosla, S., & Riggs, B. L. (2000). The expression of osteoprotegerin and RANK ligand and the support of osteoclast formation by stromal-osteoblast lineage cells is developmentally regulated. *Endocrinology, 141*(12), 4768-4776.

Gottlieb, B., Beitel, L. K., Wu, J. H., & Trifiro, M. (2004). The androgen receptor gene mutations database (ARDB): 2004 update. *Hum Mutat, 23*(6), 527-533.

Grandori, C., Cowley, S. M., James, L. P., & Eisenman, R. N. (2000). The Myc/Max/Mad network and the transcriptional control of cell behavior. *Annu Rev Cell Dev Biol, 16*, 653-699.

Gregory, C. W., Hamil, K. G., Kim, D., Hall, S. H., Pretlow, T. G., Mohler, J. L., et al. (1998). Androgen receptor expression in androgen-independent prostate cancer is associated with increased expression of androgen-regulated genes. *Cancer Res, 58*(24), 5718-5724.

Gregory, C. W., He, B., Johnson, R. T., Ford, O. H., Mohler, J. L., French, F. S., et al. (2001). A mechanism for androgen receptor-mediated prostate cancer recurrence after androgen deprivation therapy. *Cancer Res, 61*(11), 4315-4319.

Gregory, C. W., Johnson, R. T., Jr., Mohler, J. L., French, F. S., & Wilson, E. M. (2001). Androgen receptor stabilization in recurrent prostate cancer is associated with hypersensitivity to low androgen. *Cancer Res, 61*(7), 2892-2898.

Grimaud, E., Soubigou, L., Couillaud, S., Coipeau, P., Moreau, A., Passuti, N., et al. (2003). Receptor activator of nuclear factor kappaB ligand (RANKL)/osteoprotegerin (OPG) ratio is increased in severe osteolysis. *Am J Pathol, 163*(5), 2021-2031.

Guarino, M., Rubino, B., & Ballabio, G. (2007). The role of epithelial-mesenchymal transition in cancer pathology. *Pathology, 39*(3), 305-318.

Guise, T. (2010). Examining the metastatic niche: targeting the microenvironment. *Semin Oncol, 37 Suppl 2*, S2-14.

Gustafson, W. C., & Weiss, W. A. (2010). Myc proteins as therapeutic targets. *Oncogene, 29*(9), 1249-1259.

Hanada, R., Hanada, T., Sigl, V., Schramek, D., & Penninger, J. M. (2011). RANKL/RANK-beyond bones. *J Mol Med (Berl), 89*(7), 647-656.

Heinlein, C. A., & Chang, C. (2002). Androgen receptor (AR) coregulators: an overview. *Endocr Rev, 23*(2), 175-200.

Heinlein, C. A., & Chang, C. (2004). Androgen receptor in prostate cancer. *Endocr Rev, 25*(2), 276-308.

Helbig, G., Christopherson, K. W., 2nd, Bhat-Nakshatri, P., Kumar, S., Kishimoto, H., Miller, K. D., et al. (2003). NF-kappaB promotes breast cancer cell migration and metastasis by inducing the expression of the chemokine receptor CXCR4. *J Biol Chem, 278*(24), 21631-21638.

Hobisch, A., Eder, I. E., Putz, T., Horninger, W., Bartsch, G., Klocker, H., et al. (1998). Interleukin-6 regulates prostate-specific protein expression in prostate carcinoma cells by activation of the androgen receptor. *Cancer Res, 58*(20), 4640-4645.

Horwich, A. (2004). Prostate cancer management. *Ann Oncol, 15 Suppl 4*, iv307-312.

Hotz, B., Arndt, M., Dullat, S., Bhargava, S., Buhr, H. J., & Hotz, H. G. (2007). Epithelial to mesenchymal transition: expression of the regulators snail, slug, and twist in pancreatic cancer. *Clin Cancer Res, 13*(16), 4769-4776.

Hsu, T., Trojanowska, M., & Watson, D. K. (2004). Ets proteins in biological control and cancer. *J Cell Biochem, 91*(5), 896-903.

Hu, M., Yan, J., He, Y., Lu, H., Weng, L., Song, S., et al. (2010). Ultrasensitive, multiplexed detection of cancer biomarkers directly in serum by using a quantum dot-based microfluidic protein chip. *ACS Nano, 4*(1), 488-494.

Huang, L., Cheng, Y. Y., Chow, L. T., Zheng, M. H., & Kumta, S. M. (2002). Tumour cells produce receptor activator of NF-kappaB ligand (RANKL) in skeletal metastases. *J Clin Pathol, 55*(11), 877-878.

Huang, W. C., Wu, D., Xie, Z., Zhau, H. E., Nomura, T., Zayzafoon, M., et al. (2006). beta2-microglobulin is a signaling and growth-promoting factor for human prostate cancer bone metastasis. *Cancer Res, 66*(18), 9108-9116.

Huber, M. A., Azoitei, N., Baumann, B., Grunert, S., Sommer, A., Pehamberger, H., et al. (2004). NF-kappaB is essential for epithelial-mesenchymal transition and metastasis in a model of breast cancer progression. *J Clin Invest, 114*(4), 569-581.

Huber, M. A., Kraut, N., & Beug, H. (2005). Molecular requirements for epithelial-mesenchymal transition during tumor progression. *Curr Opin Cell Biol, 17*(5), 548-558.

Hung, C. M., Kuo, D. H., Chou, C. H., Su, Y. C., Ho, C. T., & Way, T. D. (2011). Osthole suppresses hepatocyte growth factor (HGF)-induced epithelial-mesenchymal transition via repression of the c-Met/Akt/mTOR pathway in human breast cancer cells. *J Agric Food Chem, 59*(17), 9683-9690.

Huynh, H., Ngo, V. C., Koong, H. N., Poon, D., Choo, S. P., Thng, C. H., et al. (2009). Sorafenib and rapamycin induce growth suppression in mouse models of hepatocellular carcinoma. *J Cell Mol Med, 13*(8B), 2673-2683.

Ikeda, T., Kasai, M., Utsuyama, M., & Hirokawa, K. (2001). Determination of three isoforms of the receptor activator of nuclear factor-kappaB ligand and their differential expression in bone and thymus. *Endocrinology, 142*(4), 1419-1426.

Iotsova, V., Caamano, J., Loy, J., Yang, Y., Lewin, A., & Bravo, R. (1997). Osteopetrosis in mice lacking NF-kappaB1 and NF-kappaB2. *Nat Med, 3*(11), 1285-1289.

Irby, R. B., & Yeatman, T. J. (2000). Role of Src expression and activation in human cancer. *Oncogene, 19*(49), 5636-5642.

Isaacs, J. T. (1994). Role of androgens in prostatic cancer. *Vitam Horm, 49*, 433-502.

Jemal, A., Tiwari, R. C., Murray, T., Ghafoor, A., Samuels, A., Ward, E., et al. (2004). Cancer statistics, 2004. *CA Cancer J Clin, 54*(1), 8-29.

Jiang, H., Sha, S. H., & Schacht, J. (2006). Rac/Rho pathway regulates actin depolymerization induced by aminoglycoside antibiotics. *J Neurosci Res, 83*(8), 1544-1551.

Jimi, E., Akiyama, S., Tsurukai, T., Okahashi, N., Kobayashi, K., Udagawa, N., et al. (1999). Osteoclast differentiation factor acts as a multifunctional regulator in murine osteoclast differentiation and function. *J Immunol, 163*(1), 434-442.

Jones, D. H., Nakashima, T., Sanchez, O. H., Kozieradzki, I., Komarova, S. V., Sarosi, I., et al. (2006). Regulation of cancer cell migration and bone metastasis by RANKL. *Nature, 440*(7084), 692-696.

Josson, S., Nomura, T., Lin, J. T., Huang, W. C., Wu, D., Zhau, H. E., et al. (2011). beta2-microglobulin induces epithelial to mesenchymal transition and confers cancer lethality and bone metastasis in human cancer cells. *Cancer Res, 71*(7), 2600-2610.

Kalluri, R. (2009). EMT: when epithelial cells decide to become mesenchymal-like cells. *J Clin Invest, 119*(6), 1417-1419.

Kang, Y., & Massague, J. (2004). Epithelial-mesenchymal transitions: twist in development and metastasis. *Cell, 118*(3), 277-279.

Karreth, F., & Tuveson, D. A. (2004). Twist induces an epithelial-mesenchymal transition to facilitate tumor metastasis. *Cancer Biol Ther, 3*(11), 1058-1059.

Kartsogiannis, V., Zhou, H., Horwood, N. J., Thomas, R. J., Hards, D. K., Quinn, J. M., et al. (1999). Localization of RANKL (receptor activator of NF kappa B ligand) mRNA and protein in skeletal and extraskeletal tissues. *Bone, 25*(5), 525-534.

Kearns, A. E., Khosla, S., & Kostenuik, P. J. (2008). Receptor activator of nuclear factor kappaB ligand and osteoprotegerin regulation of bone remodeling in health and disease. *Endocr Rev, 29*(2), 155-192.

Keller, E. T. (2002). The role of osteoclastic activity in prostate cancer skeletal metastases. *Drugs Today (Barc), 38*(2), 91-102.

Keller, E. T., & Brown, J. (2004). Prostate cancer bone metastases promote both osteolytic and osteoblastic activity. *J Cell Biochem, 91*(4), 718-729.

Kiefer, J. A., Vessella, R. L., Quinn, J. E., Odman, A. M., Zhang, J., Keller, E. T., et al. (2004). The effect of osteoprotegerin administration on the intra-tibial growth of the osteoblastic LuCaP 23.1 prostate cancer xenograft. *Clin Exp Metastasis, 21*(5), 381-387.

Kim, H. J., Litzenburger, B. C., Cui, X., Delgado, D. A., Grabiner, B. C., Lin, X., et al. (2007). Constitutively active type I insulin-like growth factor receptor causes transformation and xenograft growth of immortalized mammary epithelial cells and is accompanied by an epithelial-to-mesenchymal transition mediated by NF-kappaB and snail. *Mol Cell Biol, 27*(8), 3165-3175.

Kim, N. S., Kim, H. J., Koo, B. K., Kwon, M. C., Kim, Y. W., Cho, Y., et al. (2006). Receptor activator of NF-kappaB ligand regulates the proliferation of mammary epithelial cells via Id2. *Mol Cell Biol, 26*(3), 1002-1013.

Klymkowsky, M. W., & Savagner, P. (2009). Epithelial-mesenchymal transition: a cancer researcher's conceptual friend and foe. *Am J Pathol, 174*(5), 1588-1593.

Koeneman, K. S., Yeung, F., & Chung, L. W. (1999). Osteomimetic properties of prostate cancer cells: a hypothesis supporting the predilection of prostate cancer metastasis and growth in the bone environment. *Prostate, 39*(4), 246-261.

Koivisto, P. A., & Helin, H. J. (1999). Androgen receptor gene amplification increases tissue PSA protein expression in hormone-refractory prostate carcinoma. *J Pathol, 189*(2), 219-223.

Komori, T. (2006). Regulation of osteoblast differentiation by transcription factors. *J Cell Biochem, 99*(5), 1233-1239.

Komori, T., Yagi, H., Nomura, S., Yamaguchi, A., Sasaki, K., Deguchi, K., et al. (1997). Targeted disruption of Cbfa1 results in a complete lack of bone formation owing to maturational arrest of osteoblasts. *Cell, 89*(5), 755-764.

Kong, D., Banerjee, S., Ahmad, A., Li, Y., Wang, Z., Sethi, S., et al. (2010). Epithelial to mesenchymal transition is mechanistically linked with stem cell signatures in prostate cancer cells. *PLoS One, 5*(8), e12445.

Kong, X. L., Qi, H., Zhou, H. X., Ren, L. L., Deng, C. Y., & Li, F. R. (2010). A novel sensitive immunoassay by nucleic acid barcode dot and its application in the detection of prostate-specific antigen. *Clin Chem Lab Med, 48*(2), 279-283.

Kong, Y. Y., Yoshida, H., Sarosi, I., Tan, H. L., Timms, E., Capparelli, C., et al. (1999). OPGL is a key regulator of osteoclastogenesis, lymphocyte development and lymph-node organogenesis. *Nature, 397*(6717), 315-323.

Kowalski, P. J., Rubin, M. A., & Kleer, C. G. (2003). E-cadherin expression in primary carcinomas of the breast and its distant metastases. *Breast Cancer Res, 5*(6), R217-222.

Kuphal, S., Poser, I., Jobin, C., Hellerbrand, C., & Bosserhoff, A. K. (2004). Loss of E-cadherin leads to upregulation of NFkappaB activity in malignant melanoma. *Oncogene, 23*(52), 8509-8519.

Kwok, W. K., Ling, M. T., Lee, T. W., Lau, T. C., Zhou, C., Zhang, X., et al. (2005). Up-regulation of TWIST in prostate cancer and its implication as a therapeutic target. *Cancer Res, 65*(12), 5153-5162.

Lacey, D. L., Timms, E., Tan, H. L., Kelley, M. J., Dunstan, C. R., Burgess, T., et al. (1998). Osteoprotegerin ligand is a cytokine that regulates osteoclast differentiation and activation. *Cell, 93*(2), 165-176.

Landis, S. H., Murray, T., Bolden, S., & Wingo, P. A. (1999). Cancer statistics, 1999. *CA Cancer J Clin, 49*(1), 8-31, 31.

Lecrone, V., Li, W., Devoll, R. E., Logothetis, C., & Farach-Carson, M. C. (2000). Calcium signals in prostate cancer cells: specific activation by bone-matrix proteins. *Cell Calcium, 27*(1), 35-42.

Lee, R. J., Saylor, P. J., & Smith, M. R. (2010). Treatment and prevention of bone complications from prostate cancer. *Bone, 48*(1), 88-95.

Lemaire, V., Tobin, F. L., Greller, L. D., Cho, C. R., & Suva, L. J. (2004). Modeling the interactions between osteoblast and osteoclast activities in bone remodeling. *J Theor Biol, 229*(3), 293-309.

Lengyel, E., Prechtel, D., Resau, J. H., Gauger, K., Welk, A., Lindemann, K., et al. (2005). C-Met overexpression in node-positive breast cancer identifies patients with poor clinical outcome independent of Her2/neu. *Int J Cancer, 113*(4), 678-682.

Leung, K. (2004). Quantum dot 800-prostate-specific membrane antigen antibody J591.

Li, R., Dai, H., Wheeler, T. M., Sayeeduddin, M., Scardino, P. T., Frolov, A., et al. (2009). Prognostic value of Akt-1 in human prostate cancer: a computerized quantitative assessment with quantum dot technology. *Clin Cancer Res, 15*(10), 3568-3573.

Li, Y., Kucuk, O., Hussain, M., Abrams, J., Cher, M. L., & Sarkar, F. H. (2006). Antitumor and antimetastatic activities of docetaxel are enhanced by genistein through regulation of osteoprotegerin/receptor activator of nuclear factor-kappaB (RANK)/RANK ligand/MMP-9 signaling in prostate cancer. *Cancer Res, 66*(9), 4816-4825.

Liang, R. Q., Li, W., Li, Y., Tan, C. Y., Li, J. X., Jin, Y. X., et al. (2005). An oligonucleotide microarray for microRNA expression analysis based on labeling RNA with quantum dot and nanogold probe. *Nucleic Acids Res, 33*(2), e17.

Linja, M. J., Savinainen, K. J., Saramaki, O. R., Tammela, T. L., Vessella, R. L., & Visakorpi, T. (2001). Amplification and overexpression of androgen receptor gene in hormone-refractory prostate cancer. *Cancer Res, 61*(9), 3550-3555.

Lipton, A. (2011). Denosumab in breast cancer. *Curr Oncol Rep, 13*(1), 1-4.

Liu, J., Lau, S. K., Varma, V. A., Moffitt, R. A., Caldwell, M., Liu, T., et al. (2010). Molecular mapping of tumor heterogeneity on clinical tissue specimens with multiplexed quantum dots. *ACS Nano, 4*(5), 2755-2765.

Loberg, R. D., Logothetis, C. J., Keller, E. T., & Pienta, K. J. (2005). Pathogenesis and treatment of prostate cancer bone metastases: targeting the lethal phenotype. *J Clin Oncol, 23*(32), 8232-8241.

Lynch, C. C., Hikosaka, A., Acuff, H. B., Martin, M. D., Kawai, N., Singh, R. K., et al. (2005). MMP-7 promotes prostate cancer-induced osteolysis via the solubilization of RANKL. *Cancer Cell, 7*(5), 485-496.

Machado, J. C., Oliveira, C., Carvalho, R., Soares, P., Berx, G., Caldas, C., et al. (2001). E-cadherin gene (CDH1) promoter methylation as the second hit in sporadic diffuse gastric carcinoma. *Oncogene, 20*(12), 1525-1528.

Madrid, L. V., Mayo, M. W., Reuther, J. Y., & Baldwin, A. S., Jr. (2001). Akt stimulates the transactivation potential of the RelA/p65 Subunit of NF-kappa B through utilization of the Ikappa B kinase and activation of the mitogen-activated protein kinase p38. *J Biol Chem, 276*(22), 18934-18940.

Maeda, M., Johnson, K. R., & Wheelock, M. J. (2005). Cadherin switching: essential for behavioral but not morphological changes during an epithelium-to-mesenchyme transition. *J Cell Sci, 118*(Pt 5), 873-887.

Mancini, M., & Toker, A. (2009). NFAT proteins: emerging roles in cancer progression. *Nat Rev Cancer, 9*(11), 810-820.

Mani, S. A., Guo, W., Liao, M. J., Eaton, E. N., Ayyanan, A., Zhou, A. Y., et al. (2008). The epithelial-mesenchymal transition generates cells with properties of stem cells. *Cell, 133*(4), 704-715.

Manolagas, S. C., & Jilka, R. L. (1995). Bone marrow, cytokines, and bone remodeling. Emerging insights into the pathophysiology of osteoporosis. *N Engl J Med, 332*(5), 305-311.

Marcelli, M., Ittmann, M., Mariani, S., Sutherland, R., Nigam, R., Murthy, L., et al. (2000). Androgen receptor mutations in prostate cancer. *Cancer Res, 60*(4), 944-949.

Mason, L. I., & Patterson, R. P. (2003). Determining the relationship of heart rate and blood pressure using voluntary cardio-respiratory synchronization (VCRS). *Physiol Meas, 24*(4), 847-857.

McEwan, I. J. (2000). Gene regulation through chromatin remodelling by members of the nuclear receptor superfamily. *Biochem Soc Trans, 28*(4), 369-373.

McHugh, K. P., Hodivala-Dilke, K., Zheng, M. H., Namba, N., Lam, J., Novack, D., et al. (2000). Mice lacking beta3 integrins are osteosclerotic because of dysfunctional osteoclasts. *J Clin Invest, 105*(4), 433-440.

McKenna, N. J., Lanz, R. B., & O'Malley, B. W. (1999). Nuclear receptor coregulators: cellular and molecular biology. *Endocr Rev, 20*(3), 321-344.

Min, C., Eddy, S. F., Sherr, D. H., & Sonenshein, G. E. (2008). NF-kappaB and epithelial to mesenchymal transition of cancer. *J Cell Biochem, 104*(3), 733-744.

Miyazaki, T., Sanjay, A., Neff, L., Tanaka, S., Horne, W. C., & Baron, R. (2004). Src kinase activity is essential for osteoclast function. *J Biol Chem, 279*(17), 17660-17666.

Morel, A. P., Lievre, M., Thomas, C., Hinkal, G., Ansieau, S., & Puisieux, A. (2008). Generation of breast cancer stem cells through epithelial-mesenchymal transition. *PLoS One, 3*(8), e2888.

Morony, S., Capparelli, C., Lee, R., Shimamoto, G., Boone, T., Lacey, D. L., et al. (1999). A chimeric form of osteoprotegerin inhibits hypercalcemia and bone resorption induced by IL-1beta, TNF-alpha, PTH, PTHrP, and 1, 25(OH)2D3. *J Bone Miner Res, 14*(9), 1478-1485.

Morony, S., Capparelli, C., Sarosi, I., Lacey, D. L., Dunstan, C. R., & Kostenuik, P. J. (2001). Osteoprotegerin inhibits osteolysis and decreases skeletal tumor burden in syngeneic and nude mouse models of experimental bone metastasis. *Cancer Res, 61*(11), 4432-4436.

Muller, M. R., & Rao, A. (2010). NFAT, immunity and cancer: a transcription factor comes of age. *Nat Rev Immunol, 10*(9), 645-656.

Mundy, G. R. (1997). Mechanisms of bone metastasis. *Cancer, 80*(8 Suppl), 1546-1556.

Mundy, G. R. (2002). Metastasis to bone: causes, consequences and therapeutic opportunities. *Nat Rev Cancer, 2*(8), 584-593.

Murphy, W. L., Simmons, C. A., Kaigler, D., & Mooney, D. J. (2004). Bone regeneration via a mineral substrate and induced angiogenesis. *J Dent Res, 83*(3), 204-210.

Nakashima, K., Zhou, X., Kunkel, G., Zhang, Z., Deng, J. M., Behringer, R. R., et al. (2002). The novel zinc finger-containing transcription factor osterix is required for osteoblast differentiation and bone formation. *Cell, 108*(1), 17-29.

Nakashima, T., Kobayashi, Y., Yamasaki, S., Kawakami, A., Eguchi, K., Sasaki, H., et al. (2000). Protein expression and functional difference of membrane-bound and soluble receptor activator of NF-kappaB ligand: modulation of the expression by osteotropic factors and cytokines. *Biochem Biophys Res Commun, 275*(3), 768-775.

Nelson, W. J., & Nusse, R. (2004). Convergence of Wnt, beta-catenin, and cadherin pathways. *Science, 303*(5663), 1483-1487.

Nicolini, A., Ferrari, P., Fini, M., Borsari, V., Fallahi, P., Antonelli, A., et al. (2011). Stem cells: their role in breast cancer development and resistance to treatment. *Curr Pharm Biotechnol, 12*(2), 196-205.

Nieto, M. A. (2002). The snail superfamily of zinc-finger transcription factors. *Nat Rev Mol Cell Biol, 3*(3), 155-166.

Nomura, T., Huang, W. C., Zhau, H. E., Wu, D., Xie, Z., Mimata, H., et al. (2006). Beta2-microglobulin promotes the growth of human renal cell carcinoma through the activation of the protein kinase A, cyclic AMP-responsive element-binding protein, and vascular endothelial growth factor axis. *Clin Cancer Res, 12*(24), 7294-7305.

Odero-Marah, V. A., Wang, R., Chu, G., Zayzafoon, M., Xu, J., Shi, C., et al. (2008). Receptor activator of NF-kappaB Ligand (RANKL) expression is associated with epithelial to mesenchymal transition in human prostate cancer cells. *Cell Res, 18*(8), 858-870.

Ott, S. M. (2008). Histomorphometric measurements of bone turnover, mineralization, and volume. *Clin J Am Soc Nephrol, 3 Suppl 3*, S151-156.

Otto, F., Thornell, A. P., Crompton, T., Denzel, A., Gilmour, K. C., Rosewell, I. R., et al. (1997). Cbfa1, a candidate gene for cleidocranial dysplasia syndrome, is essential for osteoblast differentiation and bone development. *Cell, 89*(5), 765-771.

Paget, S. (1989). The distribution of secondary growths in cancer of the breast. 1889. *Cancer Metastasis Rev, 8*(2), 98-101.

Parfitt, A. M. (1994). Osteonal and hemi-osteonal remodeling: the spatial and temporal framework for signal traffic in adult human bone. *J Cell Biochem, 55*(3), 273-286.

Peinado, H., Portillo, F., & Cano, A. (2004). Transcriptional regulation of cadherins during development and carcinogenesis. *Int J Dev Biol, 48*(5-6), 365-375.

Pham, C. G., Bubici, C., Zazzeroni, F., Knabb, J. R., Papa, S., Kuntzen, C., et al. (2007). Upregulation of Twist-1 by NF-kappaB blocks cytotoxicity induced by chemotherapeutic drugs. *Mol Cell Biol, 27*(11), 3920-3935.

Pisters, L. L., Troncoso, P., Zhau, H. E., Li, W., von Eschenbach, A. C., & Chung, L. W. (1995). c-met proto-oncogene expression in benign and malignant human prostate tissues. *J Urol, 154*(1), 293-298.

Prins, G. S., Birch, L., & Greene, G. L. (1991). Androgen receptor localization in different cell types of the adult rat prostate. *Endocrinology, 129*(6), 3187-3199.

Raffo, A. J., Perlman, H., Chen, M. W., Day, M. L., Streitman, J. S., & Buttyan, R. (1995). Overexpression of bcl-2 protects prostate cancer cells from apoptosis in vitro and confers resistance to androgen depletion in vivo. *Cancer Res, 55*(19), 4438-4445.

Rajpar, S., Massard, C., Laplanche, A., Tournay, E., Gross-Goupil, M., Loriot, Y., et al. (2010). Urinary N-telopeptide (uNTx) is an independent prognostic factor for overall survival in patients with bone metastases from castration-resistant prostate cancer. *Ann Oncol, 21*(9), 1864-1869.

Roato, I., D'Amelio, P., Gorassini, E., Grimaldi, A., Bonello, L., Fiori, C., et al. (2008). Osteoclasts are active in bone forming metastases of prostate cancer patients. *PLoS One, 3*(11), e3627.

Rodan, G. A. (1998). Bone homeostasis. *Proc Natl Acad Sci U S A, 95*(23), 13361-13362.

Roodman, G. D. (2004). Mechanisms of bone metastasis. *N Engl J Med, 350*(16), 1655-1664.

Rosivatz, E., Becker, I., Specht, K., Fricke, E., Luber, B., Busch, R., et al. (2002). Differential expression of the epithelial-mesenchymal transition regulators snail, SIP1, and twist in gastric cancer. *Am J Pathol, 161*(5), 1881-1891.

Roudier, M. P., Morrissey, C., True, L. D., Higano, C. S., Vessella, R. L., & Ott, S. M. (2008). Histopathological assessment of prostate cancer bone osteoblastic metastases. *J Urol, 180*(3), 1154-1160.

Sabbota, A. L., Kim, H. R., Zhe, X., Fridman, R., Bonfil, R. D., & Cher, M. L. (2010). Shedding of RANKL by tumor-associated MT1-MMP activates Src-dependent prostate cancer cell migration. *Cancer Res, 70*(13), 5558-5566.

Saha, B., Arase, A., Imam, S. S., Tsao-Wei, D., Naritoku, W. Y., Groshen, S., et al. (2008). Overexpression of E-cadherin and beta-catenin proteins in metastatic prostate cancer cells in bone. *Prostate, 68*(1), 78-84.

Savagner, P. (2001). Leaving the neighborhood: molecular mechanisms involved during epithelial-mesenchymal transition. *Bioessays, 23*(10), 912-923.

Savagner, P. (2010). The epithelial-mesenchymal transition (EMT) phenomenon. *Ann Oncol, 21 Suppl 7*, vii89-vii92.

Schneeweis, L. A., Willard, D., & Milla, M. E. (2005). Functional dissection of osteoprotegerin and its interaction with receptor activator of NF-kappaB ligand. *J Biol Chem, 280*(50), 41155-41164.

Schramek, D., Leibbrandt, A., Sigl, V., Kenner, L., Pospisilik, J. A., Lee, H. J., et al. (2010). Osteoclast differentiation factor RANKL controls development of progestin-driven mammary cancer. *Nature, 468*(7320), 98-102.

Schramek, D., Sigl, V., & Penninger, J. M. (2011). RANKL and RANK in sex hormone-induced breast cancer and breast cancer metastasis. *Trends Endocrinol Metab*.

Schwarz-Cruz-y-Celis, A., & Melendez-Zajgla, J. (2011). Cancer stem cells. *Rev Invest Clin, 63*(2), 179-186.

Scott, L. J., & Muir, V. J. (2011). Denosumab: in the prevention of skeletal-related events in patients with bone metastases from solid tumours. *Drugs, 71*(8), 1059-1069.

Seshasayee, D., Wang, H., Lee, W. P., Gribling, P., Ross, J., Van Bruggen, N., et al. (2004). A novel in vivo role for osteoprotegerin ligand in activation of monocyte effector function and inflammatory response. *J Biol Chem, 279*(29), 30202-30209.

Sethi, S., Macoska, J., Chen, W., & Sarkar, F. H. (2010). Molecular signature of epithelial-mesenchymal transition (EMT) in human prostate cancer bone metastasis. *Am J Transl Res, 3*(1), 90-99.

Shi, C., Zhou, G., Zhu, Y., Su, Y., Cheng, T., Zhau, H. E., et al. (2008). Quantum dots-based multiplexed immunohistochemistry of protein expression in human prostate cancer cells. *Eur J Histochem, 52*(2), 127-134.

Shin, S., & Verma, I. M. (2003). BRCA2 cooperates with histone acetyltransferases in androgen receptor-mediated transcription. *Proc Natl Acad Sci U S A, 100*(12), 7201-7206.

Signoretti, S., Montironi, R., Manola, J., Altimari, A., Tam, C., Bubley, G., et al. (2000). Her-2-neu expression and progression toward androgen independence in human prostate cancer. *J Natl Cancer Inst, 92*(23), 1918-1925.

Sims, N. A., & Gooi, J. H. (2008). Bone remodeling: Multiple cellular interactions required for coupling of bone formation and resorption. *Semin Cell Dev Biol, 19*(5), 444-451.

Singh, A., & Settleman, J. (2010). EMT, cancer stem cells and drug resistance: an emerging axis of evil in the war on cancer. *Oncogene, 29*(34), 4741-4751.

Smith, D. C. (2011). Cabozantinib (XL184) Phase 2 Data Demonstrate Encouraging Clinical Activity in Patients with Castration-Resistant Prostate Cancer. *American Society of Clinical Oncology's 2011 Genitourinary Cancers Symposium (Abstract #127) in Orlando, Florida*.

Smith, D. C., Soira, A., De Greve, J., Hart, L., Holbrecht, S., Lin, C., et al. (2010). Phase 2 study of XL184 in a cohort of patients with castration resistant prostate cancer. *EORTC*, 406a.

Sosic, D., & Olson, E. N. (2003). A new twist on twist--modulation of the NF-kappa B pathway. *Cell Cycle, 2*(2), 76-78.

Sosic, D., Richardson, J. A., Yu, K., Ornitz, D. M., & Olson, E. N. (2003). Twist regulates cytokine gene expression through a negative feedback loop that represses NF-kappaB activity. *Cell, 112*(2), 169-180.

Stains, J. P., & Civitelli, R. (2005). Cell-to-cell interactions in bone. *Biochem Biophys Res Commun, 328*(3), 721-727.

Stopeck, A. T., Lipton, A., Body, J. J., Steger, G. G., Tonkin, K., de Boer, R. H., et al. (2010). Denosumab compared with zoledronic acid for the treatment of bone metastases in patients with advanced breast cancer: a randomized, double-blind study. *J Clin Oncol, 28*(35), 5132-5139.

Sturge, J., Caley, M. P., & Waxman, J. (2011). Bone metastasis in prostate cancer: emerging therapeutic strategies. *Nat Rev Clin Oncol, 8*(6), 357-368.

Sutherland, K. A., Rogers, H. L., Tosh, D., & Rogers, M. J. (2009). RANKL increases the level of Mcl-1 in osteoclasts and reduces bisphosphonate-induced osteoclast apoptosis in vitro. *Arthritis Res Ther, 11*(2), R58.

Suzuki, H., Sato, N., Watabe, Y., Masai, M., Seino, S., & Shimazaki, J. (1993). Androgen receptor gene mutations in human prostate cancer. *J Steroid Biochem Mol Biol, 46*(6), 759-765.

Sweeney, E., Ward, T. H., Gray, N., Womack, C., Jayson, G., Hughes, A., et al. (2008). Quantitative multiplexed quantum dot immunohistochemistry. *Biochem Biophys Res Commun, 374*(2), 181-186.

Szulc, P., Garnero, P., Marchand, F., Duboeuf, F., & Delmas, P. D. (2005). Biochemical markers of bone formation reflect endosteal bone loss in elderly men--MINOS study. *Bone, 36*(1), 13-21.

Takayanagi, H. (2005). Mechanistic insight into osteoclast differentiation in osteoimmunology. *J Mol Med (Berl), 83*(3), 170-179.

Takayanagi, H., Kim, S., Koga, T., Nishina, H., Isshiki, M., Yoshida, H., et al. (2002). Induction and activation of the transcription factor NFATc1 (NFAT2) integrate RANKL signaling in terminal differentiation of osteoclasts. *Dev Cell, 3*(6), 889-901.

Tarin, D., Thompson, E. W., & Newgreen, D. F. (2005). The fallacy of epithelial mesenchymal transition in neoplasia. *Cancer Res, 65*(14), 5996-6000; discussion 6000-5991.

Thalmann, G. N., Anezinis, P. E., Chang, S. M., Zhau, H. E., Kim, E. E., Hopwood, V. L., et al. (1994). Androgen-independent cancer progression and bone metastasis in the LNCaP model of human prostate cancer. *Cancer Res, 54*(10), 2577-2581.

Thalmann, G. N., Sikes, R. A., Wu, T. T., Degeorges, A., Chang, S. M., Ozen, M., et al. (2000). LNCaP progression model of human prostate cancer: androgen-independence and osseous metastasis. *Prostate, 44*(2), 91-103 Jul 101;144(102).

Theoleyre, S., Wittrant, Y., Tat, S. K., Fortun, Y., Redini, F., & Heymann, D. (2004). The molecular triad OPG/RANK/RANKL: involvement in the orchestration of pathophysiological bone remodeling. *Cytokine Growth Factor Rev, 15*(6), 457-475.

Thiery, J. P. (2002). Epithelial-mesenchymal transitions in tumour progression. *Nat Rev Cancer, 2*(6), 442-454.

Thiery, J. P. (2003). Epithelial-mesenchymal transitions in development and pathologies. *Curr Opin Cell Biol, 15*(6), 740-746.

Thiery, J. P., Acloque, H., Huang, R. Y., & Nieto, M. A. (2009). Epithelial-mesenchymal transitions in development and disease. *Cell, 139*(5), 871-890.

Thiery, J. P., & Sleeman, J. P. (2006). Complex networks orchestrate epithelial-mesenchymal transitions. *Nat Rev Mol Cell Biol, 7*(2), 131-142.

Thomas, G. H. (2001). New routes to membrane protein structures. Practical course: current methods in membrane protein research. *EMBO Rep, 2*(3), 187-191.

Thomas, R., True, L. D., Bassuk, J. A., Lange, P. H., & Vessella, R. L. (2000). Differential expression of osteonectin/SPARC during human prostate cancer progression. *Clin Cancer Res, 6*(3), 1140-1149.

Thompson, E. W., Newgreen, D. F., & Tarin, D. (2005). Carcinoma invasion and metastasis: a role for epithelial-mesenchymal transition? *Cancer Res, 65*(14), 5991-5995; discussion 5995.

Tobar, N., Villar, V., & Santibanez, J. F. (2010). ROS-NFkappaB mediates TGF-beta1-induced expression of urokinase-type plasminogen activator, matrix metalloproteinase-9 and cell invasion. *Mol Cell Biochem, 340*(1-2), 195-202.

Torres, K. E., Zhu, Q. S., Bill, K., Lopez, G., Ghadimi, M. P., Xie, X., et al. (2011). Activated MET is a molecular prognosticator and potential therapeutic target for malignant peripheral nerve sheath tumors. *Clin Cancer Res, 17*(12), 3943-3955.

Trapman, J., & Cleutjens, K. B. (1997). Androgen-regulated gene expression in prostate cancer. *Semin Cancer Biol, 8*(1), 29-36.

Tripodo, C., Sangaletti, S., Piccaluga, P. P., Prakash, S., Franco, G., Borrello, I., et al. (2011). The bone marrow stroma in hematological neoplasms-a guilty bystander. *Nat Rev Clin Oncol, 8*(8), 456-466.

van der Pluijm, G. (2010). Epithelial plasticity, cancer stem cells and bone metastasis formation. *Bone*.

van Leenders, G. J., Gage, W. R., Hicks, J. L., van Balken, B., Aalders, T. W., Schalken, J. A., et al. (2003). Intermediate cells in human prostate epithelium are enriched in proliferative inflammatory atrophy. *Am J Pathol, 162*(5), 1529-1537.

Vela, I., Gregory, L., Gardiner, E. M., Clements, J. A., & Nicol, D. L. (2007). Bone and prostate cancer cell interactions in metastatic prostate cancer. *BJU Int, 99*(4), 735-742.

Veldscholte, J., Berrevoets, C. A., Ris-Stalpers, C., Kuiper, G. G., Jenster, G., Trapman, J., et al. (1992). The androgen receptor in LNCaP cells contains a mutation in the ligand binding domain which affects steroid binding characteristics and response to antiandrogens. *J Steroid Biochem Mol Biol, 41*(3-8), 665-669.

Veldscholte, J., Ris-Stalpers, C., Kuiper, G. G., Jenster, G., Berrevoets, C., Claassen, E., et al. (1990). A mutation in the ligand binding domain of the androgen receptor of human LNCaP cells affects steroid binding characteristics and response to anti-androgens. *Biochem Biophys Res Commun, 173*(2), 534-540.

Veldscholte, J., Voorhorst-Ogink, M. M., Bolt-de Vries, J., van Rooij, H. C., Trapman, J., & Mulder, E. (1990). Unusual specificity of the androgen receptor in the human prostate tumor cell line LNCaP: high affinity for progestagenic and estrogenic steroids. *Biochim Biophys Acta, 1052*(1), 187-194.

Viatour, P., Merville, M. P., Bours, V., & Chariot, A. (2005). Phosphorylation of NF-kappaB and IkappaB proteins: implications in cancer and inflammation. *Trends Biochem Sci, 30*(1), 43-52.

Virk, M. S., & Lieberman, J. R. (2007). Tumor metastasis to bone. *Arthritis Res Ther, 9 Suppl 1*, S5.

Voulgari, A., & Pintzas, A. (2009). Epithelial-mesenchymal transition in cancer metastasis: mechanisms, markers and strategies to overcome drug resistance in the clinic. *Biochim Biophys Acta, 1796*(2), 75-90.

Wada, T., Nakashima, T., Hiroshi, N., & Penninger, J. M. (2006). RANKL-RANK signaling in osteoclastogenesis and bone disease. *Trends Mol Med, 12*(1), 17-25.

Wagner, E. F. (2002). Functions of AP1 (Fos/Jun) in bone development. *Ann Rheum Dis, 61 Suppl 2*, ii40-42.

Wagner, E. F., & Nebreda, A. R. (2009). Signal integration by JNK and p38 MAPK pathways in cancer development. *Nat Rev Cancer, 9*(8), 537-549.

Wagner, M. K., Li, F., Li, J., Li, X. F., & Le, X. C. (2010). Use of quantum dots in the development of assays for cancer biomarkers. *Anal Bioanal Chem, 397*(8), 3213-3224.

Walhout, A. J., Gubbels, J. M., Bernards, R., van der Vliet, P. C., & Timmers, H. T. (1997). c-Myc/Max heterodimers bind cooperatively to the E-box sequences located in the first intron of the rat ornithine decarboxylase (ODC) gene. *Nucleic Acids Res, 25*(8), 1493-1501.

Walsh, M. C., & Choi, Y. (2003). Biology of the TRANCE axis. *Cytokine Growth Factor Rev, 14*(3-4), 251-263.

Wang, D., & Richmond, A. (2001). Nuclear factor-kappa B activation by the CXC chemokine melanoma growth-stimulatory activity/growth-regulated protein involves the MEKK1/p38 mitogen-activated protein kinase pathway. *J Biol Chem, 276*(5), 3650-3659.

Wells, A., Yates, C., & Shepard, C. R. (2008). E-cadherin as an indicator of mesenchymal to epithelial reverting transitions during the metastatic seeding of disseminated carcinomas. *Clin Exp Metastasis, 25*(6), 621-628.

Wesselborg, S., Bauer, M. K., Vogt, M., Schmitz, M. L., & Schulze-Osthoff, K. (1997). Activation of transcription factor NF-kappaB and p38 mitogen-activated protein kinase is mediated by distinct and separate stress effector pathways. *J Biol Chem, 272*(19), 12422-12429.

Wolfer, A., Wittner, B. S., Irimia, D., Flavin, R. J., Lupien, M., Gunawardane, R. N., et al. (2010). MYC regulation of a "poor-prognosis" metastatic cancer cell state. *Proc Natl Acad Sci U S A, 107*(8), 3698-3703.

Wu, H. C., Hsieh, J. T., Gleave, M. E., Brown, N. M., Pathak, S., & Chung, L. W. (1994). Derivation of androgen-independent human LNCaP prostatic cancer cell sublines: role of bone stromal cells. *Int J Cancer, 57*(3), 406-412.

Wu, T. T., Sikes, R. A., Cui, Q., Thalmann, G. N., Kao, C., Murphy, C. F., et al. (1998). Establishing human prostate cancer cell xenografts in bone: induction of osteoblastic reaction by prostate-specific antigen-producing tumors in athymic and SCID/bg mice using LNCaP and lineage-derived metastatic sublines. *Int J Cancer, 77*(6), 887-894.

Xie, L., Law, B. K., Chytil, A. M., Brown, K. A., Aakre, M. E., & Moses, H. L. (2004). Activation of the Erk pathway is required for TGF-beta1-induced EMT in vitro. *Neoplasia, 6*(5), 603-610.

Xing, Y., Chaudry, Q., Shen, C., Kong, K. Y., Zhau, H. E., Chung, L. W., et al. (2007). Bioconjugated quantum dots for multiplexed and quantitative immunohistochemistry. *Nat Protoc, 2*(5), 1152-1165.

Xu, J., Chen, Y., & Olopade, O. I. (2010). MYC and Breast Cancer. *Genes Cancer, 1*(6), 629-640.

Xu, J., Wang, R., Xie, Z. H., Odero-Marah, V., Pathak, S., Multani, A., et al. (2006). Prostate cancer metastasis: role of the host microenvironment in promoting epithelial to mesenchymal transition and increased bone and adrenal gland metastasis. *Prostate, 66*(15), 1664-1673.

Yang, J., Mani, S. A., Donaher, J. L., Ramaswamy, S., Itzykson, R. A., Come, C., et al. (2004). Twist, a master regulator of morphogenesis, plays an essential role in tumor metastasis. *Cell, 117*(7), 927-939.

Yang, X., Matsuda, K., Bialek, P., Jacquot, S., Masuoka, H. C., Schinke, T., et al. (2004). ATF4 is a substrate of RSK2 and an essential regulator of osteoblast biology; implication for Coffin-Lowry Syndrome. *Cell, 117*(3), 387-398.

Yart, A., Laffargue, M., Mayeux, P., Chretien, S., Peres, C., Tonks, N., et al. (2001). A critical role for phosphoinositide 3-kinase upstream of Gab1 and SHP2 in the activation of ras and mitogen-activated protein kinases by epidermal growth factor. *J Biol Chem, 276*(12), 8856-8864.

Yasuda, H., Shima, N., Nakagawa, N., Yamaguchi, K., Kinosaki, M., Mochizuki, S., et al. (1998). Osteoclast differentiation factor is a ligand for osteoprotegerin/osteoclastogenesis-inhibitory factor and is identical to TRANCE/RANKL. *Proc Natl Acad Sci U S A, 95*(7), 3597-3602.

Yates, C. C., Shepard, C. R., Stolz, D. B., & Wells, A. (2007). Co-culturing human prostate carcinoma cells with hepatocytes leads to increased expression of E-cadherin. *Br J Cancer, 96*(8), 1246-1252.

Ye, L., Kynaston, H. G., & Jiang, W. G. (2007). Bone metastasis in prostate cancer: molecular and cellular mechanisms (Review). *Int J Mol Med, 20*(1), 103-111.

Yeh, S., & Chang, C. (1996). Cloning and characterization of a specific coactivator, ARA70, for the androgen receptor in human prostate cells. *Proc Natl Acad Sci U S A, 93*(11), 5517-5521.

Yeh, S., Hu, Y. C., Rahman, M., Lin, H. K., Hsu, C. L., Ting, H. J., et al. (2000). Increase of androgen-induced cell death and androgen receptor transactivation by BRCA1 in prostate cancer cells. *Proc Natl Acad Sci U S A, 97*(21), 11256-11261.

Yeh, S., Miyamoto, H., Nishimura, K., Kang, H., Ludlow, J., Hsiao, P., et al. (1998). Retinoblastoma, a tumor suppressor, is a coactivator for the androgen receptor in human prostate cancer DU145 cells. *Biochem Biophys Res Commun, 248*(2), 361-367.

Yin, J. J., Pollock, C. B., & Kelly, K. (2005). Mechanisms of cancer metastasis to the bone. *Cell Res, 15*(1), 57-62.

Yonou, H., Kanomata, N., Goya, M., Kamijo, T., Yokose, T., Hasebe, T., et al. (2003). Osteoprotegerin/osteoclastogenesis inhibitory factor decreases human prostate cancer burden in human adult bone implanted into nonobese diabetic/severe combined immunodeficient mice. *Cancer Res, 63*(9), 2096-2102.

Yurube, T., Takada, T., Hirata, H., Kakutani, K., Maeno, K., Zhang, Z., et al. (2011). Modified house-keeping gene expression in a rat tail compression loading-induced disc degeneration model. *J Orthop Res, 29*(8), 1284-1290.

Zhang, J., Dai, J., Qi, Y., Lin, D. L., Smith, P., Strayhorn, C., et al. (2001). Osteoprotegerin inhibits prostate cancer-induced osteoclastogenesis and prevents prostate tumor growth in the bone. *J Clin Invest, 107*(10), 1235-1244.

Zhang, J., Dai, J., Yao, Z., Lu, Y., Dougall, W., & Keller, E. T. (2003). Soluble receptor activator of nuclear factor kappaB Fc diminishes prostate cancer progression in bone. *Cancer Res, 63*(22), 7883-7890.

Zhang, L., Feng, X., & McDonald, J. M. (2003). The role of calmodulin in the regulation of osteoclastogenesis. *Endocrinology, 144*(10), 4536-4543.

Zhang, S., Wang, X., Osunkoya, A. O., Iqbal, S., Wang, Y., Chen, Z., et al. (2011). EPLIN downregulation promotes epithelial-mesenchymal transition in prostate cancer cells and correlates with clinical lymph node metastasis. *Oncogene*.

Zhang, S., Zhau, H. E., Osunkoya, A. O., Iqbal, S., Yang, X., Fan, S., et al. (2010). Vascular endothelial growth factor regulates myeloid cell leukemia-1 expression through neuropilin-1-dependent activation of c-MET signaling in human prostate cancer cells. *Mol Cancer, 9*, 9.

Zhang, Y., Guessous, F., Kofman, A., Schiff, D., & Abounader, R. (2010). XL-184, a MET, VEGFR-2 and RET kinase inhibitor for the treatment of thyroid cancer, glioblastoma multiforme and NSCLC. *IDrugs, 13*(2), 112-121.

Zhau, H. E., Odero-Marah, V., Lue, H. W., Nomura, T., Wang, R., Chu, G., et al. (2008). Epithelial to mesenchymal transition (EMT) in human prostate cancer: lessons learned from ARCaP model. *Clin Exp Metastasis, 25*(6), 601-610.

Zhau, H. Y., Chang, S. M., Chen, B. Q., Wang, Y., Zhang, H., Kao, C., et al. (1996). Androgen-repressed phenotype in human prostate cancer. *Proc Natl Acad Sci U S A, 93*(26), 15152-15157.

Zhou, A. X., Toylu, A., Nallapalli, R. K., Nilsson, G., Atabey, N., Heldin, C. H., et al. (2011). Filamin a mediates HGF/c-MET signaling in tumor cell migration. *Int J Cancer, 128*(4), 839-846.

Zhou, B. P., Deng, J., Xia, W., Xu, J., Li, Y. M., Gunduz, M., et al. (2004). Dual regulation of Snail by GSK-3beta-mediated phosphorylation in control of epithelial-mesenchymal transition. *Nat Cell Biol, 6*(10), 931-940.